RECENT RESULTS ON THE KINETICS OF COAL PYROLYSIS
AND HYDROPYROLYSIS AND THEIR RELATIONSHIP TO COAL STRUCTURE

K. H. van Heek and H. Jüntgen
Bergbau-Forschung, 4300 Essen 13, West Germany

1. Introduction

Pyrolysis of coal is understood to be its thermal decomposition at temperatures beyond 300 °C, whereby gas, tar and char are formed. It is the basic process of coking and the starting reaction of combustion, gasification and hydrogenation. In addition the application of pyrolysis offers the possibility to convert coal into gases and liquids in a "third way" besides gasification and hydrogenation. Thereby the yield of volatile matter can be substantially increased by hydrogen at high pressures - "hydropyrolysis".

For all these reasons coal pyrolysis has been and is being studied worldwide by many scientists. Recent reviews are owed to Howard /1/ and Gavalas /2/. For some 20 years scientists at Bergbau-Forschung have been carrying out systematic studies on the kinetics and mechanism of pyrolysis /3-8/. In continuation of this work, during the last few years, in the frame of the IEA pyrolysis project the influence of ambient gas atmosphere and pressure on course and products of coal pyrolysis have been investigated extensivelly /9-11/. Within this scope special interest was laid also on the formation kinetics of the single compounds of the BTX aromatics during pyrolysis and hydropyrolysis /12/. This contribution reviews in brief our main results on course, products, kinetics and mechanism of pyrolysis reactions on coal. Moreover it deals with a first attempt to establish a link between these findings and the most recent results on the chemical constitution of coal /13/.

2. Experimental Techniques and Basic Results

To cover a wide range of heating rates by the laboratory work different types of equipment have been used /9/. The results presented in this paper are mainly measured in a thermobalance, in which approximately 1 g of a coal sample can be heated up with some °C/min in a gas stream at pressures up to 100 bar in a temperature range between 20 and 1.000 °C. The progress of the reaction is measured by the weight loss and by the continuous analysis of the gaseous reaction products. Some additional results are presented at high heating rates, which have been achieved using the grid heater technique, whereby about 10 mg of finely ground coal are pyrolysed on a electrically heated wire mesh net. Most of the experimental results presented in this paper are measured taking coals from the Ruhr area. Here they are characterized in short by their volatile matter content (V.M.). The complete data can be found elsewhere /8,9,10/.

A characteristic result using the thermobalance is given in fig. 1, showing the formation rates of the main products. The mass loss depicts the overall reaction and thereby the formation of the char and occurs in two steps. The volatile matter - tar and gaseous products - are liberated in one or a few single reactions for each component. Fig. 2 shows the gas formation for a wide rank of German coal. In all cases - with the exception of CO_2 and the hydrogen (not given in the figure) - the curves show a systematic degradation by coalification of those groups, which have a weaker bonding and are therefore liberated at lower temperature during pyrolysis.

Course of product formation and yields are controlled by chemical reaction on the one hand and transport phenomena inside the particle on the other. The latter gains in influence, if particle diameter, heating rate and pressure increase. An example for quantitative measurements and relevant calculations is given in fig. 3. As a function of particle diameter and heating rate a curve has been established separating areas where - depending on diameter and heating rate - transport phenomena or chemical reaction controls the overall process. With higher pressure it is shifted to lower values for diameter and heating rate. The region, in which the chemical reaction is rate determining, meets to a high degree the conditions in technical reactors regarding pressure, particle size and rate of heating. Thus kinetics themselves are not influenced by transport processes, however by the different residence times of the product inside the particle secondary reactions may control yields. This is especially true for the liquid volatile matter as can be seen by the formation of the tar and - as an example of the BTX aromatics - the benzene (fig. 5), whereby pressure favours obviously the cracking of the liquids. This is true for the whole rank /10/. Fig. 7 gives quantitative data for two rates of heating. However, by comparison of low and high heating rate the latter exhibits a higher yield of liquids as the residence time of the products inside the particle is considerably smaller.

The effect of hydrogen exists mainly in an increase of the formation of liquid products, which are now formed in a two reactions (fig. 6). The peak between 350 and about 480 °C is slightly affected mainly by the influence of the pressure as discussed before and can be ascribed to pyrolysis. However with rising pressures the second reaction becomes more and more important. The enhancing influence of hydrogen pressure on the yield of tar as well as on BTX aromatics is demonstrated in fig. 9 for three different high volatile coals. It is remarkable that up to 40 % of the coal can be converted into liquids ultimately at 100 bar under low heating rates. The BTX aromatics have a share of about 10 % of the total tar. Fig. 10 summarizes results of the characterization of tar samples, taken at different temperatures during hydropyrolysis. It shows that the concentration of the aromatics in the tar increases with rising temperature and that the BTX aromatics are mainly formed at the end of the tar formation. The second reaction of tar formation mainly can be ascribed to hydrogenation and the formation of the BTX to hydrocracking.

3. **Kinetics and Mechanism**

A derivation of mathematical equations to describe product formation curves for coal pyrolysis is given in fig. 9, left side. They have been achieved under the asumption that the rate of the formation of a particular product is dependent on the concentration of functional groups in the coal, the degradation of which results in this product /3/. With these equations the measured curves can be described excellently as the examples on the right hand

side of fig. 9 confirm. This is also true for CH_4 in which formation 2 to 3 reactions participate. The values for the kinetic parameters found for these four examples depending on pressure are listed in table 1. In a similar way also the formation of other gases like H_2O, CO_2, N_2, and of tar and BTX aromatics during hydropyrolysis have been formally described and the relevant kinetic parameters have been published /12/.

The peak for tar formation can be described best by a first order reaction. Aliphates with more than two C-atoms show a curve of a simple structure, which ha been described under the assumption of a reaction order of n=1 and a distribution of E and k_o /6,8/. The support for this assumption is that the rupture of bondings is rate determining and the bonding energies are distributed because of the interactions with different neighbour groups. However, as shown in fig. 9, also n=2 together with distinct values for E and k_o formally give an excellent description of the reaction peaks. It can be interpreted by interactions of the radicals formed in the primary step. Moreover it has formal advantages in a subsequent mathematical treatment e.g., when modelling reactors. In the same way also the curves for methane can be described under the assumption of several reactions either each with distributed E and k_o-values or under the assumption of n=2 with distinct E and k_o.

The ideas about the mechanism of the product formation as mentioned before are schematically given in fig. 10. The most relevant steps are thermal activation, breaking of chemical bonds and formation of stable molecules by reactions of the radicals. The total process can be described by a first order law, when the slow step (II) is rate determining. A second order law makes sense, when the step IIIc controls the overall reaction. On the whole it can be stated that the kinetic equations and the conditions concerning E and k_o are based on assumptions, which are most compatible with possible reaction models. It follows that an extrapolation of the results, achieved with the relevant mathematical methods can be performed with a high degree of confidence. It should be mentioned that the release of H_2, being extremely wide spread over the temperature range, can only be interpreted by an overlap of many first order reactions resulting in a broad distribution of E and k_o due to the fact the C-H-bonding energies in the coal molecule are also extremely widely distributed.

4. Chemical Constitution of Coal and Kinetics of Pyrolysis

Fig. 11 gives the model molecule for a high volatile bituminous coal (83 % C) /14/. The most recent analytic diagnoses for determining both the functional CH- and CH_2-groups by NMR spectrometry as well as the functional oxygen-containing groups, entered the model. It also reflects the chemical reactions having been observed with coal. From general knowledge on bonding energies in organic molecules it can be derived, that the C-C-bonding energies at the bridges between ring systems are much weaker than those of other C-C-bonds, particularly in the aromatic structures. Thus it may be expected, that cracking of the coal molecule between the different ring systems will be a first step of coal degradation during pyrolysis being possible already at moderate temperature of about 400 °C.

Following conclusions may, therefore, be drawn when looking at the coal constitution and the kinetics of pyrolysis: the begin of tar formation at 350 °C can be assumed by the destillation and diffusion of smaller organic molecules (molecular weight below 150 - 200) having been trapped in the quite narrow pore structure of the coal. Parallel thermal degradation of the coal molecule

4

takes place at temperatures at about 400 °C according to the primary reaction steps as given schematically in fig. 10. The reactions commence at 400 °C by cracking of the bridge-carbons which have the lowest bonding energies and as a consequence by dissociating of the aromatic ring units whereby radicals are formed. Due to fast recombining reactions among the smaller radicals and their reactions with hydrogen, formation of small aliphatic gas molecules, like CH_4 and H_2O takes place. Also bigger ring fragments become hydrogen-saturated and distillate as tar with medium molecular weight. This explains the simultaneous occurence of tar CH_4, C_2-, C_3-hydrocarbons, and water above 400 °C. Also formation of coke will commence via condensation of the ring systems, under elimination of hydrogen which appears for the first time in gaseous form above 420 °C. At high temperatures there will finally be produced also CO by cracking of heterocyclic oxygen groups.

The above mechanisms are backed up by the carbon-, hydrogen-, and oxygen-balances both for the pyrolysis products as well as for the functional groups of the coal molecule /13/. The same mechanism basically applies also to high pressures and heating rates. The effect of high pressure consists, inter alia, in a shifting of tar formation towards higher temperatures due to a shifting in the boiling range so that at the expense of the tar yield the parallel coke-generating condensation will be intensified. The elementary hydrogen liberated under high pressures will beyond 700 °C lead to an increased methane yield due to a partially hydrogasification of carbon. High heating rates will result in a faster disengagement of the tar and thus reduce the proportion of condensating reactions.

If hydrogen is present the reaction mechanisms of coal pyrolysis change substantially, under additional formation of tar, aromatic compounds (fig. 6, 7, 8) and CH_4 at the expense of coke. This may be explained by the fact that beyond 500 °C, concurrently to the cracking, recombining and condensation reactions as explained, there occurs partial hydrogenation of aromatic systems which are then subject to hydrocracking. This reaction helps to increase volatile matter and reduces coke formation. The mechanism of such hydrocracking depends on whether interior or exterior aromatic rings have been hydrogenated. In the first case formation of diphenyl (under separation of methane) may occur. In the second case polynuclear aromates with aliphatic lateral chains will in a first place be formed which are decomposed partially under elimination of methane. This may be plausible explanation for the increased formation of tars, BTX aromates and methane. The additional water formation observed can be explained by hydrocracking of ether groups.

Conclusion

To sum up: Kinetic data have been evaluated to describe the formation rates of the most important products of coal pyrolysis. Also the yields depending on pressure and heating rates are well-known. Both kinetic parameters and yields have been measured covering the whole rank of hard coal. Moreover the most important liquid products evolved during hydropyrolysis can be described in the same manner. These data are now available and utilized for the modelling of pyrolysis reactors and those processes, in which pyrolysis plays an important role, like combustion, hydrogenation and fixed bed gasification. In addition the recent findings on the molecular structure of coal have lead to a detailed understanding of the single steps during pyrolysis and hydropyrolysis, thereby proving the formal kinetic approaches and showing new ways process optimisation.

References

/1/   Howard, J.B., In: Elliot, M.A.: Chemistry of coal utilisation. P. 665/784.
        John Wiley and Sons 1981

/2/   Gavalas, G.R., Coal pyrolysis. Elsevier Publishing Co. 1982

/3/   Jüntgen, H., Erdöl und Kohle 17 (1964), p. 105/114

/4/   Heek, K.H. van, Jüntgen, H., Peters, W., Ber. Bunsengesellschaft f. physik.
        Chemie 71 (1967), p. 113/121

/5/   Jüntgen, H., Heek, K.H. van, Fuel (London) XLVII (1968), p. 103/117

/6/   Jüntgen, H., Heek, K.H. van, Brennstoff-Chemie 50 (1969), p. 172/179

/7/   Koch, V., Heek, K.H. van, Jüntgen, H., Dynamic Mass Spectrometry, Vol.1,
        Heyden and Son Ltd. 1970, p. 15/21

/8/   Jüntgen, H., Heek, K.H. van, Fuel Processing Technology 2 (1979),
        p. 261/293

/9/   Arendt, P., Heek, K.H., Fuel 60 (1981), p. 779/787

/10/   Heek, K.H. van, VDI Forschungsheft Nr. 612/1982. Düsseldorf: VDI-Verlag
        GmbH (Habilitations-Thesis, Münster 1981)

/11/   Heek, K.H. van, Chem.Ing.Techn. 55 (1983), p. 777/784

/12/   Bunthoff, D., Wanzl, W., Heek, K.H. van and Jüntgen, H., Erdöl und Kohle,
        36 (1983), p. 326/332

/13/   Jüntgen, H., Fuel, 1983, (accepted for publication)

/14/   Wender, I., Heredy, L.A., Neuworth, M.B. and Dryden, G.C., In: Elliot, M.A.:
        Chemistry of coal utilisation. P. 425/521. John Wiley and Sons, 1981

pressure bar		1		100	
		E	k_O	E	k_O
tar	n = 1	138	$7.6 \cdot 10^8$	174	$1.5 \cdot 10^{11}$
benzene	1) n = 1	140	$2.1 \cdot 10^{11}$	136	$2.0 \cdot 10^{11}$
	2) n = 2	142	$6.0 \cdot 10^7$	115	$2.0 \cdot 10^6$
	3) n = 2	150	$1.0 \cdot 10^7$	149	$8.0 \cdot 10^6$
CH_4	1) n = 2	204	$7.8 \cdot 10^{11}$	214	$7.8 \cdot 10^{11}$
	2) n = 2	158	$2.7 \cdot 10^7$	141	$5.3 \cdot 10^5$
	3) n = 2	–	–	257	$1.8 \cdot 10^{11}$
C_2H_6	n = 2	210	$1.5 \cdot 10^{13}$	224	$2.2 \cdot 10^{13}$
C_2H_4	n = 2	205	$2.7 \cdot 10^{13}$	218	$7.1 \cdot 10^{13}$

E in kJ/mol; k_O for n = 1 in 1/min; k_O for n = 2 in g/cm^3 min.

Table 1: Values for kinetic parameters for the curves given in fig. 9 (right side)
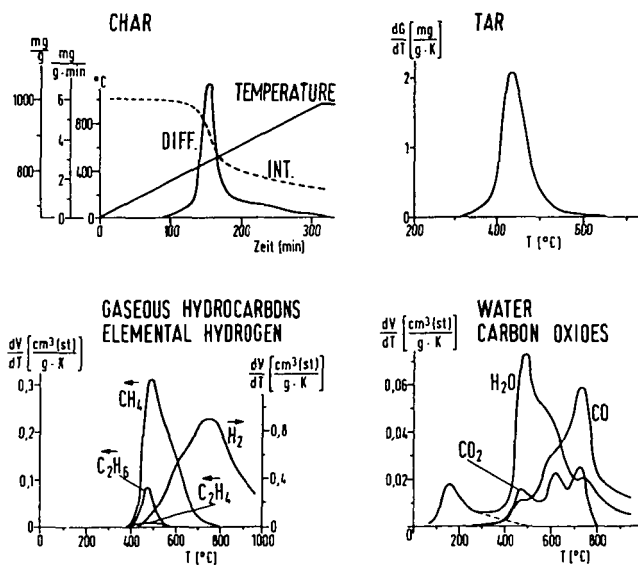

Fig. 1: Example for the product formation during pyrolysis of a German coal (32 % V.M. daf); heating rate: 3 K/min; atmosphere: N_2; total pressure: 11 bar)
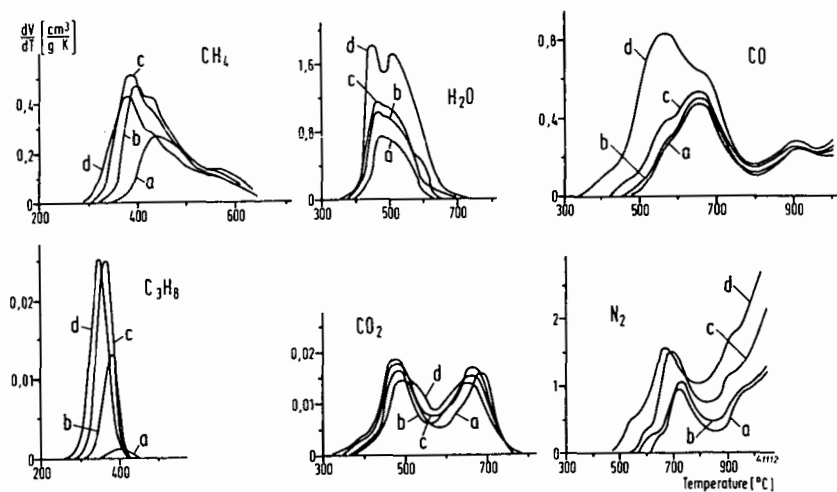
7

Fig. 2: Formation of the main pyrolysis gases for coals of
different rank
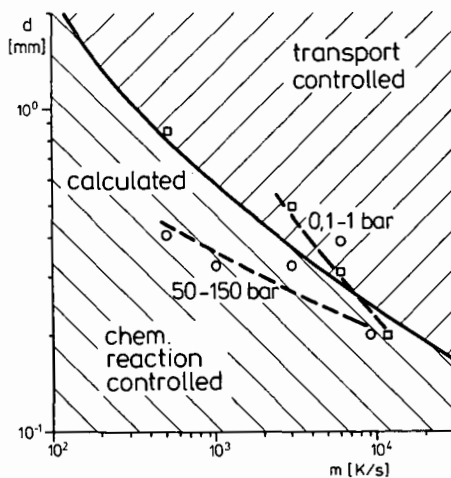(coal a: 10 % V.M.; b: 19,5 %; c: 29 %, d: 39,5 %)

Fig. 3: Influence of particle diameter (d), heating rate (m)
and pressure on the rate determining step of the pyrolysis
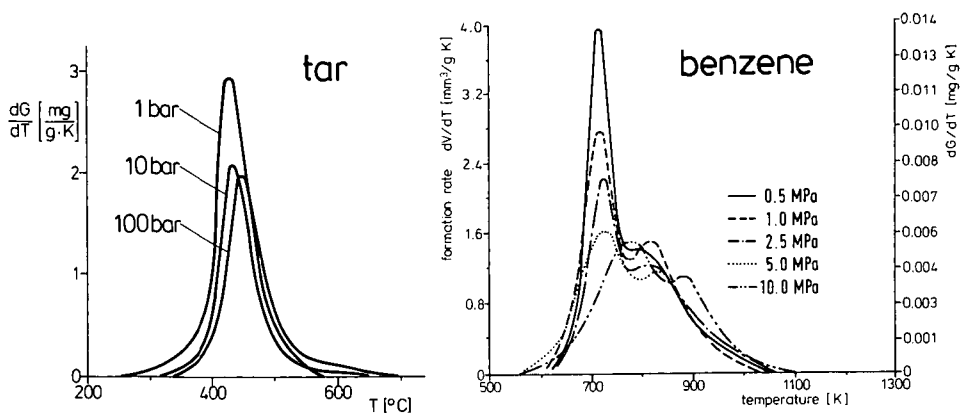for a German h.v. bit. coal

8

Fig. 4: Formation of liquid pyrolysis products depending on pressure
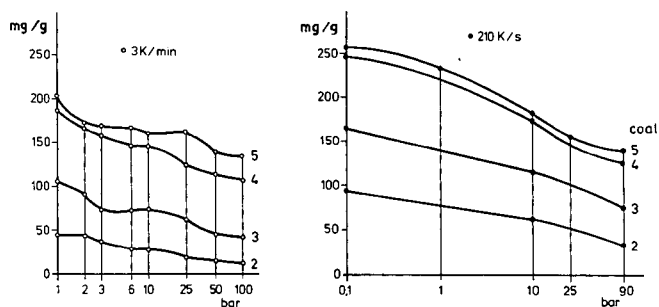(coal: 38,6 % V.M.; under N_2; 3 K/min)

Fig. 5: Influence of pressure and rate of heating on tar yield
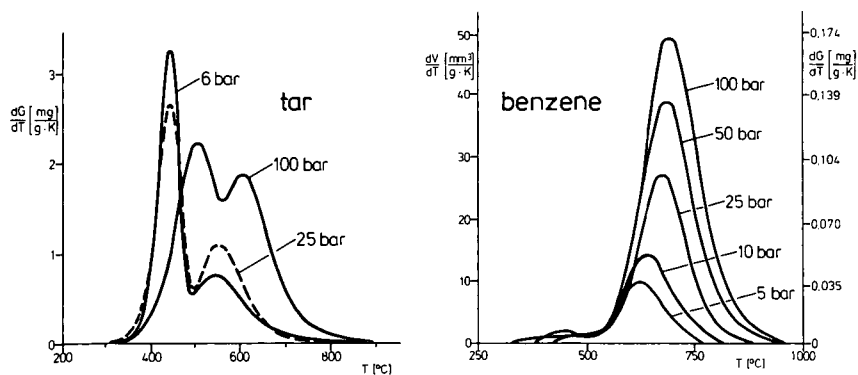for coals at different rank (coal 2: 16,2 % V.M.; 3: 23 %;
4: 32,9 %; 5: 36,3 %)

Fig. 6: Formation of liquid products during hydropyrolysis depending
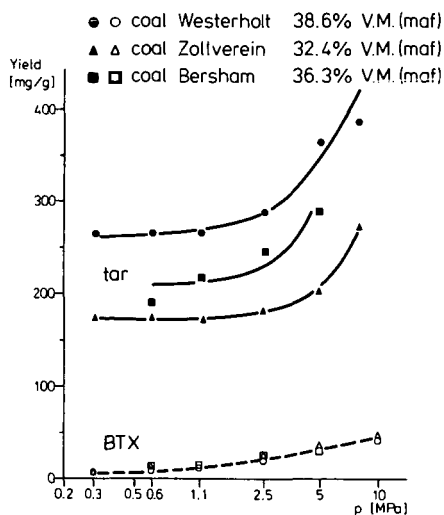on pressure (coal: 38,6 % V.M.; 3 K/min)

9

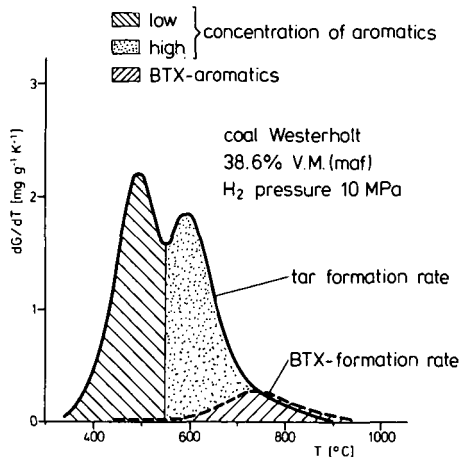Fig. 7: Yield of BTX aromatics and tar from hydro-pyrolysis

Fig. 8: Change of the contents of aromatics in the tar from hydropyrolysis

$$-\frac{dc}{dt} = k \cdot c^n$$

$$c = a \cdot (V_0 - V)$$

$$c_0 = a \cdot V_0$$

$$\frac{dT}{dt} = m = \text{const.}$$

$$k = k_0 \, \exp\left(-\frac{E}{RT}\right)$$

Integration

$$n=1 \qquad \frac{dV}{dT} = \frac{k_0 \cdot V_0}{m} \, \exp\left[-\frac{E}{RT} - \frac{k_0}{m} \, I(T)\right]$$

$$n \neq 1 \qquad \frac{dV}{dT} = \frac{k_0}{m} \, \exp\left(-\frac{E}{RT}\right) \left[V_0^{1-n} + (n-1) \, \frac{k_0}{m} \, I(T)\right]^{\frac{n}{1-n}}$$

$$\text{with} \qquad I(T) = \int_0^T \exp\left(-\frac{E}{RT}\right) \, dT$$

o measured   —— calculated
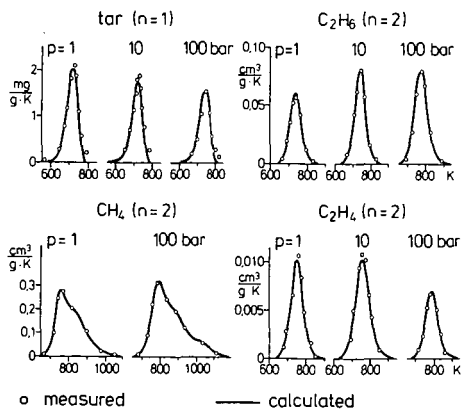
Fig. 9: Kinetic equations and description of product formation curves for pyrolysis (coal: 32,9 % V.M.; N_2; 3 K/min)

I.	Thermal activation - fast -		$R_i \diagup\diagdown R_j \diagup R_k \longrightarrow \overset{*}{R_i} \diagup\diagdown R_j \diagup R_k$
II.	Breaking of chemical bonds - slow -		$\overset{*}{R_i} \diagup\diagdown R_j \diagup R_k \xrightarrow{k_{II}} R_i \diagup\diagdown{}^{\bullet}\diagup R_k + R_j{}^{\bullet}$
III.	Formation of stable molecules by	a. Rearrangement with and without dissociation - fast -	$R_j{}^{\bullet} \longrightarrow R_l + R_n{}^{\bullet}$
		b. Intermolecular radical reactions - fast -	e.g. dimerisation $R_j{}^{\bullet} + R_m{}^{\bullet} \longrightarrow R_j - R_m$
		c. Transfer of radicals - slow	$R_n \diagup\diagdown R_l \diagup R_a + R_j{}^{\bullet} \xrightarrow{k_{IIIc}} R_j - R_l + R_n \diagup\diagdown{}^{\bullet}\diagup R_o$

Fig. 10: Steps of the primary reaction during coal pyrolysis
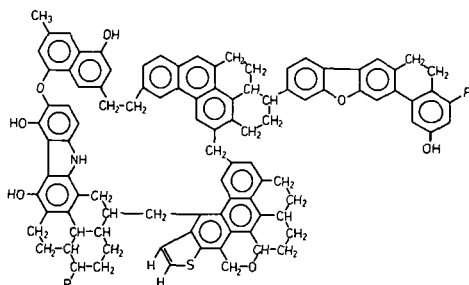

Fig. 11: Model molecule of a high volatile bituminous coal /14/

SIMULTANEOUS THERMOANALYTICAL and MASS SPECTROMETRIC INVESTIGATIONS
• of VOLATILE COMPOUNDS EVOLVED from MINERAL COAL up to a TEMPERATURE
RANGE of 1800 K.

K.-H. Ohrbach, A. Kettrup

Applied Chemistry, University GH Paderborn, P.O. Box 1621,
4790 Paderborn (F.R.G.)

The further development of simultaneous working coupling systems
basing on different physical measuring principles is one main aspect
regarding the investigation of the thermal degradation or the oxi-
dative decomposition processes of mineral coal discussed and illu-
strated in this paper.
The combination of the methods "Thermogravimetry-Derivative Thermo-
gravimetry-Differential Thermal Analysis-Mass Spectrometry" (TG-DTG-
DTA-MS) using the equipment described later offers a wide variety of
useful and practical applications in the field of mineral coal ana-
lysis respectively carbonaceous materials in general.
A working temperature of 1800 K and a stored temperature controlled
program permit long during thermal treatment of the samples in vari-
ous atmospheres as well as heating with rapid heating rates up to 20
K min^{-1} limitation of the furnace.
For monitoring the released gases and determining the mass fragments
(m/z values) a quadrupole mass spectrometer with rapid scan capabi-
lity is more convenient than a time-of-flight mass spectrometer in
many cases especially room saving construction, low cost, sufficient
sensitivity and resolution.

Experimental Section

The coal samples were given by the "Coal Mining Research Insti-
tute" at Essen (F.R.G.). The combined thermoanalytical mass spectro-
metric experiments have been carried out with a coupling system con-
sisting of Netzsch STA 429 Thermoanalyzer and Balzers Quadrupole
Mass Spectrometer QMG 511.
The main instrumental feature to record mass spectra at high tempe-
ratures at standard pressure is a special constructed interface bet-
ween thermoanalyzer and mass spectrometer, see Fig.1.. It permits
all different experimental conditions essentially at a working pres-
sure of 1 bar in various inert or reaction gas atmospheres at the sam-
ple introducing no complications with regard to high vacuum in the
mass spectrometer. Two modes of operation depending on an interface
as a pressure reduction system are possible:
1. high vacuum in the whole coupling system
2. standard pressure in different gas atmospheres in the thermoana-
   lyzer and high vacuum < 10^{-4} mbar in the mass spectrometer.
Two different pressure reduction systems have been employed, alumina
oxide tubes and quartz tubes with orifices at the bottom to reduce
pressure in two stages. A more detailed description has been given
earlier (1).
High vacuum has been the preferred method to get higher ion yields
in the upper mass range avoiding fragmentation of evolved compounds.
The storage of twelve different mass units (mass ranges) up to m/z
values of 511 including all adjustable instrumental parameters is
possible. The scan speed varies between 0.1 ms to 30 s per mass unit.

For the DTA experiments a measuring range of 0.05 mV full scale has
been applied with constant heating rates of 10 K min^{-1}.

Magnesium oxide has been used as a reference material. We have chosen
it as a dilution substance, too, when heating samples of particle
size larger than 0.2 mm diameter so that reproducible evaluation of
the DTG-DTA data can be ensured (2-7). A thermocouple Pt-Rh-Pt has
been employed for temperature measuring up to 1870 K at heating
rates from 0.1 to 20 (50) K applying various temperature programs in
the DTA measuring range from 0.05 to 100 mV. The sample mass was
taken with 10 mg and the DTG sensivity 0.5 mg/min cm .

Results

Investigations of coal pyrolysis, pyrolysis kinetics respectively
new trend analysis which is done regarding coal rank have been in-
tensively described by several authors in view of determination of
coal structure or the devolatilization process study (8-11). This
series of experiments which are reported here leads to the identifi-
cation of time temperature dependent coal devolatilization products
simultaneously. Referring to our preliminary studies into metal
complexes our interest has mainly been aimed to apply this coupling
system in the field of coal analysis, e.g. evolved gas analysis.
Regarding gasification process control the utilization of this
equipment may permit realistic experimental conditions such as tem-
perature, time and atmosphere similar to a gasification environment.
We gained our experience by exemlarily investigating a few standard
coal samples to test the capability of the apparatus as a possible
use in devolatilization analysis.
The TG-DTG-DTA data correlate reasonably. Gas evolution of a sample
results in mass loss accompanied by thermal effects exhibited as
peak width, -height, -area in the DTG (DTA) curve as illustrated in
Fig. 2. The increase in pressure as well as the temperature can be
recorded and measured at the sample. The data obtained by our ther-
moanalytical investigations have not shown striking characteristics
or significant trends with respect to coal rank as sometimes report-
ed in the literature. This is possibly due to altering the represen-
tative samples e.g. the sensivity for reproducing the data. Before
generalizing these vacuum results additional tests have been per-
formed in dynamic nitrogen and argon atmosphere showing no gradual
differences, too. Table 1 shows summarized values of the DTG experi-
ments.

Table 1

Average values of characteristic temperatures taken from the
DTG curves of three standard coal samples

Coal type[a) V.M. d.a.f.	$T_{i,I}$ [b)	$T_{f,I}$ [c)	$T_{P,I}$ [d)	$T_{i,II}$ [e)	$T_{f,II}$	$T_{P,II}$
	K	K	K	K	K	K
6.9	460	588	538	-	-	-
16.2	469	576	540	727	792	752
36.3	477	571	537	673	749	707

a) coal type, volatile matter/%, b) T_i is the temperature at which
the cumulative mass change reaches a magnitude that thermobalance

13

Resulting from our vacuum operations one striking fact seems to be very important that is to determine the gas composition of the devolatilization products in the temperature range of 1600 to 2100 K, because in our experiments we observed slightly increasing courses or maxima plateaus of ion currents when running the intensities of selected ion currents as autocontrol spectra. According to this, the begin of this phenomena is at a temperature of about 1350 K. The TG curves indicate a monotonously small decreasing mass loss. The application of a furnace working up to 2600 K for these investigations will be realized soon.

Discussion

A typical standard pressure run of a coal sample 6.9 % d.a.f. (anthracite) is shown in Fig.2. This experiment was carried out in dynamic helium atmosphere, which is not very suitable for TG-DTA-MS measurements in general. Constant heating rates up to 1800 K and constant cooling has been employed, indicating an additional mass loss in the DTG curve. The slopes of the DTG curves were similar when nitrogen or argon were used as inert gases. In this case the sample was put on a high temperature stable ceramic plate instead of platinum crucibles. The DTG curve exhibits a sharp peak at 1721 K. Observing significant mass loss in this temperature range we have to determine the m/z values of the evolved products simultaneously beginning at temperature onsets of devolatilization to final temperatures. This mode of operation yields no DTA data but more stable TG-DTG base lines. Evolution of the gases or particles are now developed from a very large surface distribution in contrast to platinum crucibles.
It is evident that thermal properties of coal samples result in different data of mass loss corresponding to the volatile matter content. A greater amount of mass loss and unavoidably less residual products can be estimated in connection with pressure and final heating time-temperature surface distribution relationships, using the above mentioned spicemen, but DTA data cannot be taken from this measuring device.
Some results concerning the different modes of operations and types of problems should be discussed exemplarily with the following examples. In Fig. 3 the TG-DTG-DTA-T-P curves of a coal sample with 36.3 % V.M. d.a.f. are shown exhibiting two peak temperatures in the DTG curve with a total mass loss of 40 %. Each step in mass loss indicated in the TG curve corresponds to an increase in pressure. The first maximum at 523 K in mass loss (endothermal slope of the DTA curve) is due to release of moisture (carbon dioxide, -monoxide equilibrium). Before reaching the second maximum temperature the mass spectrum indicates the typical breakdown pattern of homologous hydrocarbon series with increasing intensities as a function of temperature. The excitation energy applied has been 20 eV up to a mass range of 330 mass units in the temperature range from 643 to 663 K, see Fig. 4. Molecular condensation reactions cannot be excluded as well as fragmentation of higher molecular species into compounds of lower masses. In some cases we employ a rapid scan mode to observe increasing or decreasing intensities of mass fragments in a small temperature range. This is shown in Fig. 5 exhibiting the decreasing intensities of the mass range of m/z=182 to 184 which correspond to a release of compounds resulting from the diphenyl series accompanied by only a slight mass loss in this 10 K temperature interval. The investigations of a low volatile bituminous coal with 16.2 % V.M. d.a.f. is shown in Fig. 6, only monitoring six mass units corre-

14

can detect, c) T_f is the final temperature, d) T_p represents the peak temperature (12), e) I, II correspond to the first (second) mass change.

In our investigations the optimum instrumental parameters have been constant to give comparable and reproducible results. The evaluation especially the mass spectrometric data are labour-intensive and time consuming. A complete computing system RT-11 (Digital Equipment Corporation) compatible to the combined TG-DTA-MS apparatus is available and will be applied to resolve these problems soon.
The material for the most common crucibles used for TG-DTA measurements is alumina oxide, but platinum respectively tantalum has been tested in our laboratory. The yield of the evolved gases has been predicted as much higher by use of metal crucibles due to catalytic effects of Pt or Ta, but in our testswe did not observe a drastic change in gas composition or TG-DTA results by inserting constant masses of 10 mg of each coal sample and employing constant heating rates of 10 K/min.
In all runs we registered a great number of possible fragments from the macromolecular structure broken into smaller pieces. The abundance of ions in the upper mass range released from coal at higher temperatures decreases due to thermal decomposition of the species prior to ionization. The yield of fragment ions above 250 mass units increases with decreasing excitation energy at 20 eV, see Fig. 2. Thermally activated compounds always need less energy for decomposition than "cold" particles. This effect is prevailing when examining the fragmentation pattern of aliphatic molecules in contrast to aromatic devolatilization products. The influence of increasing temperature on the decomposition of the volatiles cannot be elucidated at present as well as secondary reactions of the tar when performing high vacuum analysis.
The mass fragments of structural related compounds have been monitored recording selected ion currents of different hydrocarbon series including mass values of heterocycles (sulfur and nitrogen containing compounds). Previous work has been done by Meuzelaar et al. (12). We have observed great amounts of stable polycyclic aromatic series with one or more maxima at different temperatures and the occurence of double charged positive ions as shown in Fig. 3. The typical fragmentation of alkylated benzene series has been detected in every case indicated by loss of the homologous mass unit 14. The large number of data of our experiments has to be processed on-line by the above mentioned computing system.
The yield of the devolatilization products within heating periods depends little on heating rates when coals of similar rank are investigated, but on particle size and surrounding atmosphere respectively pressure with regard to detectable fragment ions into the mass spectrometer. The experimental conditions using the high temperature stable ceramic gas inlet system in static air or employing dynamic air flow without pressure-temperature corrections during the experiment result in non reproducible mass spectral data. Small heating rates of below 5 K/min cause more rapid oxidation of the volatiles released. Accordindly the intensities of the degradation products in the low mass range show an increase corresponding to exothermal effects in the DTA curve. The peak temperatures of the DTA curves correlate with maxima in derivative thermogravimetric- and pressure curves. Therefore, most of our experiments were run in vacuum. It must be mentioned that at high temperatures the volatiles may undergo radical reactions which cannot be observed by use of the mass spectrometer.

15

sponding to the cleavage products indicated exceptionally sulfur
containing molecules in the lower mass range of interest. The evo-
lution of BTX-aromatic compounds exhibits a maximum intensity at 723
K as well as other polycyclic aromatic substances. Experiments ob-
serving the egress rates of the volatiles released are projected.

Conclusion

   Summarizing the goals of our investigations there are two categ-
ories of interest dealing on the one hand with the application of
none computerized TG-DTG-DTA-MS analysis and on the other hand with
complete on-line control of the devolatilization process in a high
temperature furnace above 1800 K. The first directly offers the
possibility to get unreliable data to study thermal decomposition
of carbonaceous material with regard to gas composition depending
on temperature-time relationships employing different atmospheres
and standard pressure. The second object is to quantify these re-
sults and data to study the kinetics during thermal degradation up
to higher mass ranges and temperatures. Practical application must
be a main feature of these investigations. Because coal structure
and the corresponding thermal decomposition process cannot be sep-
arated. Therefore the tests have to be carried out simultaneously
not basing on mathematical description of pyrolysis behaviour of
model substances which are often far away from practical utiliza-
tion.
The enhancement of the abundance of mass fragments is influenced by
catalytic effects of transition metal compounds. We are engaged to
study these effects during our continuous work as well as reactions
of tar with various test gases examining the change in gas composi-
tion. The reaction gas must be introduced by use of a capillary
inlet.
We conclude that additional instrumental modification of the meas-
uring device regarding measurements related to realistic conditions
and quantitative results is needed. Mass spectrometric and gas
chromatographic identification of the evolved compounds after ther-
mal treatment in the TG-DTA-MS apparatus above 1800 K would be well
suited in analysis of devolatilization products.

References

 (1) W.D. Emmerich, E. Kaisersberger, J.Thermal Anal., 17,197,(1979)
 (2) K.-H. Ohrbach, A. Kettrup, J. Thermal Anal., in press
 (3) K.-H. Ohrbach, G. Radhoff, J. Thermal Anal., in press
 (4) K.-H. Ohrbach, A. Kettrup, W. Klusmeier, Spectrochim. Acta,
     B, Suppl., 38, 177, (1983)
 (5) K.-H. Ohrbach, A. Kettrup, 29th Intern. Congress of Pure and
     Applied Chemistry, Cologne (F.R.G.), June 5-10, 1983
 (6) K.-H. Ohrbach, G. Radhoff, A. Kettrup, Intern. Journal of Mass
     Spectr. and Ion Phys., 47, 59, (1983)
 (7) K.-H. Ohrbach, G. Radhoff, A. Kettrup, Thermochimica Acta,
     67, 197, (1983)
 (8) J.B. Howard, W.A. Peters, M.A. Serio, EPRI-AP 1803, April 1983
 (9) P.R. Solomon, D.G. Hamlen, EPRI-AP 1654-8, July 1983
(10) H.L.C. Meuzelaar et al., Characterization of Rocky Mountain
     Coals and Coal Liquids by Computerized Analytical Techniques,
     University of Utah, DOE-DE-FG 22-80 PC 30242
(11) H. Jüntgen, K.-H. van Heek, Topics in Current Chemistry, Vol.
     13 p. 601-699, Springer, Berlin (F.R.G.) 1970
(12) G. Lombardi, For Better Thermal Analysis, Intern. Confeder.
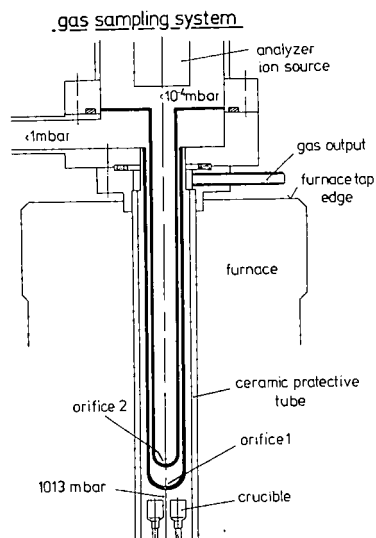   for Thermal Anal., Rome, February 1980

Fig. 1. Gas inlet system of the TG-DTA-MS apparatus showing two high temperature stable ceramic tubes for pressure reduction and the ceramic protective tube of the furnace.
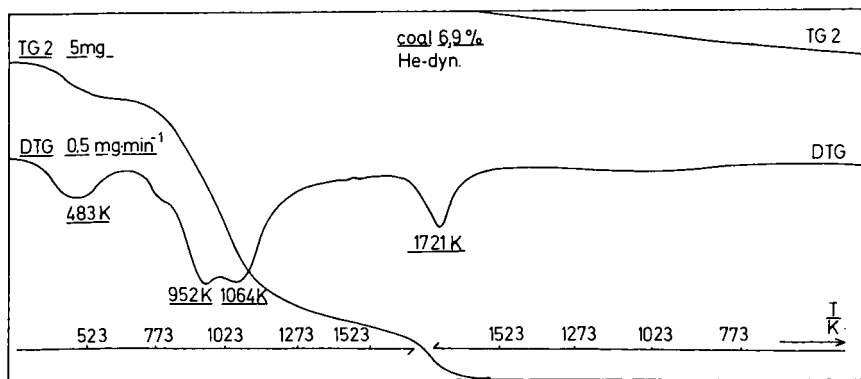

Fig. 2. The TG-DTG curves of an anthracite with 6.9 % volatile matter d.a.f. employing constant heating and cooling
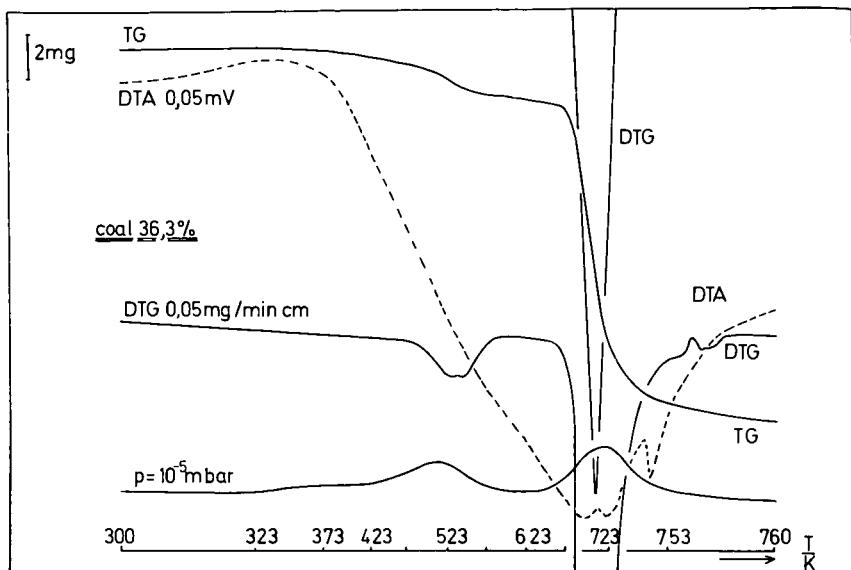
17

Fig. 3. TG-DTG-DTA-p-T curves of a coal sample with 36.3 % volatile matter d.a.f. recorded in high vacuum.
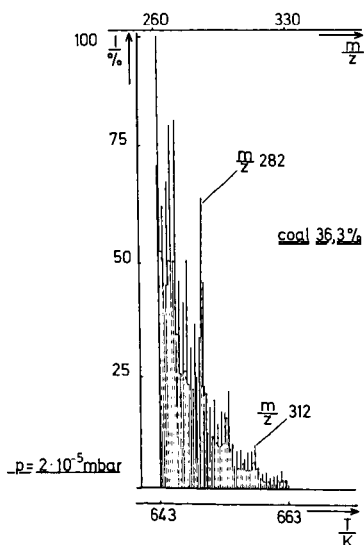

Fig. 4. Mass spectrum of a coal sample with 36.3 % volatile matter d.a.f. in the temperature range from 643 K to 663 K simultaneously recorded to the data mentioned in Fig. 3.
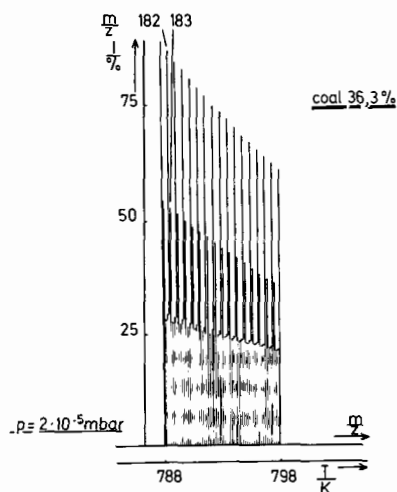
Fig. 5. Mass spectrum in the mass range from 182 to 184 mass units
in the temperature range from 788 K to 798 K of a coal sample with
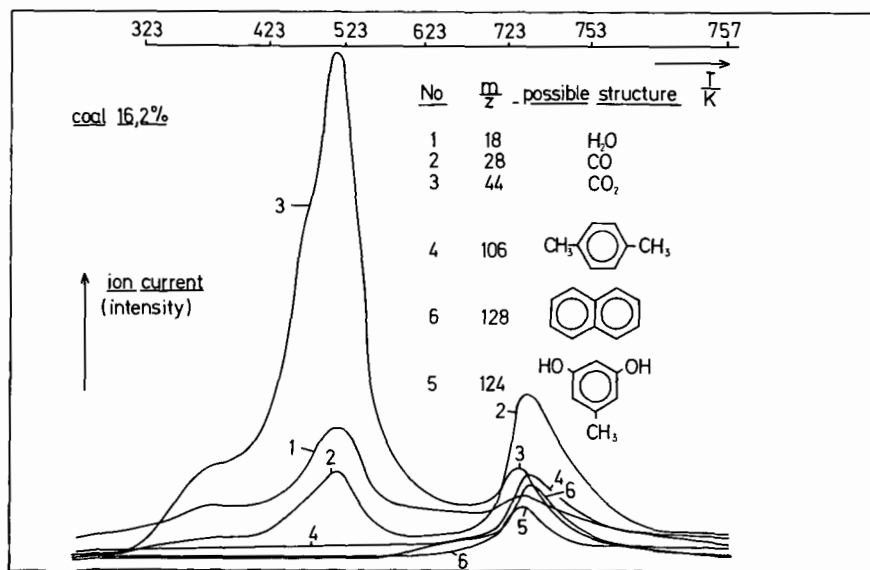36.3 % volatile matter d.a.f.

Fig. 6. Autovontrol mass spectrum of five preselected ion currents
corresponding to the mass fragments indicated as No. 1-5 of a coal
sample with 16.2 % volatile matter d.a.f. (T-from 323 K to 757 K)

MOLECULAR-BEAM SAMPLING/MASS SPECTROMETRIC STUDIES OF THE PRIMARY PYROLYSIS MECHANISMS OF BIOMASS, FOSSIL ORGANIC MATTER, AND SYNTHETIC POLYMERS

Robert J. Evans
Thomas A. Milne
Michael N. Soltys

Solar Energy Research Institute
Thermochemical and Electrochemical Research Branch
1617 Cole Blvd, Golden, CO 80401

INTRODUCTION

A major emphasis in the thermochemical conversion of biomass to fuels and chemicals is on the high heat transfer processes generally called fast pyrolysis (1). The object of fast pyrolysis is to produce high-value, low-molecular-weight products while avoiding the formation of char. This concept has been applied to the formation of hydrocarbon gases (1) and to the direct liquefaction of wood (2) as well as to the flash pyrolysis of coal (3).

One problem in these processes is that the rate and reaction conditions make it difficult to study the sequential reactions that occur, particularly the initial devolatilization or primary pyrolysis steps. This initial product slate is difficult to determine due to the reactivity, thermal lability, and molecular weight range of the products as well as the subsequent condensation or cracking reactions that mask the initial composition.

To accomplish the determination of primary product composition, the flash pyrolysis of samples in 900°C steam/He has been coupled with a molecular-beam sampling system for a mass spectrometer that permits real-time sampling and rapid quenching from ambient hot environments, while preserving reactive and condensible species. This system has been extensively described in two recent publications (4, 5) and is briefly reviewed in the experimental section below.

The major emphasis of this report is on the determination of the primary pyrolysis mechanisms of the fast pyrolysis of lignocellulosic biomass and its major constituents: cellulose, hemicellulose (particularly the pentoses, xylan and arabinan), and lignin. Other carbonaceous materials are also included for the purposes of comparison and demonstrating the technique, but pyrolysis mechanisms will not be discussed. These materials include Texas lignite, Pittsburgh #8 coal, Utah tar sand, Colorado oil shale, high-moor and low-moor peat, polyethylene, and polystyrene. The plastics are included because they are an important component of municipal solid waste and refuse-derived fuel.

EXPERIMENTAL

The fast pyrolysis/molecular-beam sampling/mass spectrometer (Fig. 1) used in this study is run by suspending a quartz boat of material (25-50 mg) in the unignited flame gases (H_2, O_2, and He) and positioned at 5 mm below the sampling orifice. At this position, residence time (5-25 ms) is insufficient for secondary cracking to occur. The flame is ignited and the 900°C steam and helium, which are maintained free of oxygen, heat the sample to pyrolysis and sweep the products away so only promptly-formed gases are introduced into the sampling orifice. Since the initial pyrolysis process is endothermic and essentially ablative, the actual process temperature is well below the 900°C steam/He (1). The sonic sampling orifice rapidly quenches the sampled gases which are subsequently collimated as a molecular beam for introduction into the ion source of a quadrupole mass spectrometer. Low energy electron impact ionization (15.5 eV) is used to minimize fragmentation. The

free-jet expansion of the sampled gases results in rapid quenching and presents internally cooled molecules to the ion source which also minimizes ionization fragmentation.

The two major disadvantages of the technique are: (1) difficulty in quantitation due to mass discrimination in the molecular beam, and variation in ionization sensitivities at low electron energy; and (2) the ambiguity in structure assignment based on only the ion mass.

RESULTS AND DISCUSSION

Biomass

Cellulose pyrolysis has been extensively investigated (6). In Fig. 3 (top) is shown the pyrolysis-mass spectrum (py-ms) of cellulose from 45 to 445 amu. Levoglucosan (Fig. 2, I) is well known to be the major primary pyrolysis product from cellulose in the high temperature pyrolysis regime (7), yet the parent ion (mass 162) is of secondary importance in the spectrum. Work with chemical ionization (8) has shown that under typical ion source conditions, levoglucosan is highly fragmented by EI. The major portion of masses 144, 73, 60, and significant portions of 98 and 126, are due to EI fragmentation of levoglucosan, so caution is required in interpreting py-ms. Nevertheless, from studying model compounds to determine the extent of EI fragmentation, a great deal of insight can be gained from this experimental system. The striking simplicity of cellulose pyrolysis, particularly in the higher mass region, is an indication of the dominance of the transglycosylation mechanism which leads to levoglucosan formation (7). The set of peaks at higher molecular weights (288, 306, 324, 325) is due to dimer formation and is analogous to the 126, 144, 162, 163 series for levoglucosan. The dimer (mass 324) could be due to a glucose-levoglucosan disaccharide, but that substance would probably be of limited thermal stability. Another possibility is the formation of 1',6:4',2-dianhydro-diglucopyranose (Fig. 2, II) by transglycosylation from the hydroxymethyl group of ring 1 to the C-1 of ring 2. Groups analogous to this dimer series have been observed up to mass 1135 (7 units). The odd masses such as 163 and 325 are thought to be EI fragments of higher polymers because the ratios 162/163 and 324/325 decrease as the EI voltage is increased from 15 to 50 eV. These observations are speculative and require collaboration with other experimental systems.

The addition of catalytic amounts of alkali salts has been known to inhibit levoglucosan formation (7). The py-ms of cellulose treated with 5% (mole) K^+ (K_2CO_3) is shown in the bottom of Fig. 3. The simplicity of cellulose pyrolysis has been replaced by a much more complicated spectrum with the noticeable absence of levoglucosan and the dimer. The masses associated with furan compounds are now predominant: 98, furfuryl alcohol; 110, 5-methyl-furfural; and 126, 5-(hydroxymethyl)-furfural. Only 110 is increased in absolute terms above what is obtained in untreated cellulose pyrolysis. Within the low-molecular-weight range, which is not shown here, masses 32 and 43 increase in yield due to methanol and carbonyl compounds, respectively. This treatment also increases the yield of char by a factor of 100. A possible explanation for these observations is that the alkali salt catalyzes the cross-linking between cellulose chains and prevents the steric rearrangements necessary for transglycosylation. This allows the simple fission reactions that yield carbonyl compounds, furans, and methanol to predominate as well as preserving more of the carbon as char.

The hemicelluloses are heterogeneous polysaccharides. Examples are xylans (hardwoods), glucomannans (softwoods), and arabinogalactanes (also classified as an extractive) (9). Only xylan and arabinose will be discussed here since the other hexopyranoses have similar pyrolysis products to cellulose. Xylan is a β-1,4 pento-pyranose polymer that differs from cellulose mostly by the missing hydroxymethyl group (C-6). In native wood, the xylan has acetyl groups bound to the C-2 position as well as minor amounts of glucuronic acid. In the separation technique these

21

groups are removed and residual salts from the process may have an effect on the pyrolysis of xylan as seen in cellulose pyrolysis. The spectrum shown in the top of Fig. 4 demonstrates that in the absence of the hydroxymethyl group, no simple high-molecular-weight pattern is present. In fact, the spectrum is similar to the one for the alkali-treated cellulose in Fig. 3. The lower-molecular-weight peaks are probably carbonyl compounds (e.g., butanedione, 86) and furan compounds (e.g., furfural, 96). Schulten and Gortz (10) proposed three basic chemical reaction mechanisms to explain the formation of the smaller pyrolysis products: dehydration, retroaldolization, and decarbonylation, but they are probably only important as primary reactions when transglycosylation is prevented, as for xylan, and are more important as secondary cracking pathways. The large peak at 114 has been identified from xylan pyrolysis as 3-hydroxy-2-penteno-1,5-lactone by Ohnishi et al. (11). This is the most characteristic peak of pentoses and is present in both xylan and arabinose although they have pyranose and furanose structures, respectively.

Arabinose is only a minor component of hemicellulose [3.5% of all sugars in softwoods and minor amounts in hardwoods (9)] and is present as copolymers with other sugars such as galactose or xylanose. However, it is discussed here because it clearly demonstrates some of the pathways discussed previously. Arabinose is a pentofuranose with a hydroxymethyl group that undergoes similar transglycosylation reactions as occurs in cellulose pyrolysis. The spectrum in the bottom of Fig. 4 shows a series of peaks, 132, 114, 96 which are analogous to 162, 144, 126 in cellulose. The 132 peak may be due to 1,5 anhydroarabinofuranose which could lose H_2O to form a double bond between C-2 and C-3 and give the peak at mass 114. Alternatively, the 114 peak may be due to 3-hydroxy-2-penteno-1,5-lactone as is proposed by Oshnishi et al. in xylan pyrolysis (11). A dimer peak is present in arabinose (mass 264) in contrast to xylan.

The third major category of biomass constituents is the lignin fraction. The py-ms of two types of separated lignin fractions derived from Aspen wood is shown in Fig. 5. In both cases, the distribution of lignin peaks is different from that observed in native aspen pyrolysis where the lignin hardwood monomers, coniferyl alcohol (180) (Fig. 2, III) and sinapyl alcohol (210) (Fig. 2, IV), clearly predominate. Of the various methods of separating lignin from wood, ball-milling followed by solvent extraction is the least destructive (Fig. 5, top). The steam explosion process (Fig. 5, bottom) changes the distribution of products giving decreased yields of the monomers and increased yields of the smaller fragments. The guaiacol (124) (Fig. 2, VI) series is derived from coniferyl alcohol (180) and includes guaiacol (124), methyl guaiacol (138), ethyl guaiacol (152), and coniferylaldehyde (178). The syringol (154) (Fig. 2, VII) series is derived from sinapyl alcohol (210) and includes methyl syringol (168), ethyl syringyl (182), vinyl syringol (180), propenyl syringol (194), 1-hydroxy-3,5-dimethoxy-benzaldehyde (182), and syringylaldehyde (208). In addition, the steam-explosion process leads to a higher abundance of the higher-molecular-weight dimer peaks (272, 280, 302, 332) which have also been found by high performance size exclusion chromatography of these materials. They probably correspond to β-O-4 alkyl aryl ether structures (Fig. 2, IX) or phenyl coumarin-derived compounds (Fig 2, X) with partially cleaved side chains (12).

Studies of the rate of product formation have shown that not only are the monomer units formed in initially high yields, but they are also the first products to form with smaller lignin fragments such as guaiacol formed later. The evolution of mass 272 reaches a maximum after the monomers, but before the lighter fragments reach maximum evolution. These results suggest that during pyrolysis further cleavage of the higher-molecular-weight polymers into the stable ether dimers occurs. This differential evolution of primary products from lignin pyrolysis is in contrast to cellulose where all products reach a maximum at the same time.

The predominance of the lignin monomers and the peak at mass 272 indicates that an alternative mechanism of formation is likely other than just random bond cleavage.

The β to α carbon-carbon bond of the propyl side chain can be cleaved under pyrolysis conditions. Ether cleavages could also occur.

Some representative biomass samples are shown in Fig. 6. No hardwood sample is shown since the whole aspen wood spectrum closely resembles the ball-milled aspen lignin spectrum in Fig. 5 with the additional contribution from the carbohydrates and the difference in proportions of lignin peaks, with 180 and 210 being the predominant lignin peaks in the whole wood pyrolysis spectrum. The pyrolysis of pine (Fig. 6, top) is typical of softwoods with the large yield of coniferyl alcohol and the presence of the group of peaks at higher molecular weight. The structures of these products are probably derived from the dimer of coniferyl alcohol with a minor peak at 342 due to the condensation of two monomers (360-18). The other peaks in this group are probably due to rearrangement reactions. Of particular interest is the peak at mass 272 since it forms earlier than the other high-molecular-weight lignin peaks and is present in higher abundances. A possible assignment is an enol ether such as (IX). This peak is present in all lignins investigated--kraft, milled wood, organosolv, and steam explosion.

The rice hull pyrolysis spectrum shown in the bottom of Fig. 6 is typical of grasses, which have an additional lignin monomer, p-coumaryl alcohol (mass 150) that is quite often the major lignin monomer peak for grasses. The peak at mass 120 is also common to most grasses and probably is due to the coumaryl alcohol fragment, p-vinyl-phenol. Mass 120 is unusual since it has the same early evolution path as the monomers 150, 180, and 210, unlike other lighter fragments, i.e., guaiacol, that reach maximum evolution significantly later than the monomers. The pentoses also make a significant contribution to the pyrolysis products of grasses judging by the increased yield of mass 114 which is charactertistic of xylan and arabinose (Fig. 4).

PRIMARY PYROLYSIS OF OTHER CARBONACEOUS MATERIAL

The more complex spectra of the pyrolysis products of several other carbonaceous materials are shown in Figs. 7-10 for comparison and are briefly described below. The spectra of two coal samples are shown in Fig. 7a. The pyrolysis products are more difficult to rationalize than the lignin peaks in wood. To facilitate discussion, homologous series of peaks are connected by lines in the figures as is used by Meuzelaar et al. (13).

The less mature Texas lignite shown in Fig. 7 is dominated by the phenolic series (94, 108, 122). Other typical lignin peaks (110, 124, 138, 150, 164) are greatly diminished in this lignite sample. Several naphthalene-derived series are present: tetralin (Fig. 2, XI) (132, 146, 160, 174, etc), dihydronaphthalene (144, 158, 172, 186), and alkyl naphthalene (142, 156, 170, 184), as well as tetrahydroanthracene (182, 196, 210, 224).

The bituminous coal sample, Pittsburgh #8, exhibits different patterns. The phenolic series is decreased in importance (as would be expected for the more mature sample) but the 110, 124, 138 series is enhanced. In addition to the lignin derived methoxyphenols this series could also be due to alkyl dihydroxybenzenes or dialkenes. The dihydronaphthalene series (144, 158, 172, 186) is much more predominant than in lignite and the tetralin and alkyl naphthalenes are not obviously present. The series, 184, 198, 212, 226, 240, which is the same sequence as alkyl naphthalenes, is in this case probably due to hexahydroanthracene, because of the higher-molecular-weight range. The last series outlined (234, 248, 262) may be due to a 4-ring naphthenoaromatic structure with the methyl derivative (248) being the predominant species. This is also the case in the hexahydroanthracene series, and the hydroxy and dihydroxybenzene series, but the dihydronaphthalene series peaks at the 2-methyl derivative (158). This predominance of the methyl

derivatives may reflect the thermal dissociation of aliphatic bonds between condensed naphthenoaromatic structures (14).

The pyrolysis of other geopolymers is shown in Fig. 8. Utah tar sands are bitumen-impregnated rocks and not strictly geopolymers, but thermal recovery is a promising method of processing tar sands to recover lighter products (15) and so tar sands are discussed here. The pyrolysis of Utah tar sand is shown in Fig. 8 and although it appears simpler than the spectra for coal, the patterns or homologous series are not as well defined. An alkene series is present (84, 98, 112, 126), but no significant series is present for the saturated hydrocarbons. The series 82, 96, 110, 124 may be due to the dialkene series although some contribution from methoxyphenol is also possible. The high abundance of mass 96 favors the dialkene interpretation since this can not be due to a phenolic or methoxyphenol ring structure.

The Colorado oil shale pyrolysis spectrum is dominated by the lighter materials including alkenes (56, 70, 84, 98), dialkenes (68, 82, 96, 110, 124), trialkenes (80, 94, 108, 122, 136), and tetraalkenes (106, 120, 134, 148, 162). The series 144, 158, 172, 186 may be due to dihydronaphthalene. The series of odd masses (195, 209, 223, etc.) could be due to fragment ions of higher-molecular-weight alkenes, although no dominant parent peaks occur at higher molecular weight.

The pyrolysis spectra of two peat types are shown in Fig. 9. Peat #1 is a high-moor peat, which is derived primarily from mosses (Sphagnum), cotton grass, and heath plants (16). The pyrolysis products are predominately carbohydrate in nature with only a minor contribution from lignin. Despite the predominant masses 144 and 162 which are attributed to levoglucosan, the higher-molecular-weight range does not show the peaks characteristic of the dimer species (see Fig. 3) for cellulose, which may be due to the heterogeneity of the sample compared to pure cellulose.

Peat #2 is a low-moor peat (composed of plants with a higher lignin content). The pyrolysis spectrum reflects the presence of lignin with the methoxyphenol series (124, 138, 152) present. The actual lignin monomers (150, 180, 210) are not as predominant as in fresh biomass materials, which may be due to the effects of diagenesis on lignin structure (17). There is also a distinct lack of prominent high-molecular-weight peaks (such as mass 272) in this sample as well; instead, all even masses are present in rougly equal abundance.

The pyrolysis spectra of two common plastics, polystyrene, and polyethylene, are shown in Fig. 10. Both these polymers show the formation of homologous series of products. The pyrolysis of other polymers yields only the monomer, such as polytetrafluoroethylene and poly(methyl methacrylate), while a third group breaks down into complex arrays of products such as polyvinylchloride and polyamide (nylon). The polystyrene and polyethylene, however, give this same repeating pattern shown in Fig. 10 to molecular weights greater than 1400 amu.

The dominant peaks in the polystyrene spectrum are due to the monomer (104), dimer (208), ad trimer (312). The other masses represent pyrolysis products not seen in other py-ms systems (13). Mass 116 could be due to indene (Fig. 2, XII), which would require cyclization of the aliphatic backbone to form the ring system. The peak at 130 could then be assigned to methylindene. Mass 142 could be assigned to methyl-naphthalene, analogously (with substantial rearrangement of the aliphatic chain).

There are several ion series present in the polyethylene spectrum: alkyl fragment ions (57, 71, 85, 99, 113, . . .), alkenyl fragment ions (55, 69, 83, 97, 111, 125, . . .), alkenes (196, 210, 224, 238, 252, 266, . . .), and dialkenes (194, 208, 222, 236, 250, . . .). These products indicate that random bond cleavage is occurring followed by hydrogen rearrangement to yield a saturated end and an unsaturated end (the alkenes), although there is a high proportion of molecules having two unsaturated ends (the dialkenes). The extent of condensation reactions is unknown.

24

CONCLUSIONS

Biomass samples give a relatively simpler spectrum of products compared to the product slate obtained from organic geochemical samples. In the latter materials, a higher degree of sample heterogeneity, diagenesis, and humification may explain most of the differences.

Cellulose pyrolysis at high temperature is dominated by levoglucosan possibly as a result of transglycosylation reactions, which depend on the hydroxy methyl group for sterically favored attack. Higher anhydro-polymers may also be formed by inter-ring attack by the primary hydroxyl group. A competing mechanism is evident in the presence of alkali metal salts: bond fission reactions which yield carbonyl compounds, furans, and methanol.

Lignin, although of a more complicated structure, also yields relatively simple primary pyrolysis products dominated by the three precursor monomers that make up the macromolecule, although the contribution from smaller fission products is more significant than in the homogeneous polymer, cellulose. The formation of higher-molecular-weight products from lignin also indicates the predominance of specific rearrangemnt reactions over simple bond fission. An example is the predominance of the peak at mass 272 in all the lignin samples investigated, irrespective of genetic origin or method of preparation.

The complexity of the pyrolysis spectra of coal, tar sands, oil shale, and to a lesser extent, peat indicates the greater importance of labile bond fission in the pyrolysis of geopolymers.

REFERENCES

1. J. Diebold, Workshop Chairman, Proceedings of a Specialists Workshop on the Fast Pyrolysis of Biomass, SERI/CP-622-1096, (1980).

2. D. S. Scott, Specialists Meeting on Biomass Liquefaction (eds: R. L. Eager, J. F. Mathews, and T. M. Peppers) (1982).

3. M. Steinberg and B. Bhatt, Proceedings of a Specialists Workshop on the Fast Pyrolysis of Biomass, SERI/CP-622-1096, (1980).

4. T. Milne and M. Soltys, J. Anal. Appl. Pyrol., 5, 93-110, (1983).

5. T. Milne and M. Soltys, J. Anal. Appl. Pyrol., 5, 111-31 (1983).

6. M. J. Antal, Jr., in K. W.Boer and J. A. Doffle (eds), Advances in Solar Energy, Annual Review of R&D 1, ASES Publications, N.Y. (1982), in press.

7. F. Shafizadeh, J. Anal. Appl. Pyrol., 3, 283-305, (1982).

8. T. A. Milne, M. N. Soltys, and R. J. Evans, Fundamental Pyrolysis Studies Annual Report, Dec. 1982 - September 1983, SERI/PR-234-2152.

9. C. Schuerch in B. L. Browning (ed.), The Chemistry of Wood, Krieger Publishing Co., NY, (1975).

10. H.-R. Schulten and W. Gortz, Anal. Chem 50, 428-433 (1978).

11. A. Ohnishi, E. Takagi and K. Kato, Carb. Res. 50, 428-33, (1978).

12. M. Himmel, K. Oh, K. Spencer, D. W. Sopher, and H. L. Chum, J. Chromatog., 267, 249-65, (1983).

13. H. L. C. Meuzelaar, J. Haverkamp, and F. D. Hileman, Pyrolysis Mass Spectrometry of Recent and Fossil Biomaterials, Elsevier Pub. Co., Amsterdam, (1982).

14. P. P. Soloman in B. D. Blaustein, B. C. Bockrath, and S. Friedman (eds), New Approaches in Coal Chemistry, ACS Symposium Series 169, (1981).

15. K. M. Jayakar, J. D. Seader, A. G. Oblad, and K. C. Hanks, in H. C. Stauffer (ed.), Oil Shale, Tar Sands, and Related Materials, ACS Symposium Series 163, (1981).

16. C. H. Fuchsman, Peat: Industrial Chemistry and Technology, Academic Press, N.Y., (1980).

17. J. M. Bracewell, G. W. Robertson, and B. L. William, J. Anal. Appl. Pyrol., 2, 53-62 (1980).
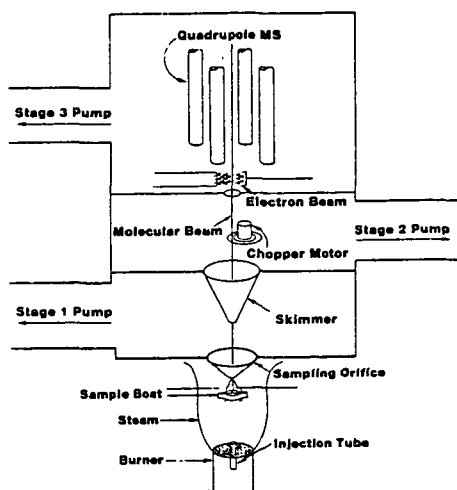
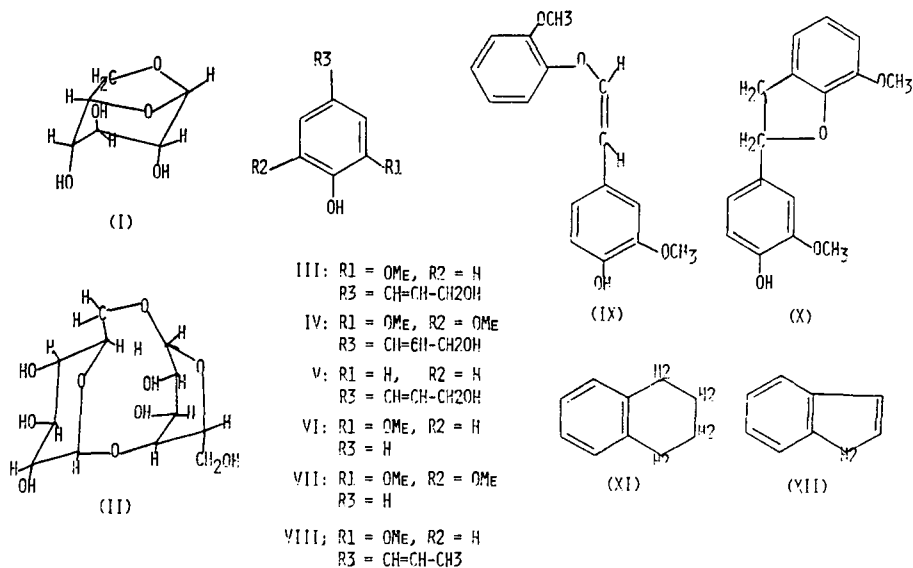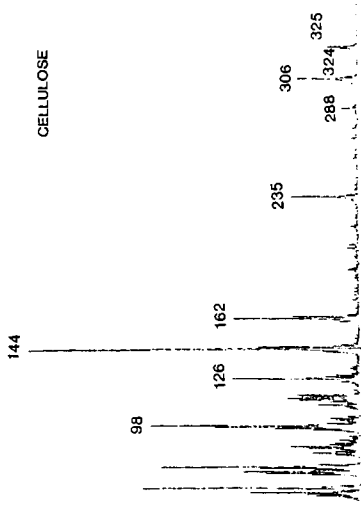**Figure 1. Molecular-Beam Apparatus for Fast Biomass Pyrolysis.**

III: R1 = OME, R2 = H
R3 = CH=CH-CH2OH

IV: R1 = OME, R2 = OME
R3 = CH=CH-CH2OH

V: R1 = H, R2 = H
R3 = CH=CH-CH2OH

VI: R1 = OME, R2 = H
R3 = H

VII: R1 = OME, R2 = OME
R3 = H

VIII: R1 = OME, R2 = H
R3 = CH=CH-CH3

Figure 2. Selected Structures Referred to in Text.
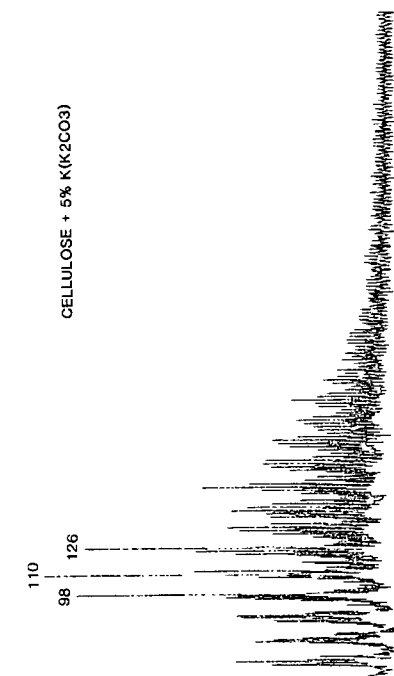
CELLULOSE

XYLAN

CELLULOSE + 5% K(K2CO3)

ARABINOSE

Figure 3. Mass Spectra of Primary Pyrolysis Products From Cellulose (Top) and Alkali Treated Cellulose (Bottom).
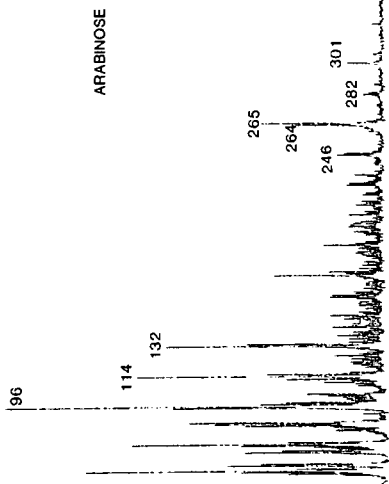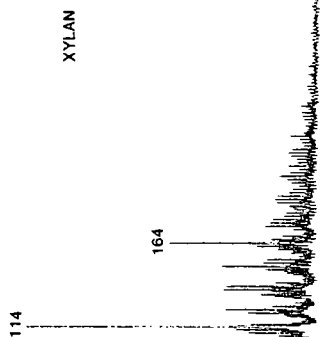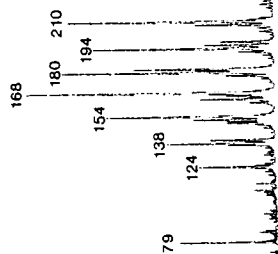
Figure 4. Mass Spectra of Primary Pyrolysis Products From Xylan (Top) and Alkali Treated Aribinose (Bottom).

28

BALL-MILLED ASPEN LIGNIN

MEOH EXTRACTED
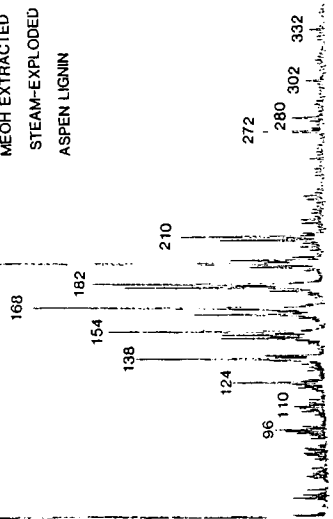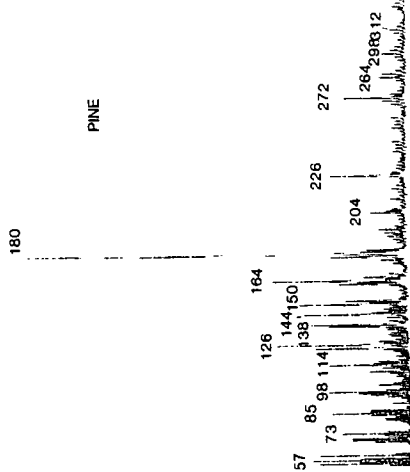STEAM-EXPLODED
ASPEN LIGNIN

Figure 5. Mass Spectra of Primary Pyrolysis Products From Ball-Milled Aspen Lignin (Top) and Steam-Exploded Aspen Lignin (Bottom).

PINE

RICEHULL
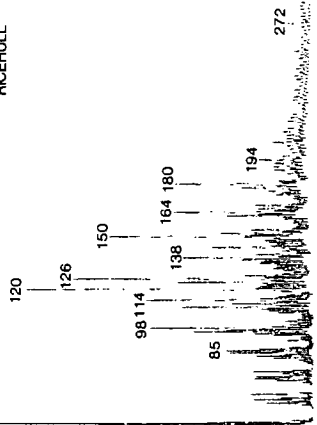
Figure 6. Mass Spectra of Primary Pyrolysis Products From Pine (Top) and Rice Hulls (Bottom).

29

COLORADO
OIL SHALE

TEXAS LIGNITE

UTAH TAR SAND
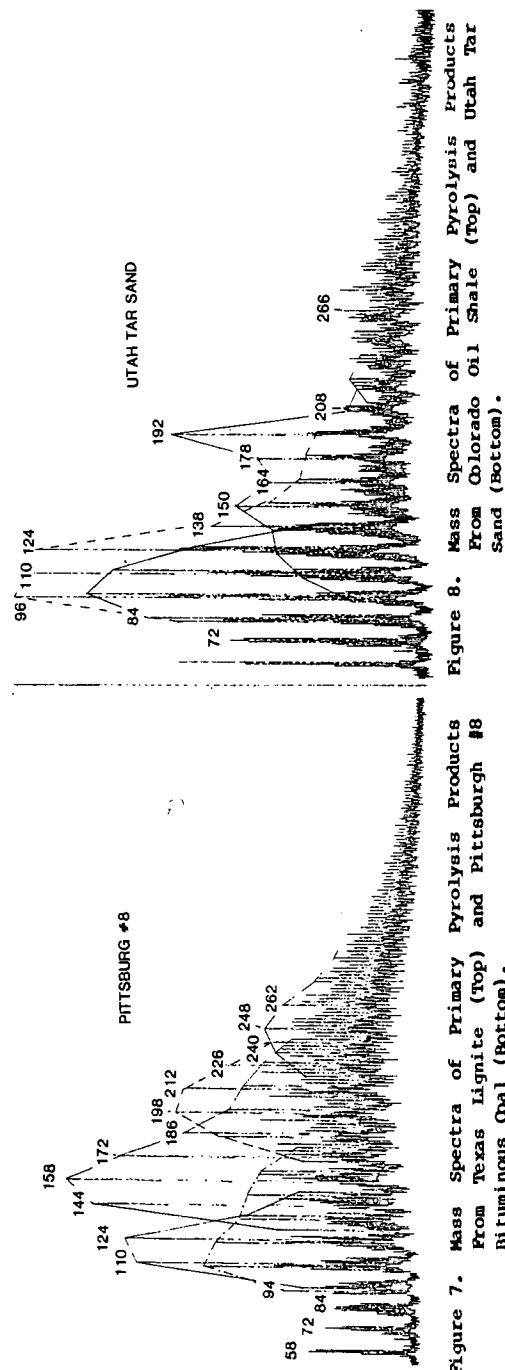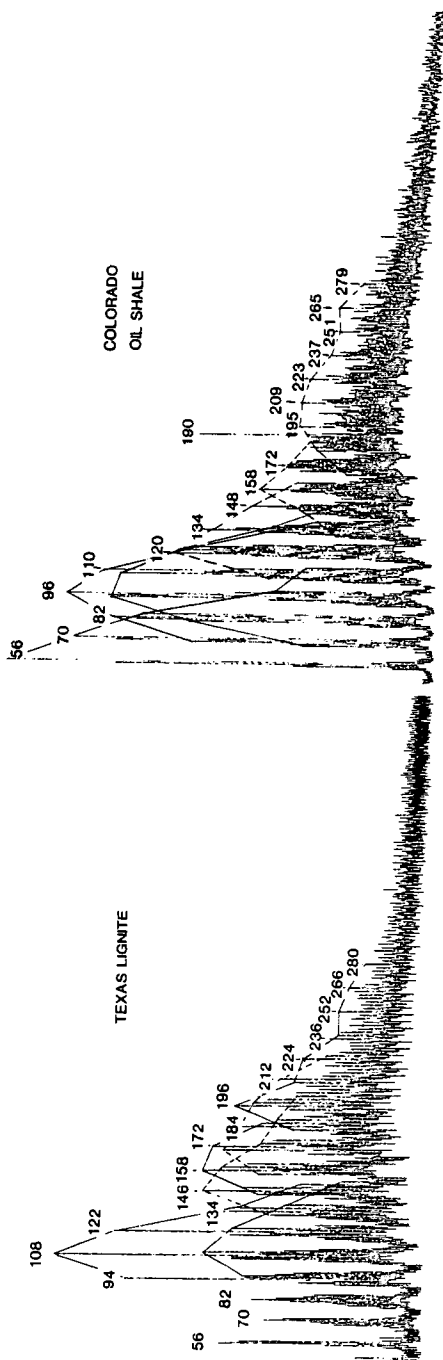
PITTSBURG #8

Figure 7. Mass Spectra of Primary Pyrolysis Products From Texas Lignite (Top) and Pittsburgh #8 Bituminous Coal (Bottom).

Figure 8. Mass Spectra of Primary Pyrolysis Products From Colorado Oil Shale (Top) and Utah Tar Sand (Bottom).

30
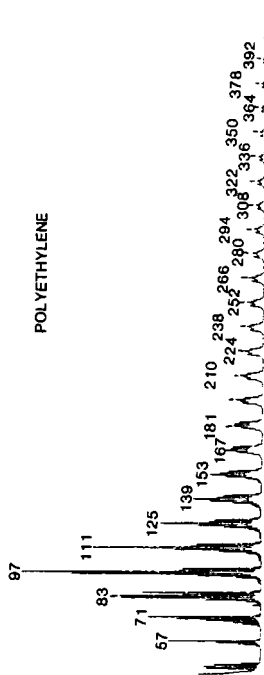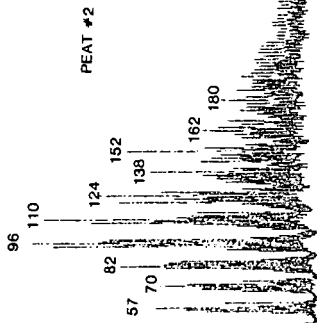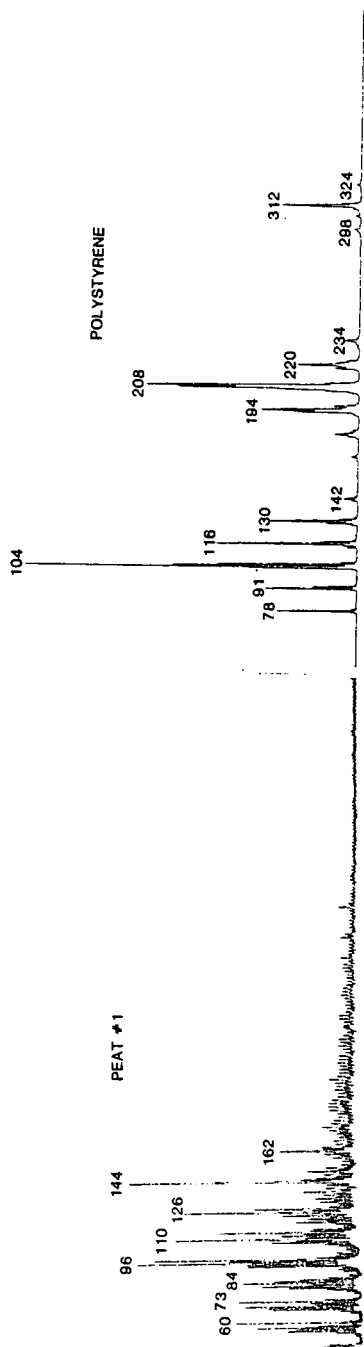
Figure 9. Mass Spectra of Primary Pyrolysis Products from High-Moor Peat (Top) and Low-Moor Peat (Bottom).

Figure 10. Mass Spectra of Primary Pyrolysis Products From Polystyrene (Top) and Polyethylene (Bottom).

31

THE PREPARATION AND PYROLYSIS OF O- AND C-BENZYLATED ILLINOIS NO. 6 COAL

G. R. Rose and R. F. Zabransky
Institute of Gas Technology, IIT Center, Chicago, Illinois 60615

L. M. Stock, C. B. Huang, V. R. Srinivas, and K. Tse
Dept. of Chemistry, University of Chicago, Chicago, Illinois 60637
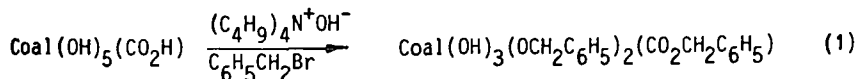
INTRODUCTION

Recent thoughtful reviews of gasification research have stressed the deficiencies in our knowledge of coal pyrolysis and the need for a greater understanding of the reactions responsible for the decomposition of coal molecules and for the formation of products.[1,2] We have taken a new approach for the study of this issue by the pyrolysis of coals that have been modified by the introduction of labeled structural fragments. The labels were selectively introduced into the structures so that the reactions of the new structural element could be readily traced. This approach enables the reaction chemistry of a variety of different structural elements to be investigated within the environment of the coal molecules and offers great advantages for the definition of the course of the reactions in the medium, i.e. coal, that is of principal interest.

This report concerns the methods used for the selective O- and C-benzylation of an Illinois No. 6 coal and the pyrolysis of these materials in a wire screen reactor.

RESULTS AND DISCUSSION

Illinois No. 6 coal was benzylated using the method described by Liotta and his coworkers.[3] The extent of the alkylation reaction was controlled by limiting the quantities of base, the alkylating agent, and the reaction time. O-Benzyl, O-benzyl-$\underline{d}_7$, and O-benzyl-$\underline{1}$-$^{13}\underline{C}$ coal were prepared using this method. The microanalytical data imply that three benzyl groups were incorporated per 100 carbon atoms of the coal. The presence of the unreacted hydroxyl groups (two to three free groups per 100 carbon atoms) and other structural features were established by infrared spectroscopy. These results are semiquantitatively in accord with the transformation shown in equation (1).

$$\text{Coal(OH)}_5(\text{CO}_2\text{H}) \xrightarrow[\text{C}_6\text{H}_5\text{CH}_2\text{Br}]{(\text{C}_4\text{H}_9)_4\text{N}^+\text{OH}^-} \text{Coal(OH)}_3(\text{OCH}_2\text{C}_6\text{H}_5)_2(\text{CO}_2\text{CH}_2\text{C}_6\text{H}_5) \qquad (1)$$

The C-benzylation of Illinois No. 6 coal was carried out in three steps. Several procedures were evaluated, but the reaction sequence shown in equations (2)-(4) proved to be most suitable.

$$\text{Coal(OH)}_6 + 6\text{CH}_3\text{I} \xrightarrow[\text{THF}]{\text{Bu}_4\text{N}^+, \text{OH}^-} \underset{\text{A}}{\text{Coal(OCH}_3)_6} \qquad (2)$$

$$\underset{\text{A}}{\text{Coal(OCH}_3)_6} + n\text{C}_6\text{H}_5\text{CH}_2\text{Br} \xrightarrow[\text{NH}_3]{\text{NaNH}_2} \underset{\text{B}}{\text{Coal(OCH}_3)_6(\text{CH}_2\text{C}_6\text{H}_5)_n} \qquad (3)$$

$$\underset{\text{B}}{\text{Coal(OCH}_3)_6(\text{CH}_2\text{C}_6\text{H}_5)_n} \xrightarrow[\text{Collidine}]{\text{LiI}} \underset{\text{C}}{\text{Coal(OH)}_6(\text{CH}_2\text{C}_6\text{H}_5)_n} \qquad (4)$$
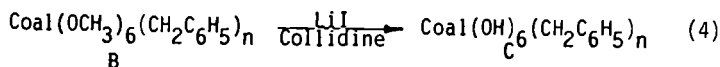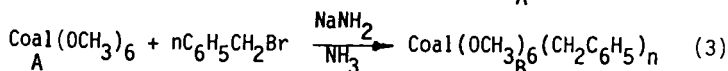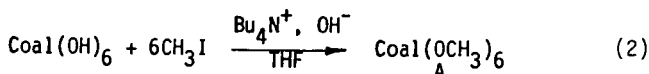
The course of each reaction was followed by infrared spectroscopy. For example, O-methyl-d_3 coal was treated with lithium iodide in collidine, no carbon-deuterium stretching frequencies were observable in the infrared spectrum of the product and the absorptions of the benzyl group appear in the C-benzylated products, B and C, whereas the hydroxyl absorption is absent in the infrared spectra of A and B, but is present in C.

The pyrolyses were carried out without difficulty in a wire screen reactor.[4] The mass balances generally exceeded 97%. A high sensitivity GC-MS procedure was used for the determination of the important gaseous reaction products. The results are summarized in Table 1.

The char, tar, and gas yields for the pyrolysis of whole Illinois No. 6 coal obtained in this investigation are comparable with the well known data of Suuberg[5] for whole Pittsburgh No. 8 coal. The two coals provide different amounts of char and tar, but quite comparable quantities of gas. The similarity in the total quantity of the gaseous products is also apparent when the yields of methane and carbon monoxide from these two coals are compared, Figure 1. These findings suggest that the patterns of reactivity found for the gaseous products of the Illinois No. 6 coal are representative of the behavior of other bituminous coals.

The quantities of char formed from the benzylated coals are significantly lower than the amounts obtained from the whole coals or the reaction blank at temperatures less than 800°C. On the other hand, methane and carbon monoxide are generally obtained in greater quantity from the alkylated coals than from the whole coal or the reaction blank.

The distribution of the deuterium and ^{13}C labels in the gaseous products obtained from the modified coals were studied to provide additional information about the principal reaction pathways. The yields of methane and the distribution of the label within the methane produced during the pyrolyses of the O- and C-benzylated coals are summarized in Table 2.

The pyrolysis of the exhaustively O-methylated coal, as expected, provides much more methane than the whole coal or the reaction blank at the same temperature. The enhanced yield of methane could be attributed to the low energy requirements for the cleavage of the carbon-oxygen bonds in the methyl esters and methyl aryl ethers. However, the finding that the yields of methane and carbon monoxide obtained from the O- and C-benzylated coals are also enhanced negates this simple interpretation. Only a small portion of the methane and carbon monoxide arise from the benzyl groups. Thus, the experimental results indicate that the structural modifications enhance the formation of these products in indirect ways.

The structural modifications may increase the concentration of radicals within the coal particles because the bond dissociation energies of the newly formed carbon-oxygen and carbon-carbon bonds in the modified coals are less than the bond dissociation energies of the linkages native to the coal. The radicals formed in these processes may initiate reaction sequences that lead to decarbonylation and demethylation via well known processes such as β-scission, ipso substitution and radical displacement. In addition, the O-methyl and O- and C-benzyl groups in the modified coals considerably increase the quantity of effective hydrogen atom donors within the coal particles. Productive abstraction reactions would also enhance the conversion of the macromolecular coal molecules to gaseous products.

Significantly more deuteriomethane is produced from the O-benzyl-d_7 derivatives than from the C-benzyl-d_7 derivatives, Table 2. This observation strongly suggests that the methyl radicals formed in the decomposition reactions of the coal molecules abstract hydrogen (deuterium) selectively from the methylene fragment of the O-benzyl group. Hence, the methyl radicals produced in the pyrolyses exhibit a reasonable degree of selectivity even at temperatures approaching 850°C. Significantly greater quantities of methane-d_2 and methane-^{13}C are formed during the pyrolysis of the labeled O-benzylated coals than from the corresponding C-benzylated coals. Although a portion of the methane-d_2 must arise via the exchange reactions of methane-d, the fact that a larger quantity of methane-d_2 is formed from the O-benzyl-d_7 coal suggests that this labeled methane is also formed by a reaction sequence unique to the O-benzylated material. One plausible reaction pathway involves the rearrangement of the benzyloxy radical.[6]

Deuterium labeled ethene, propene, and butene are formed in readily detectable amounts during the rapid pyrolyses of the O- and C-benzyl-d_7 coals. Similar amounts of deuterium are incorporated into the ethene produced from each coal. The most plausible reaction pathways for the formation of ethene-d involve exchange reactions prior to the formation of ethene via pericyclic processes or β-scission reactions or subsequent exchange reactions via rapid addition-elimination reactions.

34

These formulations all require that the primary reactive products formed in the original decomposition reactions undergo secondary reactions within the small coal particles even in this reaction system where the secondary reactions of the stable reaction products are minimized.

The benzylation of the Illinois No. 6 coal enhances the production of benzene and toluene. The results summarized in Table 3 indicate, not unexpectedly, that the aromatic compounds are formed more efficiently from the O-benzylated coal and that the products of the pyrolysis of the O-benzyl-d_7 coal are extensively exchanged. The results can be analyzed semiquantitatively under the reasonable assumption that the hydrogen atoms of toluene formed in the reaction undergo exchange much more slowly than the hydrogen atoms of the O-benzyl group from which it is produced. This analysis suggests that about 40-45% of the O-benzyl-d_7 and 55-60% of the C-benzyl-d_7 groups experience exchange before undergoing homolysis to yield toluene at temperatures between 600 and 850°C. The difference presumably reflects the differences in the rates of the decomposition (O-benzyl > C-benzyl) which requires that the C-benzyl fragment remain bonded to the coal molecule for a longer time. These results also imply that the non-volatile coal macromolecules undergo more chemical reactions than the volatile reaction products. The results are compatible with the idea that the reactive radicals are more abundant in the plastic phase than in the rapidly cooled vapor.

CONCLUSIONS

Several conclusions emerge from the results discussed in the previous paragraphs and from other information obtained in the course of the study. First, the modified coals are generally more reactive than the unmodified starting materials. This enhanced reactivity is particularly evident in the increased yields of carbon monoxide and methane from the O-benzylated coals. The enhancement of the production of carbon monoxide suggests that the increased radical density resulting from the modification of the coal promotes other secondary radical reactions, possibly chain processes, that lead to demethylation and decarbonylation. Hence, the results strongly infer that the extent of small fragment molecule formation depends in a direct way upon the concentration of radicals within the coal particles. The enhancement of the production of methane, on the other hand, may be attributed to the increased concentration of effective hydrogen donor groups which terminate undesirable char-forming reactions. Second, the exchange patterns strongly suggest that the energetically more favorable reactions occur reversibly and that radical addition and recombination reactions compete favorably with fragmentation and radical substitution reactions. Third, the non-random distribution of the isotopic labels in the products, for example, the selective abstraction of hydrogen from the benzylic ether, indicates that the reactions underway within the coal particle are kinetically-controlled rather than

35

equilibrium-controlled processes even at temperature near 850°C. Fourth, the distribution of the labels in the water and ethene reveal that non-radical processes contribute significantly. Thus, theories of pyrolysis that are based exclusively on radical processes may be seriously misleading.

ACKNOWLEDGEMENT

REFERENCES

1. J. B. Howard, "Fundamentals of Coal Pyrolysis and Hydropyrolysis," in "The Chemistry of Coal Utilization," Wiley-Interscience, Inc. NY (1981). Chapter 12.

2. G. R. Gavalas, "Coal Pyrolysis," Elsevier Scientific Publishing Company, New York (1982).

3. R. Liotta, Fuel 58, 729 (1979). R. Liotta, K. Rose and E. Hippo, J. Org. Chem., 46, 277 (1981).

4. D. B. Anthony, J. B. Howard, H. P. Meissner, and H. C. Hottel, Rev. Sci. Instrum., 45, 992 (1974).

5. E. M. Suuberg, Sc. D. Thesis, Massachusetts Institute of Technology Library, Cambridge (1977).

6. C. J. Collins, V. F. Raaen, B. M. Benjamin, P. H. Maupin, and W. H. Roark, J. Am. Chem. Soc., 101, 5009 (1979).
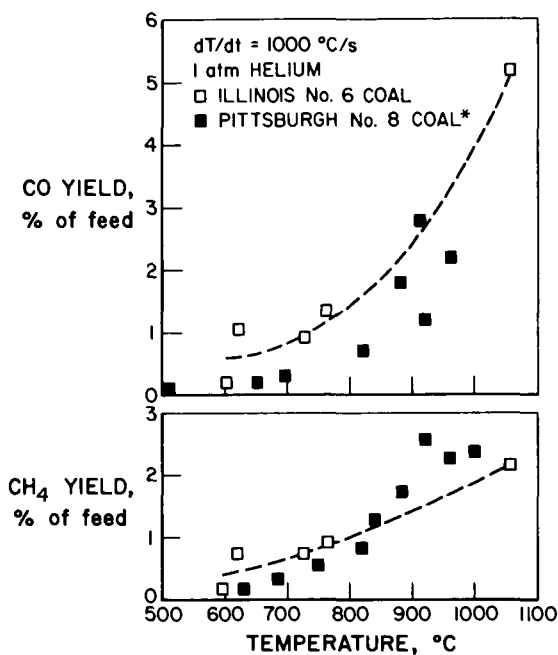
Figure 1. The yields of carbon monoxide and methane in the pyrolysis of whole Illinois No. 6 coal, open squares, and whole Pittsburgh No. 8 coal, solid squares. The data for the Pittsburgh coal were obtained by E. M. Suuberg, ref. 4.

37

Table 1. A summary of the results for the pyrolysis of
Illinois No. 6 coal and its alkylated derivatives.

Coal type	------------------------Illinois No. 6------------------------					
Final temperature, °C	598	619	723	761	921	1057
Coal wt., mg.	11.4	14.3	7.6	12.4	5.3	9.5
Char, % of coal	78.1	70.6	59.2	56.5	55.8	50.5
Tar, % of coal	13.2	12.6	32.9	33.1	33.7	35.8
Gas, % of coal	5.9	4.2	5.4	9.6	10.5	12.6
Gas yields, wt. % of coal						
CH_4	0.2	0.8	0.8	0.9		2.2
CO	1.2	1.1	1.0	1.4		5.2
CO_2	1.5	0.08	1.4	0.59		1.2
H_2O	3.5	2.0	1.3	6.2		3.0
C_2H_6	0.1	0.07	0.3	0.1		0.2
C_2H_4	0.1	0.04	0.3	0.2		0.4
C_6H_6	0.009	0.001	0.001	0.00		0.02
C_7H_8	0.05	0.001	0.005	0.008		0.04

Coal type	-----------Blank--------------			--O-Methyl--	
Final temperature, °C	634	718	834	550	848
Coal wt., mg.	9.6	6.9	7.4	6.5	6.4
Char, % of coal	72.9	56.5	51.4	60.0	54.7
Tar, % of coal	9.4	20.3	21.6	27.7	23.4
Gas, % of coal	5.0	7.9	18.4	9.2	12.5
Gas yields, wt. % of coal					
CH_4	0.2	0.9	2.4	1.8	3.4
CO	0.8	1.4	3.7	1.1	3.3
CO_2	1.0	3.0	3.7	1.6	1.6
H_2O	1.5	0.8	4.4	3.6	2.5
C_2H_6	0.4	0.3	0.7	0.2	0.3
C_2H_4	0.2	0.5	1.5	0.3	0.7
C_6H_6	0.006	0.002	0.004	0.01	0.01
C_7H_8	0.01	0.0008	0.008	0.04	0.02

Table 1. A summary of the results for the pyrolysis of
Illinois No. 6 coal and its alkylated derivatives.

Coal type	-O-Benzyl-		-O-Benzyl-$\underline{d_7}$		
Final temperature, °C	532	724	508	617	745
Coal wt., mg.	13.3	13.4	10.8	13.6	10.7
Char, % of coal	60.9	53.7	68.5	57.4	51.4
Tar, % of coal	15.8	23.9	15.7	25.0	28.0
Gas, % of coal	7.8	17.2	10.3	11.8	9.7
Gas yields, wt. % of coal					
CH_4	0.4	2.3	0.4	1.0	1.8
CO	0.7	4.4	1.0	0.6	3.1
CO_2	3.6	4.6	3.7	1.0	1.7
H_2O	2.1	2.7	3.4	6.5	0.7
C_2H_6	0.2	0.7	0.2	0.2	0.3
C_2H_4	0.1	0.7	0.3	0.07	0.6
C_6H_6	0.03	0.1	0.3	0.2	0.05
C_8H_8	0.2	1.1	0.1	1.4	0.3

Coal type	-O-Benzyl-$\underline{1}$-$^{13}\underline{C}$-		-C-Benzyl-$\underline{d_7}$		C-Benzyl-$\underline{1}$-$^{13}\underline{C}$
Final temperature, °C	840	865	611	854	758
Coal wt., mg.	3.7	3.2	9.8	8.7	7.5
Char, % of coal	51.4	50.0	67.4	51.7	52.0
Tar, % of coal	29.7	28.1	18.4	24.1	24.0
Gas, % of coal	14.1	17.6	8.9	17.2	22.7
Gas yields, wt. % of coal					
CH_4	1.6	2.6	0.8	2.1	3.9
CO	2.5	7.1	0.6	3.3	3.8
CO_2	3.0	2.4	0.9	2.4	0.7
H_2O	6.2	4.0	5.9	8.9	11.1
C_2H_6	0.1	0.3	0.1	0.04	1.0
C_2H_4	0.2	0.4	0.1	0.1	0.9
C_6H_6	0.07	0.06	0.04	0.003	0.01
C_8H_8	0.1	0.2	0.2	0.01	0.05

Table 2. The yields and isotopic composition of the methane produced in the pyrolyses of the benzylated coals.

Modified Coal	Temperature (°C)	Methane (%)			
		Yield	CH_4	CH_3D	CH_2D_2	$^{13}CH_4$ [a]
O-Benzyl-d_7	617	1.0	70	25	5	-
O-Benzyl-d_7	745	1.8	64	30	6	-
C-Benzyl-d_7	611	0.8	90	10	BDL	-
C-Benzyl-d_7	845	2.1	86	14	BDL	-
O-Benzyl-1-^{13}C	828	1.0	-	-	-	1.8
O-Benzyl-1-^{13}C	840	1.6	-	-	-	1.3
O-Benzyl-1-^{13}C	865	2.6	-	-	-	3.1
C-Benzyl-1-^{13}C	758	3.9	-	-	-	BDL

[a] The amount of this product in excess of natural abundance is reported

Table 3. The composition of the benzene and toluene produced in the pyrolysis of the modified coals.

	O-Benzyl-$\underline{d}_7$		C-Benzyl-$\underline{d}_7$	
	At 617°C	At 745°C	At 611°C	At 845°C
Total Yield (Weight % of coal sample)				
Benzene	0.2	0.05	0.04	0.003
Toluene	1.4	0.3	0.2	0.01
Isotopic Composition (mole %)				
C_6H_6	8	10	82	40
$C_6H_2D_4$	14	17	1	11
C_6HD_5	70	56	15	37
C_6D_6	8	8	BDL	BDL
C_7H_8	BDL	BDL	5	16
$C_7H_3D_5$	18	11	17	26
$C_7H_2D_6$	25	25	17	20
C_7HD_7	54	52	37	35
C_7D_8	3	4	BDL	BDL

CHEMICAL FUNDAMENTALS OF COAL CHAR
FORMATION

S. E. Stein, R. L. Brown, L. L. Griffith, and M. Manka

Chemical Kinetics Division, The National Bureau of Standards
Washington, DC 20234

Recent results and current directions of our program aimed at
elucidating fundamental chemical features of carbonization processes will
be discussed. This program is divided into three related components:
(1) elementary rate constant determinations; (2) mechanistic studies
of polyaromatic pyrolysis and; (3) theoretical studies of very large,
highly-condensed polyaromatic molecules. Each of these areas are discussed
below.

## (1) Elementary Rate Constant Determination

Analyses of complex reaction mechanisms generally require numerous
rate constant estimates. While rate constants for many reactions of
concern in thermal aromatic chemistry may be estimated with reasonable
accuracy [1], several serious problem areas exist. Our rate constant
measurements are devoted to such areas.

We have completed a study of relative rates of radical-radical
disproportionation and recombination, k_d/k_r, for reactions involving
hydroaromatic radicals, $M\overset{\bullet}{H}$,

$$M\overset{\bullet}{H} + \overset{\bullet}{R} \xrightarrow{\quad k_d \quad} M + RH$$

$$\xrightarrow{\quad k_r \quad} MH\text{-}R$$
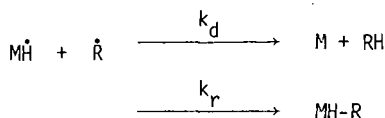
These ratios were derived from product concentrations in experiments
where a free-radical initiator (di-tert-butyl peroxide) was decomposed
at 150°C in the presence of MH_2 and RH molecules.

Results of these studies are shown in Figure 1 where they are
plotted against disproportionation enthalpy, ΔH_d. Recombination rate constants
are known to be relatively independent of reaction thermochemistry.
Particularly noteworthy is the finding that radicals I are much more
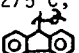prone to disproportionation than are radicals II
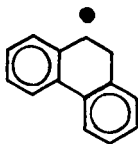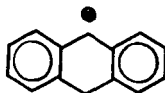
I   II

The overall correlation between ΔH_d and k_r/k_d is only fair (correlation coefficient = 0.7), but is apparently real and might be substantially improved when more accurate bond strength data are available. Moreover, based on known activation energies for related H-atom abstraction reactions [2], it would be surprising if such a dependence did not occur at low enough exothermicities. The above correlation does not hold for reactions of non-aromatic radicals [3]; this is presumably a result of the generally higher exothermicity for these reactions.

These results suggest that the highly-stabilized radicals detected in coal reactions by ESR [4] may be ineffective H-transfer agents since the only thermodynamically feasible H-transfer path open to these radicals involves disproportionation [1c].

In a series of experiments involving polyaromatic free radicals it was found that steric effects can have a profound influence on radical reactivity. For instance at 300°C H-transfer to diphenylmethyl radicals, $\phi_2\overset{.}{C}H$, from the sterically-crowded molecule 1,1,2,2-tetraphenylethane, $\phi_2CHCH\phi_2$, occurred only 1/400 as fast as transfer from tetralin. In another series of experiments it was found that at 275°C, homolysis of

1,1,2,2-tetraphenylethane and 9,9'-bifluorene ( ) occurred > 100 times faster than predicted in the absence of strain due, presumably, to relief of steric crowding during bond breaking. Because of the large sizes of molecules and radicals involved in carbonization processes, such steric effects may be major factors controlling these reactions.

(2) Mechanistic Studies of Polyaromatic Pyrolysis

Reaction mechanisms involved in the initial stages of carbonization are being investigated in model systems. Studies have focused on the liquid-phase pyrolysis of anthracene and phenanthrene. We have found that mechanisms of pyrolysis of these two seemingly related substances are entirely different.

In the pyrolysis of neat anthracene, An, at 350-470°C, the observed stoichiometry at low extents of reaction was,
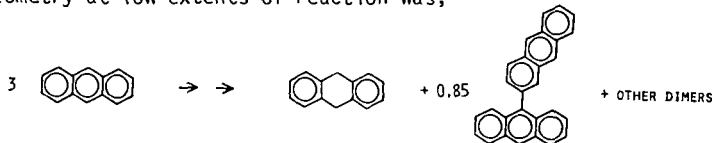

Production of anthracene dimers followed the rate expression (in moles $l^{-1}s^{-1}$),

$$\frac{d[dimers]}{dt} = 10^{8.0} \exp\{-22900/T(K)\} [An]^2$$

Anthracene-solvent adducts were formed readily even in relatively inert "solvents" such as biphenyl. These adducts were generally formed with a rate constant within a factor of two of that for anthracene dimer formation.

Rates of these reactions were only slightly affected by addition of radical-forming agents such as 9,10-dihydroanthracene. In the gas phase, four dimers were formed at comparable rates and kinetics followed a more complex rate law.

The overall kinetics for the condensed-phase reaction is consistent with the following mechanism,
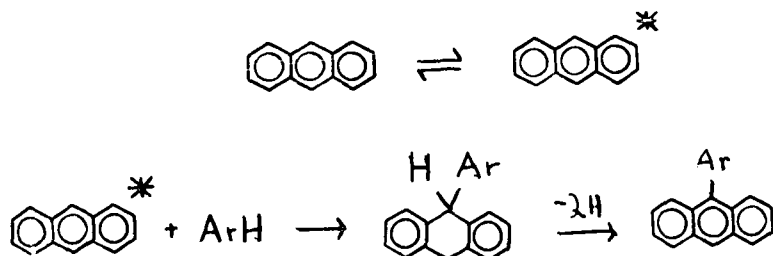
where ArH may be any aromatic molecule (including anthracene itself).

Our working hypothesis is that the species   is a highly reactive, charge-transfer-like intermediate. This mechanism was very unexpected on the basis of known mechanisms for gas-phase pyrolysis and differs substantially from a mechanism proposed by one of us using free-radical reaction rate arguments [5].

Phenanthrene thermolyzes much more slowly than does anthracene and displays different kinetics. At low extents of reactions in pure phenanthrene, at 400°-500°C dimers are formed according to the following (preliminary) pseudo-first-order rate expression, $10^{8.6}$ exp($-25500/T$)s^{-1}. The rate is accelerated by free-radical generating additives (9,10-dihydrophenanthrene, for instance), the mechanism is very unselective (eight dimers of comparable amounts are formed), and gas- and condensed-phase product distributions are similar. The reaction appears to proceed via an aryl free radical-chain mechanism,
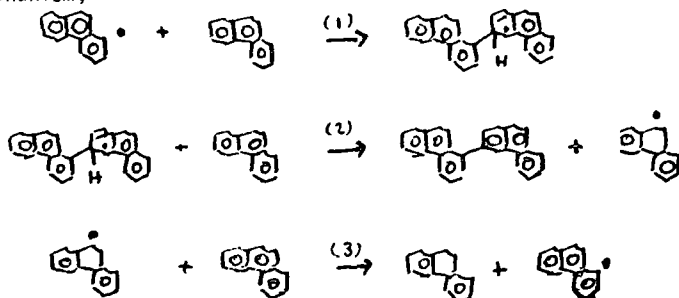
Steps 2 and 3 may involve free H-atom intermediates.

We presume that the primary factor causing the difference in mechanism between anthracene and phenanthrene is the presence of much more accessible (lower energy) "excited states" in anthracene. The triplet state energy, for instance, is 20 kcal mol^{-1} lower for anthracene than phenanthrene.

Based on several preliminary studies of other model pyrolytic systems, the above aryl chain mechanism seems to be rather typical. It may also explain the gas-phase anthracene results. However, mechanisms more closely related to the one proposed for anthracene may become increasingly important as reacting molecules grow in size during carbonization and more accessible "excited states" become available.

(3) Theory of Very Large Aromatic Molecules

In order to analyze reactions occurring in the late stages of carbonization, it is necessary to deal with very large, highly aromatic molecules. Since these molecules are too large to study experimentally, we are developing a theoretical approach intended to allow extrapolation of known reactivity properties of small molecules to these large structures.

In order to treat very large molecules, we are forced to use very simple theories [6]. Using a HP-1000 computer, we have examined molecules containing as many as 3300 carbon atoms. The theories used are Herndon's structure-resonance theory (SRT) [7] and Hückel Molecular Orbital Theory (HMO) [8]. Despite their simplicity, these theories are generally regarded as good predictors of chemical properties for benzenoid polyaromatic molecules, the type of primary concern in carbonization.

Our present work focuses on properties of hexagonally-symmetric molecules containing a single edge type. Initial members of two of these series are given in Figure 2. Thermodynamic stabilities of four series were determined by SRT and results are shown in Figure 3.

Reactivity indicies derived from perturbational HMO theory [8] are illustrated in Figure 4 for a member of the most stable and least stable series. The area of each circle in this figure represents the energy required to fix a π-electron at the carbon atom represented by the circle. These energies are generally considered to be proportional to activation energies for reaction [8].

Hückel MO theory is used to obtain electronic energy levels. The upper third of the occupied energy levels for series A and B are shown in Figure 5. These levels, particularly the highest one for each molecule, contain the electrons that are involved in chemical reactions.

These calculations establish a logical framework which may be used to examine reactions at edges of very large polyaromatic molecules. We are currently applying more accurate theories and introducing other chemical features (strain energy, for instance) with the ultimate aim of deducing chemical reaction mechanisms.

1a. Benson, S. W., "Thermochemical Kinetics" Wiley and Sons, N.Y., 1976.

 b. Stein, S. E., in "New Approaches in Coal Chemistry", ACS Symp. Ser. 69, Blaustein, et al., eds., Pittsburgh, PA, 1981, pp 97-130.

 c. Stein, S. E. in "Chemistry of Coal Conversion", Schlosberg, R. D., Pergamon Press, NY, 1984 (in press).

2. Kerr, J. A.; Moss, S. J., "CRC Handbook of Bimolecular and Termolecular Reactions", Vols. 1, 2, CRC Press Boca Raton, FL., 1981.

3. Gibian, M. J. and Corley, R. C., Chem. Rev., $\underline{73}$, 44 (1973).

4. Retcofsky, H. L. in "Coal Science", Vol. 1, Gorbaty et al., eds., Academic Press, 1982, pp 43-83.

5. Stein, S. E., Carbon, $\underline{19}$, 421 (1981).

6. Brown, R. L., J. Computational Chem. 1983 in press.

7. Herndon, W. C., Isr. J. Chem. $\underline{20}$, 270 (1980); J. Org. Chem. $\underline{40}$, 3548 (1975); ibid $\underline{46}$, 2119 (1981).

8. Heilbronner, E., Bock, H., "The HMO Theory and its Application", Interscience, N.Y., 1976.

Figure 1.   Plot of Measured k_r/k_d per Transferrable H-atom vs. ΔH for Disproportionation. ΔH estimates were made using data discussed in reference 1c and recent data given in D. F. McMillen and D. M. Golden in Ann. Revs. Phy. Chem., Ann. Rev. Inc., Menlo Park, 1982.

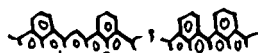Figure 2.   Illustrations of First Few Members of Series A and B.

Figure 3.   Log of Kekulé Structures per π-electron (KSPE $\equiv n_\pi^{-1}$ ln {# Kekulé structures}) Versus $n_\pi^{-1/2}$ (n_π = no. π-electrons). Note that ln(KSPE) is proportional to the resonance energy per electron [7] and $n_\pi^{1/2}$ is (nearly) proportional to the number of edge C-atoms. Series C and D have edges Three different "corner" types are given for series C.

Figure 4.   Electron Localization Energies for a Member of Series A(a) and B(b).

Figure 5.   Upper Third of HMO Energy Levels for Series A (upper) and B(lower).
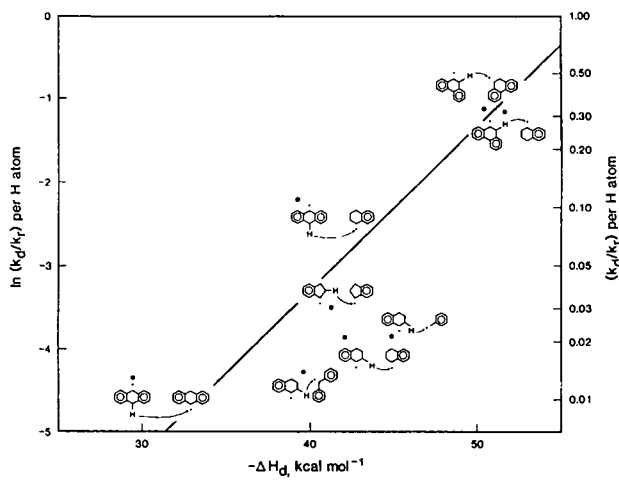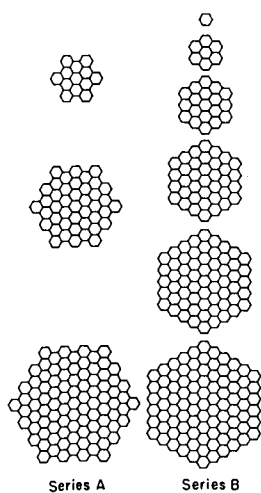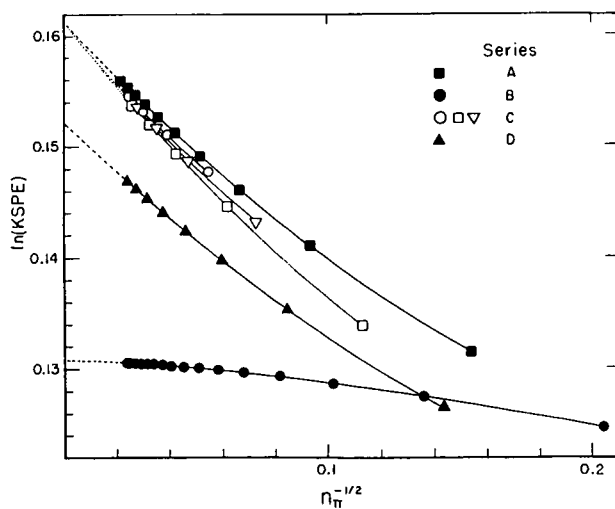
Figure 1

Series A   Series B
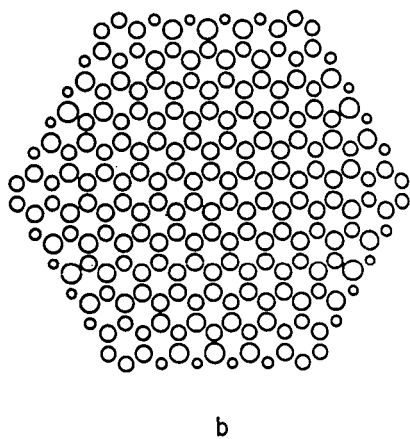
Figure 2

Figure 3

a   b

Figure 4
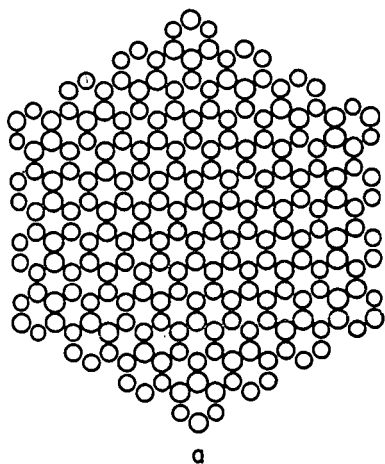

C_{1350}
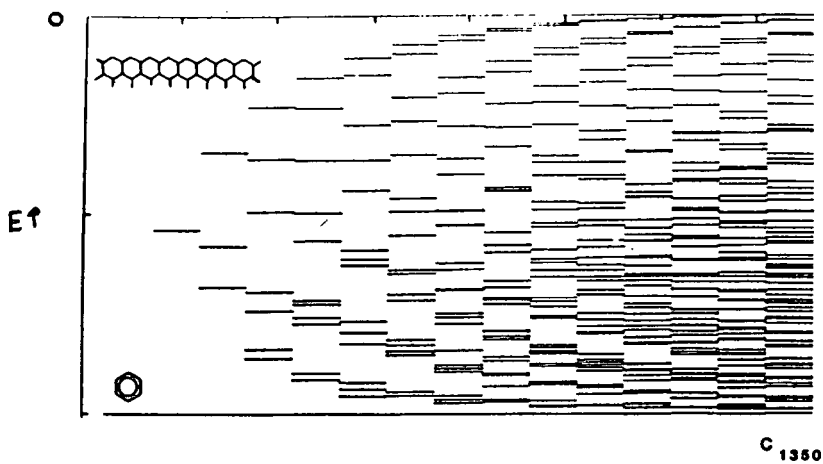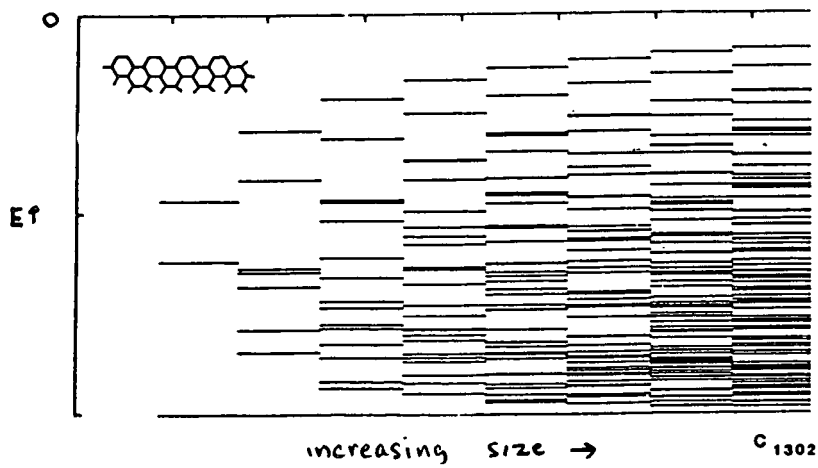
Figure 5

increasing   size → C_{1302}

48

PYROLYSIS STUDIES OF ILLINOIS #6 AND ITS TAR
USING MATRIX ISOLATION FTIR SPECTROSCOPY

C. Judith Chu, Leif Fredin, Robert H. Hauge and John L. Margrave

Department of Chemistry, Rice University, Houston, Texas 77251

INTRODUCTION

The various experiments in this study are performed with the objective of better understanding the initial reaction steps in coal gasification. Emphasis is placed on clarifying and understanding the structure of coal and its tars through pyrolysis studies designed to enhance formation of reactive gas phase intermediate species. Our main concern is centered on the characterization of unknown intermediates and better understanding the mechanism of tar formation. The experiments are designed such that reactive gas phase intermediates can exit the reaction zone rapidly and be trapped with inert matrix gas on a cold (12°K) matrix surface. Identification of these species and possibly free radicals are performed in a newly designed Rice University multisurface matrix isolation FTIR-MS apparatus[1].

EXPERIMENTAL

The Rice University multisurface matrix isolation FTIR-MS apparatus was used in the slow pyrolysis studies of Illinois #6 and flash pyrolysis of its tars. The multisurface MI-FTIR apparatus possesses a large number (60) of deposition surfaces which are useful for pyrolysis studies over a wide range of temperatures. This large number of surfaces is very valuable in detecting small changes occuring as a result of variations in reaction temperature or other reactor conditions. The system is integrated to a high resolution Fourier transform i. r. spectrometer covering a spectral range from the far i. r. to the near i. r. A detailed schematic diagram of the MI-FTIR apparatus is shown in Figures 1a and 1b.

The reactor used in our slow pyrolysis experiments is shown in Figure 2. It consists of a water cooled radiation shield; a hot furnace resistively heated through a cylindrically shaped thin tantalum foil (.001 inches) which has been spot wielded to an outer cylinder of a thicker tantalum tube (.020 inches); and a graphite sample cell. Finely divided powders of coal, between 20-100 mg. of <500 mesh particle size, are place into the graphite cell inside the reactor. After evacuation, the sample is slowly heated from room temperature to approximately 1450°C. The gaseous pyrolysis products are then immediately directed over the very cold depostion surface (12°K) which quenches reactions and traps the species in an inert matrix gas of either argon or nitrogen. In general, one deposition surface is used for each $60-100^{O}$C increment rise in temperature over a 10 minute trapping period. The frozen transient products are later analyzed off-line with the FTIR spectrometer.

Figure 3 presents the reactor used in the flash pyrolysis studies of coal tar. The reactor is essentially the same as described for the slow

pyrolysis studies with the exception of the sample cell. Since tar evolves
at relatively low temperatures ($\sim$100-300°C), it became essential to
maintain the coal within this low temperature range to ensure generation of
tar. The evolved tar should then pass through a hot zone of $\sim$1200°C for
pyrolysis to occur. These requirements have been achieved by the design
of a copper sample cell cooled by flowing either nitrogen or helium gas
through small stainless steel tubing (1/16") silver soldered to the back of
the copper cell (see details in Figure 3). A piece of 4 mm quartz tubing
is attached to the front of the copper cell. This is the hot reactor zone
where the flash pyrolysis occurs. When assembled and placed into the
furnace, the relatively non-conducting quartz tube becomes positioned at
the front of the furnace, in the hot zone, and the copper cell containing
the coal sample becomes positioned at the relatively cool back section of
the furnace. By varying the flow of the cooling gas from 30 to 0 psi, the
temperature of the copper cell can be successfully maintained in the tar
evolution range (between room temperature to $\sim$321°C) when the temperature
of the quartz tube reaches $\sim$1180°C. Under these conditions, evolution of
tar is easily controlled. During the experiment, the temperature of the
coal powder was closely monitored with a Chromel-Alumel thermocouple in
direct contact with the copper cell. Tar molecules are pyrolyzed as they
pass through the hot quartz tube through surface heating. The transient
pyrolysis products are trapped onto the 12°K deposition surface along with
the inert matrix gas to be analyzed later by FTIR spectroscopy.

RESULTS

1. Slow Pyrolysis of Illinois #6
    Slow pyrolysis studies are performed as a basis for
    characterizing coal and for comparison to other heating
    techniques. Approximately 28 mg. of Illinois #6 ($<$500 mesh) coal
    powder is placed in the graphite cell (see Figure 2) and slowly
    heated. Gaseous products obtained at different temperatures are
    trapped in 10 minute intervals with nitrogen onto the 12°K matrix
    isolation surface and subsequently examined. The resulting
    MI-FTIR spectra are presented in Figure 4. Variations in gaseous
    pyrolysis products are easily followed in the three-dimensional
    plot. As can be seen from the plots, coal devolatilization is
    characterized by: the immediate evolution of CO_2, H_2O and SO_2 as
    well as traces of small carbonyls such as acetone[1],
    formaldehyde[2], formic acid[3] and acetic acid[4] at low
    temperatures; evolution of tar at 150-400°C with simultaneous
    evolution of CH_4, C_2H_4, C_2H_6, C_3H_6 and COS; coupled evolution of
    CO_2, CO, H_2O, HCN and CH_4 from 400-850°C; and higher temperature
    evolution of CS_2, CO, H_2O and C_2H_2 as well as nitric oxide[5] and
    other as yet unidentified species. The interesting observation
    that carbon monoixide reaches maximum yield at two different
    temperatures, first at $\sim$800°C and then at $\sim$1350°C indicate two

different sources of CO in the parent coal. This has also been
observed by Soloman and co-workers[6].

   Tar formation with simultaneous evolution of CH_4, C_2H_4, C_2H_6
and C_3H_6 suggests aliphatic linkage groups in the parent coal.
Our studies also indicate the evolution of tar as discrete
molecules (perhaps in the form of free radicals) which
re-polymerize to give a structure similar to the parent coal.
Characteristic tar absorptions in matices are broad absorptions in
the C-H stretching region of 3100-2800 cm^{-1}, C-H bending region of
1500-1400 cm^{-1} and C-O stretching regions of ~1100 cm^{-1}. More
detailed tar spectra and their variations with temperature are
shown in Figure 5.

   Sulfur in Illinois #6 coal is evolved in the form of SO_2 and
COS at low temperatures and CS_2 at higher temperatures. Traces of
H_2S and NH_3 are also observed at low temperatures.

2. **Pyrolysis of Illinois #6 Tar**

   Pyrolysis studies of Illinois #6 tar were carried out to gain
a better understanding of its structure and of how it differs from
the parent coal. Approximately 100 mg. of Illinois#6 powder
(< 500 mesh) is placed in the copper cell (see Figure 3). After
assembling the reactor and attaching it to the matrix isolation
apparatus, the system is slowly evacuated to 10^{-6} torr. The front
furnace is then immediately heated to and maintained at 1180°C
throughout the length of the experiment. A constant flow of
helium gas is passed through the stainless steel cooling tube at a
starting pressure of 30 psi to keep the copper tube at a low
temperature. With gradually decreasing helium flow, the
temperature of the coal can be raised slowly to induce tar
evolution. The tar then passes through the hot quartz tube,
becomes pyrolyzed and gaseous intermediates are trapped in 10
minute intervals with nitrogen onto the 12°K deposition surface.
The temperature range studied was from room temperature to 321°C.
The evolution of tar was found to be a continuous process starting
from 120°C and reaching maximum yield between 206-238°C. The
resulting MI-FTIR spectra of tar pyrolysis products are shown in
Figure 6. It can be seen clearly that the characteristic broad
tar absorptions have disappeared indicating pyrolysis of tar. The
appearance of several new species as well as increased absorptions
of several existing species are observed in place of tar. They
are: increased yeilds of CO, C_2H_4 and C_2H_6; appearance of HCN,
CS_2, benzene[7] and the methyl radical[8], CH_3; approximately the
same yields of CO_2, H_2O, CH_4, C_3H_6, SO_2, COS and the carbonyls
(acetone, acetic acid, formaldehyde, formic acid). Traces of NH_3
and H_2S are also observed. The presence of acetylene as one of
pyrolysis products is inconclusive since C_2H_2 has the same
absorptions as HCN in nitrogen matrices(7,9).

In summary, pyrolysis of Illinois #6 tar was found to produce CO, C_2H_4, C_2H_6, HCN, CS_2, C_6H_6 and the methyl radical CH_3. The formation of C_2H_4, C_2H_6 and benzene as pyrolysis products points to the presence of aromatic hydrocarbons in the tar structure since pyrolysis of other aromatic hydrocarbons are known to produce similar results[10]. CO, HCN and CS_2 indicate presence of oxygen, nitrogen and sulfur in tar. Finally the formation of methyl radicals indicate that the design of our reactor favors and promotes the formation of free radicals which can rapidly exit the reactor chamber without secondary reactions with other species. By varying the diameter of the quartz tube, we hope to further enhance the chances of observing other free radicals.

3. **Slow Pyrolysis of Oxidized Illinois #6**

Effects of oxidation on Illinois #6 powder were studied. Illinois #6 powder ($<$ 500 mesh) was oxidized by heating the coal in an oven at $\sim$180°C for 4 hours. Formation of carbonyl functional groups in the oxidized coal was observed along with a reduction in aliphatic C-H groups. Results of slow pyrolysis studies of the oxidized coal using the same experimental procedures as described for the unoxidized coal are shown in Figure 7. When compared with results of the unoxidized coal (Figure 4), a clear increase in CO_2 absorption is observed. Oxidation also appears to increase the carbon monoxide absorptions at the lower temperatures (r. t. to 850°C) while CO at higher temperatures remain uneffected. Oxidation also retards formation of tar. Only traces of tar are observed during slow pyrolysis of the oxidized sample.

DISCUSSION

At the present time our work has shown that our pyrolysis technique can be developed as a valuable tool in characterizing different ranks of coal. It is also a highly sophiscated tool for identifying unknown intermediates. As of yet our limited library of refernce data has prevented the identification of all pyrolysis intermediates and products. We will be making numerous additions to this library in the near furture.

ACKNOWLEDGEMENT

REFERENCES

1. R.H. Hauge, L. Fredin, J. Chu and J.L. Margrave, "The Identification and Chemistry of Species Resulting from the Rapid Pyrolysis of Small Coal Particles in Vacuum and in the Presence of

Reactive Gases", American Chemical Society, Division of Fuel
Chemistry, Preprints, 28, 1, 35, (1983).

2. K.B. Harvey and J.F. Ogilvie, Canadian Journal of Chemistry, 40,
85, (1962).

3. R.C. Millikan and K.S. Pitzer, J. Amer. Chem. Soc., 80, 3515,
(1958).

4. C.V. Berney, R.L. Redington and K.C. Lin, J. Chem. Phys., 53,
1713, (1970).

5. W.A. Guillory and C.E. Hunter, J. Chem. Phys., 50, 3516, (1969).

6. P.R. Solomon, "The Evolution of Pollutants During Rapid
Devolatilization of Coal", Rep. R76-952588-2, United Technologies
Research Center, East Hartford Conn. 1977,
Rep. NSF/Ra-770422,NTISPB, 278496/AS, 1977.

7. M.M. Rochkind, in "Spectrometry of Fuels, ed. R.A. Friedel,
p. 280, Plenum Press, 1970.

8. D.E. Milligan and M.E. Jacox, J. Chem. Phys., 47, 5146, (1967)..

9. C.M. King and E.R. Nixon, J. Chem. Phys., 48, 1685, (1968).

10. Adv. in Chem. Series, 183, "Thermal Hydrocarbon Chemistry",
ed. A. G. Oblad, H. G. Davis, R. T. Eddinger, ACS., (1979).

Fig. 1a. Matrix Isolation – FTIR Mass Spectrometer – Side View

QUADRUPOLE MASS SPECTROMETER

VACUUM

HIGH TEMPERATURE FURNACE

CLOSED CYCLE CRYOSTAT

MULTISURFACE 10X TRAPPING BLOCK

IBM VACUUM FTIR

LASER

QUADRUPOLE MASS SPECTROMETER

LASER

TRAPPING COLD BLOCK

SAMPLE INLET

HIGH TEMPERATURE FURNACE

SAMPLE INLET

IBM-98 FTIR
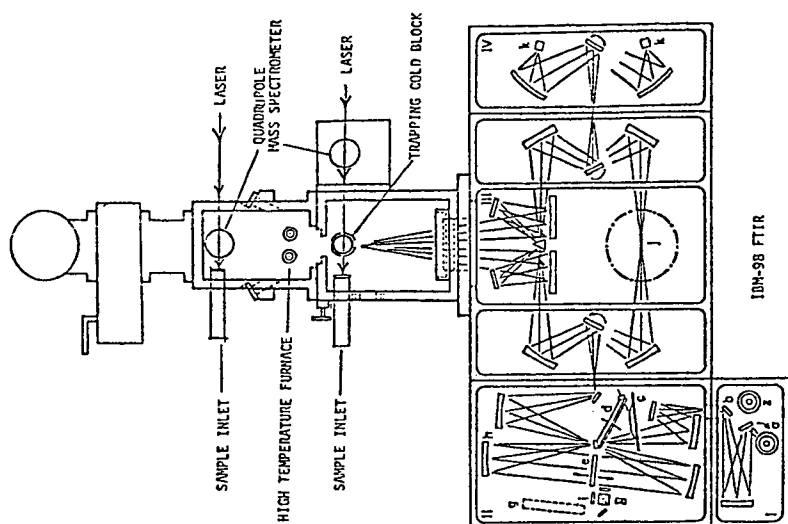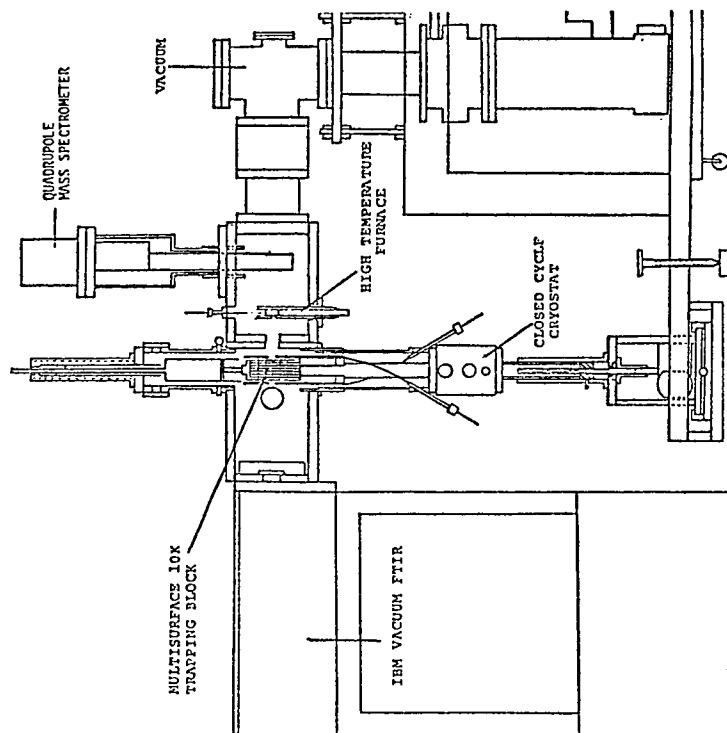
Fig. 1b. Matrix Isolation –FTIR Mass Spectrometer – Top View

54

Fig. 2 Slow Pyrolysis Reactor

Vacuum

Argon

MATRIX
BLOCK
13K

Water Cooled Shield   Graphite Cell
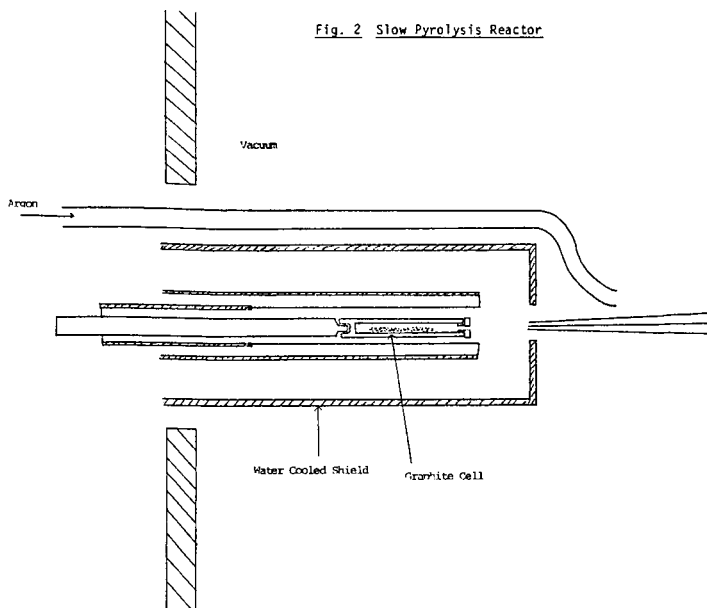
Fig. 3 Reactor for Pyrolysis of Tar

Vacuum

Argon
or N₂

He or
N₂

Thermocouple

MATRIX
BLOCK
13K

Quartz
tube

Gas cooled
copper cell

Water cooled
shield

55

Fig. 4 Slow Pyrolysis of Illinois #6 (500 mesh) from RT to 1499°C in N₂ Matrix (12°K)
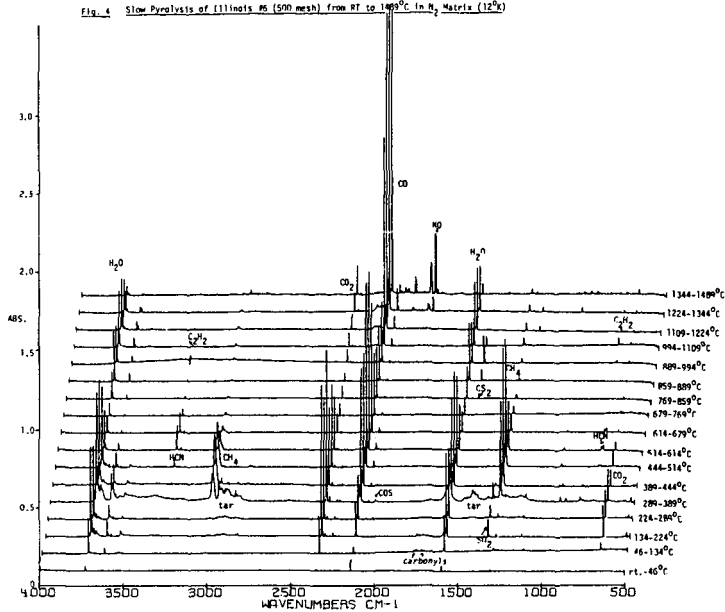
Fig. 5 Slow Pyrolysis of Illinois #6 (500 mesh) in Nitrogen Matrix (12°K)
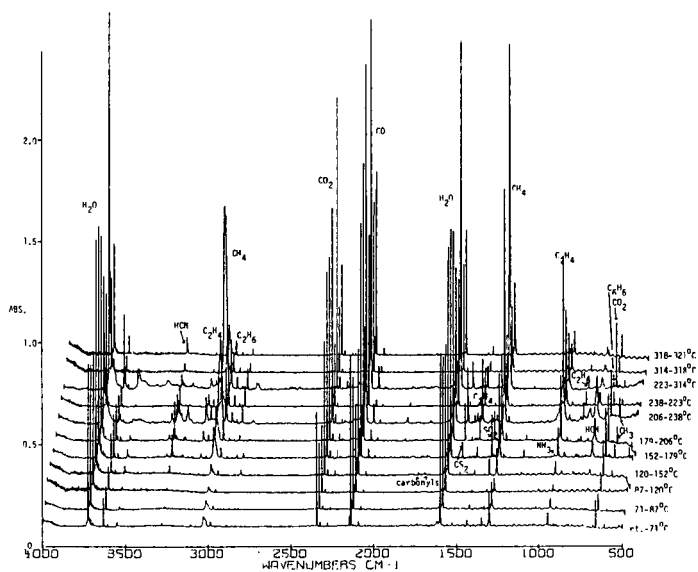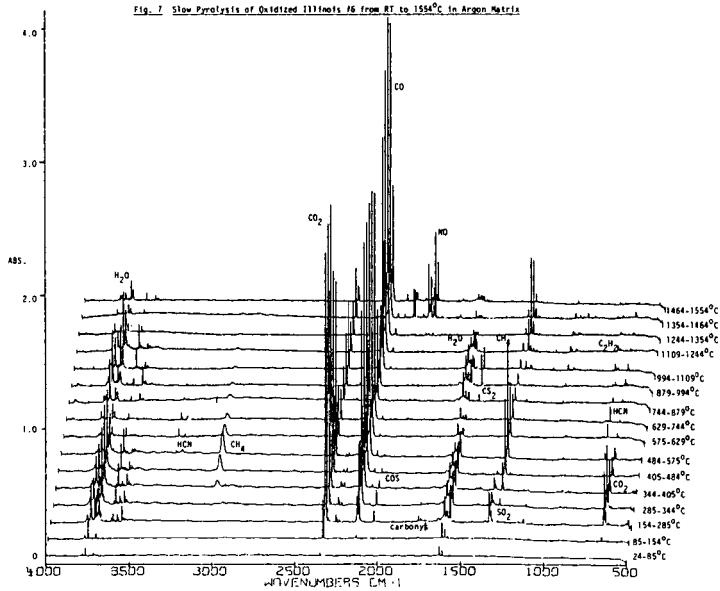
PARTICLE SIZE LIMITATIONS DUE TO HEAT
TRANSFER IN DETERMINING PYROLYSIS KINETICS
OF BIOMASS

George M. Simmons

Department of Chemical Engineering
University of Idaho
Moscow, Idaho 83843

A simplified heat transfer model is analyzed in order to estimate an upper
bound for biomass particle size in conducting experimental pyrolysis kine-
tics. In determining intrinsic kinetic rates, it is desirable that the
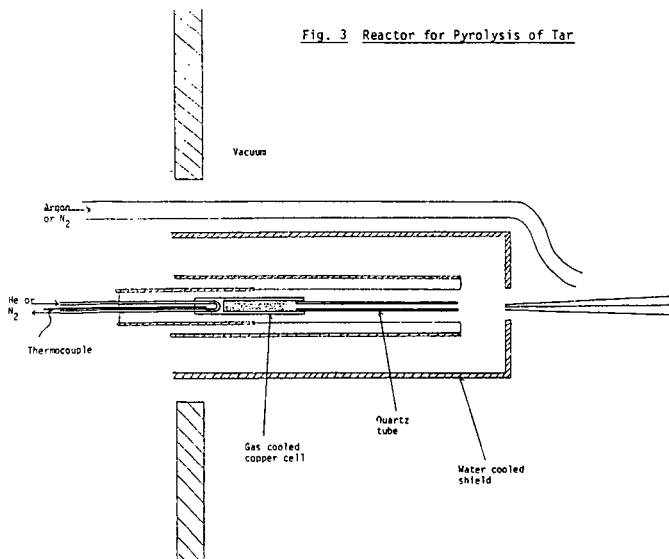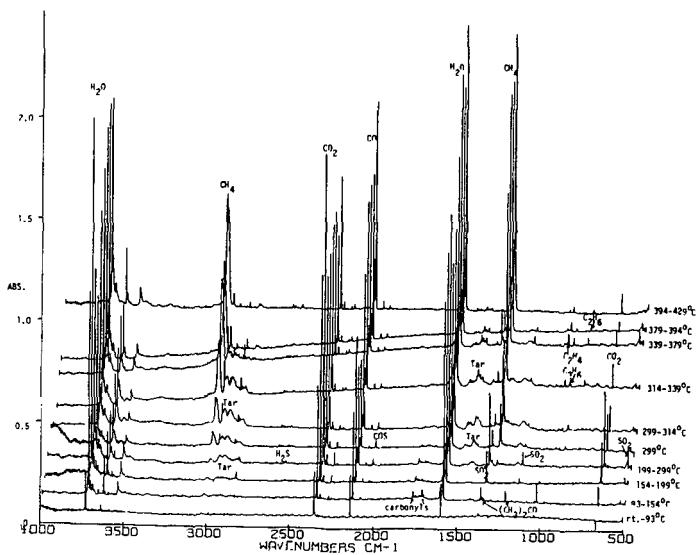entire particle be at reactor temperature for the duration of the chemical
reaction. By comparing characteristic times for reaction rates versus heat
up rates, an approximate boundary for particle size can be constructed as
a function of temperature; above this boundary, the reaction rate is strongly
heat transfer dominated, and below the boundary the reaction rate is kinetic-
ally controlled. Using parameters for cellulor pyrolysis, it is estimated
that a 100 µ particle will be heat transfer limited due to internal heat
transfer at temperatures above 500°C.

In order to experimentally determine kinetic parameters for pyrolysis decomposition
of biomass materials, it is typically assumed that the reactions are first order with
respect to mass and that the solid material is at uniform temperature. As the reac-
tion temperature is increased, the kinetic rates eventually become faster than the
associated heat transfer rates (internal and external). At higher temperatures,
the decomposition rate becomes heat transfer limited, and any kinetic interpreta-
tion must include a transport model of the process. Since the temperature region
over which the transition from kinetic control to heat transfer control takes place
is a strong function of particle dimension, it is important for the kineticist to use
relatively small particles if the temperature uniformity assumption is made. A
simplified model will be presented for determining the particle size limit for the
kinetic controlled regime.

In this development, several simplifying assumptions are made in order to achieve
readily interpreted results. Within the region of interest, that is the transition
from a kinetic rate controlled mechanism to that influenced by heat transfer limita-
tions, the assumptions are reasonable and lead to meaningful results. The goal is
to quantify the dimension referred to as "thermally thick" and to develop an under-
standing of how this characteristic dimension changes with temperature. The ratio-
nale is to define the region in which kinetic data may be safely interpreted without
the necessity to model the heat and mass transfer process.

In the light of recent work by Chan and Krieger (1), it is clear that transport
limitations play an important role in governing the overall rate of solid decom-
position for large particles. Several detailed and well developed solutions are
available (2, 3, 4, 5), however, an interpretation of what these considerations
mean to the kineticist is needed.

Model Development and Solution

The simplest geometry to assume is that of the semi-infinite slab of defined thick-
ness. There is also some practical justification as wood chips could be so described.
The starting energy equation (simplified) is

$$\rho C_p \; \frac{\partial T}{\partial t} = k \frac{\partial^2 T}{\partial X^2} + k_{rx} \, \lambda \rho \qquad \qquad \text{1)}$$

$$k_{rx} = \text{1st order rate constant}$$
$$\lambda = \text{heat of reaction}$$
$$\rho = \text{particle density}$$

The energy transport due to volatile evolution and diffusion is neglected, recognizing that the resulting solution will hold only for relatively slow (compared to heat transfer) kinetic rates. Since this is the region of interest, no loss of information results. In addition, recognizing that we are considering cases for relatively slow kinetic reactions or for initial rate studies, it is also assumed that we have constant densities and constant physical properties.

The reaction rate coefficient is "exponential" with temperature, however a linearized form expanded about the reactor temperature results in significant simplification and is justified since the rate drops so rapidly with temperature. It also turns out that the region of primary interest is within about 10°C of the reactor temperature, so that a linearized rate constant is a good approximation:

$$k_{rx} = k_0 \left\{ 1 + \frac{E}{RT_o^2} (T - T_o) \right\} \qquad \qquad \text{2)}$$

$$k_0 = \text{rate coefficient at } T_c$$

If we define dimensionless coordinates

$$\tau = t/(\rho C_p B^2 / k)$$
$$\xi = \frac{X}{B}$$

where $2B$ = particle thickness

and a dimensionless temperature

$$\phi = \frac{T - T_o}{T_1 - T_o}$$

$$T_o = \text{surface temperature}$$

$$T_1 = \text{initial temperature}$$

the energy equation reduces to

$$\frac{\partial \phi}{\partial \tau} - \frac{\partial^2 \phi}{\partial \xi^2} - \alpha \gamma \phi = \alpha \qquad \text{where } \alpha = \frac{-\rho \lambda k_0 B^2}{k(T_1 - T_o)} \qquad \text{3)}$$

$$\gamma = \frac{E(T_1 - T_o)}{RT_o^2}$$

59

The initial condition is

$$\phi(0) = 1 \qquad \text{from } T(x,o) = T_1 \qquad \qquad 4)$$

and the boundary conditions used are

i) $\dfrac{\partial \phi}{\partial \xi}(0,\tau) = 0$ symmetry about x = 0   5)

ii) $\phi(1,\tau) = 0$ from $T = T_o$ at x = B

The second boundary condition assumes that the surface temperature can be speci-fied with high external heating fluxes available using fluid beds, radiation, or other devices. It is important to note that external heat transfer is also often limiting and that the estimate to be presented here for an upper bound particle dimension would need to be revised downward in such cases.

This "initial-boundary value" problem can be solved analytically following the development in Bird, et. al. (6) or Carslaw and Jaeger (7).

For endothermic reactions (λ = negative):

$$\phi = \phi_{ss} + \phi_t \qquad \qquad 6)$$

$$\phi_{ss} = \text{steady state solution}$$

$$\phi_t = \text{transient solution}$$

$$\phi_{ss} = \frac{1}{\gamma}\left[\frac{\exp(\sqrt{\alpha\gamma}\,\xi) + \exp(-\sqrt{\alpha\gamma}\,\xi)}{\exp\sqrt{\alpha\gamma} + \exp - \sqrt{\alpha\gamma}} - 1 \right] \qquad \qquad 6a)$$

$$\phi_t = e^{-\alpha\gamma\tau} \sum_o^\infty C_n \, e^{-[(n+\frac{1}{2})\pi]^2 \tau} \cos(n+\tfrac{1}{2})\pi\xi \qquad \qquad 6b)$$

$$\text{with } C_n = \frac{2(-1)^m}{(n+\frac{1}{2})\pi}\left[1 + \frac{1}{\gamma} - \frac{1}{\gamma}\left(\frac{1}{1+\dfrac{\alpha\gamma}{(n+\frac{1}{2})^2\pi^2}} \right) \right]$$

Cellulose and wood pyrolysis are thought to be endothermic (3, 5), however for completeness the solution for exothermic reactions is also given:

$$\phi = \phi_{ss} + \phi_t \qquad \qquad 7)$$

$$\phi_{ss} = \frac{1}{\gamma}\left[\frac{\cos\sqrt{\alpha\gamma}\,\xi}{\cos\sqrt{\alpha\gamma}} - 1\right] \qquad\qquad 7a)$$

$$\phi_t = e^{+\alpha\gamma\tau}\sum_o^\infty C_n\, e^{-\left[\left(n+\frac{1}{2}\right)\pi\right]^2\tau}\cos\left[\left(n+\frac{1}{2}\right)\pi\,\xi\right] \qquad\qquad 7b)$$

$$Cn = \frac{2(-1)^n}{\left(n+\frac{1}{2}\right)\pi}\left[1 + \frac{1}{\gamma} - \frac{1}{\gamma}\left(\frac{1}{1 - \frac{\alpha\gamma}{\left(n+\frac{1}{2}\right)^2\pi^2}}\right)\right]$$

The solutions presented are composed of a steady state and a transient solution. The steady state solution is correct mathematically but does not represent a true steady state solution for real situations, with time varying densities and physical properties. We can nevertheless develop useful information from this solution if we recognize its limitations. Figure 1 shows the analytical solution (Equation 6) for ϕ as a function of ξ and τ for typical values of α and γ.

Defining the Region Free of Heat Transfer Limitations

Solid decomposition reactions are difficult to conduct in a totally repeatable and precise manner. The main difficulties are associated with sample uniformity, sample location in the reactor, temperature, and composition.

It could be argued that, since rates are repeatable only to within, say, 10 to 20% accuracy, that the temperatures within the sample should also be within the same limit. This means that if the local rate is everywhere within this 10 to 20% limit, then we can define an allowable temperature profile associated with this position dependent reaction rate. In the present case, with the center of the particle being the coolest, we may determine the temperature at the center associated with 90% (or 80%) of that at the reactor temperature, T_o.

Using an Arrhenius expression for the rate constant, k, we have the temperature limit, T_ℓ, defined as follows:

$$T_\ell = \frac{T_o}{1 - \frac{R\,T_o}{E}\ln 0.9} \qquad\qquad 8)$$

This in turn defines a minimum centerline particle temperature and dimensionless temperatures

$$\phi_\ell = \frac{T_\ell - T_o}{T_1 - T_o} \qquad\qquad 9)$$

As a first attempt to fix an appropriate particle size, we can estimate, from Equation 6, the time required for the temperature at the centerline to reach T_ℓ, or ϕ_ℓ. This time can then be used to estimate an approximate extent of reaction to determine how much of the particle may have pyrolyzed in that time period. The actual extent of reaction would be lower since the particle is not uniformly at T_o; the estimate or particle size limits will therefore be conservative.

61

Specific Examples of Cellulose Kinetics

The results of examining cellulose decomposition as a specific case are shown in Figure 2. Example calculations for 450°C are shown as follows:

$$\frac{d\rho}{dt} = -k\rho \qquad\qquad 10)$$

where $k = 9.32(10^{11})\exp(-35960/RT)$ min^{-1} (ref. 8)

The time to reach 10% ($\rho/\rho_0 = 0.9$) decomposition at reactor temperature is then determined by integrating to get

$$t_{10} = \frac{\ln 0.9}{-k_0} = .0084 \text{ min} \qquad\qquad 11)$$

The dimensionless time, τ, associated with this 10% decomposition value is dependent on particle size

$$\tau_{10} = \frac{t_{10}}{(\rho C_p B^2/k)} \qquad\qquad 12)$$

Using literature values for cellulose properties

$$\rho = 0.5 \text{ g/cm}^3$$

$$C_p = 0.32 \text{ cal/g-°C}$$

$$k = 0.0003 \text{ cal/(cm-sec-°K)}$$

$$\lambda = -100 \text{ cal/g}$$

the following mathematical procedure was conducted. For a given temperature and and particle size, the time required for the centerline temperature to reach that temperature (T_ℓ) associated with 90% of the ultimate rate was determined. This heat up time was then compared to the kinetic time for 10% decomposition. The particle size was then increased and the calculation repeated.

In all cases, the limitation imposed by the steady state (or maximum possible) centerline temperature was first reached. This result validates the basic assumptions used in the derivation. It is therefore apparent that just the steady state portion of the solution can be used to obtain an estimated limit for particle size. Specifically, at the centerline,

$$\phi_{ss} = \frac{1}{\gamma} \left[\frac{2}{\exp(\sqrt{\alpha\gamma}) + \exp(-\sqrt{\alpha\gamma})} - 1 \right] \qquad\qquad 13)$$

Only α depends on particle size, so for a given temperature limit, the particle size associated with that steady state limit is readily calculated. The results of these calculations are shown on Figure 2 for both 10% and 20% deviations from the ultimate rate.

If the heat of reaction is considered to be zero, then the transient solution must be used to determine the particle size limit in the manner as just described. This limit

is also shown on Figure 2 for 10% and 20% deviations from the ultimate rate.

Summary

Using various assumptions as described, it is seen that, for example, a particle dimension of 0.01 cm (thickness = 0.02 cm or 200 microns) might be investigated kinetically up to about 450-500°C without taking transport limitations due to internal particle profiles into account. If external heat transfer to the particle surface is also slow, then even lower temperature limits would occur. In many cases, Equation 13 can be used to estimate the maximum particle size for various values of the dimensionless parameters. It should also be noted that the characteristic dimension for a bed of fine particles would be bed depth rather than particle size.

References

1. Chun, R.W.C., and Krieger, B. B., "Analysis of Chemical and Physical Processes During Devolatilization of a Single, Large Particle of Wood," Seventh International Symposium on Chemical Reaction Engineering, Boston, Massachusetts, Oct, 1982.

2. Kanury, A. M. "Thermal Decomposition Kinetics of Wood Pyrolysis," Combustion and Flame, 18, 75-83 (1972)

3. Kung, H-C., "A Mathematical Model of Wood Pyrolysis," Combustion and Flame, 18, 185-195 (1972)

4. Kung, H-C., and Kalelkar, A.S., "On the Heat of Reaction in Wood Pyrolysis," Combustion and Flame, 20, 91-103 (1973)

5. Kansa, E.J., Perlee, H.E., and Chaiken, R.F., "Mathematical Model of Wood Pyrolysis Including Internal Forced Convection," Combustion and Flame, 29, 311-324 (1977)

6. Bird, R.B., Stewart, W.E. and Lightfoot, E.N., Transport Phenomena, John Wiley & Sons, Inc., New York, 1960

7. Carslaw, H.S., and Jaeger, J.C. Conduction of Heat in Solids, Oxford University Press, (1959), Second Edition.

8. Simmons, G.M., and Lee, W.H., "Kinetics of Gas Formation from Cellulose and Wood Pyrolysis," presented at International Conference "Fundamentals of Thermochemical Biomass Conversion", Estes Park, Colorado, November, 1982. (submitted for publication)

Figure 1. Temperature Profile vs. Time (Equation 6) with $\alpha = -0.5$, $Y = -15$

$$\tau = \frac{t}{(\rho C_p B^2/k)}$$

$$\alpha = \frac{\rho \lambda k_0 B^2}{k(T_1 - T_0)}$$

$$Y = \frac{E(T_1 - T_0)}{R T_0^2}$$

$\tau = \infty$

1.0

0.5

0.3

0.2

0.1

0.01

$\tau = 0.0$

$\phi = \frac{T - T_0}{T_1 - T_0}$

0.0   0.2   0.4   0.6   0.8   1.0

$\xi = \frac{x}{B}$

-1.0   0   +1.0
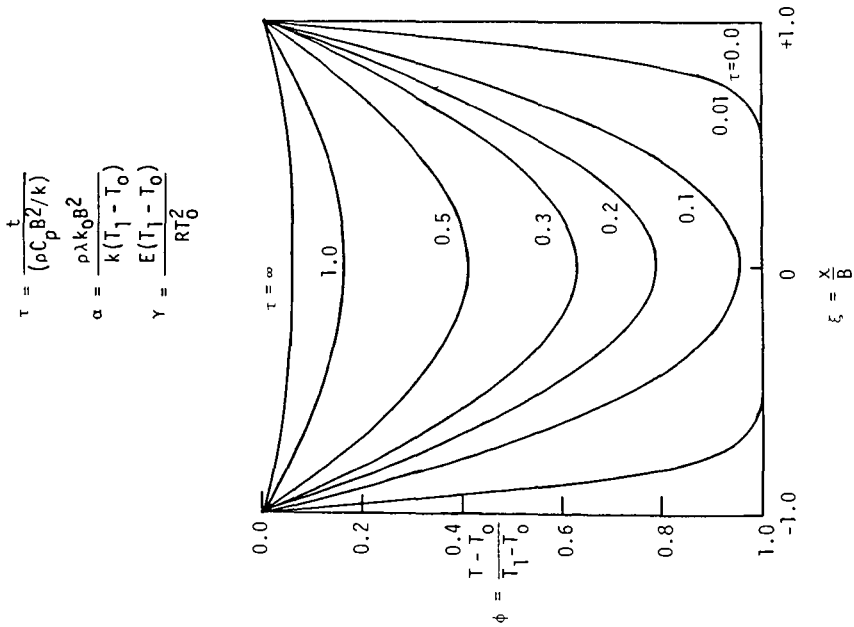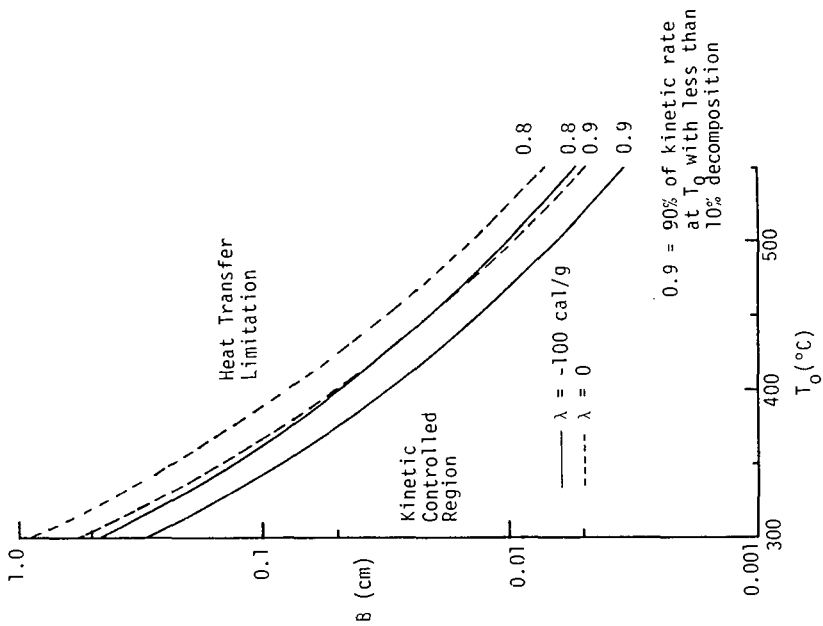
Figure 2. Particle Size Limit vs. Temperature for Kinetic Controlled Region (using parameters for cellulose)

Heat Transfer Limitation

Kinetic Controlled Region

$\lambda = -100$ cal/g
$\lambda = 0$

0.9 = 90% of kinetic rate at T_0 with less than 10% decomposition

0.8
0.8
0.9
0.9

B (cm)

1.0

0.1

0.01

0.001

T_0 (°C)

300   400   500

Global Kinetics of Primary and Secondary Reactions in
Hydrocarbon Gas Evolution from Coal Pyrolysis

Michael A. Serio, William A. Peters, Ken Sawada, and Jack B. Howard

Department of Chemical Engineering and Energy Laboratory,
Massachusetts Institute of Technology
Cambridge, Massachusetts   02139

Introduction

The global pyrolysis kinetics of a Pittsburgh No. 8 Seam bituminous coal were studied previously (1,2) in a reactor where volatiles are rapidly diluted and quenched upon exiting the coal, thereby reducing the extent of secondary reactions of primary products. Despite this feature, a significant decrease in tar yield occurs as the pressure is increased, implying that the nascent tar contains reactive components capable of significant secondary reactions under conditions of interest in commercial coal processing. A study was undertaken to systematically determine the effects of temperature (500 to 900°C), residence time (0.6 to 1.1 s), and contacting surfaces (coal char, active carbon, and quartz) on the homogeneous and heterogeneous secondary reactions of tar from a Pittsburgh Seam bituminous coal.

In this paper, results for the formation kinetics of CH_4, C_2H_4, C_2H_6, and C_3's by primary pyrolysis of the coal and of CH_4 and C_2H_4 by vapor-phase cracking of the tar are presented. An earlier paper (3) focused on the overall kinetics of the homogeneous and heterogeneous cracking of tar.

The kinetic parameters presented in this paper are understood to be global parameters, i.e., they represent the kinetics for the overall reaction A → B rather than any elementary step involving radical species. Consequently, the values obtained for activation energies correlate with the strengths of the bonds which are being broken, but are not equivalent.

Experimental

The apparatus is a reactor containing two independently heated, series-connected stages for controlled generation and reaction of volatiles (3,4,5). A thin bed of coal, diluted with sand to prevent agglomeration, is pyrolyzed in the upstream stage at a low heating rate (3°C/min) in order to produce fresh volatiles at temperatures (<500°C) which are unfavorable to secondary reactions. These volatiles are then rapidly transported by an inert carrier gas to a second (isothermal) stage, held between 500 and 900°C, and then to a collection system. In preliminary experiments (referred to as "base case"), the volatiles generated in the first stage pass directly to the collection system.

In the second (reaction) stage, the separate effects of temperature and residence time (0.6–1.1 s) on the homogeneous secondary reactions of the primary tars are systematically studied. Conditions are chosen such that the cracking reactions of light oils and light hydrocarbon volatiles are relatively unimportant. Consequently, changes in the composition of volatiles within the second stage are attributed solely to secondary reactions of the tar.

Results and Discussion

Kinetics of Tar Formation and Tar Cracking
Cumulative yields of tar as a function of formation temperature are shown in

Fig. 1. Since the heating rate is constant, the abscissa can also be considered a time axis. This figure includes data from base case experiments (no cracking stage) and homogeneous cracking experiments with a gas-phase residence time (V/F, plug flow) of 1.1 s and a temperature ranging from 700 to 900°C in stage 2.

The base case data in Fig. 1 were obtained with a carrier-flow rate equivalent to a nominal stage-2 residence time of 1.1 s. Other base case runs having nominal stage-2 residence times from 0.5 to 3.0 s gave very similar tar yields and evolution profiles (4,5). This result indicates that the evolution of tar from the bed is not limited by mass-transfer into the bulk gas. The independence of tar evolution rate with respect to carrier gas flow rate is important since this parameter is used to control volatiles residence time in the second stage.

The base data also show that the maximum rate of tar formation occurs at relatively low temperatures (~430°C) and that over 90 percent of the tar is formed below 500°C. Consequently, one can assume that the tars being formed in the first stage are "primary," i.e., they have not yet been subjected to significant secondary reactions.

The dotted curve drawn through the base data in Fig. 1 has been generated by fitting with a kinetic model which assumes an infinite set of parallel, first-order decomposition reactions with a Gaussian distribution of activation energies (6). The parameters obtained by fitting this model or a simple, single first-order reaction model to the tar formation data are given in Table 1, below.

TABLE 1. TAR FORMATION KINETIC PARAMETERS					
Model Type	A 1/s	E (kcal/mole)	σ (kcal/mole)	V* (wt. % of coal	RMS Error
Single Reaction	2.56×10^5	27.1	--	23.03	0.026
Multiple Reaction	4.54×10^7 3.80×10^{13}	34.2 52.8	1.1 2.5	23.27 23.41	0.024 0.025

Depending on the initial guess used to initiate the numerical data fitting routine, the multiple reaction model gives two sets of kinetic parameters, which fit the data equally well. Discriminating between these sets will require data from experiments at different heating rates. Since, in all cases, the activation energy for tar formation is higher than would be expected for a physical process, and because of the flow-independence, it is likely that the rate-controlling mechanism for tar evolution is chemical kinetics. This result differs from the study of Unger and Suuberg (7), where evaporation of tar was thought to be rate-limiting. This difference can probably be attributed to the reactor system used in their study, in which a thin layer of coal is heated in the absence of a forced convective flow.

The success of the single reaction model and the small values of σ for the multiple-reaction model indicate that the formation reactions for tar involve only a small range of activation energies, suggesting that primary tar is formed by decomposition of only a few types of bonds in the coal.

The other data sets in Fig. 1 were fitted with an equation with the form of the multiple reaction model but these plots reflect the combined influence of tar generation and tar secondary reactions. Consequently, no kinetic parameters were obtained directly from this fit. However, by using the asymptotic values of tar yield the overall conversion of tar (relative to the base case) was calculated. These data are shown in Fig. 2 for several homogeneous cracking experiments performed at temperatures between 500 and 900°C and nominal residence times of 0.6 and

1.1 s. The data were fit to a model which assumes that the tar consists of three "lumps" of different reactivity, which react independently. The first lump, "A" tar, is the most reactive and is assumed to decompose via a first-order reaction into gases and light oils at relatively low severities. The "B" tar is moderately reactive and decomposes to similar products by a parallel first-order reaction with a presumably higher global activation energy than that of lump "A." The "C" tar is assumed to be unreactive under the present conditions. The percentages of A, B, and C were obtained by inspection of the apparent plateaus in the conversion data (Fig. 2). This resulted in values of 33, 27, and 40 wt. percent for A, B, and C, respectively. Additional details of the model have been discussed previously (3). The kinetic parameters are given in Table 2.

TABLE 2. TAR SECONDARY REACTIONS/KINETIC PARAMETERS FOR 3-LUMP MODEL

LUMP	A 1/s	E (kcal/mole)	T^* (wt. % of tar)
A	1.25×10^9	39.4	33.0 (fixed)
B	8.04×10^{12}	65.2	27.0 (fixed)
C	--	--	40.0 (fixed)

Hydrocarbon Gas Formation

The evolution rates of primary hydrocarbon gases (CH_4, C_2H_4, C_2H_6, C_3H_6 + C_3H_8) are presented in Figures 3-6, respectively. The data clearly show that the gas formation kinetics are independent of carrier flow rate. (This same result was observed for the tar).

These data were obtained from base case experiments where the bed temperature in stage-1 is increased at 3°C/min to 550°C and then held at 550°C for 30 minutes. Only the non-isothermal data have been plotted in Figs. 3-6 and used in the modeling calculations. The gas data are fit to a single reaction first-order model and also to a multiple independent-parallel reaction model, in the same manner as the tar data. The kinetic parameters obtained from a least-squares fit are given in Table 3, below.

TABLE 3. LIGHT GAS FORMATION/KINETIC PARAMETERS

Gas	A (1/s)	E (kcal/mole)	σ (kcal/mole)	V^* (wt. % of coal)	RMS Error
- single rxn model					
CH_4	7.52×10^5	30.3	--	1.44	0.073
C_2H_4	2.75×10^5	29.2	--	0.13	0.027
C_2H_6	3.05×10^6	31.6	--	0.51	0.054
C_3's	8.90×10^{11}	48.6	--	0.12	0.085
- multiple rxn model					
CH_4	4.68×10^{11}	50.0	2.5	1.59	0.064
C_2H_4	2.79×10^{12}	53.1	2.8	0.14	0.020
C_2H_6	$+1.00 \times 10^{13}$	52.9	2.1	0.53	0.047
C_3's	7.33×10^{13}	55.0	1.2	0.13	0.081

[+]indicates a parameter which is fixed during the fitting routine

With the exception of methane, both models describe the data fairly well although the multiple parallel reaction model gives more reasonable parameters (A and E), a better overall fit to the data (smaller RMS error), and a value of V^* that is closer to the experimental value. For methane, it appears that there is an overlapping set of reactions which cannot easily be fit with a single reaction or a Gaussian distribution of reactions. Other studies have fit methane formation data with a set of 2 to 4 parallel first-order reactions (8,9,10). A similar approach has been used for other gases, when necessary.

Gas Formation from Tar Cracking

A determination was made of how well the kinetics for "secondary" CH_4 and C_2H_4 formation in the volatile cracking experiments agreed with the kinetics for disappearance of tar based on the three-lump model. Only CH_4 and C_2H_4 were examined because these gases are the most stable, being resistant to secondary cracking at temperatures below 800°C. For the same reason, only low-temperature (<800°C) tar cracking and secondary gas formation were considered. This regime corresponds to decomposition of the "A" lump in the 3-lump cracking model discussed above (see also Fig. 2).

These two gases account for about 1/3 of the products of low temperature decomposition, while an additional 1/3 is estimated to be light oil (4,5). However, the light oil (primarily benzene, toluene, and xylenes) is not as easily quantified due to difficulties in collection, so it was not considered in this analysis.

The yields of secondary CH_4 and C_2H_4 were determined by subtracting their corresponding base case yields (no cracking stage) from their yields in a homogeneous cracking experiment. These results are plotted in Figs. 7 and 8, for CH_4 and C_2H_4, respectively.

The kinetic analysis was done by fixing the preexponential factor at the value obtained for the "A" lump of tar. Then the V^* was fixed at a value corresponding to the yield at 750°C and a regression analysis was done to calculate the value of the activation energy. The results are given in Table 4.

TABLE 4. SECONDARY REACTION KINETIC PARAMETERS

SPECIES	A (1/s)	E (kcal/mole)	T^* (wt % of tar)	V^* (wt. % of coal)
− Secondary Formation				
CH_4	+1.25x10^9	40.2	+4.6	+1.1
C_2H_4	+1.25x10^9	39.4	+5.8	+1.4
− Secondary Decomposition				
"A" tar	1.25x10^9	39.4	+33.0	+8.0

+indicates a parameter which is fixed during the fitting routine.

In both cases, the value of the activation energy was very close to that for decomposition of lump "A."

These results indicate that:

1) The additional ethylene and methane formed in secondary reactions are predominantly from tar cracking rather than cracking of other gases. This

result supports one of the key assumptions of the reactor system;

2) The two gases are formed from tar by breaking bonds of similar strength and/or type, which supports the concept of dividing the tar into "lumps" containing bonds of similar reactivity.

Comparison of Gas Formation from Coal Pyrolysis and Tar Decomposition
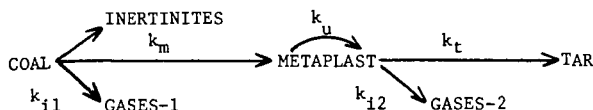
It is instructive to compare the rate constants for the formation of CH_4, C_2H_4, C_2H_6, C_3's, and tar from the primary pyrolysis of coal with those for the low-temperature (vapor-phase) decomposition of tar to form CH_4 and C_2H_4 (among other products). These are plotted in Fig. 9 for the temperature range of 300 to 700°C. The rate constants were calculated from the Arrhenius parameters in Tables 3 and 4. Because of the similarity of the parameters for secondary formation of CH_4 and C_2H_4 from tar with those for the overall decomposition of tar (lump "A"), only the latter values were used.

One conclusion from this plot is that, even at relatively low temperatures (350-500°C), the intrinsic rate of tar decomposition to form CH_4, C_2H_4, etc., is greater than or equal to the intrinsic rate of formation of these gases from primary pyrolysis of the coal. This result is not surprising, in light of the fact that these gases are formed from cracking of side chains of aromatic units in either case. The only difference is that the side chains are attached to a volatile species in the case of tar. The fact that the rate of gas formation from tar is actually somewhat greater than that from the coal can be explained based on the sequence of product evolution indicated in the composite plot shown in Fig. 10. It is apparent that significant light gas formation occurs after the maximum rate of tar evolution has ended. Consequently, it would be expected that the viscosity of the coal melt would be increasing as the evolution of light gas proceeds. It is known that the rates of bond homolysis reactions in the gaseous and liquid phases are generally the same within a factor of 2, but the latter tend to decrease with increasing melt viscosity due to so-called "cage" effects (11).

Comparison of the Rates of Tar Formation and Tar Decomposition

From Fig. 9, it is also apparent that the intrinsic rate of tar cracking is comparable to or greater than that of tar formation over a wide range of temperature. This fact underscores the necessity of removing the tar quickly from the generation zone in order to prevent cracking of side chains and aliphatic (or etheric) linkages. Failure to do so will result in increased yields of light gases (e.g., CH_4, C_2H_4) and light oil at the expense of tar. Consequently, it would be expected that, in coal pyrolysis, factors which affect the time-temperature history of the tar and/or the escape of tar from the coal will also affect the yield of light hydrocarbon products. These factors would include the heating rate, which can affect both the time-temperature history and the evaporation rate of the tar. (Note: For the purpose of this discussion, it is assumed that the coal of interest is a softening bituminous coal and that the tar does not react further once it escapes from the melt.)

The phenomenon is best understood by first considering the behavior of tar during pyrolysis according to the model proposed by Unger and Suuberg (12) for a softening bituminous coal:

$$\text{COAL} \underset{k_{i1}}{\overset{k_m}{\rightleftarrows}} \text{METAPLAST} \overset{k_u}{\underset{k_{i2}}{\longrightarrow}} \overset{k_t}{\longrightarrow} \text{TAR}$$

INERTINITES ... GASES-1 ... GASES-2

In this scheme, which is well supported by the body of evidence in the literature, the metaplast is the tar precursor. It can be evaporated as tar (k_t), undergo repolymerization to form char (k_u), or give rise to additional gas formation via side-chain cracking (k_{12}). In the case where formation of tar is rate-limiting ($k_t \gg k_m$), it would be expected that an increased heating rate would lead to increased light gas formation since the temperature interval of tar formation would be shifted upward (13) to temperatures where the rate of tar cracking becomes greater than the formation rate (see Fig. 9).

If the evaporation rate of tar is rate-limiting ($k_m \gg k_t$) the light gas yields would be increased over the case of no mass-transfer limitations but would not be sensitive to heating rate, provided that the final temperature is the same in every case. This is a result of the fact that, while the tar is formed at lower temperatures as the heating rate is reduced, it still cannot escape until relatively high temperatures are reached. Consequently, there is ample opportunity for side-chain cracking at any value of the heating rate.

The above hypotheses can be tested by examining some recent work from the literature. Suuberg (13,14) used a captive sample, screen-heater apparatus to study changes in volatiles composition with heating rate for the Pittsburgh No. 8 Seam coal. Over a range from 350–15,000°K/s, no significant effect was observed. Conversely, Stangeby and Sears (15) studied a comparable Canadian coal using a similar system and found a significant increase in CH_4 and C_2H_4 yield as the heating rate was raised from 250 to 6000°K/s. Desypris et al. (16) found the same result for an Australian bituminous coal over the range from 450 to 1800°K/s. In all of the above studies the reactor system, final temperature (~1000°C), and pressure (~1 atm) were similar. However, in the latter two studies a gas flow was superimposed on the screen-heater during pyrolysis to enhance mass-transfer of the volatile species.

This disagreement can be explained based on the presence or absence of mass-transfer effects. In Suuberg's experiment it is likely that the rate of tar evolution was limited by tar evaporation. This conclusion is based on recent studies, using gel permeation chromatography, of tars from a similar experiment (17). In the work of Stangeby and Sears and Desypris et al., it is likely that such limitations were not a factor. This concurs with results from the present study (discussed above) for a gas-swept fixed-bed and explains the sensitivity to heating rate.

While high heating rates can promote tar cracking in experiments where tar evaporation is rate-limiting, they are not always detrimental. If the heating rate is too slow, the low volatility of the tar will cause it to accumulate, thus providing an opportunity for repolymerization reactions to occur. In practice, the reduction in tar yield by this mechanism may be more important than by side chain cracking as evidenced by the dramatic reduction in tar yield and corresponding increase in char yield observed when tar escape is inhibited by increasing the ambient pressure (13,14).

An example of how the heating rate can affect such reactions is the work by Warren (18,19,20), who did a series of studies on pyrolysis of packed beds of coal. It was found that the yield of tar increased at the expense of gas and coke when the heating rate was increased from 0.7 to 21.80°C/min.

A theoretical basis for this phenomenon can be found in the model compound work of Van Krevelen (21). An increase in heating rate was observed to increase the yield of volatiles from pyrolysis of a hydroxyl-substituted polycondensed aromatic system, but had no effect on the unsubstituted polycondensate. Van Krevelen theorized that, in the former case, evaporation of tar competed with repolymerization via hydroxyl groups.

It should be noted that in the high heating rate studies discussed above (14,15,16) the total yield of volatiles was found to be independent of heating rate in all cases. This result implies that the repolymerization reactions are not influenced by heating rate at values above ∿100°K/s.

Conclusions

The above discussion would indicate that there is an optimum heating rate for tar yield. This has been found by Freihaut and Seery (22), who studied the vacuum pyrolysis of a variety of coals in a captive sample reactor at heating rates of $1-10^3$°C/s. They found a variation in tar yield for two high volatile bituminous coals, with an optimum value of 10^2°C/s (for maximum tar yield). Other coals were not nearly as sensitive to heating rate.

In theory, if the rates of tar formation, tar evaporation (which depends on the molecular weight distribution), tar cracking, and tar recombination reactions are well-known, the optimum time-temperature path to maximize tar yield could be predicted. The model proposed by Unger and Suuberg (12) does incorporate most of the important features of the chemistry and transport of tar, but requires better information on the tar molecular weight distribution and the kinetics of tar formation and secondary reactions. The overall objective of the present study is to provide some of the information on tar which is now lacking.

Acknowledgements

References

1. Anthony, D. B., J. B. Howard, H. C. Hottel, and H. P. Meissner, 15th Symp. (Int.) on Comb., p. 1303, 1974.
2. Suuberg, E. M., W. A. Peters, and J. B. Howard, Adv. Chem. Series, No. 183, pp. 239-257, ACS, Washington, D. C. (1979).
3. Serio, M. A., W. A. Peters, K. Sawada, and J. B. Howard, Proc. Int. Conf. on Coal Science, pp. 533-536, Pittsburgh, Pa. (1983).
4. Serio, M. A., Ph.D. Thesis, Dept. of Chem. Eng., M.I.T., Cambridge, Ma., in preparation.
5. Sawada, K., S. M. Thesis, Dept. of Chem. Eng., M.I.T., Cambridge, Ma., 1982.
6. Anthony, D. B., and Howard, J. B., AIChE J., 22, 625 (1976).
7. Unger, P. E., and E. M. Suuberg, ACS Div. of Fuel Chem. Prepr., 28(4), 278 (1983).
8. Weimer, R. F., and D. Y. Ngan, ACS Div. of Fuel Chem. Prepr., 24(3), 129 (1979).
9. Suuberg, E. M., W. A. Peters, and J. B. Howard, Ind. Eng. Chem., Proc. Des. Dev. 17, 37-46 (1978).
10. Campbell, J. J., and D. R. Stephens, ACS Div. of Fuel Chem. Prepr. 21(7), 94 (1976).
11. Stein, S. E., ACS Symp. Ser., No. 169, pp. 98-129, ACS, Washington, D. C. (1981).
12. Unger, P. E., and E. M. Suuberg, 18th Symp. (Int.) on Comb., p. 1203, 1981.
13. Howard, J. B., in Chem. of Coal Util., Suppl. Vol. (M. A. Elliott, Ed.), pp. 665-784, Wiley, 1981.
14. Suuberg, E. M., Sc.D. Thesis, Dept. of Chem. Eng., M.I.T., Cambridge, Ma., 1977.

15. Stangeby, P. C., and P. L. Sears, Fuel 60, 131 (1981).
16. Desypris, J., P. Murdoch, and A. Williams, Fuel 61, 807 (1982).
17. Unger, P. E., and E. M. Suuberg, paper submitted to Fuel (1983).
18. Warren, W. B., Ind. Eng. Chem. 30, 136 (1938).
19. Warren, W. B., Ind. Eng. Chem. 27, 72 (1935).
20. Warren, W. B., Ind. Eng. Chem. 27, 1350 (1935).
21. Van Krevelen, D. W., Coal, Elsevier, Amsterdam (1961).
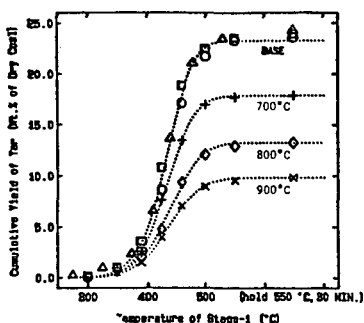22. Freihaut, J. D., and D. J. Seery, ACS Div. of Fuel Chem. Prepr. 28(4), 265
        (1983).

Figure 1. CUMULATIVE YIELD OF TAR vs. FORMATION TEMPERATURE
Data for base case and homogeneous reaction
at 1.1 s residence time; (·····) Multiple
reaction model; Parameters for base case
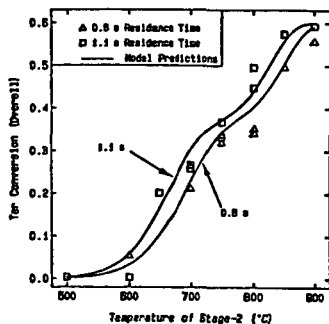are given in Table-1.

Figure 2. TAR CONVERSION FOR HOMOGENEOUS REACTION
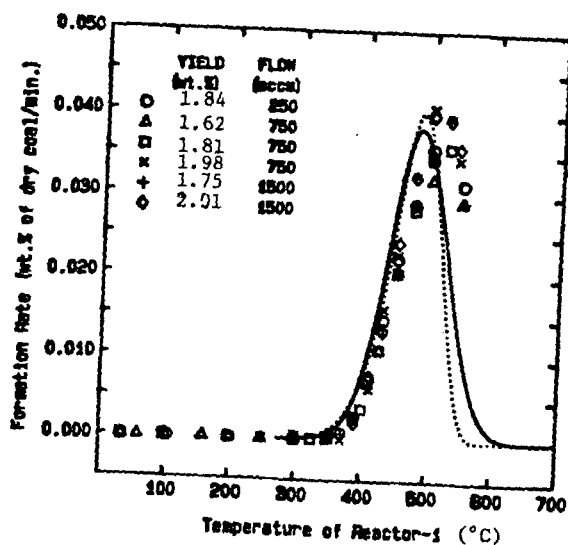Parameters for model are given in
Table-2.

Figure 3 FORMATION RATE OF PRIMARY METHANE
(·····) single reaction model
(———) multiple reaction model
Parameters are given in Table 3.
Yields are experimental values.

Figure 4 FORMATION RATE OF PRIMARY ETHYLENE
(·····) single reaction model
(———) multiple reaction model
Parameters are given in Table 3.
Yields are experimental values.

73

Figure 5   **FORMATION RATE OF PRIMARY ETHANE**
(·····) single reaction model
(——) multiple reaction model
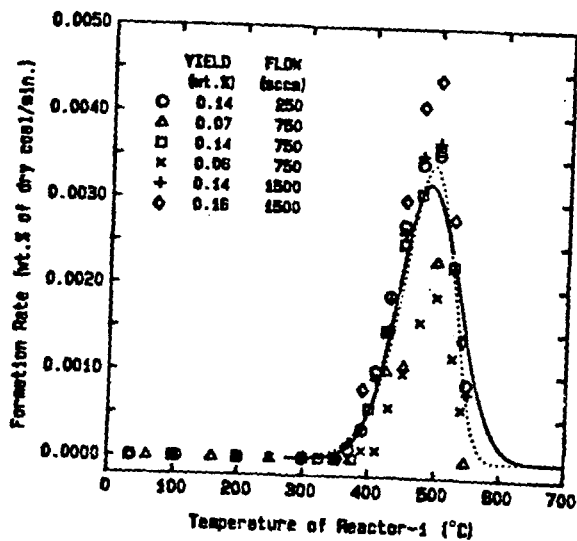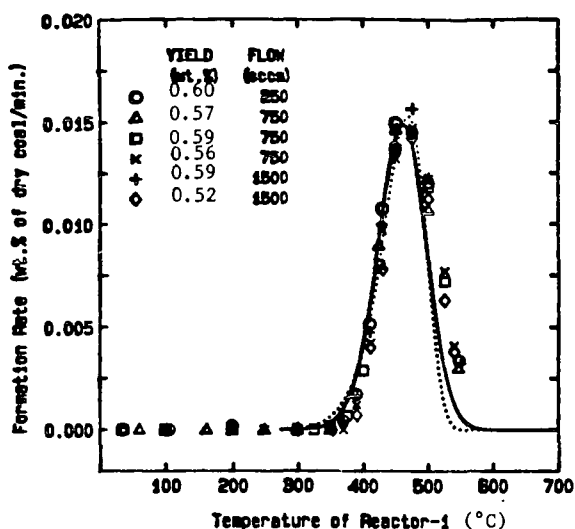Parameters are given in Table 3.
Yields are experimental values.
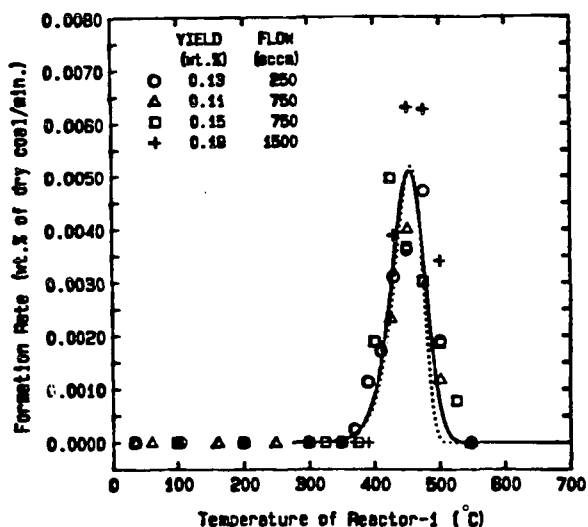
Figure 6   **FORMATION RATE OF PRIMARY PROPANE (AND PROPYLENE)**
(·····) single reaction model
(——) multiple reaction model
Parameters are given in Table 3.
Yields are experimental values.

74
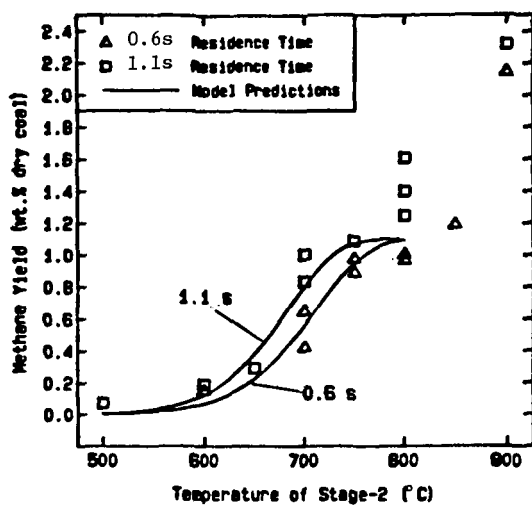
Figure 7 **METHANE YIELD FROM SECONDARY REACTIONS**
Parameters for model are given in
Table 4.
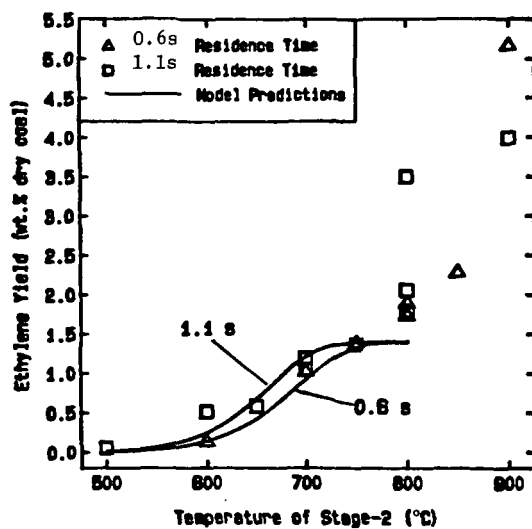
Figure 8 **ETHYLENE YIELD FROM SECONDARY REACTIONS**
Parameters for model are given
in Table 4.

75

Figure 10
FORMATION RATE OF PRIMARY GAS AND TAR

Calculated from parameters in Tables 1 and 3.

Figure 9
RATE CONSTANTS FOR PRIMARY GAS AND TAR FORMATION AND TAR CRACKING

Calculated from parameters in Table 3 and 4.

76

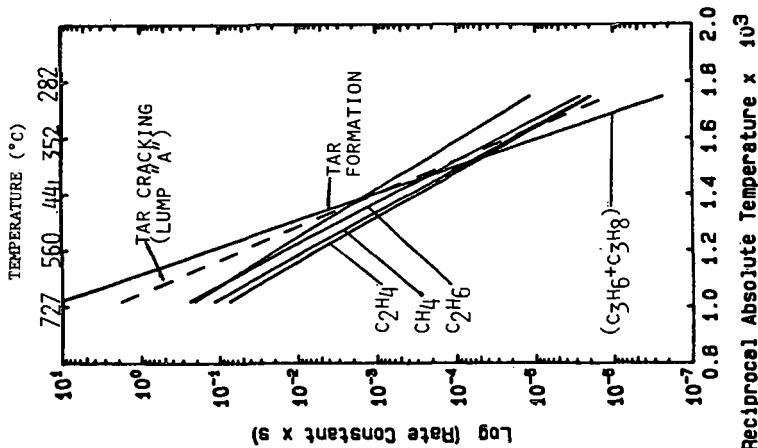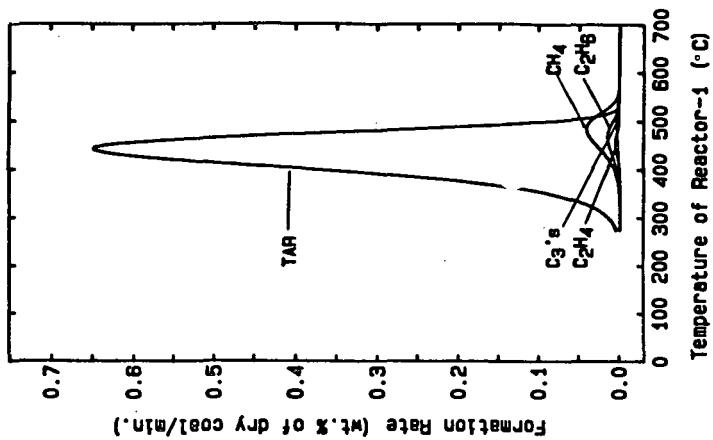# THERMAL EFFECTS ON THE RAPID DEVOLITIZATION OF COAL

O. Morel and F. J. Vastola

Department of Materials Science and Engineering
The Pennsylvania State University
University Park, PA   16802

INTRODUCTION

One of the major difficulties in the calculation of the kinetics of coal pyroly-
sis under conditions of rapid heating is the determination of the temperature history
of the coal during the pyrolysis event. The temperature at which the pyrolysis oc-
curs when a particle of coal is injected into a hot environment is dependent on the
rate of heat transfer to the particle surface and the rate at which heat is trans-
ported through the particle. This latter transfer is further complicated by the
heat adsorbed or released by the pyrolysis reaction as well as phase changes that
can occur within the particle. One method of obtaining data on the thermal response
of coal under rapid heating conditions is to measure the variation in gas temperature
when particles are injected into a hot gas environment where gas convection will
play a significant role in the heat transfer process. By measuring local gas temp-
erature in the vicinity of a particle injected into a hot environment the time of
the heating-pyrolysis period can be measured and an estimate can be made of the rela-
tive contributions of gas convection and radiation to the process.

EXPERIMENTAL

Figure 1 illustrates the design of the captive particle isothermal flow reactor
used in this investigation. Single or multiple particles of coal or char are placed
on a solenoid controlled platform. A rapid withdrawal of the platform allows the
particle(s) to fall into a preheated reaction environment. The time of entry into
the reaction zone is detected by the perturbation of a light beam located at the
entrance of the reaction zone. Preheated He was used as the gaseous pyrolysis en-
vironment. To detect temperature transients induced by sample injection a 0.13 mm
cross section chromel-alumel thermocouple was placed in the reactor in such a manner
that the samples after injection would be extremely close to the thermocouple tip.
The thermocouple output was amplified and the resulting signal was digitized with
a computer controlled 12-bit analog to digital converter. The converter had an ac-
quisition time of 20 μs the sampling period used in this study was 1 ms. The coal
used was PSOC-640 a HVA bituminous coal, its analysis is given in Table 1. Multiple
coal particles in sized ranges of 80-220 μm in diameter and single particles of ap-
proximately 2 mm in diameter were used.

RESULTS AND DISCUSSION

Figure 2 shows the gas temperature in the vicinity of an injected 4.8 mg, 2 mm
coal particle vs time. The reactor temperature was 1072 K and the gas environment
was quiescent He. The second plot was obtained by reinjecting the 2.5 mg char par-
ticle resulting from the pyrolysis of the coal particle. The thermocouple is rapidly
cooled on particle injection then is slowly reheated as the sample and the gas
surrounding the sample approach the reactor temperature. The differences in the
extent of the temperature perturbation between the coal and char are due to the
change in mass resulting from the loss of VM from the coal and the endothermicity
of the pyrolysis process. By slightly changing the position of the thermocouple
for different runs, it was observed that the cooling effect was a localized phe-
nomenon, taking place only in the very close neighborhood of the sample. This in-
dicated that the bulk temperature of the gas remained constant during the pyrolysis-
heating period.

TABLE 1

CHEMICAL DATA FOR HIGH VOLATILE A BITUMINOUS PSOC 640

Analyses, Weight %	PROXIMATE ANALYSIS Dry	DMMF (Parr)
Ash	8.1	
Volatile Matter	37.3	39.6
Fixed Carbon	54.6	60.4

	ULTIMATE ANALYSIS	
Ash	8.1	
Carbon	74.7	83.3
Hydrogen	5.2	5.8
Nitrogen	1.3	1.4
Sulphur	2.8	-
Oxygen (diff)	7.9	9.5

Energy transfer from a hot environment to a particle is by both gaseous convection and thermal radiation. The magnitude of the radiative transfer can be readily estimated. The maximum rate of radiant energy delivered to the particle by its surroundings is equivalent to the energy radiated by the particle at the temperature of its surroundings.

$$P = \sigma \epsilon A T^4 \qquad (1)$$

P = maximum radiative power, W
σ = Stephan-Boltzman constant, 5.67×10^{-8} W/m^2-K
ϵ = emissivity of particle, 0.7
A = area of particle, 1.36×10^{-5} m^2
T = reactor temperature, 1072 K

In this case $P = 0.71$ watts.

The amount of energy required to heat a particle of coal to the temperature of its environment when that temperature is sufficiently high to allow the pyrolysis to go to completion in a measurable time would be:

$$q = M_p C_p \Delta T + M_p \Delta H \qquad (2)$$

where M_p is the mass of the particle, C_p is its heat capacity, ΔT the initial particle-environment temperature difference and ΔH is the heat of pyrolysis. If, for example, the 2 mm particle of the previous calculation was taken and the following characteristics assumed,

$M_p = .0048$ g
$C_p = 1.6$ J/g-K
$\Delta H = 700$ J/g

the energy required to heat the particle from 300 K to 1072 K would be 9.29 J. If this particle was to be heated by radiation alone the heating time would be greatly in excess of that measured experimentally. For the single particle experiments the small contact area of a spherical particle contacting the silica surface of the reactor would tend to minimize the contribution of solid-solid heat conduction. Consequently the major reason for the shortening of the pyrolysis period from that calculated by radiative transfer alone is heat transfer via gas conduction.

78

A more exacting calculation can be made by making an energy balance for the particle taking into account convection, radiation, heat capacity and the heat of pyrolysis.

$$hA_p(T_g-T_p) + \sigma A_p \epsilon_p(T_w^4-T_p^4) + RH_p = M_p C_p dT_p/dt \tag{3}$$

The values used to model the 2 mm coal and char particles in Figure 2 are:

h = heat transfer coefficient, W/m^2-K
A_p = area of particle, 1.36×10^{-5} m^2
T_g = gas temperature, 1072 K
T_p = particle temperature, K
ϵ_p = particle emissivity, .7
T_w = wall temperature, 1072 K
R = pyrolysis rate, g/s
H_p = heat of pyrolysis of coal, 700 J/g
M_p = mass of particle, coal .0048 g, char .0025 g
C_p = particle heat capacity, J/g-K.

The heat capacities of coal and char as a function of temperature were obtained using the following equation:

$$C_p(T) = a + bT + cT^2 + dT^3 + eT^4 \tag{4}$$

Coal		Char	
a	− 0.685	a	2.673
b	9.235 x 10^{-3}	b	2.617 x 10^{-3}
c	− 1.262 x 10^{-2}	c	1.169 x 10^{-5}
d	7.865 x 10^{-3}		
e	− 1.85 x 10^{-12}		

The data used for fitting the equation for coal was extrapolated from that given by Merrick (1). The heat capacity of graphite (2) was used to approximate that of char. The rate of pyrolysis was assumed to be a first order reaction with a pre-exponential of 10^{-5}/s and an activation energy of 83.6 kJ/gmole.

This model was able to fit the temperature profile of a single coal particle and when setting the reaction term to zero the profile of the reinjected char particle. Figure 3 shows the experimental thermocouple response for the injection of a 2 mm diameter char particle, curve a, along with the calculated particle surface temperature profile, curve c. During the temperature perturbation experiments, the thermocouple was not measuring the temperature of the particle surface but rather a temperature intermediate between that and the temperature of the bulk gas,

$$T_{AV} = \frac{mT_g - nT_p}{m + n} \tag{5}$$

where n and m > 1. This equation represents a weighted average between the bulk gas and the particle surface temperature. These values were adjusted to fit the experimentally measured temperature, curve b. This correction does not change the calculated particle temperature history but only adjusts the calculation to give the gas temperature at a given distance from the particle surface. A similar calculation was used to model the data obtained from the injection of a 2 mm particle of coal, in this case the term accounting for the heat of pyrolysis is included in the model. Figure 4 shows the experimental data along with the adjusted model data. Other than the front edge of the experimental temperature curves good agreement is found between the model and the experimental data for both coal and char. The

79

difference on the front edge is a consequence of the thermocouple being at reactor temperature prior to particle injection. In Figure 4 an inflection point can be n seen at the onset of rapid pyrolysis for both the experimental and calculated data.

The heat transfer coefficient, h which was used as the main adjustable parameter in the model, gave the best fit value, 123 W/m^2-s. Using this value the maximum convective heat flux would be,

$$q = hA\Delta T = 1.28 \text{ W} \tag{6}$$

this value is greater than the maximum radiative heat flux calculated in equation (1), 0.71 W. Under these circumstances convective heat transport is playing a dominant role.

Although many assumptions on values have to be made in the model, the values used in the calculation and the values obtained from the model do not appear unrealistic. However, the experimental measurement of significant temperature depressions in the vicinity of the injected particle is strongly indicative of the major role played by gas thermal transport.

When groups of small sized particles (80-500 μm) were introduced into the reactor, it was found that the heating times as measured by the thermocouple perturbation were only slightly shorter than that of a single particle of equivalent mass. If resistance to heat transfer occurs in the gas phase surrounding the particle, a temperature gradient would be expected to be found extending some finite distance from the particle surface to the bulk gas phase. If the particle density is such that the distance between particles would be less than the thickness of this boundary layer their inter particle interaction will result in longer heating times.

The modeling of the pyrolysis of coal under conditions of rapid heating relies on the knowledge of the temperature history of the coal during the pyrolysis process. From the results of this investigation it can be seen that a significant portion of the pyrolysis of a particle will occur at a temperature considerably lower than the reactor temperature. The assignment of the pyrolysis temperature is further complicated by intra particle temperature gradients. With the data currently available on heat capacity, thermal conductivity and heat of pyrolysis of coal, the temperature history of a rapidly heated coal particle cannot be reliably calculated a priori. It is essential that more accurate data on these properties be obtained.

REFERENCES

1. Merrick, D., Fuel, 62, p. 540 (83).

2. Perry, H. P. and Chilton, C. H., Chemical Engineers Handbook, McGraw-Hill, Fifth Edition.
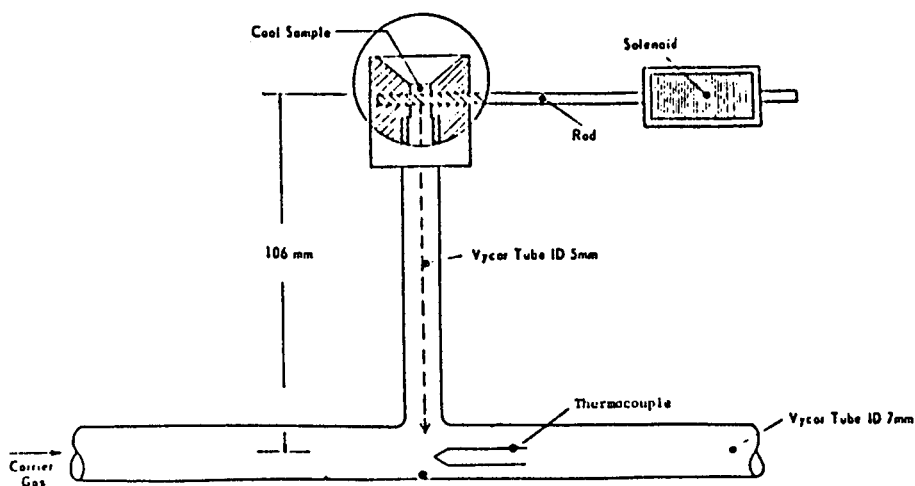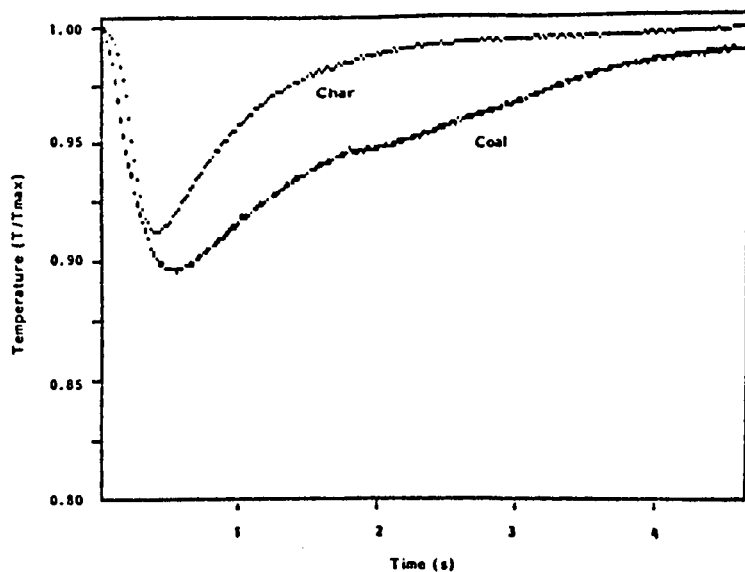
Figure 1. COAL INJECTION SYSTEM

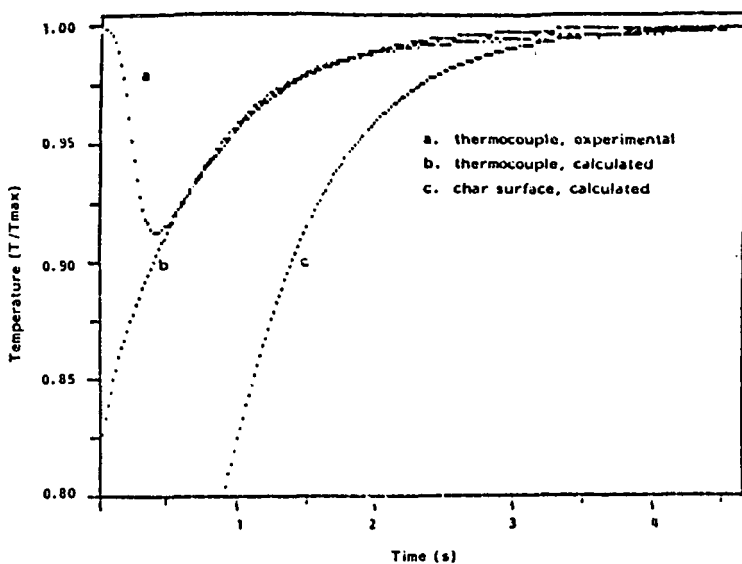FIGURE 2. Temperature perturbation for single char and coal particles.

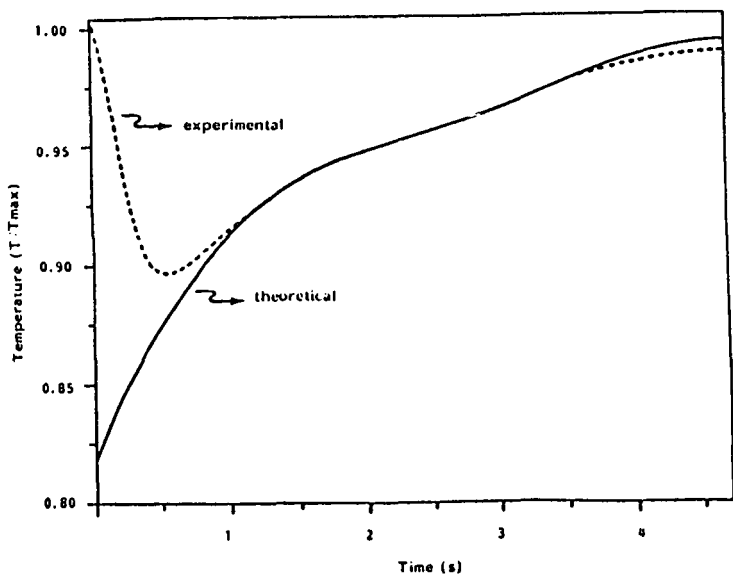FIGURE 3. Temperature perturbation for a single char particle.

FIGURE 4. Temperature perturbation for a single coal particle.

82

THE VARIATION OF COAL PYROLYSIS BEHAVIOR WITH RANK

Peter R. Solomon, David G. Hamblen, Robert M. Carangelo,
James R. Markham and Marie B. DiTaranto

Advanced Fuel Research, 87 Church Street, East Hartford, CT 06108

Coal pyrolysis is important since it is the initial step in most coal conversion processes and is the step which is most dependent on the properties of the coal. Recent reviews of the pyrolysis literature (1-3) present a complicated profusion of results in which it is difficult to identify any simplifying order. The purpose of this paper is to provide some understanding of the diversity in the reported data.

The problem of interpreting kinetic rate constants in coal pyrolysis is illustrated in Fig. 1 adapted from (2). The figure presents a summary of reported rate constants (4-21) for weight loss, most of which are derived assuming a simple first order process. Figure 1 shows that at any given temperature, there is between a two and four order of magnitude variation in reported rate constant, as well as wide variations in slope (acitvation energy). For coal pyrolysis in the absence of external reacting gases, the possible causes for such variations are: 1) coal type; 2) the assumptions used for deriving a kinetic expression; 3) reaction conditions (reaction time, pressure, particle size, heating rate, final temperature and mass transfer rates).

A recent review, (22) considered whether coal type was a cause for such variation. A number of experiments were examined in which coal rank alone was varied. The conclusion of this review was that at low temperature, where chemical kinetic rates can be most easily measured, the rates for hydrocarbon evolution vary by at most a factor of 5 between lignite and bituminous coals. Significant rank variations were also absent in high temperature experiments. Therefore, rank variation is probably the least important cause for scatter.

One cause for variations in reported activation energy is the assumption of a single first order process when a number of parallel reactions with different rates contribute to weight loss. In this case, the use of a single rate constant will lead to anomalously low activation energies. If there are no heat transfer limitations, the rate constant will be reasonable at the temperature of the reaction. This problem has been discussed by a number of investigators (5,18,21-24).

The major causes for rate variations, therefore, appear to be heat and mass transfer limitations. To separate these effects from the chemical kinetic rate, coal pyrolysis was measured in two experiments designed to minimize heat and mass transfer limitations. Coals of different rank were used to provide additional data on rank variations. The first experiment is a constant heating rate experiment in which the coal is heated slowly enough (30°C/min) that heat transfer to the coal particle is not a problem. The major weight loss occurs at about 500°C. The second experiment provides for rapid heating (3 to 5 x 10^4 °C/sec) so that weight loss occurs between 700 and 900°C.

The results of both experiments confirm that variations in coal rank cause at most a factor of 5 variation in the rate constant for weight loss. The latter experiment yields very high rates in line with those reported by Badzioch and Hawksley (4) and Freihaut (15). The result suggests that lower rates reported at these temperatures and comparable rates reported at higher temperatures were due to heat transfer limitations. That is, these experiments have measured the rate of heat transfer to the coal particle, not a chemical kinetic rate constant for weight loss.

SLOW HEATING EXPERIMENT

Pyrolysis was carried out by heating the coal in a wire grid rapidly to 150°C and then at approximately 30°C/min to 900°C. The grid is located within an infrared cell swept by 0.7 liter/min of nitrogen at 1 atmosphere. Infrared spectra of the

evolving products are obtained every 15 seconds with a Nicolet 7199 FT-IR. The spectra for pyrolysis of a coal maceral are illustrated in Fig. 2. Specific regions of the spectra are integrated to give the amounts of a particular gas in the cell as a function of time. The ordinate is proportional to evolution rate. The tar amounts are indicated by scattering of the IR beam which shifts the base line absorbance at high wavenumbers. While the tar measurement is not quantitative, it does indicate the onset, peak and conclusion of tar evolution.

Data for 10 coal samples are presented in Figs. 3 and 4. The data include one repeated experiment for a Pittsburgh Seam bituminous coal and samples of this coal which oxidized during 13 and 504 hours of drying at 110°C. The points are data from individual FT-IR spectra.

Tar evolution (Fig. 3) exhibits the narrowest peak. The rank variations in the temperature of the peak evolution are small. The lignites peak at about 490°C while the highest rank bituminous coals peak at about 530°C. This corresponds to about a factor of 5 in rate. The data can be modeled with a single source with a Gaussian distribution of activation energies (Fig. 3c). This approach to modeling individual species has been discussed previously (22-25). It avoids the anomanously low activation energies obtained from assuming a single first order process. The rate parameters for tar evolution are presented in Fig. 1. The second term in the exponent is the width of the gaussian. The tar rate plotted in Fig. 1 fits the bituminous and subbituminous coals best. It is a little low for the lignite.

The evolution data for heavy aliphatic gases are presented in Fig. 4. The peaks are slightly wider than for tar. The high temperature tail on the peak may be an artifact of the experiment which is caused by gas not immediately swept from the cell. This tail has not been modeled. Rank variations in the data are small. The lowest peak at 500°C is for a lignite and the highest at 540°C is for a high rank bituminous. Rank variations, therefore, can produce a factor of 5 variations in kinetic rate for heavy aliphatics. Aliphatic evolution is modeled in Fig. 4c. The rate parameters are presented in Fig. 1.

Tar and heavy aliphatics typically account for 50 to 75% of the volatiles and up to 90% of the initially released volatiles. Thus, on the basis of the above results, rank variation in initial volatile release must be small.

Data for additional species and analyses of the coals will be presented in (22). Similar rank insensitivity was observed for CH_4, CO, CO_2, C_2H_4 and H_2O.

RAPID HEATING EXPERIMENT

The reactor consists of a 1/4" diameter stainless steel tube which is heated electrically. Coal entrained in cold carrier gas is injected at the top of the tube. The coal is fed using a previously described entrainment system (23,25). The coal-gas mixture enters the heated section of tube and heats rapidly. The heat transfer rate is large because of the small tube diameter and the high thermal conductivity and small heat capacity of the helium carrier gas. After a variable residence time, the reacting stream is quenched in a water cooled section of tube. The product collection train was described previously (23,25). It consists of a cyclone to separate the char followed by a collection bag to collect the gas, tar and soot. The gas from the bag is analyzed by FT-IR and the solids and liquids are collected on the bag surface and in a filter.

The temperature of the gas has been measured with a thermocouple under conditions of constant tube current. At constant current, the tube will reach an equilibrium temperature such that the power radiated is equal to the electrical power input. With gas or coal flowing in the tube, the tube is initially cooler than the equilibrium temperature as heat is used to raise the temperature of the reactants. When the reactants reach the equilibrium temperature, the outside of the tube reaches a constant temperature, so the heating region is directly observable.

Figure 5a shows the measured gas temperature with no coal flow at a tube equilibrium temperature of 800°C. The gas velocity, coal velocity and coal particle temperature have been calculated (Figs. 5a, b and c) as functions of time and distance assuming that the coal provides no additional heat load, (in agreement with only a small change in the observed temperature of the tube exterior when coal is

introduced). The gas velocity is calculated from the measured temperature using the ideal gas law. The coal velocity is obtained by integrating the acceleration determined by applying Stokes and Newton's laws. The heat up time at 800°C is calculated to be approximately 18 msec. The heat up time at 900°C and 700°C are 16 msec and 21 msec respectively. The times required to get from 600°C to equilibrium temperature, are on the order of 3-5 milliseconds.

Results for a North Dakota lignite and an Illinois #6 coal are compared in Fig. 6. The data are for weight loss and aliphatic gas evolution. The aliphatic gas evolution data have been fit using the same rate (see Fig. 1) as for the low temperature experiment. The parameters which describe the species amount are the same as previously used to model these coals in the constant heating rate experiment (22) and in the entrained flow reactor (23,25). No attempt has been made to optimize the parameters for the new data. The fit is good for the Illinois #6 but could be improved with a higher rate (about a factor of 5) for the North Dakota lignite.

The weight loss data have been modeled (lines in Fig. 6c and d) using a previously described theory (23-25) which combines the weight loss due to the evolution of individual species (tar, paraffin, water, CO, etc). There is reasonable agreement with the data. To compare these data to the other data in Fig. 1, a single first order rate constant has been computed. The weight loss is dominated by the tar and aliphatic loss so this "rate constant for weight loss" should be between the rate for these two products as shown in Fig. 1. A minimum possible weight loss rate constant was derived by fitting the data as a single first order process assuming that the particles never accelerated above the initial cold gas velocity and were at the tube equilbrium temperature for the whole distance. This estimated rate is plotted on the low end of the vertical lines at 700, 800 and 900°C. The worst case assumptions, agree with Badzioch and Hawksley (4) and Freihaut (15) which were also done under conditions which favor high heat transfer. A higher rate is obtained by assuming that the coal is at the equilbrium tube temperature only for the time it takes to transit the hot section at the calculated velocity of the coal. This assumption over-estimates the rate because weight loss during heat up is neglected. This rate is plotted as the top of the vertical lines (700, 800, and 900°C). They fall between the aliphatic rate and the tar rate as expected.

DISCUSSION

Based on the information available it is possible to identify the probable cause for much of the scatter in Fig. 1. The data presented here confirm previous suggestions that coal kinetics are relatively insensitive to coal rank, ruling out rank variations as the cause. On the other hand, heat transfer limitations appear to be a primary factor. If the rate for tar evolution presented in Fig. 1 is correct, weight loss will be almost completed in 1 millisecond at 800°C. Any experiment which attempts to get data at higher temperatures must heat the coal from 600°C to the reaction temperature in less than 1 msec, requiring heating rates in excess of $2-5 \times 10^{5}$ °C/sec. The weight loss measured in the entrained flow reactors at temperatures above 800° to 900°C (12,23,25) most likely occurs during particle heat up. Support for this suggestion comes from the observation that the better the heat transfer in the experiment, the higher has been the reported rate. The high heating rate experiments reported here have yielded the highest kinetic rates reported at 900°C. The new data are in reasonable agreement with the data of Badzioch and Hawksley (4) who used very fine coal and Freihaut (15) who dropped small amounts of coal alone, without cold carrier gas into a hot furnace. Both of these experiments provide high heating rates to moderate temperatures. Entrained flow reactor data of Maloney (19) and Solomon and Hamblen (26) show higher rates when helium (which has a high thermal conductivity) is used as the carrier gas rather than nitrogen. If weight loss occurs at temperatures less than the reactor temperature, the reported data would shift to lower temperatures.

This explanation runs into trouble for three experiments (14,16,20) which have measured the coal particle temperature during pyrolysis by two or three color

pyrometry. So, additional discrepancies exist which may be caused by such factors as mass transfer limitations or non-isothermal particle temperatures (a hot particle surface or hot soot or tar surrounding the particle). These possibilities must be examined in more detail.

CONCLUSIONS

1. Kinetic rates for individual species evolution in coal pyrolysis at low and high temperatures are relatively insensitive to coal rank.

2. High kinetic rates were measured at 700 to 900°C when the heat transfer rate is maximized.

3. Lower rates at these temperatures and comparable rates at higher temperatures which have been reported from heated grid and entrained flow reactor experiments were most likely heat transfer limited.

4. Comparable rates reported at higher temperatures in experiments which employ surface temperature measurements by two or three color pyrometry have not been explained.

ACKNOWLEDGEMENT

REFERENCES

1. Anthony, D.B., and Howard, J.B., Coal Devolatilization and Hydrogasification, A.I.Ch.E. Journal, 22, 625, (1976).
2. Howard, J.B., Peters, W.A.; and Serio, M.A., Final Report, EPRI Project No. 986-5, Coal Devolatilization Information for Reactor Modeling, (1981).
3. Howard, J.B., Chapter 12 in Chemistry of Coal Utilization, John Wiley & Sons, New York, (1981), Elliot, M.A.
4. Badzioch, S. and Hawksley, P.G.W., Kinetics of Thermal Decomposition of Pulverized Coal Particles Ind. Eng. Chem. Process Design Develop ,9, 521, (1970).
5. Anthony, D.B., Howard, J.B., Hottel, H.C. and Meissner, H.P., Rapid Devolatilization of Pulverized Coal, 15th Symposium (International) on Combustion, The Combustion Institute, Pittsburgh, PA, (1975) p. 1303.
6. Shapatina, E.A., Kalyuzhnyi, V.V., and Chukhanov, Z.F., Technological Utilization of Fuel for Energy, 1-Thermal Treatment of Fuels, (1960), (Reviewed by Badzioch, S., British Coal Utilization Research Association Monthly Bulletin 25, 285, (1961).
7. Howard, J.B. and Essenhigh, R.H., Pyrolysis of Coal Particles in Pulverized Fuel Flames, Ind. Eng. Chem., Process Design and Develop., 6, 74 (1967).
8. Stone, H.N., Batchelor, J.D., and Johnstone, H.F., Lower Temperature Carbonization Rates in a Fluidized Bed, Ind. Eng. Chem., 46, 274, (1954).
9. van Krevelen, D.W., van Heerden, C., and Huntjens, F.J., Fuel, 30, 253, (1951).
10. Boyer, A.F., Assoc. Tech. de L'Indus. du Gaz en France Congres, (1952).
11. Wiser, W.H., Hill, G.R., and Kertamus, N.J., Kinetic Study of the Pyrolysis of a High-Volatile Bituminous Coal, Ind. Eng. Chem. Process Design Develop. 6, 133, (1967).
12. Kobayashi, H., Howard, J.B., and Sarofim, A.F., Coal Devolatilization at High Temperatures, 16th Symposium (International) on Combustion, p. 411, The Combustion Institute, Pittsburgh, PA (1977).

13. Wegener, D.C., M.S. Thesis, Kansas State Univ., 1978, as reported in
Lester, T.W., Polavarapu, J. Merklin, J.F. Fuel, 61, 493, (1982).
14. Ballantyne, A., Chou, H.P., Orozvo, N. and Stickler, D., Volatile
Production During Rapid Coal Heating, Presented at the DOE Direct
Utilization AR & TD Contractors Review Meeting, Pittsburgh, PA, (1983).
15. Freihaut, J.D., A Numerical and Experimental Investigation of Rapid Coal
Pyrolysis, Ph. D. Thesis, Pennsylvania State University, (1980).
16. Witte, A.B. and Gat, N., Effect of Rapid Heating on Coal Nitrogen &
Sulfur Release, Presented at the DOE Direct Utilization AR & TD
Contractors Review Meeting, Pittsburgh, PA, (1983).
17. Kennedy, J.M., Garman, A.R., Pessagno, S.L. and Krill, W.V., Kinetics of
NO Formation During Early Stages of Pulverized Coal, Presented at the
DOE Direct Utilization AR & TD Contractors Review Meeting, Pittsburgh, PA,
(1983).
18. Suuberg, E.M., Peters, W.A., and Howard, J.B., Ind. Eng. Process Des.
Dev., 17, #1, p. 37 (1978).
19. Maloney, D.G., Ph.D. Thesis, Penn State University, 1983, and Maloney,
D.G. and Jenkins, R.G., ACS Div. of Fuel Chemistry, 27, #1, p. 25,   (1982).
20. Seeker, W.R., Samuelsen, G.S., Heap, M.P. and Trolinger, J.D., Eighteenth
Symposium (International) on Combustion, p. 1213 (1981).
21. Niksa, S., Russel, W.B. and Saville, D.A., 19th Symposium (International)
on Combustion, The Combustion Institute, Pittsburgh, PA, (1982) p. 1151.
22. Solomon, P.R. and Hamblen, D.G., Finding Order in Coal Pyrolysis
Kinetics, DOE Topical Report for contract #DE-AC21-81-FE05122 (1983) and
Progress in Energy and Combustion Science (to be published).
23. Solomon, P.R. and Hamblen, D.G., Measurement and Theory of Coal
Pyrolysis Kinetics in an Entrained Flow Reactor, EPRI Final Report for
Project RP 1654-8, (1983).
24. Solomon, P.R., Hamblen, D.G. and Carangelo, R.M., Coal Pyrolysis,
AICHE, Symposium on Coal Pyrolysis (1981).
25. Solomon, P.R., Hamblen, D.G., Carangelo, R.M. and Krause, J.L., 19th
Symposium (International) on Combustion, The Combustion Institute, Pittsburgh,
PA, (1982), p. 1139.
26. Solomon, P.R. and Hamblen, D.G., Final Report, EPRI Project No. 1654-7,
Characterization of Thermal Decomposition of Coal in Experimental Reactors,
(1982).

TEMPERATURE, °C

Aliphatics $0.17 \times 10^{15} e^{-(30,000 \pm 1500)/T}$

Tar $0.45 \times 10^{14} e^{-(26,400 \pm 1500)/T}$

Bituminous (16)

(13)

(17)

(14)

(20)

(12)

(19)

(19)

Coal "F"
Coal "B" (4)

Tar-1 (18)

53-106 μ
(15)
850-1000 μ

zone 1 (6)
zone 2

(7)

Tar-2
(18)

(5) Bituminous
Lignite

(21)

zone 3

Subbituminous (16)

(8)
zone 1

Brown Coal
Bituminous Coal

(9)

zone 2

zone 3

(11)

(zone 2)

(10)

RATE CONSTANT (k), s⁻¹

RECIPROCAL ABSOLUTE TEMPERATURE, $10^{-3} °K^{-1}$
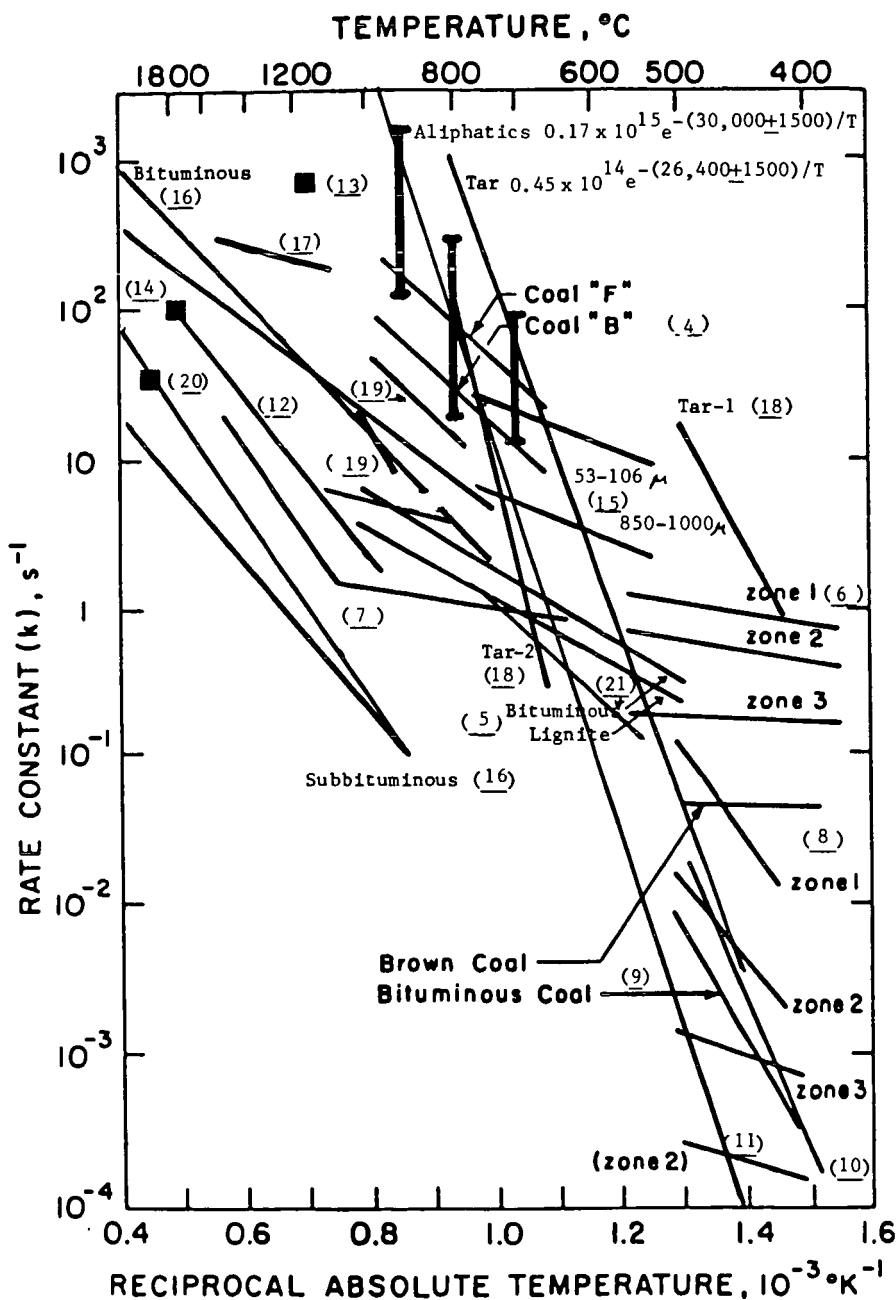
Figure 1. Comparison of Kinetic Rates for Weight Loss (or Tar Loss) from a number of Investigators.
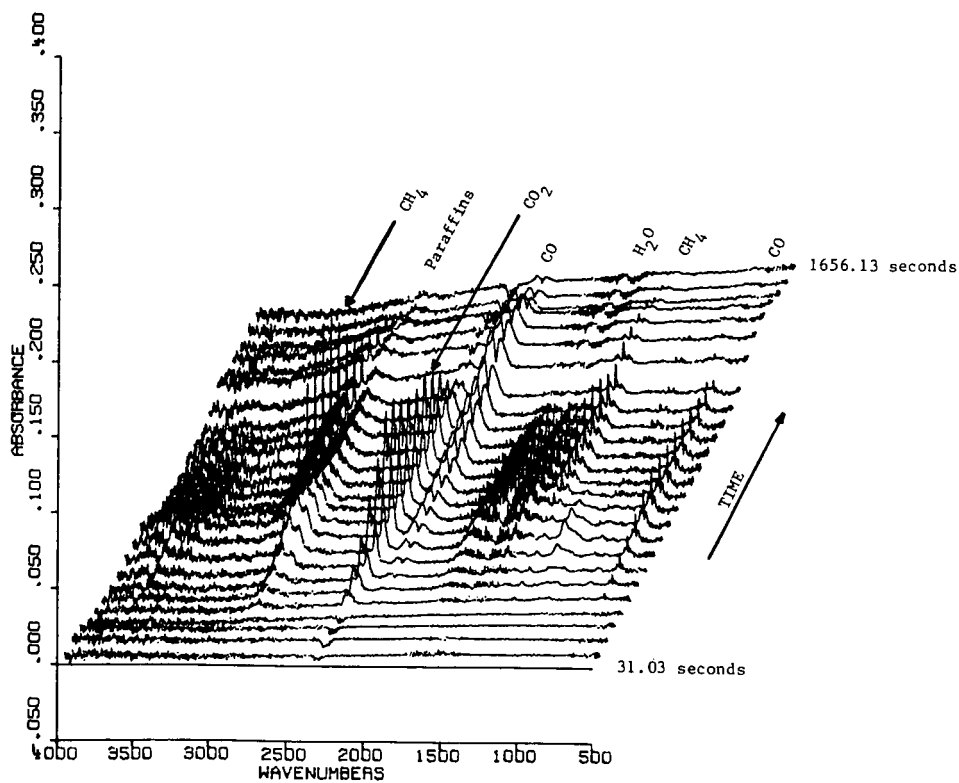
Figure 2. FT-IR Spectra obtained during Pyrolysis for a Pure Vitrinite Maceral in 1 Atmosphere of Nitrogen, Flowing at 0.7 liter/min. The Coal is Heated Rapidly at 150°C and at 30°C/min to 900°C.
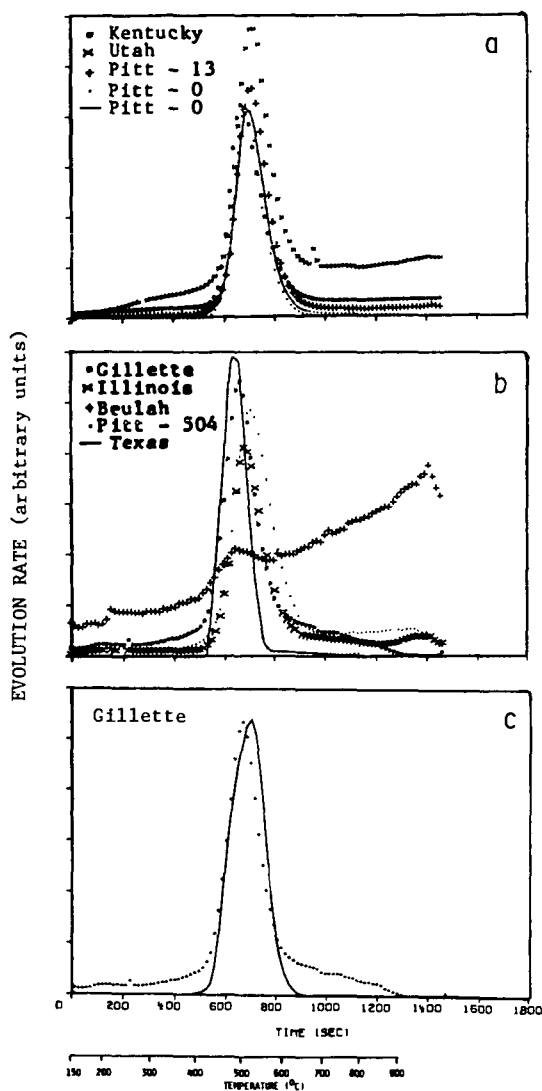
Figure 3. Evolution of Tar for 10 Coal Samples Pyrolyzed in 1
Atmosphere of Nitrogen, Flow ing at 0.7 liter/min. The Coal is
Heated Rapidly at 150°C and at 30°C/min to 900°C.

90
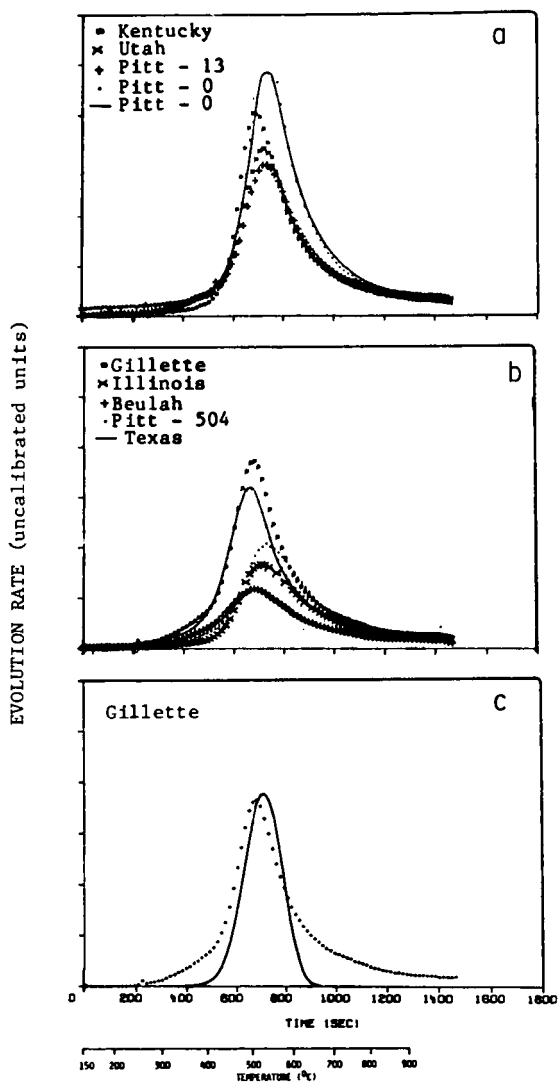
Figure 4. Evolution of Aliphatic Gases for 10 Coal Samples Pyrolyzed in 1 Atmosphere of Nitrogen, Flowing at 0.7 liter/ min. The Coal is Heated Rapidly at 150°C and at 30°C/min to 900°C.
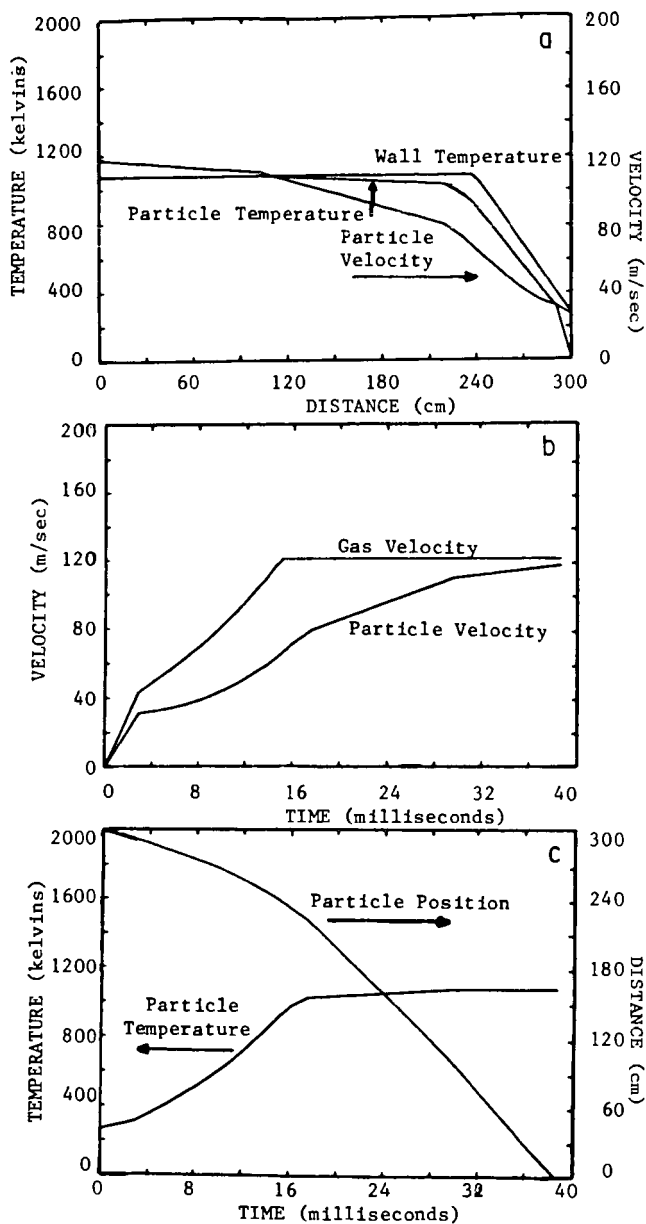
Figure 5. Measured Reactor Wall Temperature
and Calculated Gas Velocity, Particle Velocity
and Particle Temperature as Functions of Time
and Distance.
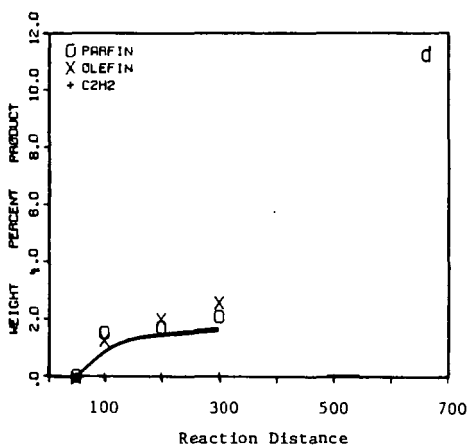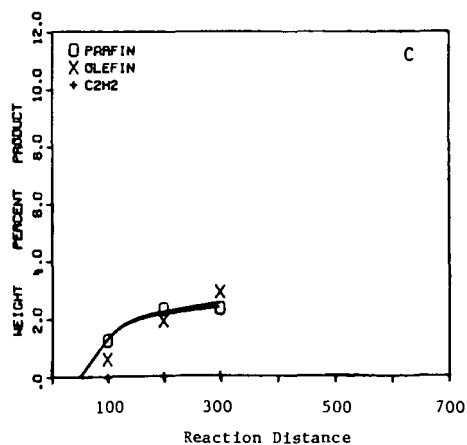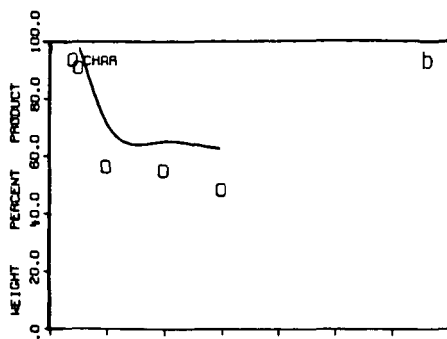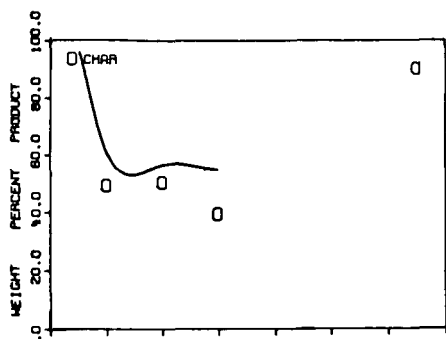
Figure 6. Weight Loss and Evolution of Aliphatic Gases for two Coals Pyrolyzed in the Heated Tube Reactor at an Equilbrium Temperature of 800°C. a and c Illinois #6 and b and d Beulah, North Dakota Lignite.

93

DRYING AND DEVOLATILIZATION OF MISSISSIPPI LIGNITE IN A FLUIDIZED BED

Pradeep K. Agarwal, William E. Genetti, Yam Y. Lee

Chemical Engineering Department
University of Mississippi, University, MS 38677

INTRODUCTION

Fluidized bed combustion offers a means of burning coal and other low grade fuels with high moisture and ash content in an economical and environmentally acceptable way. Fluidized bed combustors can be made to reduce SO_2 and NO_x emission by suitable control of the combustion process eliminating the need for flue gas treatment (1,2).

Low rank coals such as Mississippi lignite contain appreciable amounts of moisture in their "as-mined" state. Hence, lignite particles being introduced into the combustor will undergo several processes before they are completely burned. These processes include, drying (with or without shrinkage), devolatilization, and combustion of volatiles and residual char. All these processes are expected to occur in overlapping time periods and their interactions are not well understood (3).

In this paper, a model is presented which describes the coupled drying and devolatilization of low rank coals in fluidized beds. Experiments are also performed in a three inch ID fluidized bed unit using alumina as bed particles to obtain data for drying and devolatilization of Mississippi lignite. The model predictions are then compared with the experimental data obtained.

BACKGROUND

The complexity of the drying process has led to large disparity between science and application (4). Based on the various mechanisms proposed for the movement of moisture in porous media, and at different levels of complexity and detail, several models have been reported. Dayan (5), however, points out that most of the models proposed may not be valid for intense drying conditions.

In fluidized beds operating at high temperatures, the drying process involves finite sized particles and finite drying times. Hence, semi-infinite strip formulations and asymptotic time domain solutions may not be valid. Moreover, using the reported correlations for gas solid heat exchange within fluidized beds and the thermophysical properties of coal, it may be shown that the heat transfer Biot numbers – for particle sizes and operating conditions of interest in FBC – may also vary within the range of 1 to 20 (6). This implies that instantaneous surface heat-up boundary conditions may also not be valid.

Rigorous and approximate methods for analyses of heat transfer problems with moving boundaries have been reviewed by Mori and Araki (7). Several numerical schemes have been proposed (8). However, numerical solutions have been found to be time consuming and difficult to implement. Additionally convective boundary conditions (of the second kind), which could reasonably describe the intense fluidized bed drying, have been noted to give rise to special difficulties both numerically as well as analytically (9,10).

Extensive reviews dealing with pyrolysis of predried coals are available in literature (11, 12, 13). The majority of the studies have focused on the determination of the kinetic mechanism and parameters using pulverized coal. It is becoming increasingly accepted that the overall coal decomposition kinetics cannot be represented by simple nth order kinetic expressions because of two major reasons. The first is their inability to account for the observed final temperatue dependent yields and the second is the lower activation energies and preexponential factors for the Arrhenius rate expressions (11,12).

Large particle coal decomposition studies, which would involve consideration of the decomposition kinetics as well as transport processes, are comparatively few. Mechanisms proposed include heat (14, 15, 16) as well as mass transfer controlled devolatilization rates (17,18). Available experimental evidence for devolatilization in inert atmospheres suggests that the total devolatilization time would be proportional to d^2, where d is the particle diameter. However, since the transient transport of heat as well as mass is represented in terms of $Fo = \alpha t/d^2$, the experimental evidence does not directly distinguish between heat and mass transfer control.

THE MODEL

The proposed model for coupled drying and devolatilization of coal is based on the models proposed earlier for drying (6) and devolatilization of predried coal (19).

The moisture and volatile species are assumed to be evenly distributed within the spherical particle of radius R_0. The particle is assumed to retain its shape during the process. Devolatilization is assumed to be thermally neutral. Mass transfer is assumed to be rapid. Heat transfer – to and through the particle – is assumed to be the rate controlling mechanism for drying which is assumed to take place from a receding drying (phase change) front constituting a moving boundary. Heat transfer in conjunction with the overall coal decomposition kinetics is assumed to be the rate controlling step for devolatilization.

From the time the wet coal particle is introduced into the fluidized bed, there would be two different stages which are analyzed separately in the following:

Stage 1

When the wet coal particle is introduced into the fluidized bed, drying would commence almost immediately with the moving boundary constituting the drying front moving inwards. The heat conduction equation, with a constant effective thermal diffusivity, may be written for the dry shell region as

$$\frac{\partial T}{\partial t} = \frac{\alpha}{r^2} \frac{\partial}{\partial r} (r^2 \frac{\partial T}{\partial r}) \qquad r_e \leq r \leq R_o \qquad 1)$$

The convective boundary condition (of the second kind) at the particle surface is

$$\left. k_s \frac{dT}{dr} \right|_{r = R_o} = h (T_a - T_s) \qquad \text{for finite h and } T_s \neq T_a$$

$$= a(t) \qquad \text{in general} \qquad \Biggr\} \quad 2)$$

At the receiving wet dry interface, a heat balance leads to

$$k_s \frac{dT}{dr}\bigg|_{r = r_e} = \lambda \; C_o \, \rho_s \frac{dr_e}{dt} \tag{3}$$

The moving boundary may be immobilized by a transformation of the space variable as $\phi = (r - r_e)/(R_o - r_e)$. The temperature profile, assumed to be quadratic with coefficients evaluated by the initial and boundary conditions, may be found to be

$$T(r,t) = T_e + (T_s - T_e)(2\phi - \phi^2) + a(t)((R_o - r_e)/k_s)(\phi^2 - \phi) \tag{4}$$

Use of the heat balance integral approach leads to an equation involving integrals which can be evaluated given the particle surface temperature as a function of time. The assumption that a pseudo steady state formulation (20) may be used to estimate the surface temperature then leads to the following governing equation to describe the drying

$$B\phi_m^3 + (D - E_1 - B)\phi_m^2 + (C - B - D)\phi_m + B - C + E_1 - A.F = 0 \tag{5}$$

where $\phi_m = \dfrac{r_e}{R_o}$ and the coefficients A, B, C, D, E_1 and F are tabulated in Table 1.

TABLE 1. Coefficients of the Governing Equation of Drying (Equation 5)

$A = (\dfrac{T_e + L}{2}) - \dfrac{T_e + 5 T_s \big|_{\theta=1}}{12} + \dfrac{Bi \; \phi_{ms}\big|_{\theta=1}}{12(2\phi_{ms}\big|_{\theta=1}} \dfrac{(T_a - T_e)}{+ Bi \; (1 - \phi_{ms}\big|_{\theta=1}))}$		
$B = \dfrac{\phi_{ms} \; Bi \; (T_a - T_e)}{12 \; (2\phi_{ms} + Bi \; (1 - \phi_{ms}))}$	$C = \dfrac{T_e + 5 T_s}{12}$	
$D = \dfrac{T_e + T_s}{4}$	$E_1 = (\dfrac{T_e + L}{2})$	$F = (\dfrac{\phi_{ms}^2 - 1}{\phi_{ms}\big|_{\theta=1}} - 1)$
$L = \dfrac{\lambda \; C_o}{C_p}$	$\lambda' = \lambda + (T_e - T_o)(C_{pw} + C_p/C_o)$	

The volumetric average fractional devolatilization is given by

$$X_c = \frac{3}{R_o^3} \int_o^{R_o} X \, r^2 \, dr \tag{6}$$

where X is the point devolatilization expression given by the non-isothermal kinetic expression proposed by Anthony et al. (11)

$$X = \int_0^\infty \exp(-k_o \int_0^t e^{-E/RT}) \, f(E) \, dE$$

$$f(E) = [\sigma(2\pi)^{\frac{1}{2}}]^{-1} \exp[-(E - E_o)^2/2\sigma^2]$$

(7)

Recognizing that there would be no devolatilization in the wet region and that $\int_0^\infty f(E) \, dE = 1$, it may be shown

$$X_c = \frac{3}{R_o^3}\left[\frac{r_e^3}{3} + \int_{r_e}^{R_o} [\int_0^\infty \exp(-k_o \int_0^t e^{-E/RT} \, dt) \, f(E) \, dE] \, r^2 \, dr\right]$$

(8)

Equation 8 may be integrated numerically with the temperature profile given by equation 4 to characterize devolatilization in the presence of simultaneous drying.

Stage 2

After the drying is completed, the particle would still devolatilize until the remaining possible devolatilization at the operating temperature is completed. Writing the heat conduction equation with time $t' = t - \tau$, where τ is the time required for the completion of drying

$$\frac{\partial T}{\partial t'} = \frac{\alpha}{r^2} \frac{\partial}{\partial r} (r^2 \frac{\partial T}{\partial r}) \qquad\qquad 0 < r < R_o$$

(9)

The boundary conditions for finite Biot numbers may be written as

$$k_s \frac{dT}{dr}\Big|_{r = R_o} = h(T_a - T_s)$$

$$\frac{dT}{dr}\Big|_{r = o} = 0$$

(10)

The initial condition is derived from equation 4 with $r_e = 0$. Then

$$T(r, t' = 0) = T(r, t = \tau) =$$

$$T_e + (T_s\Big|_{\theta=1} - T_e)(2 \, (\frac{r}{R_o})^2 - (\frac{r}{R_o})) + a(t)\Big|_{\theta=1} (\frac{R_o}{k_s})((\frac{r}{R_o})^2 - \frac{r}{R_o})$$

(11)

Following the analysis methods described by Jakob (21), it is possible to show that during this stage

$$T(r,t) = T_a - \sum_{i=1}^\infty N_i (\frac{\sin \beta_i \, r/R_o}{\beta_i \, r/R_o}) e^{-\frac{\beta_i^2 \, t}{R_o^2}}$$

(12a)

where β_i's are the roots of the equation

$$\beta \cos \beta = (1 - Bi) \sin \beta$$

(12b)

and $N_i = 2 [C_1 A_1 - (2C_2 - C_3)A_2 - (C_3 - C_2)A_3]/A_4$. The expressions for C_1, C_2, C_3. A_1, A_2, A_3 and A_4 are tabulated in Table 2.

TABLE 2. Coefficients Defining Equation 12

$A_1 = \sin \beta_i - \beta_i \cos \beta_i$		$A_2 = \cos \beta_i (\frac{2}{\beta_i} - \beta_i) + 2 \sin \beta_i - \frac{2}{\beta_i}$	
$A_3 = \cos \beta_i (\frac{6}{\beta_i} - \beta_i) + 3 \sin \beta_i (1 - \frac{2}{\beta_i^2})$		$A_4 = \beta_i - \sin \beta_i \cos \beta_i$	
$C_1 = (T_a - T_e)$	$C_2 = (T_s - T_e)$		$C_3 = a(t) \frac{R_o}{k_s}$

The temperature profile given by equation 12 may now be used in the expression for volumetric average fractional devolatilization to characterize the devolatilization in the second stage.

The flow chart of the computational procedure is shown in Figure 1.

EXPERIMENTAL APPARATUS

The fluidized bed used was 7.6 cm in diameter. The bed was filled to a static height of 12.7 cm with 6-10 mesh alumina beads. Preheated air/nitrogen, introduced into the bed through a perforated steel place distributor, was used to fluidize the bed. The air/nitrogen flow rate into the bed and the bed temperatures were measured by an orificemeter and thermocouples respectively. A schematic diagram of the experimental set up is given in Figure 2.

Large chunks of Mississippi lignite were broken and crushed to 4-7 mesh size. Samples were stored in polyethylene bags to prevent loss of moisture and shaken virorously to ensure a homogeneous mixture. Random samples were withdrawn and analyzed on Fischer Proximate Analyzer to determine initial moisture and volatile content (given in Table 3).

A cylindrical cage shaped sampler was constructed from woven mesh (10 mesh aperture size) of steel. The bottom of the sampler was fixed and the top was a removable cap. The sampler was provided with a handle to facilitate insertion into and withdrawal from the bed. The bed was brought up to the required temperature with air as the fluidizing medium. Nitrogen, however, was used during the actual experiment to prevent combustion. The empty sampler was inserted into the bed to permit it to reach the bed temperature. It was then withdrawn, a batch of lignite particles was put into the sampler and the cap closed. The sampler, with the lignite, was inserted within the bed for the desired time period and then withdrawn. The lignite particles were quenched, weighed and analyzed for the residual amount of moisture and volatiles in the Proximate Analyzer. Several readings were taken for each time period to ensure reproducibility.

RESULTS AND DISCUSSION

Experimental data for drying (6) for Mississippi lignite (for temperatures <200°C) and for devolatilization (22) of predried Mississippi lignite (for a different bed particle size and fluidizing velocity) have been reported earlier. The above are the limiting cases for the general model presented in this paper. Hence, the data presented earlier may be viewed in conjunction with the data presented here. The comparison of the data for the coupled process - for drying (O) with model calculations (—) and for devolatilization (◻) with model calculations (— - —) - are shown in Figures 3 and 4. The parameters used in the present model calculations are the same as used in the studies of the phenomena examined separately (6, 22) and are tabulated in Table 3.

<div align="center">

Table 3.

</div>

I. Experimental Operating Conditions:
u = 1.5 m/s $\qquad$ C_o = 0.68 gm/gm dry coal
Initial volatile content = 0.5 gm/gm dry coal
Coal Particle Sizes: 4-7 mesh (average d = 3.8 mm)
T_a = 713°K $\quad$ - $\quad$ Bi ≈ 3.0
T_a = 613°K $\quad$ - $\quad$ Bi ≈ 4.0
II. Kinetic and Thermophysical Properties (6,22)
α = 0.1 mm^2/s $\qquad$ T_o = 283°K $\qquad$ λ = 570 cal/gm
ρ_s = 1.25 gm/cm^3 $\qquad$ T_e = 373°K $\qquad$ C_p = 0.3 cal/gm°K
E_o = 192 kJ/mol $\qquad$ σ = 40 kJ/mol

The agreement of the model calculations with the data is seen to be good. The heat transfer approach, as presented here, is felt to be adequate at least for low rank coals (with low tar yields). A more accurate representation of the phenomena would require the use of the coupled heat and mass transfer solutions to describe the drying. Mass transport may also have to be included in describing the devolatilization of other types of coal with higher tar yields. However, it must be recognized that for FBC there is also the need to couple the phenomena of combustion of volatiles and the residual char. Thus, simplicity in model formulations is essential in order to make a complete analysis tractable. The strength of the model presented here is its ability to provide a reasonably rigorous and computationally tractable base to formulate an integrated approach for describing the various interactive processes occuring during the fluidized bed combustion of wet low rank coals.

NOMENCLATURE

A	coefficient, defined in Table 1
A_1	coefficient, defined in Table 2
A_2	coefficient, defined in Table 2
A_3	coefficient, defined in Table 2
A_4	coefficient, defined in Table 2
a	heat flux at the surface, watts/cm^2
B	coefficient, defined in Table 1
Bi	heat transfer Biot number, dimensionless
C	coefficient, defined in Table 1
C_1	coefficient, defined in Table 2

C_2	coefficient, defined in Table 2
C_3^2	coefficient, defined in Table 2
C_o	initial moisture content, gms moisture/gm dry coal
C^o	specific heat of coal, cal/gm°K
C^p	specific heat of water, cal/gm°K
D^{pw}	coefficient, defined in Table 1
d	particle diameter, mm
E_1	coefficient, defined in Table 1
E	activation energy, kJ mol^{-1}
E_o	mean activation energy, kJ mol^{-1}
F	coefficient, defined in Table 1
Fo	Fourier number, dimensionless
$f(E)$	Gaussian distribution function
h	heat transfer coefficient, cal/sec cm^2°K
k_o	pre-exponential factor in Arrhenius rate expression, sec^{-1}
k_s	thermal conductivity of coal, cal/cm sec°K
N_i	coefficients
R	gas constant, kJ/mol°K
R_o	particle radius, mm
r_e	radial position of the drying front, mm
r	radial position within a particle, mm
T	temperature, °K
T_a	ambient/bed temperature, °K
T_e	temperature at the drying front, °K
T_o	initial particle temperature, °K
t'	$t - \tau$, redefined time variable, sec
t	time, sec
X_c	fractional amount of volatiles retained
X	devolatilization at any point within the volume of the particle

Greek Letters

α	thermal diffusivity of coal, mm^2/sec
ϕ	$(r-r_e)/(R_o-r_e)$, transformed space variable
ϕ_m	r_e/R_o
τ	total drying time, sec
θ	t/τ, dimensionless time
ρ_s	particle density of the coal, gm/cm^3
λ	latent heat of vaporization of water, cal/gm
λ'	defined in Table 1
σ	standard deviation in activation energies, kJ mol^{-1}
β_i	ith root of equation 12b

REFERENCES

1. Yaverbaum, L.H., 'Fluidized Bed Combustion of Coal and Waste Materials', Noyes Data Corporation (1977).

2. Selle, S.J., Honea, F.I. and Sondreal, E.A., in 'New Fuels and Advances in Combustion Technology', Institute of Gas Technology, Chicago, 1979.

3. Jung, K. and Stanmore, B.R., Fuel, 1980, Vol. 59, p. 74.

4. Keey, R.B., in 'Advances in Drying', (Ed. A.S. Mujumdar), Hemisphere Publishing Corporation, Washington, 1980, Vol. I, p. 1.

5. Dayan, A., Int. J. Heat Mass Transfer, Vol. 25, 1982, p. 1469.

6. Agarwal, P.K., Genetti, W.E., Lee, Y.Y. and Prasad, S.N., to appear in Fuel.

7. Mori, A. and Araki, K., Intl. Chem. Eng., Vol. 16, 4, 1976, p. 734.

8. Crank, J. in 'Moving Boundary Problems in Heat Flow and Diffusion', (ed.   ' Ockendon, J.R. and Hodgkins, W.R.), Clarendon Press, Oxford, 1975, p. 192.

9. Tao, L.N., Quarterly J. of Mech. and Appl. Math., Vol. 32, Pt. 2, 1979, p. 175.

10. Shamsundar, N. in 'Moving Boundary Problems', (ed. Wilson, D.G., Solomon, A.D. and Boggs, P.T.), Academic Press, New York, 1978, p. 165.

11. Anthony, D.B. and Howard, J.B., AIChE J., Vol. 22, 4, 1976, p. 625.

12. Gavalas, G.R., 'Coal Pyrolysis', Elsevier Scientific Publishing Co., New York, 1982.

13. Juntgen, H. and van Heek, K.H., Fuel Processing Technology, 2 (1979), p. 261.

14. Peters, W. and Bertling, H., Fuel, Vol. 44, 1965, p. 317.

15. Borghi, G., Sarofim, A.F. and Beer, J.M., paper presented AIChE 70th Annual Meeting, New York, November, 1977.

16. Mills, A.F., James, R.K. and Antoniuk, D., in 'Future Energy Production Systems', Vol. 2, (ed. Denton, J.C. and Afgan, N.H.), Washington, 1976, p. 537.

17. Essenhigh, R.H., J. Eng. Power, Vol. 85, 1963, p. 183.

18. LaNauze, R.D., Fuel, Vol. 61, 1982, p. 771.

19. Agarwal, P.K., Genetti, W.E. and Lee, Y.Y., (Submitted for publication).

20. Agarwal, P.K., Genetti, W.E. and Lee, Y.Y., to appear in Chem. Engg. Comm.

21. Jakob, M., 'Heat Transfer', John Wiley and Sons, New York, 1959.

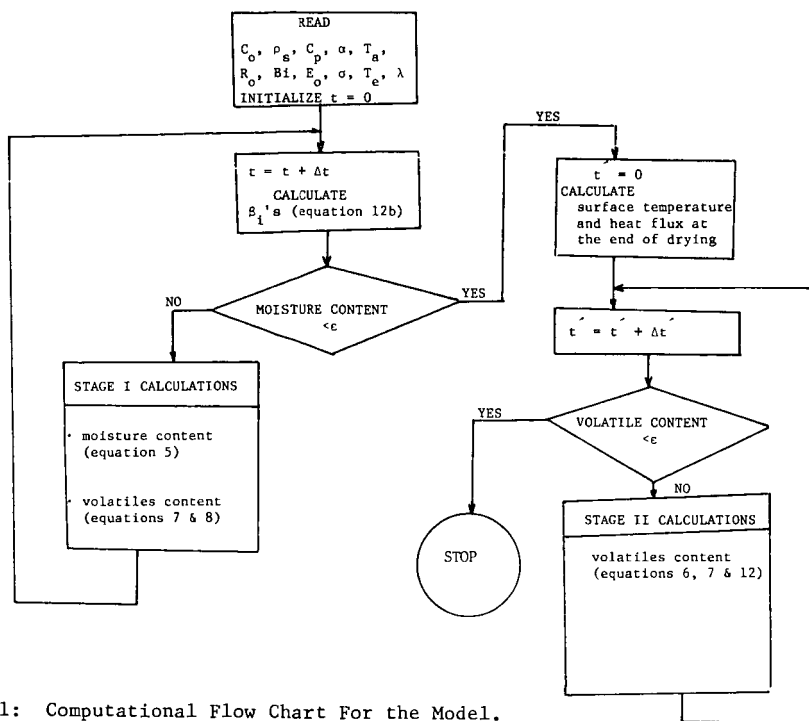22. Agarwal, P.K., Genetti, W.E., and Lee, Y.Y. (Submitted for publication).

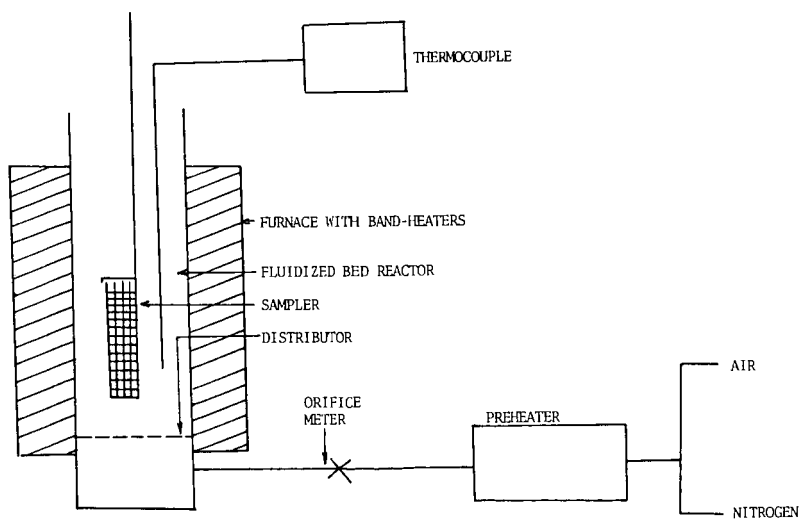Figure 1: Computational Flow Chart For the Model.

Figure 2: Experimental Apparatus Schematic.
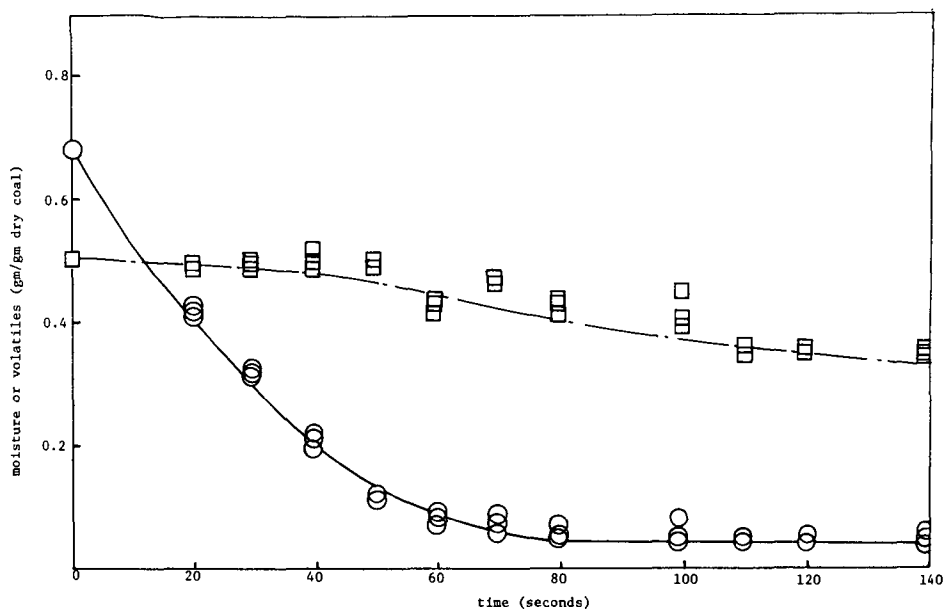
Figure 3: Experimental Data and Model Predictions for Drying (0, —) and Devolatilization (, — - —) at 613°K
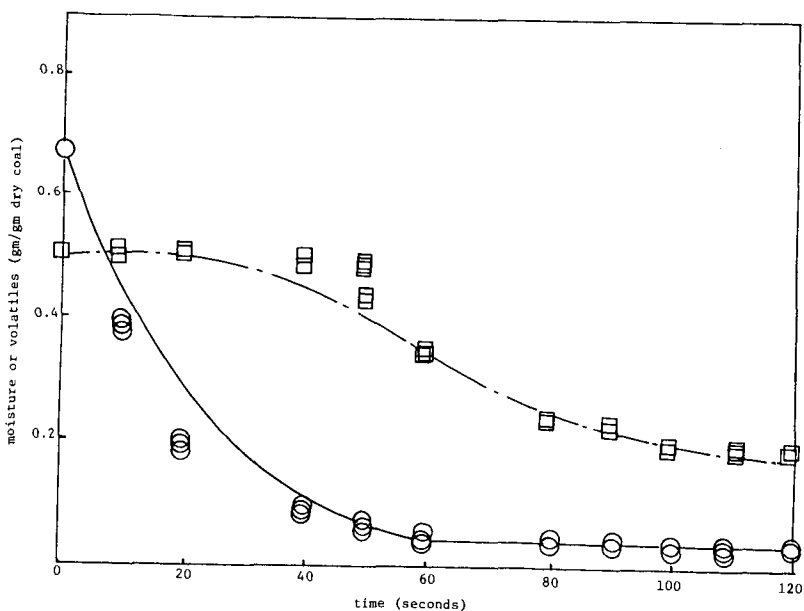

Figure 4: Experimental Data and Model Predictions for Drying (0, —) and Devolatilization (, — - —) at 713°K.

103

COAL LIQUEFACTION BY STEAM PYROLYSIS

Robert A. Graff and Susan D. Brandes

The Clean Fuels Institute, The City College CUNY
New York, NY 10031

Introduction

A key to obtaining high liquid yields in steam pyrolysis of coal has been found to be pretreatment in steam at low temperature. In tests reported here, coal is pyrolyzed in steam at a pressure of 50 atm. by flash heating to temperatures from 870 to 980°C. In the absence of pretreatment about 23% of the coal's carbon is converted to liquid product. If, however, the coal is first exposed to 50 atm. of steam for less than 30 min. at temperatures from 320 to 360°C, over 50% carbon conversion to liquids is obtained in subsequent pyrolysis.

Experimental Methods

These experiments were conducted in a bench-scale batch reactor (Fig.1). In order to obtain rapid heating of coal, the sample is held in an external injection tube while the reactor is brought to temperature under a flow of superheated steam. The reactor is constructed of 2.5 cm i.d., 3.8 cm o.d. 304 stainless steel pipe and is 25 cm. in length. A trap of -8 + 10 mesh quartz chips, 2.5 cm deep, supported by a drilled steel plate is located at the center of the reactor. Heating is provided by an external furnace and electrical windings. Reaction temperature is read from a thermocouple in a well inserted from the bottom of the reactor and in contact with the trap.

Coal, held in the injection tube (5.1mm i.d.) by two quartz wool plugs, is injected into the reactor by a pulse of helium obtained from a 32.5 cc pulse tank charged to 82 atm. by opening a solenoid valve for a nominal 0.1 sec. Upon injection into the incoming stream of superheated steam, the sample is carried downward and deposited on the trap. It is rapidly heated by conduction from steam, radiation from reactor walls, and by direct contact with the trap.

Volatiles released from coal are carried by flowing steam to the reactor outlet and expanded to atmospheric pressure with a residence time of 3 to 5 seconds. A fraction of the product gas stream is conducted to an on-line mass spectrometer for analysis. The only carbon containing gases observed in significant amounts (over 1%) are CO, CO_2, and CH_4. The reaction is terminated by flooding the reactor with helium. Following steam pyrolysis, the residual char is burned with oxygen at 14 atm and the amount of CO_2 produced is used to determine the quantity of carbon remaining in the reactor (the amount of CO produced has been found to be negligible).

This information is used to construct a carbon balance. Total volatile yield is obtained by subtracting carbon determined in residual char from the carbon content of the coal sample charged. The difference between the carbon yields of these gases and the total volatiles yield is ascribed to liquids.

Both pretreated and raw coal are injected into the reactor and pyrolyzed following identical procedures as described above. Pretreatment when desired, is carried out in a preliminary step on the coal charged to the injection tube. An auxiliary heating mantle is

placed around the injection tube which is then heated to above the steam condensation point (264°C) while charged with helium. Steam is then admitted to the reactor, and its flow through the coal sample regulated by the vent valve above the injection tube. Temperature during pretreatment is read with a thermocouple spot welded to the outside of the injection tube and controlled by adjustments to the power supplied to the auxiliary heater and the steam flow. Pretreatment is terminated by lowering the temperature while flushing with helium. The sample may then be injected at any time without any intervening exposure to air.

In separate experiments it has been determined that a 7% weight loss occurs by volatilization during pretreatment. This is reported as part of the total volatiles yield. Even though some fraction of volatile material produced during pretreatment is condensable liquid, this has not been included in the liquid yields given below.

Tests were conducted using a batch of Illinois No. 6 coal ground under inert atmosphere to pass 200 mesh and having the following elemental analysis (wt. %) on a moisture free basis: 69.1 C, 5.2 H, 1.2 N, 3.0 organic S, 9.2 organic O, 12.3 mineral matter.* Coal was charged to the reactor with a moisture content of 2.3%.

From 150 to 250 mg. of coal were charged to the reactor in each run. Charges larger than 250 mg. give lower liquid yields, possibly exceeding the ability of the system to rapidly heat injected material.

Further details of equipment and methods are given in Graff, et al, (1983).

Experimental Results
Fig. 2 shows yields obtained from Illinois No. 6 coal over a range of pyrolysis temperatures both with and without pretreatment. In each case pyrolysis was carried out in pure steam at 50 atm. pressure under rapid heating conditions. When the coal is not pretreated, no more than about 23% of its carbon is converted to liquid, the same as has been reported in the literature for pyrolysis in an inert atmosphere at the same pressure (Howard, 1981). Pretreated samples in Fig. 1 were exposed to 50 atm. of steam for 30 minutes at temperatures from 300 to 360°C. By this pretreatment, at a pyrolysis temperature of about 940°C, the liquid yield is more than doubled and the total volatiles yield is increased by about 20%.

While some variation in temperature during pretreatment could not be avoided, it is possible to give approximate limits within which the procedure is effective. Steam was admitted when the saturation temperature had been safely passed, usually at about 300°C. If the sample was not then allowed to reach at least 320°, little, if any, yield improvement resulted. If a temperature much above 360° was reached at any time, the benefits of pretreatment were lost. These limits are likely peculiar to the coal, the pressure, and the exposure time employed and are expected to be different if any of these parameters are changed.

————————————————————

*We thank Dr. Ronald Liotta of Exxon Research and Engineering Co., Clinton, NJ, for this sample, its preparation and analysis.

For commercial processes shorter pretreatment times will be desirable. This possibility has been tested in a few exploratory runs (Table 1). Two runs were made for 15 min. of pretreatment and two for 5 min. of pretreatment. Yields are more sensitive to pretreatment temperature at these shorter times than for the 30 min. pretreatments. In run E113, the sample was pretreated for 15 min. at temperatures mostly around 320°C. Both total volatiles and liquid yields were considerably lower than for 30 min. pretreatments. Yields were brought into agreement with the 30 min. pretreatment in run E114 by keeping the pretreatment temperature mostly in the 330 to 340°C range. A 5 min. pretreatment, mostly at about 340°C, gave low volatiles yield but good liquids yield (E115). When the sample was held at about 350°C for the 5 min. pretreatment, the volatiles yield was raised to the value obtained in 30 min., liquid yield not determined (E117).

The equipment used here is not suitable for studies of pretreatments less than 5 min. in duration. However, results so far suggest that good liquid yields can be maintained with even shorter pretreatments.

A second series of runs were made to test the effect of sample storage between pretreatment and pyrolysis (Table 2). In runs E93, 95 and 98 batch samples of about one gram were pretreated. After cooling in helium, the light agglomerates which had formed were easily broken up and stored in small vials. During handling and storage, no precautions were taken to exclude air. After the time period noted, the sample was reacted in the usual way. All samples show volatiles yields less than that for untreated coal and liquid yields about the same as untreated coal. One sample (E126) was contacted with air for only 2 min. after cooling in helium. Volatiles yield was slightly higher and liquids yield the same as for untreated coal.

It seems possible, however, to store pretreated coal under inert gas. Storage for four hours in helium (Table 2) gave the same volatiles yield as pretreated and promptly injected coal (E120, no liquids yield available). We have no explanation for the anomalously high yield in E118 and have disregarded this run for the present. A sample stored for 18 hours in helium gave higher yields of both volatiles and liquids than promptly injected coal (E127). However, this sample was heated to 226°C and may have received further exposure to steam in the minutes before injection; verification of the results of run E127 will be required.

Six coal samples have been pretreated in helium at 50 atm. pressure. In the temperature range between 315 and 350°C an increase in volatiles yield is observed over that obtained from raw coal. Whether this increase is as much as that obtained from steam is not yet certain; the one available liquid yield is not better than for untreated coal.

Discussion
In general, scant attention has been given to processes occurring in coal below 350°C. In spite of reports to the contrary (vide infra), the prevailing opinion seems to be that little of interest occurs below this temperature. For example, Brown and Waters (1966) state that initial softening takes place between 350 and 400°C. Similarly, Neavel (1982) gives 350-450°C as the range in which plastic

coals soften and become deformable when heated in an inert atmosphere.
We have observed, however, that our sample of Illinois No. 6 coal
looses volatile matter and becomes lightly agglomerated during the
pretreatment process even at temperatures as low as $320^{\circ}C$.
Consequently, plastic development has at least been initiated. That
this has occurred at an unusually low temperature may be a result, in
part, of the elevated pressure which retards loss of volatiles. Some
chemical, or physical activity of steam may also play a role.
The literature does contain reports of coal activity below $350^{\circ}C$
(Kirov and Stephens, 1967). Berkowitz (1957) reported exotherms
commencing near $200^{\circ}C$ which reached a maximum between 260 and $280^{\circ}C$
and the appearance of slight exotherms around 320 to $340^{\circ}C$ in the
differential thermal analysis of five bituminous and sub-bituminous
coals. Some very pronounced endotherms appear in differential
scanning calorimetry curves at about $300^{\circ}C$ for various coals
(particularly for an HVB coal from Illinois) published by Mahajan, et
al. (1976).
Thermally induced alterations to the organic structure of coal at
low temperature were demonstrated by Chakrabartty and Berkowitz (1977)
using sodium hypochlorite oxidation. Heating of Kentucky hvb coal
samples for 2 hrs. at temperatures as low as $150^{\circ}C$ produced observable
changes in carboxylic acid yields from which it was concluded that
isomerization was already beginning.
Squires, et al. (1983) found that heating of Illinois No. 6 coal
in vacuum caused a reduction in its pyridine solubility beginning at
$200^{\circ}C$. A parallel effect was observed when samples heated in flowing
methanol were subsequently extracted with pyridine.
These literature references suggest that coal is labile at the
temperatures used in the pretreatment process. The limited
volatilization and agglomeration observed in the process may result in
part from bond rupture. Elevated pressure acts to retard volatiles
loss, particularly of heavier species, increasing mobility. This may
improve the accessibility of internal donatable hydrogen to free
radicals formed by thermal rupture (following the discussion of
Neavel, 1982) inhibiting repolymerization and resulting in a partially
depolymerized material. All of these effects could occur during
heating in an inert atmosphere under pressure, and we have observed
increased volatiles yields resulting from such treatment. In steam,
these effects may be enhanced or supplemented by other processes
discussed below.
Pretreated coal has been found to be very sensitive to exposure
to air. Oxidation of coal is known to reduce its plastic properties
and lower liquefaction yields, an effect attributed to the formation
of cross-links. A similar effect may be operative when pretreated
coal is exposed to air. It's extreme sensitivity suggests that the
material is somehow unstable and quite susceptible to cross-linking by
oxygen.
Our observations indicate that steam is considerably more
effective in pretreatment than an inert atmosphere. An explanation
may be found in the work of Ross et al.(1982) who reacted anisole at
$400^{\circ}C$ in 184 atm. (estimated) of D_2O. At this temperature the
calculated half-life of the ether linkage for thermal rupture is 29
hours. Yet, in deuterated steam the observed conversion is about 30%
in 20 minutes. To the extent that anisole is a model for ether-aryl

linkages in coal, this implies that steam has the ability to "depolymerize" coal by cleaving these thermally stable linkages. Ross (1983) has further found that steam, under the same conditions, removes 40% of the coal's oxygen. Although his work was carried out at higher temperatures and pressures, it nevertheless suggests that steam has important chemical activity in the pretreatment process.

Another effect at work in pretreatment is the mutual solubility of water and hydrocarbons. Although mutual solubility is quite low at ordinary conditions, they become miscible in all proportions at high temerpature and pressure (Schneider, 1970). In the naphthalene-water system, for example, the critical solution temperature is as low as 310°C and 100 atm. Even though miscibility may not be complete at pretreatment conditions (the pressure is lower) wide regions of solubility are likely. This would have the following consequences: to the extent that water dissolves in the plastic or molten coal, its mobility is increased thus improving transfer of internal donatable hydrogen. It also places water into intimate contact with coal for chemical reaction, and makes ionic reactions possible. To the extent that large aromatic hydrocarbon fragments dissolve in a water phase, the rate of their repolymerization is reduced by dilution.

Conclusions

From the experimental results and discussion above, we conclude that important changes in the structure of coal occur at temperatures below 350°C. Although a number of potential explanations may be suggested, it seems likely that coal is partially depolymerized during pretreatment, resulting in higher yields of volatiles in a subsequent pyrolysis. The effect is not solely thermal; the presence of water significantly improves product yields.

An evaluation of liquid quality is needed to evaluate the full potential of steam pretreatment. However, provided the liquids are of acceptable quality, the beneficial effects of pretreatment are such as to increase liquid yields in pyrolysis to levels of commercial importance.

Acknowledgement

REFERENCES

1. Berkowitz, N. (1957), "On the Differential Thermal Analysis of Coal," Fuel, 36, 355.

2. Brown, H.R. and Waters, P.L., (1966), "The Function of Solvent Extraction Products in the Coking Process 1 - Yields Properties and Mode of Release of Chloroform Extracts," Fuel, 45, 17.

3. Chakrabartty, S.K. and N. Berkowitz (1977), "Early Stages of Coal Carbonization: Evidence for Isomerization Reactions," ACS Division of Fuel Chemistry Preprints, 22, No. 5, 107.

4.   Deno, N.C., B.A. Greigger, L.A. Messer, M.D. Meyer, and
        S.G. Stroud (1977), _Tetrahedron Letters_, 1703.

5.   Deno, N.C., B.A. Greigger, and S.G. Stroud (1978) _Fuel_,
        _57_, 455.

6.   Graff, R.A. and A.I. LaCava (1983) "Studies Toward Improved
        Techniques for Gasifying Coal," Annual Reports for 1982 and
        1983, USDOE Contract No. DE-AC21-80MC14875, in preparation.

7.   Howard, J.B. (1981) "Fundamentals of Coal Pyrolysis and
        Hydropyrolysis," Ch. 12, p.665 ff, in "Chemistry of Coal
        Utilization, 2nd Supplementary Volume," M.A. Elliot, Ed.,
        John Wiley and Sons, New York.

8.   Kirov, N.Y. and J. N. Stephens (1967), "Physical Aspects of
        Coal Carbonization," Ch. 12, Research Monograph, University
        of New South Wales, Sidney Australia.

9.   Mahajan, OmP., A. Tomita, and P.L. Walker, Jr. (1976),
        "Differential Scanning Calorimetry Studies on Coal. 1.
        Pyrolysis in Inert Atmosphere," _Fuel_, _55_, 63.

10.   Neavel, R.C. (1982), "Coal Plasticity Mechanism: Inference
        from Liquefaction Studies," in "Coal Science," M.L.
        Gorbaty,   J.W. Larsen, and I. Wender, editors, vol. 1, p.
        1, Academic Press, NY.

11.   Ross, D.S. (1983) private communication, November 30.

12.   Ross, D.S., D.F. McMillen, W.C. Ogier, R.H. Fleming and
        G.M. Hum (1982) "Exploratory Study of Coal Conversion
        Chemistry," Quarterly Report No.4, Feb. 19 - May 18,
        p. 26 ff., DOE/PC/40785-4.

13.   Schneider, G.M. (1970) "Phase Equilibria in Fluid Mixtures
        at High Pressures," _Advances in Chemical Physics_, _17_, 1.

14.   Squires, T.G., T. Aida, Y.-Y. Chen, and B.F. Smith (1983),
        "The Role of Thermal Chemical Processes in Supercritical
        Gas Extraction of Coal," _ACS Division of Fuel Chemistry
        Preprints_, _28_, _No. 4_, 228.

Table 1. Steam Pyrolysis of Pretreated Coal.Prompt Injection

| Run No. | Pretreatment | | | Pyrolysis Temp.(C) | Carbon Conversion(%) | | | | |
	Time Min.	Temp. Range(C)	Wt. Loss%		CH$_4$	CO	CO$_2$	Liquids	Total Volatiles
E113	15	301-348	(7)	933	3.9	12.7	12.2	35.9	71.7
E114	15	260-353	(7)	923	2.4	3.7	10.1	54.9	78.1
E115	5	286-340	(7)	918	1.8	1.6	5.6	49.4	65.4
E117	5	313-370		946					82.5

Table 2. Effect of Storage in Air and Helium on Steam Pyrolysis Yields of Pretreated Illinois No. 6 Coal

| Run No. | Pretreatment | | | Storage | | Pyrolysis Temp.(C) | Carbon Conversion(%) | | | | |
	Time (Min)	Temp. Range(C)	Wt. Loss%	Time	Medium		CH$_4$	CO	CO$_2$	Liquids	Total Volatiles
E93	30	265-339	7.8	12 days	Air	920	2.9	5.4	13.7	25.7	55.5
E95	30	289-335	(8)	4 days	Air	914	2.0	5.4	20.7	14.8	53.4
E98	30	289-335		25 days	Air	924					44.5
E118	15	274-358		4 hrs.	He	914					94.0
E120	15	288-377		4 hrs.	He	913					74.9
E126	15	311-358	(7)	2 min.	Air	920	3.9	7.4	20.2	25.5	64.0
E127	15	299-362	(7)	18 hrs.	He	912	3.4	2.1	12.7	61.3	86.5

( ) estimated from direct measurements on other samples.

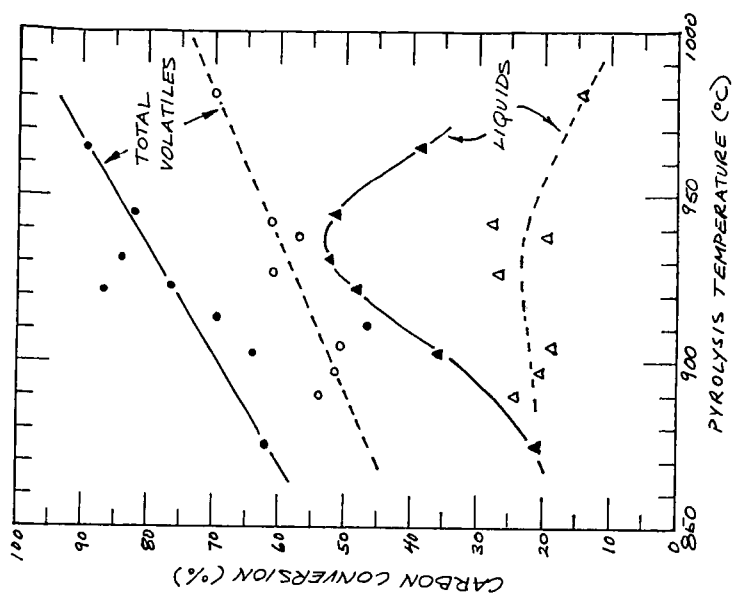Fig. 2. Comparison of Steam Pyrolysis Yields obtained from As-received (open points) and Pretreated (closed points) Illinois No. 6 Coal at 50 Atm.

Fig. 1. Coal Injection Reactor for Pretreatment and Flash Pyrolysis

Coal: Kinetic Analysis of Thermogravimetric Data-(II)
by
M.A. Serageldin and Wei-Ping Pan
Michigan Technological University
Houghton Michigan, 49931

INTRODUCTION

It is customary to use a thermogravimetric analyzer (TGA) to determine the kinetic parameters during coal decomposition. Several workers [1-3] have however, shown that a differential thermal analyzer (DTA) which is used to monitor the change in enthalpy [4] during decomposition can also be used to evaluate the experimental activation energy E, the order of reaction and the pre-exponential factor. This work compares results obtained using a DTA to those obtained using a TGA. For the purpose of statistical evaluation of the variance resulting from using the two methods, the effect of additives was also included.

THEORETICAL

The rate of coal devolatilization may be represented as follows [4-6]:

$$\frac{dC}{dt} = A(1-C)^n \exp[-E/RT] \qquad (1)$$

where dC/dt is the rate of reaction, C is the fraction reacted ($0 \le C \le 1$), A is the pre-exponential factor, n is the order of reaction, E is the activation energy, R is the gas constant and T is the absolute temperature. Equation 1 can be rearranged and modified to incorporate the heating rate, dT/dt:

$$\log_e[(dC/dt)/(1-C)^n] = \log_e[A/(dT/dt)] - (E/RT) \qquad (2)$$

A plot of the left hand side of equation (2) vs (1/T) for various assumed values

112

of n provides a number of curves. The kinetic parameters are obtained when the results fall along a straight line. A number of such curves are shown in Figures 1 and 2. However, the values of n and E shown in Table 1 were machine computed. The assumed values of n were increased from 0 to 2 in fractions of ten. In DTA work C is the ratio of the reaction enthalpy of the sample at given temperature divided by the total sample enthalpy, and is therefore obtained by dividing the area under the peak at this temperature by the total peak area [1] as illustrated in Figure 3.

EXPERIMENTAL

1. ### Material
   A subbituminous coal (-270 and +320 U.S. mesh) was used which was provided by the Institute of Mineral Research at Michigan Technological University. The properties of the coal are given elsewhere [7-8].

   The gas atmosphere was oxygen-free nitrogen and was provided by the Matheson Company. The flow rate was fixed at 50ml/min at STP.

   The additives were group 1A metal salts, certified grade Li_2CO_3 from Research Organic/Inorganic Chemical Corporations; k_2CO_3 (anhydrous) from Fischer Chemical Company; and Na_2CO_3 (anhydrous) from J.T. Baker Chemical Company.

2. ### Apparatus
   A DuPont Differential Thermal Analyzer with a 1200°C was used. The DTA was operated at a linear heating rate of 20° C/min.

RESULTS AND DISCUSSION

Table 1 summarizes values of E and n for the temperature range (523-923K)

obtained using both DTG and TGA, as well as the effect of alkali metal salts.

The corresponding values of n and E obtained using DTA and TGA (method 2) show

little variance. Both methods are similar in that the order of reaction is

determined by trial and error. The better agreement of E values, obtained by

DTA and method 1 (TGA) is interesting considering that in the latter procedure,

n was assumed equal to unity in equation 1.

To determine the significance of the observed variations in the values of

the activation energy resulting from the use of different instruments, methods

and metal salts, the variance was analyzed using an Anaylsis of Variance Table

(Table 2). On the basis of the F-ratio test it was possible to conclude that the

variance due to the methods and instruments was not statistically significant.

However, changing the additive type produced a significant effect.

The good agreement between corresponding values of E and n may have been

due to the similarity of a DTA curve and the curve representing the rate of

conversion (dC/dt) obtained using a TGA [9]. Another factor may have been that

the maximum difference temperature ΔT_{max} and $(dC/dt)_{max}$ occurred at nearly the

same temperatures. This was found to be the case (Table 3), however, ΔT_{max}

occurred at a slightly higher temperature. The thermocouple in DTA work was

touching the sample holder which may have reduced the actual heating rate of the

sample. This was not expected to affect the measured peak temperature due to

the small radius of the sample [10]. The shape of the sample holder and loose

packing in the case of the TGA provided better contact between the flowing gas

and the sample, which may have accounted for the occurence of $(dC/dt)_{max}$ at a

lower temperature.

Two other DTA methods [2,3] for measuring E and n were also considered and

found to be less attractive than the method adopted in this work. Both involved

114

measuring an inflection temperature, T_i, and the temperature at which ΔT_{max} occurred off a DTA thermogram. It was therefore to be expected that the precision would be low. This was especially true when plots were small or not very smooth. Also, in the method proposed by Kissinger [2] two thermograms were required to evaluate E and therefore, the results would depend on the heating rate combination used [5].

CONCLUSIONS

A DTA thermogram may be used to obtain kinetic data given that the variance between DTA and TGA results was statistically insignificant.

References

1. Haddadin, R.A. and Tawarah, K.M., Fuel, 59 (1980), p.539.

2. Kissinger, H.E., J. Res. Nat. Bur. Standards, 57(1956), p.217.

3. Yang, R.T. and Steinberg, M., J. Physical Chem. Vol. 80, No. 9, (1976) p.965.

4. Wendlandt, W.W., "Thermal Methods of Analysis," 2nd Edition, John Wiley and Sons, N.Y.(1974).

5. Serageldin, M.A. and Pan, W.P., "Coal: Kinetic Analysis of Thermogravimetric Data," To be published in Thermochimica Acta.

6. Flyn, J.H. and Wall, L.A., J. Res. Nat. Bur. Standards, 50A(1966), p.487.

7. Serageldin, M.A. and Pan, W.P., "Coal Analysis Using Thermogravimetry," Presented at the 185th ACS Seattle Meeting, March (1983).

8. Serageldin, M.A. and Pan, W. P., Proceeding of the 32nd Canadian Chemical Engineering Conference, Vancouver, Canada, Vol. 1(1982), p.442.

9. Murray, P. and White, J., Trans. Brit. Ceram. Soc., 54(1955), p.204.

10. Melling, R., Wilburn, F.W. and McIntosh, R.M. Anal. Chem., Vol. 41, No. 10(1969), p.1275.

Table 1

Kinetic Parameters: Influence of Method and Alkali Metal Salts

Experimental	TGA [7]				DTA	
Conditions	Method 1		Method 2			
	n	E_{II}	n	E_{II}	n	E_{II}
Coal	1.0	50.9±2.3	0.52±0.04	46.1±1.2	0.6	51.2±2.7
Coal + Li_2CO_3	1.0	35.2±3.1	0.38±0.04	41.7±0.9	0.4	39.6±2.2
Coal + Na_2CO_3	1.0	45.6±2.5	0.44±0.04	43.1±1.1	0.5	46.6±2.6
Coal + K_2CO_3	1.0	49.1±2.3	0.48±0.04	45.0±1.1	0.5	50.4±2.6

E= KJ/mol ; n=order of reaction

Table 2

Analysis of Variance Table (ANOVA)

Source of Variation	Degree of Freedom	Sum of Squares	Mean Square	F-ration	F-ratio (from table)
Additives	3	200.59	66.86	9.35	$F_{3,6,0.95}=4.76$
Methods	2	17.88	8.94	1.25	$F_{2,6,0.95}=5.14$
Error	6	42.89	7.15		
Total	11	261.36			

Table 3

Furnace Temperatures at Which ΔT_{max} and $(dm/dt)_{max}$ Occurred

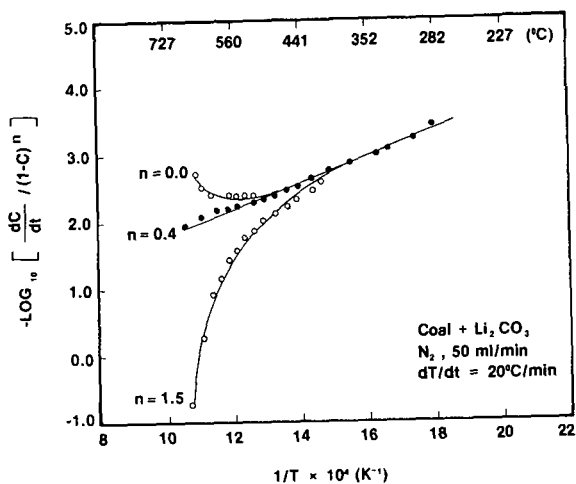| Experimental Conditions	TGA [7] $(dm/dt)_{max}$	DTA ΔT_{max}
Coal	720K	753K
Coal + Li_2CO_3	698K	728K
Coal + Na_2CO_3	708K	743K
Coal + K_2CO_3	713K	748K

116

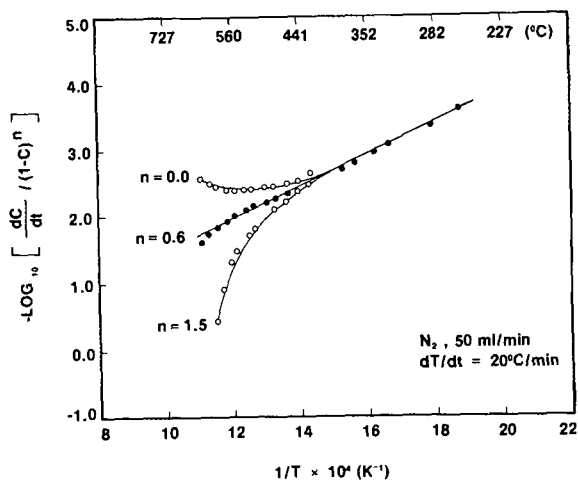Figure 2: Plots of nth order equation for coal – Li_2CO_3 mixture

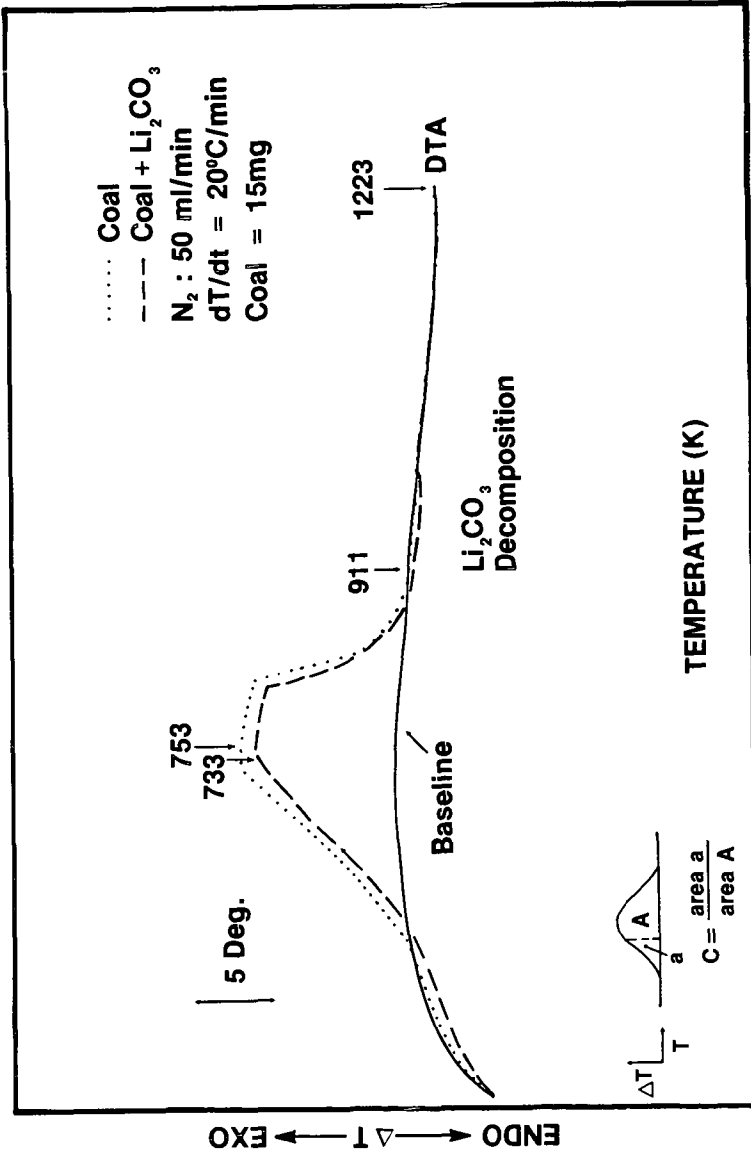Figure 1: Plots of nth order equation for coal

117

Figure 3: DTA heating curve for coal
and Li_2CO_3 – coal mixture in nitrogen
($10^5 N/m^2$)

COLD ATMOSPHERE PYROLYSIS OF PULVERIZED COAL USING 10.6μM LASER HEATING

A. Ballantyne, H. Chou, K. Neoh, N. Orozco, D. Stickler

Avco Everett Research Laboratory, Inc.
2385 Revere Beach Parkway, Everett, MA 02149

ABSTRACT

The pyrolysis behavior of three different coals was explored in a unique experimental arrangement that inhibited secondary reactions of the primary volatiles. They were transported as particulate suspensions in room temperature nitrogen, and heated to particle temperatures in the range 1300–1800K at about 10^5K/s by a 10.6μm laser beam. This approach allows well-controlled heating with good time/space resolution, and very rapid thermal quenching of primary volatiles by diffusion into the cold nitrogen. A key result is that gas phase C species account for less than one percent of the coal C although H_2O comparable to the coal moisture content is evolved. Residual solids have proximate and ultimate analyses very close the raw coals but significantly enhanced solubility. It appears that tarry volatiles are produced with minimal change in chemical bonding and recondense in the cold gas flow. This suggests that primary coal volatiles are of high molecular weight, with subsequent gas phase decomposition giving low molecular weight products in hot atmospheres.

INTRODUCTION

The extensive measurements of coal devolatilization performed over the past two decades have almost exclusively employed conductive heat transfer from a hot environment to the coal sample under test[1-5]. This results in a significant volatile residence time in a hot environment, relative to the time scale required for particle devolatilization. Consequently, it is difficult to give assurance that the observed product species are in fact primary volatiles. It is also unclear to what extent the composition of the gas environment used in various experiments affects primary volatile yield, and to what extent it reacts at elevated temperatures to stabilize volatiles as lower molecular weight or hydrogenated species.

It has also proven to be difficult to explore heating rate and temperature regimes corresponding to pulverized fuel combustion or entrained flow gasification, typically in the range 10^4-10^6 K/s, and with peak temperature approaching 2000K. Heated grid experiments have been limited in absolute heating rate and peak temperature, and leave some uncertainty regarding coal particle tracking of the grid temperature.[1] Also, the physical scale of the heater and typical experiment time scales suggest that the primary volatiles may be cooled relatively slowly by diffusive mixng. Flow tube reactors of course allow relatively rapid diffusion of primary volatiles away from the parent particle, but into a hot gas environment.[3,4,6] Further, the usual use of hot walls for the reactor renders particle temperature measurement by pyrometry questionable, and predictive approaches based on particle dispersion and heat transfer modeling are quantitatively uncertain.

A third experimental approach uses radiative heating to establish particle temperatures sufficient for devolatilization measurements under high heating rate, high temperature conditions. Initial experiments used pulsed laser heating of relatively large particles, followed by averaged product analysis.[7,8]

Transient thermal diffusion into the bulk sample resulted in a wide range of thermal history contributing to the total yield. The product appeared to range more or less continuously from H_2 to "tars". More recently, the availability of high power, constant output infrared lasers has allowed the development of steady, entrained flow particle heating experiments. This is analogous to a flow tube reactor concept, except that heating is radiative, with the carrier gas and local structures remaining cold.

Radiative heating of an entrained flow of particles allows several gains in experimental environment control and diagnostics.[9] The primary advantage results from particle dispersion in a carrier gas, with gas heating occurring only indirectly, by diffusion from the radiation absorbing particles. This results in complete decoupling of bulk gas temperature from the particle heating rate and temperature. Consequently, primary volatiles diffuse into a cold environment on a minimal time scale. It corresponds to 5ms or less for spherically symmetric diffusion from a 50µm nominal particle diameter in a room temperature N_2 atmosphere. The observed phenomenon of volatile jetting would result in much more rapid cooling. While not instantaneous, the cooling time scale appears to approach a practical minimum. This results in minimum decomposition or reaction of primary volatile species after leaving the parent particle. Use of laser heating of a dilute entrained particle flow also allows the imposition of arbitrary temperature-time profiles by tailoring of the spatial laser beam power distribution. This allows, for example, exploration of the relative effects of heating rate and final temperature on devolatilization behavior, and correspondingly a possible gain in basic understanding of devolatilization mechanisms.

Structurally, the need for a hot walled flow confinement structure is eliminated. For one atmosphere experiments, no wall structure is required, with all flow control based on aerodynamic techniques. This allows very extensive diagnostic and radiative heating access, and eliminates secondary wall radiation as a factor in direct particle temperature measurement.

EXPERIMENT DESIGN

The overall experiment approach was based on the time shared availability of a 15 KW CW CO_2 laser, (Avco HPL®). It provides a continuous output at 10.6µm wavelength, with power level adjustable by the user. It was used to irradiate a dilute coal particle suspension transported in a room temperature gas. Figure 1 shows the key experiment components in block diagram format. They break down into three major groupings: Fluid supply and flow control; radiative heating system; and diagnostics. These are discussed in sequence below.

Fluid Supply and Flow Control

This has as its purpose the establishment of a well defined, steady flow of pulverized coal entrained in a carrier gas. A fluidized bed feeder is used as the primary coal supply, with the feeder supported on a precision electronic balance to give time averaged flow rate information. The coal/carrier stream is delivered to a nozzle designed to homogenize the particle dispersion and give a uniform velocity distribution. Dispersion was checked for space and time uniformity using HeNe beam transmittance, and velocity monitored using an LDV. As shown in Figure 2, a shield flow was also used. Nitrogen was chosen to avoid air entrainment and consequent oxidation reactions with the coal, and velocity matched to the core flow. This coaxial flow passed through the heating and diagnostic volume, and was then collected using an extractor fan and particles filtered out before venting to the atmosphere.
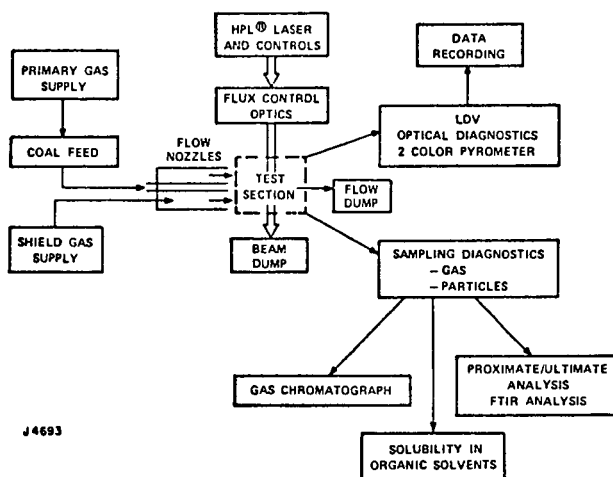
120

Figure 1 - Component Schematic of Experimental System for Steady
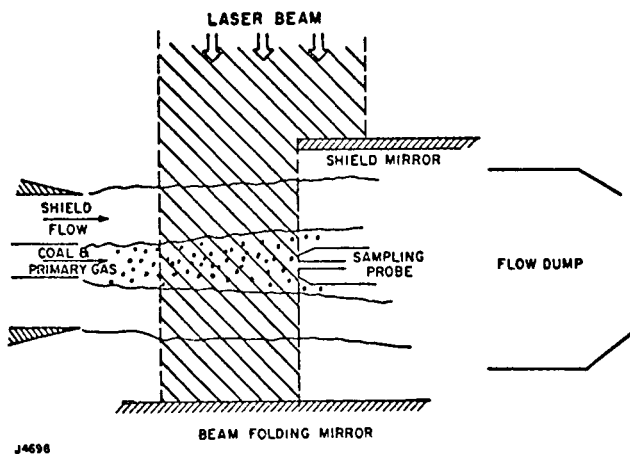Flow Radiative Coal Devolatilization

Figure 2 - Conceptual Schematic of Flow Structure in Radiative
Heating Zone

121

Coal particle loading was chosen as a compromise between uniform radiative heating across the flow, and sufficient concentration to permit quantitative analysis of the expected gas phase volatiles. Dimensions were chosen to ensure existence of an undisturbed potential flow core for measurements over a residence time up to 30ms, with high spatial, and hence time resolution. This is related to particle heating rate and laser beam power as shown in Figure 3. The "Experimental Resolution Parameter" plotted is equivalent to the number of discrete data points obtainable at a given particle heating rate. For fixed input power, higher rate implies a smaller heated volume, which for fixed spatial resolution in the flow gives fewer data points. As shown, heating rates of direct interest to pulverized fuel applications require about 10KW delivered laser power for useful time resolution of data points.

Radiative Heating System

The laser source used delivers an output at 10.6μm wavelength, with power adjustable up to 15KW. The output is spatially nonuniform and requires optical homogenization for this experiment, although not for normal metalworking applications. Optics are fabricated from copper, highly polished, and actively water cooled. A beam integrator was used to spatially overlay multiple segments of the source beam to give a spatially uniform structure. To provide relatively uniform particle heating, this is split into two beams using a roof prism mirror. They are again reflected to cross at circa 160 degrees in the coal flow, defining the heating zone. This gives uniform heating of both sides of the particles, and appears to be an adequate approach to 4π steradian illumination. Uniform particle heating across the flow implies limited beam absorption, resulting in significant (>90 percent) power wastage. This is absorbed on zirconia faced water cooled copper beam dumps, maintained at low temperature to avoid secondary thermal radiation.

Diagnostics

Diagnostic systems include monitoring of input flows and laser power, real time optical measurement of particle conditions, and post-test analysis of gaseous and solid samples. As discussed above, particle flow is monitored using a precision balance with the fluidized bed feeder. Gas flows are set, and monitored using rotameters. Laser power is set at the source, using the HPL^R control system.

Particle conditions are monitored using a single component LDV and a two-color pyrometer. These are mounted with a sampling probe and ancillary shield mirrors on a traverse system, set up to move the sampling point along the flow axis. The physical relationship of some of these components is shown in Figure 4. The velocity measurement is used to relate position to particle heating time scale. It was found, as anticipated, that particle velocity and gas velocity are defined by the nozzle source condition, with downstream heating effects negligible. Particle cloud temperature is monitored using a unique two color pyrometer. It was built around two cooled PMTs with extended red sensitivity ($\lambda \leq 8500A$), and was calibrated in the range 670 to 2000K. Use of a 10.6μm laser heating source, and cooling of the beam dumps to minimize re-radiation, precludes direct optical interference effects.

Interpretation of the pyrometer output signal in this experiment requires a priori knowledge of the particle size distribution, and some modeling of their thermal behavior. Very good spatial resolution, together with extremely low particle loading, could preclude this difficulty by presenting individual particle radiators to the system. This was not feasible for the product sampling approach
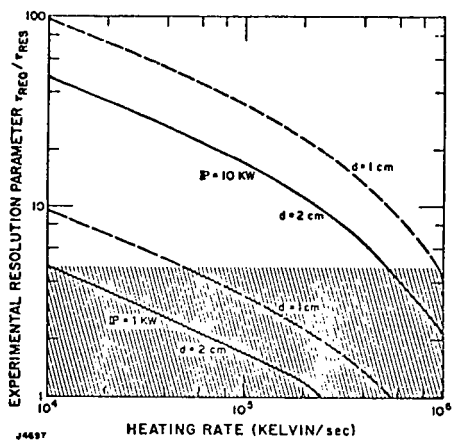
Figure 3 - Dependence of Discrete Sample Resolution on Heating
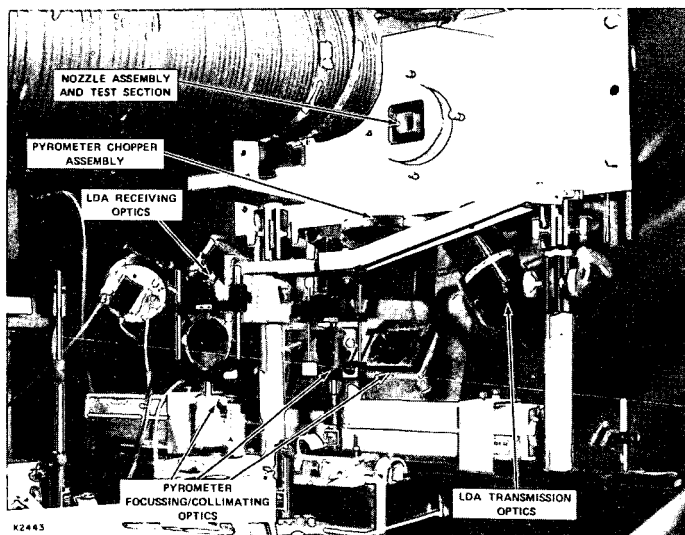Rate and Laser Source Power

Figure 4 - Experimental Hardware Layout, Showing Flow Source and
Optical Diagnostics

123

TABLE 1

COAL SOLIDS ANALYSIS

Sample No.	Coal Mass Loading	Gas Comp.	Residence Time (ms)	Local Coal Temp., K	Proximate Anal.*				Ultimate Analysis					Solubility % WGT DAF
					H_2O	Vol.	F.C.	Ash	C	H	N	S	Ash	
Coal: Wyoming Subbituminous														
1	0.026	0.91 H_2, 0.09 CO_2	0	300	2.8	37.9	48.8	10.6	64.9±0.3	4.34±0.03	1.14±0.09	-	-	3.7
2	0.026	.	2.5	1680±60	3.3	37.3	48.1	11.3	64.2±0.2	4.02±0.05	1.22±0.06	-	-	8-12
3	0.026	.	10	1780±50	2.0	38.8	48.9	10.3	66.0±0.8	4.05±0.09	1.20±0.03	-	-	45-51
4	0.026	.	12	1440±35	2.7	37.0	48.1	11.5	64.5±0.1	4.18±0.09	1.43±0.27	-	-	19-36
5	0.026	.	16	1264±40	1.6	38.9	48.9	10.6	66.5±0.3	3.95±0.02	1.19±0.04	-	-	10-22
6	0.037	N_2	3.5	1665±100	2.3	38.3	48.1	11.4	-	-	-	-	-	8-14
7	0.037	N_2	6	1450±36	3.1	36.4	47.8	12.7	-	-	-	-	-	10
8	0.037	N_2	8.5	--	2.2	37.3	48.8	12.2	-	-	-	-	-	14-16
9	0.037	N_2	11	1340±40	2.0	38.2	47.7	12.2	-	-	-	-	-	27
Coal: Montana Rosebud														
10	-	N_2	0	300	9.7	34.6	42.0	13.7	59.3±0.1	2.94±0.01	0.82±0.14	0.29±0.12	16.4±0.3	3
11	0.071	N_2	13.8	1660±130	4.8	31.9	46.2	17.1	57.0±0.7	3.34±0.10	0.61±0.12	0.17±0.06	14.8±1.6	11-12
12	0.059	N_2	13.8	1390±40	5.5	35.0	43.0	16.9	57.6±0.3	3.62±0.10	0.85±0.01	0.12±0.03	12.5±0.3	8-10
Coal: Pittsburgh No. 8														
13	-	N_2	0	300	1.4	39.0	53.4	6.2	75.2±0.1	5.03±0.01	1.56±0.04	0.25±0.1	6.14±0.02	4-9
14	0.042	N_2	4.6	1930±300	1.4	39.0	53.0	6.6	74.9±0.1	5.23±0.8	1.79±0.5	0.28±0.1	6.72±0.15	7
15	0.033	N_2	21.8	1570±75	1.6	39.0	53.5	6.0	75.3±0.3	4.72±0.05	1.64±0.05	0.06±0.01	6.06±0.20	14-18
16	0.051	N_2	14.8	1330±40	1.4	38.6	54.0	6.1	76.0±0.1	4.76±0.04	1.86±0.4	0.18±0.05	6.74±0.01	15-17
17	0.059	N_2	6.9	1585±20	0.8	39.2	53.5	6.5	74.9±0.2	4.71±0.03	1.74±0.02	0.20±0.02	6.62±0.14	11-17
18	0.056	N_2	27.6	2090±120	0.6	36.8	55.8	6.7	76.4±0.2	4.38±0.3	1.62±0.3	0.15±0.05	5.85±0.05	24-27

* Repeatability ±0.5%

124

chosen, so an attempt was made to provide a relatively monodisperse coal particle
size distribution. Figure 5 shows results of a prediction of radiative heating of
such a distribution, together with the inferred pyrometric temperature. It is
based on an area weighted sum of the predicted particle size group contributions at
the two measurement wavelengths. For this calculation, the heating source beam is
a triangular waveform, of duration 16ms (controlled by particle/carrier gas flow
through the heating volume) and spatial mean flux 500 w/cm^2.
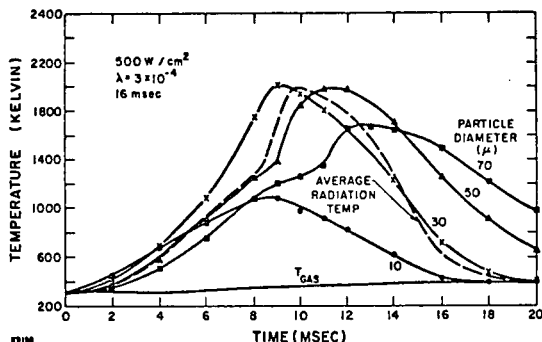

Figure 5 - Predicted Thermal History of Coal Particle Flow in
Nitrogen, and Corresponding Radiation Temperature at
Pyrometer Wavelengths

        Particle thermal behavior is somewhat different in this environment than in
a hot flow experiment. The low thermal inertia of small particles, relative to
their surface area, results in a rapid initial temperature rise. However, the
achievable steady state temperature decreases with decreasing particle size, due to
increased thermal diffusive loss to the cold carrier gas. As a result, very fine
particles roughly track the spatial flux distribution of the laser beams.
Consequently, at longer times the larger particles can overshoot the fines in
temperature. Local slope discontinuities in the curves for 50 and 70μm particle
sizes result from use of an assumed endothermic devolatilization
process.[4,10,11] Curves for 20, 40, 60 and 80μm particles were also obtained
for the size distribution, but not included on the plot. Heat transfer from
particles to gas results in limited gas temperature change, in this case from 300K
to 400K. The predicted radiation temperature curve is shown as a dashed line. It
is close to the temperature of the mass mean particle size, and hence may be a
useful indicator of mean temperature. However, the wide distribution of
temperatures of the various size particles during the transient heating period
renders direct inference of kinetic rates difficult, except for the case of a
nearly monodisperse supply. Use of the fluidized bed feeder, while appropriate
from a feed rate and control viewpoint, may have exaggerated the size distribution
via preferential elutriation.

        Flow sampling was based on a simple tubular stainless steel probe, aligned
coaxially with the flow. It was protected from the incident laser beam using
shield mirrrors, as shown schematically in Figure 2. No probe cooling or quenchant
was used, as the sampled particles were in a cold gas environment, and additional
cooling would be ineffective. The sample stream was drawn through a filter system
to capture condensed phase material, and samples taken of the cleaned gas stream
using one liter pyrex bottles. As indicated on Figure 1, subsequent sample
analysis included gas chromatography, and extensive measurement of the condensed
phase material properties. This analysis is continuing, and further data will be
reported separately.

125

EXPERIMENTAL RESULTS

Data was taken over a limited range of heating conditions using three coals; Pittsburgh No. 8, Wyoming sub-bituminous, and Montana Rosebud. Heating rates in the range 1-3 10^5K/s to temperatures in the range 1000-2000K were obtained, with heating times up to 30 ms. Test conditions are given in Table 1 for the three coals used. While calibrated screen sample sizing was used in an effort to minimize the range of particle size distribution, sample analysis shows considerable variability.[9] Overall, negligible gaseous products were observed, and no liquids found. Color and physical appearance of the collected solids differed from the raw coal, and solubility of the solids was considerably increased, while ASTM ultimate and proximate analysis of the bulk samples showed little change from the raw coals.

Gas Analysis

Gas samples from all test conditions were analyzed using a chromatograph, calibrated usng a dilute mixture of expected light volatiles in nitrogen carrier.* This gave detection limits corresponding to expected sample conditions, typically 10^{-4} by volume. At this level of sensitivity, in no case were any gaseous products observed other than H_2O, which was found at concentrations consistent with the raw coal moisture content. These results imply that not more than two to four percent of the feed coal carbon content is converted to light volatiles in this environment, and that negligible free hydrogen was produced. Table 2 shows results for two gas samples analyzed using a flame ionization detector. Samples were chosen for maximum heating and residence time conditions. As shown, the Wyoming sub-bituminous coal gave less than 0.2 percent carbon conversion to light volatiles, and the Pittsburgh No. 8 less than 0.01 percent. Since heating time and measured area mean temperature were comparable to those for extensive devolatilization to light species in hot gas environments, these results suggest that the primary volatiles are of relatively high molecular weight.

TABLE 2

ANALYSIS OF GAS SAMPLES FOR VOLATILES

			Gas Concentration (ppm)					Coal Mass Loading in N_2	Volatile Carbon Yield
	CH_4	C_2H_2	C_2H_4	C_2H_6	C_3H_6	C_3H_8	C_4		
Sample # 1 Wyoming (1700K, 30ms)	49.7	2	16.4	7.6	5.0	2.0	ND*	0.025	<0.2%
Sample # 11 Pitt #8 (1560K, 30ms)	8.9	ND	2	ND	ND	ND	ND	0.075	<0.01%

* ND = < 1 ppm, resolution limit of G.C.

Solids Analysis

Captured solids were examined in several ways, at various levels of detail. These include visual observation; particle size analysis; ASTM ultimate and proximate analysis; FTIR spectroscopy**; and solvent extraction. Further study using SEM of the collected solids, GPC of the solvent extract, and particle size analysis has been initiated, and will be reported separately.

* Species calibrated were: H_2O, H_2, CO_2, CO, CH_4, C_2H_2, C_2H_4, C_3H_4, C_3H_6, C_3H_8, C_4H_x, H_2S, COS.

** Performed by Advanced Fuel Research, East Hartford, CT.

126

Both raw coal and heated samples were gathered on the sample filters using the complete feed, flow, and sampling system. These raw coal samples were used for subsequent baseline analysis. Visually, samples subjected to heating showed a progressive tendency to clump or cake on the filter elements and a distinct color shift from black toward dark brown. Results of proximate and ultimate analysis of various coal samples are given in Table 1. These are readily summarized, as indicating very little or no change in properties between raw coal and radiatively heated samples, except some moisture loss from the Montana Rosebud samples. Since samples were stored in the laboratory environment, with no control of atmospheric moisture absorption, the measured H_2O content is perhaps not surprising. FTIR analysis* of Wyoming samples 1, 5, and 9 of Table 1 gave no discernable indication of structural bond changes between the raw coal and extensively heated samples.

Solvent extraction tests were carried out, using a reflux of stabilized THF* in air at one atmosphere pressure. Temperature in the extraction volume was about 310 to 320K, and reflux period was typically two hours. Results are given in Table 1. Dried extract was typically a brown to black tarry material. Overall, the radiatively heated samples had significantly increased solubility, relative to the parent coals. Some limited extractions with MEK and with hot dilute $NaOH/H_2O$ showed similar behavior. While the range of heating rates and temperatures attained preclude direct comparison, there may also be some decrease in yield with increasing coal rank. Also, for each coal, there may be a trend toward increased soluble fraction with increased heating rate or peak temperature, which is related to size distribution as well as heating environment.

DISCUSSION

The observations given above are consistent with a phenomenological picture of evolution of primary volatiles from the heated particles as high molecular weight compounds. Rapid diffusion of them into the cold gas atmosphere minimizes secondary decomposition, and results in some homogeneous nucleation and condensation.[1] Sample withdrawal through a fine filter results in capture of a mixture including decomposed coal particles, volatile condensate particles, and trapped volatile vapors. The volatiles, possibly together with a direct contribution from the heated coal particles, appears to be the component extracted by solvent treatment. This is supported by preliminary SEM images of fresh and solvent extracted solid material samples. The soluble product yield is observed to be generally lower than the ASTM proximate analysis, and much lower than volatile yield observed at high heating rate and temperature conditions. This may be due to the effect of particle size distribution on achievable particle temperature, shown in Figure 5. In particular, preferential elutriation of fines from the coal feeder could result in most of the input solids feed being temperature limited by diffusive heat transfer to the gas while a minor fraction of coarse particles provides the pyrometer signal, as well as pyrolysate.

Based on these observations, it would appear that primary volatile species are of high molecular weight, with the gaseous products in other experiments resulting from secondary decomposition or reactions in hot environments. Also, the proximate and FTIR results can be interpreted as suggesting that the devolatilization process may involve very limited chemical bond breaking or rearrangement.

(1)   Resulting particles are small, and equilibrate at low to moderate temperature in the heating volume.

*   Tetrahydrofuran; suggested by Dr. Peter Solomon of Advanced Fuel Research.

CONCLUSIONS

Use of an high powered laser as a means of providing a controlled heating environment for particles in a gas flow has been shown to be practical. This approach allows decoupling of the particle heating from fluid stream mixing and gas composition and temperature. It also allows choice of background gas composition, for example for study of high temperature heterogeneous reactions. Choice of background gas temperature also allows rapid cooling of vapor phase products, and the potential for selective gas phase reaction conditions.

Measurement of devolatilization behavior of three coals resulted in no observable gaseous products, and enhanced solubility of the solid product. Also, the solid product showed minimal change in proximate and ultimate analyses relative to the raw coal, and minimal change in its FTIR spectrum. These results suggest that primary devolatilization may occur with minor change of chemical structure of the organic material.

ACKNOWLEDGEMENTS

REFERENCES

1.   Anthony, D.B., Howard, J.B., Hottel, H.C., and Meissner, H.P., 15th International Symposium on Combustion, p. 1303 (1975).

2.   Badzioch, S., and Hawksley. P.G.W., Ind. Engg. Chem., 9, p. 521, (1970).

3.   Kimber, G.M., and Gray, H.D., Combus. Flame 11, p. 360 (1967).

4.   Kobayashi, H., Howard, J.B., and Sarofim, A.F., 16th Symposium (International) on Combustion, Cambridge, MA August 15-21 (1976b).

5.   Lowenstein, A.I., and von Rosenberg, Jr., C.W., 11th International Symposium on Shock Tubes and Waves, Seattle, WA, July 11-14 (1977).

6.   Solomon, P.R., Hamblen, D.G., Carangelo, R.M., and Kraus, J.L., 19th International Symposium on Combustion (1982).

7.   Karn, S.F., Friedel, R.A., Sharkey, A.G., Fuel 49, p. 297 (1969).

8.   Karn, F.S., Friedel, R.A., Sharkey, A.G., Fuel 51, p. 113 (1972).

9.   "Volatile Production During Preignition Heating", Final Report, Final Report No. DE-AC22-84PC30291, prepared by Avco Everett Research Laboratory, Inc..

10.   Stickler, D.B., Gannon, R. E., and Kobayaski, H., Eastern States Section, Fall Meeting of the Combustion Institute, Applied Physics Laboratory, Maryland, MD November 12-13 (1974).

11.   Ubhayakar, S.F., Stickler, D.B., and Gannon, E.R., Fuel 56, p. 281 (1977).

Enhanced Ethylene Production via Flash Methanolysis of Coal

Muthu S. Sundaram, Meyer Steinberg, and Peter Fallon

Process Sciences Division
Department of Applied Science
Brookhaven National Laboratory
Upton, NY   11973

INTRODUCTION

According to a recent report, an estimated 31 billion pounds of ethylene was produced in the U.S. alone (1). Ethylene is an important raw material in the vast plastic and polymer markets. An upward trend in the demand for ethylene has been predicted for the future years. Currently, ethylene is produced mainly through thermal and catalytic hydrocracking of ethane and other hydrocarbons. Although a large amount of work has been performed on the production of gaseous and liquid fuels from coal, much less attention has been focused on the production of ethylene using coal as the raw material. In an on-going pyrolysis research project at the Brookhaven National Laboratory, the methods to increase the yield of ethylene through flash methanolysis of coal is being investigated. Flash methanolysis is defined as pyrolysis of coal under pressure in an atmosphere of methane. This study attempts to identify the influence of important process variables such as reaction temperature, gas pressure, solids residence time, gas/solids ratio etc. on the production characteristics of ethylene and other pyrolysis products.

EXPERIMENTAL

Much of the work discussed in this paper was done using a New Mexico sub-bituminous coal. Other coals of ranks varying from lignite to bituminous were used for comparison purposes. These included North Dakota lignite, Wyodak lignite, Montana Rosebud sub-bituminous and Illinois no. 6 bituminous coals. The proximate and ultimate analyses of these coals are given in Table 1.

The methanolysis experiments were carried out in a highly instrumented down-flow entrained tubular reactor. The reactor, made of Inconel 617 alloy, is heated electrically by four clam-shell type heaters and designed for a maximum pressure of 4000 psi. The detailed description of the design, construction and operation of the reactor has been published (2). The schematic representation of the complete reactor set-up is shown in Figure 1. Coal particles of 150 μm or less in diameter, mixed with 10% by weight of Cab-O-Sil, are fed by gravity at the rate of approximately 500 gm/hour into the top of the 1-in.-i.d. by 8-ft-long reactor. Methane is preheated to 600°C before feeding into the tubular reactor held at isothermal conditions along the length of the reactor at the temperature of interest. The gas samples could be taken from any one of the four sample taps located at 2-ft intervals along the length of the reactor and analyzed via an on-line GC. Products heavier than BTX ($>C_9$) are collected in the water-cooled condensers and analyzed separately. The individual product yields are determined as percent of carbon contained in the feed coal.

RESULTS AND DISCUSSION

Pyrolysis of coal at temperatures higher than 600°C generally results in the formation of light hydrocarbon gases, oxides of carbon, BTX and tar. The product distribution, however, depends on the coal type, the processing conditions, the pyrolysis atmosphere and the method of heating.

A survey of the recent research literature on coal pyrolysis and the composition of various pyrolysis products is available (3). Traditionally, the pyrolysis of coal has been carried out in H_2, He, N_2 or CO atmospheres; Ar, H_2O and CO_2 have also been used in a few instances. Except the previous reports from our laboratory (4), the pyrolysis of coal in an atmosphere of methane, to our knowledge, has not been documented in the literature. The main interest in the use of methane as the pyrolysis medium lies in the fact that for hydrogenation of coal, a large resource of natural gas can be used in the place of hydrogen which has no known natural sources.

The flash methanolysis of New Mexico sub-bituminous coal at temperatures higher than 700°C, produced significant quantities of CO, ethylene, BTX and tar; small amount of CO_2 also was detected. Methane produced due to pyrolysis of coal could not be distinguished from the entraining methane gas. In order to determine the net production or consumption of methane, a calibrated mass flowmeter was placed on the methane inlet to the reactor; the experimental set-up already contained a calibrated positive displacement meter at the reactor outlet. The mole percent of methane in the product-laden gases was determined via GC analysis. The methane and total gas flow data, at steady reactor operating conditions, are shown in Table 2 for several runs. The difference between the methane flows, calculated from the limited data available and shown in the last column of Table 2, indicates a negligible net consumption or production of methane within the limits of combined experimental errors which has been estimated to be approximately ±5%.

At 900°C and 50 psi total gas pressure, 21.4% of carbon in the feed coal was converted to products of which approximately half was made up of ethylene. The remaining products were BTX (2.9%C) and CO_x(8.5%C). Table 3 shows that the total carbon conversion tends to increase with pressure up to 200 psi before falling off to a lowest level of 20.0%C at 500 psi. The decrease in total conversion at 500 psi is mainly due to the decrease in the yields of CO and ethylene. There is very little variation in the yield

131

of CO_2 as a function of pressure. The separate curves for BTX and tar yields, in Figure 2, go through a maximum and minimum respectively at 200 psi. An increase in the methane pressure had an adverse effect on the ethylene yield. At higher pressures, the hydrogenation of ethylene to produce ethane is facilitated.

Table 4 shows the effect of reactor temperature on the methanolysis product distribution and illustrated in Figure 3. There is a marked increase in the total carbon conversion with increasing temperature; this is mainly due to a pronounced increase in the yield of ethylene and BTX. As high as 12.7% carbon was converted to ethylene at 1000°C and approximately 9% was converted to BTX. In contrast, pyrolysis in inert helium atmosphere produced only 2.2% ethylene and 7% BTX under the same conditions. Thus, at 1000°C, 5-6 times greater yield of ethylene is produced during flash methanolysis when compared to helium pyrolysis. When the New Mexico coal was pyrolyzed in the atmospheres of He or N_2 or CO, the maximum yield of ethylene obtainable at 50 psi was approximately 6% and as shown in Figure 4, the maxima occurred around 900°C. A comparison of the maximum yields of ethylene shows that more than twice the amount of ethylene is produced in an atmosphere of methane than any other pyrolysis atmospheres investigated. The ethylene yields from methanolysis experiments were somewhat closer to ethylene yields from pyrolysis in other atmospheres up to 800°C. At temperatures higher than 800 °C, only methanolysis experiments recorded a continued increase in the yield of ethylene with increase in the reactor temperature. This clearly indicates the effectiveness of methane atmosphere for enhanced yield of ethylene during pyrolysis of coal. Several blank runs, in the absence of coal, confirmed that reactor walls do not catalyze the decomposition of methane to form products, including ethylene. Blank runs with pyrolysis char, coconut char and Cab-O-Sil additive also showed no formation of ethylene under the same conditions.

In addition to the effect of temperature and pressure, the effect of methane to coal feed ratio on the methanolysis product distribution was investigated. The results are shown in Table 5. In these experiments, the
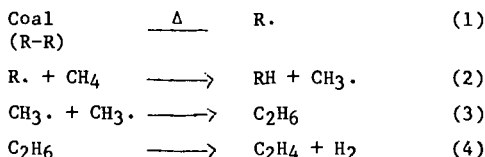
methane feed rate was held almost constant while varying the coal feed rate. This table shows that an increase in the methane to coal feed ratio favors the production of ethylene and BTX as well. However, the ethylene concentration in the product stream follows an opposite trend as seen in Table 5. The maximum concentration of ethylene obtainable, under the conditions investigated, is slightly over 2% and the dependence of ethylene concentration on the coal feed rate, rather than on the methane to coal feed ratio, is apparent.

Using the data in Table 5, a linear regressional analysis was made to describe the relation between the individual product yields and the methane/coal feed ratio. The following expressions were obtained:

$$\%C_{C_2H_4} = 2.39 \ x + 3.11; \ R^2 = 0.90$$
$$\%C_{H.C. \ Gases} = 2.57 \ x + 3.05; \ R^2 = 0.91$$
$$\%C_{BTX} = 1.89 \ x + 1.30; \ R^2 = 0.94$$
$$\%C_{Total \ H.C.} = 4.46 \ x + 4.36; \ R^2 = 0.93$$
$$\%C_{CO_x} = 0.67 \ x + 3.89; \ R^2 = 0.63$$
$$\%C_{Total \ Conv.} = 5.98 \ x + 6.90; \ R^2 = 0.90$$

where x = methane/coal feed ratio and R^2 = the correlation coefficient. The rather low correlation coefficient for CO_x is attributed to errors occasionally encountered in the measurement of CO during on-line GC analysis of the product gases.

The enhanced yield of ethylene in flash methanolysis experiments probably has a free radical origin. An abundance of thermal free radicals from coal at elevated temperatures facilitates the decomposition of methane to produce methyl radicals which can lead to the formation of ethylene, probably with an ethane intermediate, as follows:

$$Coal \xrightarrow{\ \Delta\ } R \cdot \qquad\qquad (1)$$
$$(R-R)$$
$$R \cdot + CH_4 \longrightarrow RH + CH_3 \cdot \qquad (2)$$
$$CH_3 \cdot + CH_3 \cdot \longrightarrow C_2H_6 \qquad\qquad (3)$$
$$C_2H_6 \longrightarrow C_2H_4 + H_2 \qquad (4)$$

133

High temperatures favor reaction (4) in the forward direction as written. Other free radical reactions, leading to the formation of higher hydrocarbons and heavy materials are also possible which might explain the increased liquid product yields in these experiments. Since no net consumption of methane was noticed, it is reasonable to assume that (1) a part of ethylene comes from coal due to thermal effects as in the case of straight inert helium gas pyrolysis and (2) the remaining ethylene comes from the methyl radicals generated from coal which would have been converted to methane in helium pyrolysis via autohydrogenation effect. In other words, methane, at high concentrations, causes part of the coal radicals to form ethylene instead of methane. The methane formed from coal appears to be in balance with the reacted methane gas. For example, at 1000°C and 50 psi helium pressure, the total hydrocarbon gases yield was 10.9% (5.5% CH_4 + 5.4% ethylene) which compares well with 12.1% total hydrocarbon gases (12.0% C_2H_4 + 0.1% C_2H_6) in Table 5 under an identical gas to coal feed ratio. Thus it is seen that methane acts as a shuttler in methanolysis experiments.

Table 6 summarizes the results of flash methanolysis of other coals under identical temperature and pressure conditions. Difficulties were encountered in closely controlling the coal feed rates during some experiments as a result of which the methane to coal feed ratios could not be kept uniform in all cases. At this time, it is not known whether the effect of methane to coal feed ratio on the methanolysis product distribution from these coals is similar to what was seen in the case of New Mexico sub-bituminous coal. Apparently, there is no clear trend in the yields of ethylene or BTX with respect to the coal rank. Correlation of the data with volatile matter content, fixed carbon or ash content also did not reveal any trend. For example, a comparison of the data from the two lignites, obtained under similar reaction conditions, in Table 6, shows a wide variation in the producer yields despite the fact that the proximate and ultimate analyses of these coals, in Table 1, do not show any remarkable difference between them. The change in the product distribution

134

between different coals might then be due to important structural differences among the coals. This is supported by the recent findings of Calkins who was able to correlate the pyrolysis ethylene yields to polymetheylene contents of coals successfully (5).

CONCLUSIONS

We have shown that there are definite advantages in the use of methane as an atmosphere in the flash pyrolysis of coal. At temperatures higher than 800°C, 2 - 5 times greater yields of ethylene is obtainable in methane atmosphere when compared to flash pyrolysis in an inert helium atmosphere. An enhancement in the yield of ethylene and BTX is seen at a lower coal feed rate. Since ethylene and BTX are important raw materials in the vast polymer and plastic markets, flash methanolysis of coal has potential process applications.

ACKNOWLEDGEMENT

REFERENCES

1.   Chem. and Eng. News, 61 (43), 13 (1983).

2. (a) Fallon, P. T. and Steinberg, M., "The Design, Construction, Operation, and Initial Results of a Flash Hydropyrolysis Experiment Unit", BNL 22519 and BNL 50698. Presented at ACS 173rd National Meeting, New Orleans, March 1977.

   (b) Sundaram, M. S., Steinberg, M. and Fallon, P. T., "Flash Hydropyrolysis of Coal for Conversion to Liquid and Gaseous Fuels: Summary Report", DOE/METC/82-48 (May 1982).

3.   Howard, J. B., "Fundamentals of Coal Pyrolysis and Hydropyrolysis", Chapter 12 in Chemistry of Coal Utilization, Elliott, M. A., Editor, John Wiley and Sons, New York, NY, pp. 665-784 (1981).

4.   Steinberg, M. and Fallon, P. T., "Make Ethylene and Benzene by Flash Methanolysis of Coal", Hydrocarbon Processing 61 (11), 92-6 (Nov.1982).

5.   Calkins, W. H., Prepr. Pap. - Am. Chem. Soc., Div. Fuel Chem. 28, 85 (1983).

Table 2

Mass Flowmeter Data

Run No.	Pressure (psi)	Temp. (°C)	Feed Methane-in (SCF/Min)[1]	Total Gases out (SCF/Min)	% Methane in the exit gases	Methane-out (SCF/Min)	% Difference in CH₄ Flow
643[2]	20	1000	0.88	1.06	82	0.87	-1.1
644[2]	50	1000	0.93	1.06	88	0.93	0
650[3]	50	900	1.00	1.10	88	0.97	3.0

1) SCF= Standard Cubic Feet at 15°C and 1 atm.
2) New Mexico sub-bituminous coal
3) Montana Rosebud sub-bituminous coal

Table 1

Analyses (Wt%) of Coals Used

	Wyodak Sub-bit.	North Dakota Lignite	Ill. No. 6 Bit.	New Mexico Sub-bit.	Montana Rosebud Sub-bit.
Moisture*	3.0	9.6	6.83	7.8	9.1
Proximate Analysis					
Dry Ash	10.0	10.0	12.4	22.8	11.8
Dry V.M.	43.8	46.2	38.5	34.9	46.8
Dry FC	46.2	43.8	49.1	42.4	41.4
Ultimate Analysis					
Carbon	55.3	59.0	68.8	55.9	67.7
Hydrogen	4.1	4.0	5.0	4.3	4.8
Nitrogen	0.9	0.9	1.2	1.1	0.9
Sulfur	0.9	0.5	3.4	1.0	2.2
Oxygen**	28.8	25.6	9.2	14.9	12.6

* As received; ** By difference.

Table 4

Flash Pyrolysis of New Mexico Sub-Bituminous Coal with Methane
Effect of Reactor Temperature

Run No.	685	683	683	683	692	692	692	684
Reactor Temperature (^oC)	800	800	850	900	900	950	1000	1000
Reactor Pressure (psi)	50	50	50	50	50	50	50	50
Coal Feed Rate (lb/hr)	1.01	0.99	0.99	0.99	0.90	0.90	0.90	1.00
Methane Feed Rate (lb/hr)	4.1	4.05	4.05	4.05	4.15	4.15	4.15	4.05
Coal Particle Residence Time (sec)	1.5	1.5	1.5	1.5	1.5	1.5	1.5	1.4
Methane/Coal Ratio	4.1	4.1	4.1	4.1	4.6	4.6	4.6	4.6
% Carbon Converted to Product								
C_2H_4	6.1	5.1	10.2	10.0	8.9	12.6	12.7	12.0
C_2H_6	0.5	0	0	0	1.1	1.1	1.2	0.1
BTX	0.6	0.8	2.1	2.9	3.1	4.2	8.8	9.0
CO	5.2	5.2	5.7	6.8	3.8	4.2	5.4	8.0
CO_2	1.4	1.5	1.8	1.7	1.3	1.3	1.2	1.7

Table 3

Flash Pyrolysis of New Mexico Sub-Bituminous Coal with Methane
Effect of Gas Pressure

Run No.	683	454	451	424
Reactor Temperature (^oC)	900	900	900	900
Reactor Pressure (psi)	50	100	200	500
Coal Feed Rate (lb/hr)	0.99	1.22	0.85	1.05
Methane Feed Rate (lb/hr)	4.05	3.5	4.0	5.6
Coal Particle Residence Time (sec)	1.5	1.8	2.7	3.0
Methane/Coal Ratio	4.1	2.9	4.7	5.3
% Carbon Converted to Product				
C_2H_4	10.0	8.3	7.1	4.3
C_2H_6	0.0	1.4	3.9	3.5
C_3H_8	0.0	0.9	0	0
Total Gaseous H.C.	10.0	10.6	11.0	7.8
BTX	2.9	3.4	6.5	3.6
>C_9	ND	6.9	5.2	7.1
Total Liquid H.C.		10.3	11.7	10.7
CO	6.8	4.6	5.5	0
CO_2	1.7	1.7	2.2	1.5
Total CO_x	8.5	6.3	7.7	1.5
Subtotal	21.4	27.2	30.4	20.0
Char	ND	ND	ND	58.7
Total				78.7

137

Table 6

Flash Pyrolysis of Coals with Methane
Effect of Coal Type

	Wyodak Lignite			North Dakota Lignite			Illinois No. 6 Bituminous			Montana Rosebud Sub-Bituminous		
Run No.	722	722	722	731	731	731	720	720	720	708	708	708
Reactor Temperature (^{o}C)	900	950	1000	900	950	1000	900	950	1000	900	950	1000
Reactor Pressure (psi)	50	50	50	50	50	50	50	50	50	50	50	50
Coal Feed Rate (lb/hr)	0.93	0.93	0.93	1.00	1.00	1.00	0.60	0.60	0.60	1.45	1.45	1.45
Methane Feed Rate (lb/hr)	3.85	3.85	3.85	4.1	4.1	4.1	3.88	3.88	3.88	3.81	3.81	3.81
Coal Particle Residence Time (sec)	1.6	1.5	1.5	1.6	1.6	1.5	1.6	1.5	1.5	1.3	1.3	1.3
Methane/Coal Ratio	4.14	4.14	4.14	4.1	4.1	4.1	6.5	6.5	6.5	2.6	2.6	2.6
% Carbon Converted to Product												
C_2H_4	7.6	8.9	11.0	4.0	4.5	5.1	4.5	7.0	11.1	4.3	4.9	6.2
BTX	4.6	6.6	9.9	1.7	2.4	3.9	2.2	6.0	12.8	1.7	2.6	3.9
Total H.C.	12.2	15.5	29.9	5.7	6.9	9.0	6.7	13.0	23.9	6.0	7.5	10.1
CO	7.0	9.1	8.0	5.7	8.6	9.6	2.2	2.5	3.4	4.0	5.1	6.3
CO_2	5.0	4.7	3.0	4.9	5.9	5.2	0.8	0.8	0.9	2.6	2.5	2.5
Total CO_x	12.0	13.8	11.0	10.6	14.5	14.8	3.0	3.3	4.3	6.6	7.6	8.8

Table 5

Flash Pyrolysis of New Mexico Sub-bituminous Coal with Methane
Effect of Methane/Coal Ratio

| Run No.	684	692	703	704	705	706
Reactor Temperature (^{o}C)	1000	1000	1000	1000	1000	1000
Reactor Pressure (psi)	50	50	50	50	50	50
Coal Feed Rate (lb/hr)	1.0	0.90	1.89	1.9	2.77	5.08
Methane Feed Rate (lb/hr)	4.05	4.15	3.79	3.77	3.77	3.75
Coal Particle Residence Time (sec)	1.5	1.5	1.5	1.5	1.5	1.5
Methane/Coal Ratio	4.05	4.61	2.01	1.98	1.36	0.74
% Carbon Converted to Product						
C_2H_4	12.0	12.7	9.0	10.4	8.3	4.6
C_2H_6	0.1	1.2	1.0	0.0	0.0	0.0
Total Gas H.C.	12.1	13.9	10.0	10.4	8.3	4.6
BTX	9.0	8.8	7.2	5.7	4.1	2.2
Total H.C.	21.1	22.7	17.2	16.1	12.4	6.8
CO	8.0	5.4	6.0	ND	5.1	2.2
CO_2	1.7	1.2	2.0	1.5	1.8	0.9
Total CO_x	9.7	6.6	8.0	1.5+	6.9	3.1
Total	30.8	29.3	25.2	18.0+	17.3	9.9
Methane Concentration (%)	93	94	87	84	83	81
Methane Partial Pressure (psi)	46.5	47	43.5	42	41.5	40.5
Ethylene Concentration (Vol%)	1.1	1.1	1.7	1.9	2.3	2.3
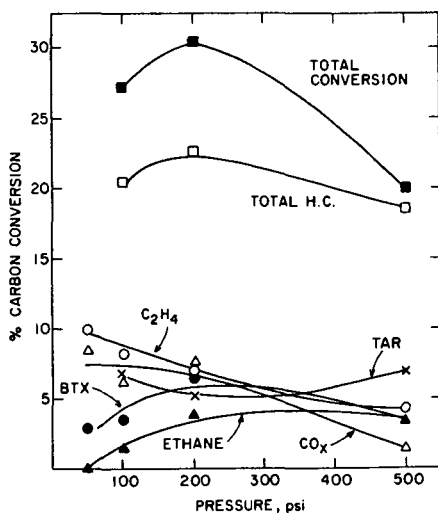
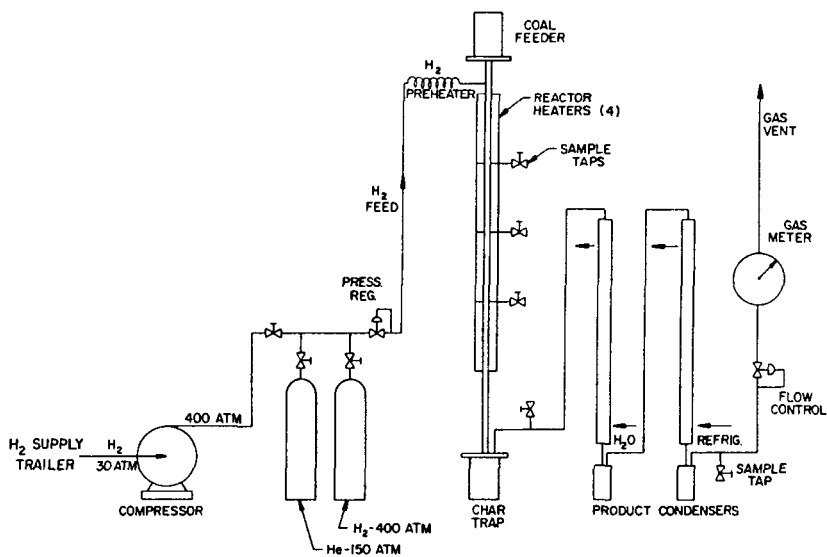FIGURE 2.   EFFECT OF PRESSURE ON PRODUCT DISTRIBUTION.

FIGURE 1.   Schematic representation of the pyrolysis reactor.
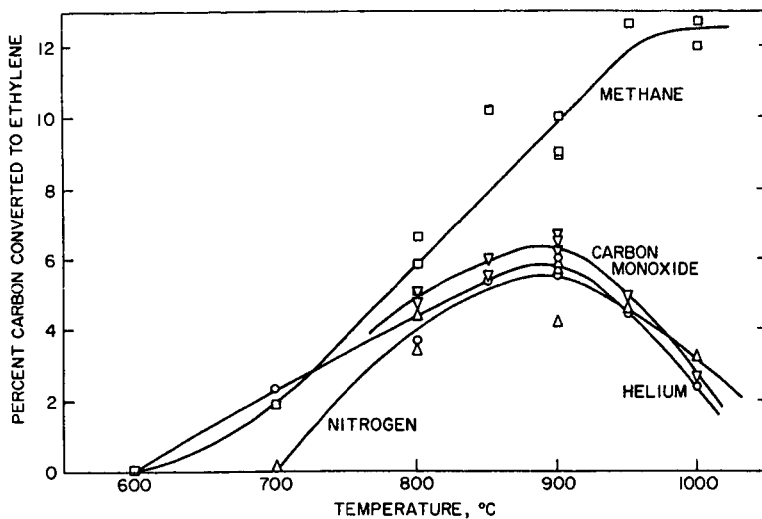
139

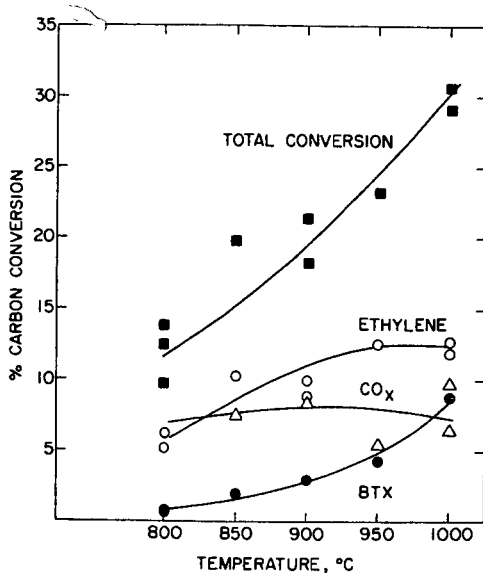Figure 4. Effect of Temperature and Pyrolysis Atmosphere on Ethylene Yield.

FIGURE 3. EFFECT OF TEMPERATURE ON PRODUCT DISTRIBUTION.

140

ROLE OF EXCHANGEABLE CATIONS IN CONCURRENT GASIFICATION/PYROLYSIS OF LIGNITES

Mark E. Morgan* and Robert G. Jenkins

Department of Materials Science and Engineering
The Pennsylvania State University
University Park, PA   16802

INTRODUCTION

Gasification and combustion of the large reserves of American lignites is an area of intense research. This research, coupled with economic incentives, has led to the current project to build and operate the first large-scale coal gasifier using lignites from North Dakota. However, much work is necessary in order to be able to understand and predict the behavior of these coals. In this paper, the role of ion-exchangeable alkali and alkaline-earth metals in the gasification/pyrolysis of lignites is addressed. These cations, which are peculiar to low-rank coals, are known to have a significant influence on the utilization behavior of lignites. Exchangeable metal cations have been found to affect coal pyrolysis (1,2) and coal-char gasification (3). The goal of this paper is to illucidate the way in which exchangeable cations affect coal gasification in terms of their role in coal pyrolysis, char gasification and the interaction between the two.

EXPERIMENTAL

Pyrolysis was carried out in a dilute-phase entrained-flow reactor. The system is a modified version (4) of that utilized by Scaroni et al. (4). The system allows pyrolysis to be studied under high heating and cooling rates ($10^4 - 10^5$ K/s). Under these conditions, examination of pyrolysis over residence times from 0.03 to 0.30 s and at temperatures up to 1300 K is possible. Pyrolysis occurs in a dilute stream in order to reduce the role of secondary reactions resulting from contact between the pyrolysis products. Because of experimental conditions, weight loss was determined by using ash as a tracer. This technique has been used previously by a number of workers (4,5,6). Weight loss data are reported on a Dry Inorganic Content Free (DICF) basis in order to account for the presence/absence of metal cations.

In this work, four pyrolysis atmospheres were utilized; they are nitrogen, air, carbon dioxide and wet-nitrogen. It should be noted that the volumetric flow rates and gas velocities were the same for all four cases. The wet-nitrogen referred to is saturated nitrogen produced by bubbling dry nitrogen through water at room temperature (2.7% water by volume).

A Montana lignite (Fort Union Seam) was utilized in this study. Details of the organic and inorganic analyses of this coal can be found elsewhere (2). In this study, two types of samples were utilized: raw lignite and acid-washed lignite. In the acid-washing procedure, 50 g of raw lignite, with a mean particle size of 46 μm, were mixed with 900 ml of 0.1 N HCL for 16-24 hours, filtered, and washed repeatedly. It was then refluxed in 1000 ml of boiling distilled water for 1 hour to remove excess HCL (7).

RESULTS AND DISCUSSION

Air and Nitrogen -- The pyrolysis of lignites in air and nitrogen will be discussed first. Combustion in air is treated separately because the highly exothermic oxidation reactions make it difficult to control and predict particle temperature. Thus, the results gained have to be discussed in terms of this experimental difficulty.

* Current Address: Atlantic Research Corporation, Alexandria, VA, 22314.

The results for pyrolysis of the raw and acid-washed lignites in air and nitrogen at 1173 K can be seen in Figure 1. For the sake of clarity, the discussion of these results will be broken into two parts: the effect of the presence of air and the effect of metal cations in air.

In Figure 1, it can be seen that the weight loss behavior is dramatically different in air when compared to nitrogen. While maximum weight loss in nitrogen are 50% for the acid-washed coal and 30% for the raw coal, both coals lose about 90% in air. It should also be noted that major differences between the behavior in nitrogen and air occur at very early residence times. During this initial period, it is assumed that the pyrolysis process dominates the weight loss behavior. Because these increases in weight loss in air occur so rapidly, there are, at least, three proposed mechanisms suggested: oxidation of primary volatiles to reduce secondary char-forming reactions, oxidation of unstable nascent sites in the pyrolyzing char (8), and/or increases in the rate and yield of pyrolysis due to increases in particle temperatures from oxidation reactions.

It can be seen that the presence of metal cations, in air, results in a decrease in the rate of weight loss when compared to the behavior of the acid washed lignite. Figure 1 shows that after approxiamtely 0.05 s the acid-washed lignite has lost 80 wt% whereas the raw lignite has only lost about 30 wt%. It appears that the reason for the observed influence of metal cations is a decrease in the rate of volatile evolution and, thus, oxidation. This view is substantiated by the observation that metal cations have been shown to affect the amount, rate of release and chemical nature of the volatile material (1,2). From Figure 1, it can also be seen that after about 0.15 s the two curves obtained from the runs in air become almost coincident.

Wet-Nitrogen and Carbon Dioxide -- Potentially reactive atmospheres of carbon dioxide and wet-nitrogen were also examined. Analysis of lignite behavior in these atmospheres is somewhat simpler than in air because of the lack of exothermic reactions; especially in any carbon gasification reactions (9).

The results of pyrolyzing the lignite in these two atmospheres can be seen in Figures 2 and 3. In Figure 2, the results for pyrolysis of the raw coal in nitrogen, carbon dioxide and wet-nitrogen are presented. It can be seen that initially weight loss in nitrogen and carbon dioxide are similar but they are greater than in wet-nitrogen. This indicates, probably, a slower heating rate of the particles when wet-nitrogen is the secondary gas. Secondly, it is observed that, at some stage, significant weight loss ceases for all three gases. This leveling off occurs at about 39 wt% in carbon dioxide.

Results for pyrolysis of the acid-washed samples in the three atmospheres are presented in Figure 3. In the case of this sample, similar effects of atmosphere on initial weight loss are observed. That is, initially the weight loss in nitrogen and carbon dioxide are similar and, yet, greater than that observed in wet-nitrogen. However, the most important observation is that there is little, if any, effect of atmosphere on final weight loss in the reactor. After about 0.20 s this acid-washed lignite loses almost 50 wt% in all three gases.

If one compares Figures 2 and 3, an additional interesting result can be found. In all cases, the presence of metal cations in the lignite causes a decrease in total weight loss in the reactor. Although there is a significant increase in weight loss when the raw coal is pyrolyzed in the reactive gases, the largest weight loss for the raw coal is about 40% while the acid-washed sample loses almost 50%. This is in contrast to the weight loss behavior in air where the raw and acid-washed samples have similar weight loss values after about 0.15 s.

As stated previously, during pyrolysis in wet-nitrogen or carbon dioxide, it is possible to eliminate large differences in particle time-temperature history as a source of differences in gasification behavior. Therefore, the two major causes of the observed behavior in these atmospheres are related to reactions of the atmospheres with the pyrolyzing solid surface and/or reactions with the volatile materials released. Of these two explanations, it appears that the second is more likely to be dominant. This suggestion arises from two observations. Firstly, the increases in weight loss occur most dramatically during the initial 0.15 s when the release of volatile species should dominate the coal's behavior. Secondly, these gases appear to have little influence on the ultimate pyrolysis behavior of the acid-washed lignite. It has been shown that the presence/absence of metal cations in lignites profoundly affects the evolution of volatile species at short residence times. Thus, removal of the metal cations enhances volatile yield to such a degree that the presence of the various gases has little or no effect on the observed behavior.

ACKNOWLEDGEMENTS

REFERENCES

1.   Morgan, M. E. and Jenkins, R. G., A.C.S. Fuel Chemistry Preprints, 1983, (28), 4, 138.

2.   Morgan, M. E., Ph.D. Thesis, The Pennsylvania State UNiversity, University Park, PA, 1983.

3.   Walker, P. L., Jr., Matsumoto, S., Hanzawa, T., Miura, T. and Ismail, J. M. K., Fuel, (62), 1983, 140.

4.   Scaroni, A. W., Walker, P. L., Jr. and Essenhigh, R. H., Fuel, 1981, (60), 71.

5.   Anthony, D. B. and Howard, J. B., AIChE Journal, 1976, (22), 625.

6.   Badzioch, S. and Hawksley, P. G. W., Ind. Eng. Chem. Process Des. Dev., 1970, (9), 521.

7.   De, G. S., Tumuluri, S. and Lahari, K. C., Fuel, 1971, (50), 272.

8.   Johnson, J. L., Kinetics of Coal Gasification, John Wiley and Sons, Inc., NY, 1979.

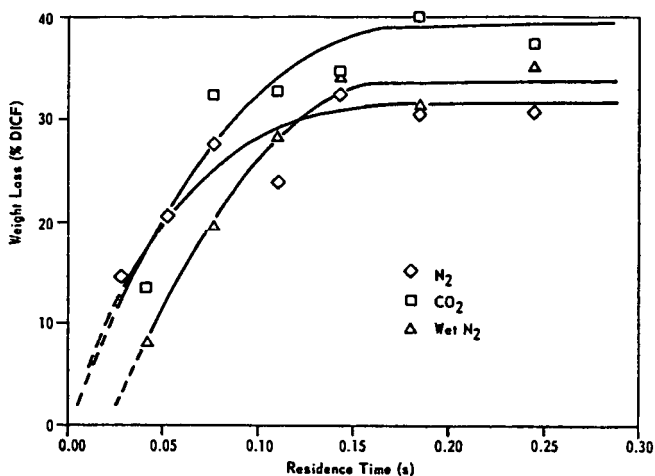9.   Walker, P. L., Jr., Rusinko, F. and Austin, L. G., Adv. in Cat., 1959, (11), 133.

Figure 2. WEIGHT LOSS IN ENTRAINED FLOW REACTOR
IN N_2, CO_2 AND WET N_2
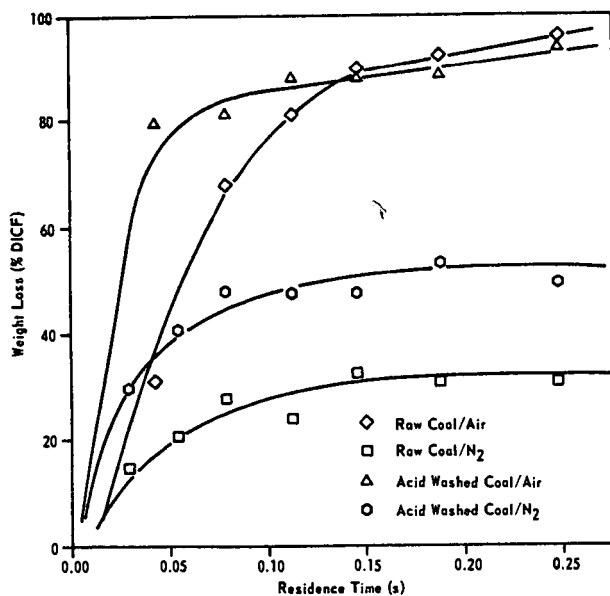Raw Montana Lignite, 270 x 400 Mesh

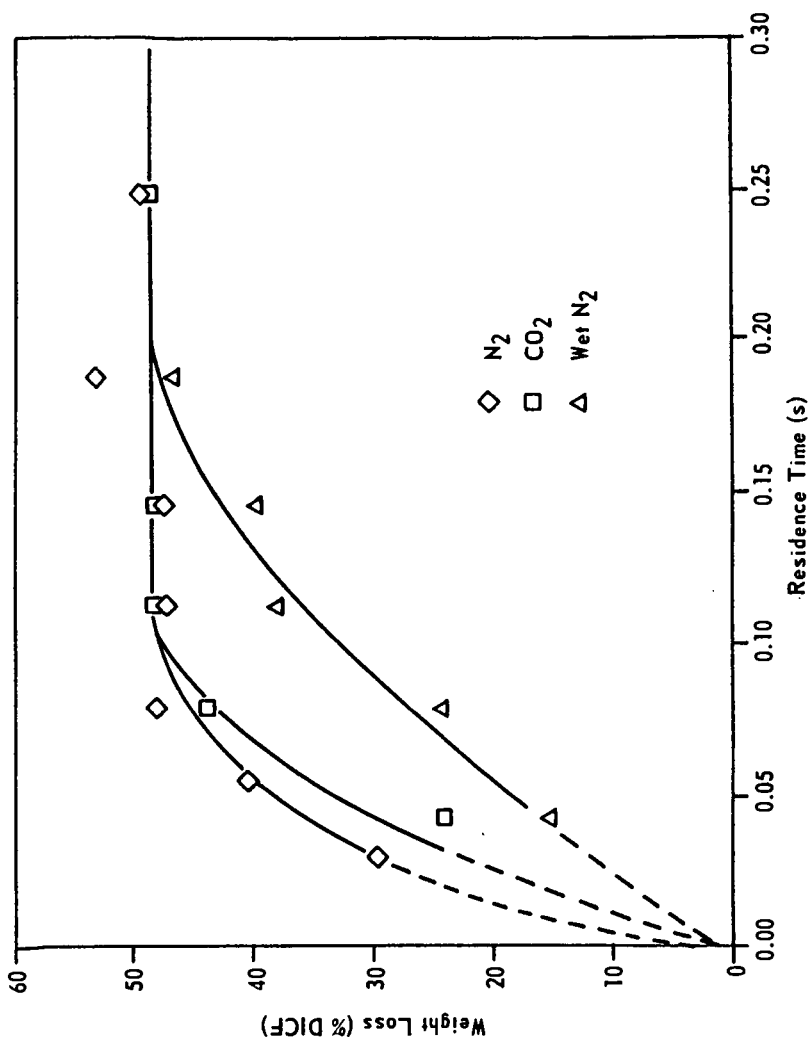Figure 1. WEIGHT LOSS IN ENTRAINED FLOW REACTOR
IN AIR, 1173K

144

Figure 3. WEIGHT LOSS IN ENTRAINED FLOW REACTOR
IN N_2, CO_2 AND WET N_2
Acid Washed Montana Lignite, 270 x 400 Mesh

145

THE EFFECT OF INORGANIC SPECIES ON CHAR FORMATION FROM BIOMASS FUELS

William F. DeGroot and Fred Shafizadeh[1]

Wood Chemistry Laboratory
University of Montana
Missoula, Montana   59812

INTRODUCTION

Inorganic species naturally present in biomass play a dual role in terms of the thermochemical properties of biomass and its char. They dramatically affect the temperature and extent of pyrolysis, and many are effective catalysts for combustion and gasification reactions of the resulting char. Previous work in this laboratory (1) on the effect of prepyrolysis treatment of wood with gasification catalysts has indicated that inorganic species naturally present in wood are exchangeable with ions added from solution. Glucuronic acid groups which are present in the hemicellulose fraction of wood, particularly in the acetyl 4-0-methylglucuronoxylans which comprise the hemicellulose fraction of hardwoods, are the most likely sites for ion exchange. Free phenolic groups in the lignin fraction are another probable exchange site. This study was undertaken to determine the role of exchangeable cations on char formation and to further examine the nature of ion exchange in wood. Thus, samples of untreated and acid-washed wood were treated with solutions of the two most prevalent naturally-occurring inorganic species in wood, calcium and potassium; and the effect of the treatments on the thermal decomposition of the wood was determined by thermogravimetry (TG) and derivative thermogravimetry (DTG). The results indicate the mode of addition of gasification catalysts added to wood and their effects on carbonization.

EXPERIMENTAL

The primary sample used in this study was a well-characterized sample of black cottonwood, _Populus trichocarpa_, a common North American hardwood. Douglas fir, _Pseudotsuga menzeisii_, was used as a secondary sample to confirm specific trends in a softwood species. Samples were ground and sieved and the 20-40 mesh fraction was retained. The chemical composition of both samples is given in Table I.

TABLE I
ANALYSIS OF WOOD SAMPLES AND THEIR ASH CONTENT

Species	Percent Ash	Percent Lignin	Inorganic Analysis ($\mu g/g$ wood)					
			Na	K	Mg	Ca	Mn	Fe
Cottonwood	0.41	20.3	18	668	324	869	<5	5
Douglas fir	0.10	27.4	3	32	53	314	20	<3

Wood samples were treated with potassium carbonate or calcium acetate for TG analysis by soaking in a 0.013 N solution of the salt for 30 minutes and removing excess solution by filtration with suction. For preparation of ion-exchanged samples, the filtered wood was then stirred for 30 minutes in distilled, degassed water to remove adsorbed salts and dried at 40°C under reduced pressure. In some cases, the distilled water wash was eliminated to provide samples treated at a level beyond the exchange capacity of the wood with adsorbed salts.

Acid-washed wood and cellulose samples were prepared by placing 10 g of the sample in 200 ml of 0.1 N HCl and stirring for 4 hours at room temperature. The suspension was then filtered and the wood was washed with 2 liters of distilled water, covered with distilled water and stirred overnight. The sample was filtered again,

---

placed in a cellulose extraction thimble and washed for 4 hours in a Soxhlet extractor. The sample was then dried at 70°C under reduced pressure.

Thermogravimetry was carried out using a Perkin-Elmer TGS-2 system which was interfaced to a microcomputer for data acquisition and temperature program control. For determination of char yields, one milligram of sample was heated in a platinum pan to the desired temperature at 25°C/min under flowing nitrogen. This system was also used for ash determinations, in which case the sample was heated to 550°C at 20°C/min under a mixture of O_2 and N_2 and held at 550°C for 10 min. Ash determinations made in this way agreed with those determined on a large scale by standard methods to within 0.02%.

Surface areas of chars were determined gravimetrically using a Cahn R-100 electrobalance (sensitivity = 0.1 µg) equipped with a Cahn adsorption tube. Isotherms were determined for 5-10 mg samples by monitoring carbon dioxide adsorption at room temperature. Surface areas were calculated by application of the Dubinin-Polanyi equation (2).

RESULTS AND DISCUSSION

The effects of acid washing and addition of calcium and potassium salts on the ash content, char yield and decomposition temperature of cottonwood, Douglas fir and cellulose samples are shown in Table II. The ash contents of the ion-exchanged

TABLE II

EFFECTS OF VARIOUS TREATMENTS ON MINERAL CONTENT, CHAR YIELD (HTT 600°C)
AND TEMPERATURE OF MAXIMUM WEIGHT LOSS IN WOOD AND CELLULOSE

Sample and Treatment	Ash Content (%, d.a.f.)	Char Yield (%, d.a.f.)	Temperature of DTG Peak (°C)
COTTONWOOD			
Untreated	0.40 ± 0.03	12.8 ± 0.1	387 ± 2
Acid washed, 0.1% HCl	<0.01	9.8 ± 0.4	379 ± 1
Acid washed, potassium added from solution	0.40 ± 0.05	17.2 ± 0.4	366 ± 1
Acid washed, calcium added from solution	0.27 ± 0.04	12.7 ± 0.3	394 ± 1
Acid washed, calcium and potassium added from solution	0.36 ± 0.01	12.4 ± 0.3	393 ± 3
Potassium added from solution	0.45 ± 0.05	14.1 ± 0.5	375 ± 1
Calcium added from solution	0.34 ± 0.03	11.5 ± 0.3	389 ± 1
Hot water, 6 hr. @ 60°C	0.26 ± 0.01	11.2 ± 0.3	391 ± 1
DOUGLAS FIR			
Untreated	0.10 ± 0.01	15.7 ± 0.3	385 ± 1
Acid washed, 0.1% HCl	<0.01	13.4 ± 0.3	388 ± 1
CELLULOSE (CF-11)			
As received	<0.01	5.4 ± 0.3	367 ± 1
Acid washed, 0.1% HCl	<0.01	3.6 ± 0.1	354 ± 2
Acid washed, potassium added from solution (no H_2O wash)	0.09 ± 0.04	10.6 ± 0.1	392 ± 1
Acid washed, calcium added from solution (no H_2O wash)	0.13 ± 0.01	5.7 ± 0.1	365 ± 1

cottonwood samples are similar to that of the untreated sample, suggesting that the factors controlling the ash content in wood are related to some extent to ion-exchange capacity. As expected, the calcium-exchanged samples contain less ash in every case because the wood has lower exchange capacity for the divalent calcium cation.

Comparison of the char yields and decomposition temperatures of untreated, acid-washed and ion-exchanged cottonwood samples provides some insight into the overall effect of inorganic species on char formation, as well as contribution of specific cations to the overall effect. It is apparent from the data given in Table II that both the natural ash components and the ions added from solution significantly increase the char yield above that obtained for the ash-free sample. The difference in char yields from untreated and acid-washed Douglas fir samples is less, apparently because of the lower ash content of that sample. As shown in Figure 1, acid washing also has a profound effect on the physical properties of the char. Char from untreated wood retains the original cellular structure of the wood, whereas the original structural features of the wood are lost during carbonization of acid-washed wood. Chars were formed from several substrates under a variety of conditions in order to determine the requirements for loss or retention of physical structure. In general, we found that the physical structure was lost only in acid-washed wood samples and particularly when heated at high rates (>500°C/min). Acid-washed cellulose retained its cellular structure even when heated at very high rates, however.

Because of the possible implications of loss of cellular structure in terms of available surface areas, we measured surface areas of chars prepared at high heating rates from untreated and acid-washed samples of Douglas fir and cellulose. All of the samples had total surface areas of between 800 and 1000 m^2/g, indicating the total available surface area is not significantly reduced due to loss of cellular structure in the wood. As seen in Figure 1, it is very likely that the loss of cellular structure in the acid-washed wood is counteracted by foaming of the intermediate char during carbonization.

The most pronounced effect of added inorganics is due to addition of potassium ions, which resulted in an 80% increase in char yield, even at the low concentration afforded by ion exchange. The char yield from the calcium-exchanged cottonwood is more like that of the untreated sample, which suggests that calcium content strongly influences the char yield in this sample. The effect of ion-exchange treatments on the decomposition temperature adds further support to this hypothesis. Potassium treatment reduces the temperature of decomposition, while calcium treatment increases the decomposition temperature. Therefore, the higher temperature of decomposition of untreated wood compared to acid-washed wood can be attributed to the dominant effect of calcium on the decomposition. Addition of potassium and calcium from the same solution (0.007 N in each) gives results very similar to those found for the calcium treatment, which indicates that the calcium is bound preferentially.

The characteristic effects of calcium and potassium on the thermal decomposition of cottonwood provide a means of determining the extent of exchange of ions from solution with naturally-occurring inorganic species. As shown in Table II, addition of potassium and calcium to previously untreated cottonwood results in the same changes in the thermal decomposition patterns as observed for treatment of acid-washed cottonwood, although the effects are less pronounced. Addition of potassium increases the char yield and reduces the decomposition temperature, while addition of calcium reduces the char yield and increases the decomposition temperature slightly. These results indicate that the original ash components can be replaced to some degree by elements added from solution through ion exchange.

Table II also shows the TG results for a cottonwood sample extracted with hot water. This treatment was included primarily to determine whether the hot water Soxhlet extraction step after acid washing might have resulted in swelling of the wood, which could be expected to affect the extent of charring of the wood. As shown in

Table II, the char yield was reduced somewhat by this treatment, but not to the degree observed with acid washing. Furthermore, the hot water extraction increased the decomposition temperature while acid washing decreased the decomposition temperature. In fact, the decomposition pattern is very much like that of calcium-treated cottonwood; thus the reduction in char yield does not appear to be due to physical changes, but rather results from removal of elements such as potassium which tend to reduce the decomposition temperature and enhance charring, allowing the opposing effect of calcium to be more pronounced. The tendency of calcium to be removed less readily from wood by hot water treatment, combined with its preferential addition to wood from solutions containing both potassium and calcium, indicate stronger binding by wood of calcium ions and presumably other alkaline earth metals such as magnesium, which is also present in substantial quantities in many species of wood.

The effects of acid washing and ion exchange treatments on wood decomposition are further illustrated by the DTG's shown in Figures 2 and 3. Figure 2 shows the effect of acid washing on the rate of thermal decomposition of cottonwood and Douglas fir. In both samples, acid washing results in a lower rate of decomposition at low temperatures (250-350°C) and enhances the primary decomposition which peaks near 385°C. Since the low temperature 'shoulder' in the DTG of wood is generally attributed to decomposition of hemicelluloses (3,4), it is apparently the decomposition of this fraction which is most affected by the acid washing. The likelihood of association of inorganic species with the hemicellulose fraction through the glucuronic acid groups further suggests that inorganic species act primarily on the hemicellulose fraction and reduce its decomposition temperature. In the absence of exchanged cations, the hemicelluloses decompose at higher temperatures and produce less char.

Figure 2 shows the effects of several treatments on the DTG of acid-washed cottonwood. The DTG of untreated cottonwood is shown by dotted lines for comparison. The DTG of the potassium-exchanged sample [Figure 2(A)] shows that the low temperature 'shoulder', which was reduced by acid washing is restored by the potassium treatment. The 'cellulose peak' has the same general shape, but is shifted to much lower temperature. With addition of calcium to acid-washed cottonwood [Figure 2(B)], the low temperature shoulder is restored to a lesser extent. When the wood is treated with a solution containing potassium and calcium [Figure 2(C)], the decomposition is identical to that of the calcium-treated wood, except the low temperature shoulder is restored to a greater extent. The DTG of cottonwood which was extracted with hot water, shown in Figure 2(D), is also very much like that of calcium-treated cottonwood. These results indicate that potassium has the greatest effect on the decomposition of the hemicellulose fraction, even though calcium is preferentially bound by ion exchange. However, the overall decomposition of untreated cottonwood, as indicated by the char yield and temperature of the cellulose decomposition is more closely related to the effect of calcium, as discussed previously.

The effects of acid washing and addition of potassium and calcium salts to pure cellulose are also shown in Table II. In this case, the water extraction after the exchange treatment was eliminated, since pure cellulose has few exchange sites and all of the salt was removed by water extraction. These data show that the effects of adsorption of potassium or calcium salts on cellulose decomposition are very different from the effects of the corresponding salts added to wood through ion exchange. Potassium treatment dramatically increases the decomposition temperature of acid-washed cellulose, while it decreases that of wood. The char yield increased in both wood and cellulose. Conversely, treatment of acid-washed cellulose with calcium increases the decomposition temperature only slightly, whereas it dramatically increased the decomposition temperature of wood. Some of these differences may be due to counterion effects, which would be absent in the ion-exchanged wood samples, although these effects are expected to be minimal with the acetate and carbonate salts used in this study. The increase in cellulose decomposition temperature after treatment with potassium has also been noted with other alkali metal salts, particularly sodium (5,6).

The effects of addition of salts to wood beyond the exchange capacity are shown in Figures 4 and 5. These samples were prepared by reducing or eliminating the water wash after ion exchange treatment. Figure 4 shows that the effect of both salts on char yield continues to increase as the level of addition is increased. Thus, adsorbed salts and exchanged cations appear to have similar effects on the char yield in wood, as would be predicted on the basis of the results for adsorption of salts on cellulose.

The dependence of the temperature of the maximum rate of weight loss on level of addition of salts is shown in Figure 5. Surprisingly, adsorption of potassium salts beyond the exchange capacity continues to reduce the decomposition temperature, whereas potassium dramatically increased the decomposition temperature of cellulose. The most likely explanation for this behavior is that the increased potassium treatment continues to decrease the decomposition temperature of the hemicelluloses, and the decomposition products of the hemicellulose fraction catalyze decomposition of the cellulose fraction. Adsorption of calcium on wood reduces the initially high decomposition temperature slightly, which is predictable on the basis of the effects of calcium on cellulose decomposition.

CONCLUSIONS

The results of this study show that inorganic species, whether present as components of the natural ash fraction or as added catalysts, have a significant effect on temperature and extent of pyrolysis of wood and even the physical structure of the resulting char. The effects of specific cations added to wood by ion exchange are different from the effects of the corresponding salts adsorbed on cellulose. The overall decomposition of untreated cottonwood appears to be affected primarily by the presence of calcium, which is the predominant component of the ash. However, the decomposition of the hemicellulose fraction, which precedes the primary decomposition of the wood, depends in large part on the presence of potassium ions. The loss of cellular structure in acid-washed wood is believed to be due to enhanced volatilization of the fibrous carbohydrate components which provide the structure of the cell wall. The char then arises primarily from lignin, an amorphous polymer which can flow at high temperatures. Because of the close association of inorganic species with the hemicelluloses through ion exchange, it is very likely that decomposition of the hemicelluloses contributes significantly to char formation in wood.

ACKNOWLEDGEMENT

REFERENCES

1. W.F. DeGroot and F. Shafizadeh, "Kinetics of Gasification of Douglas Fir and Cottonwood by Carbon Dioxide", accepted for publication in Fuel.

2. H. Marsh and W.F.K. Wynne-Jones, Carbon, 1, 269 (1964).

3. F. Shafizadeh and G.D. McGinnis, Carbohydr. Res., 16, 273 (1971).

4. F.C. Beall, Wood and Fiber, 1, 215 (1969).

5. F. Shafizadeh, P.S. Chin, and W.F. DeGroot, J. Fire Flamm./Fire Retardant Chemistry, 2, 195 (1975).

6. Y. Sekiguchi and F. Shafizadeh, "The Effect of Inorganic Additives on the Formation, Composition and Combustion of Char", J. Appl. Polym. Sci., accepted for publication.

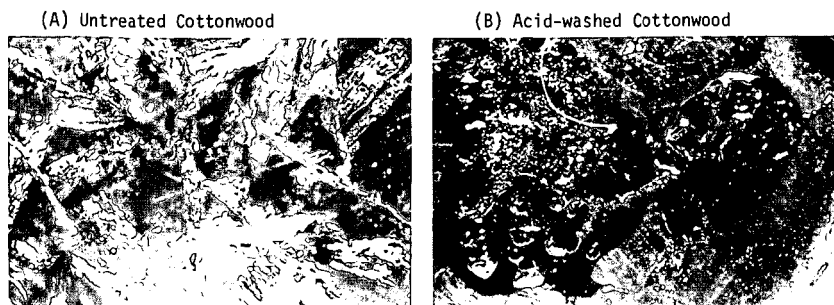(A) Untreated Cottonwood   (B) Acid-washed Cottonwood

Figure 1.   Photomicrographs of chars prepared from untreated and acid-washed cottonwood. (Magnification: 60X)
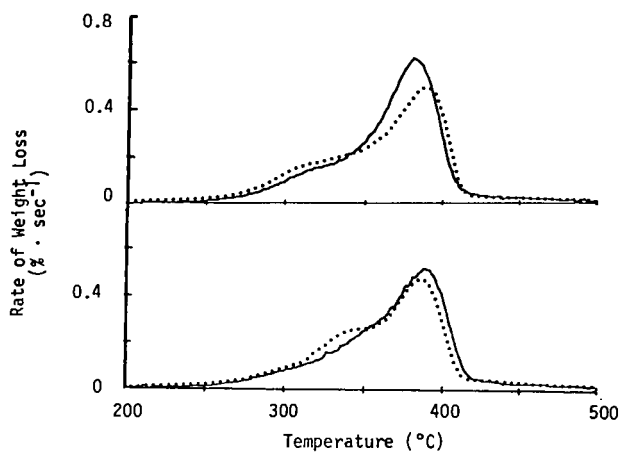

Figure 2.   Effects of acid washing on the rate of weight loss (DTG) from cottonwood and Douglas fir. The DTG of the untreated sample is indicated by dotted lines.
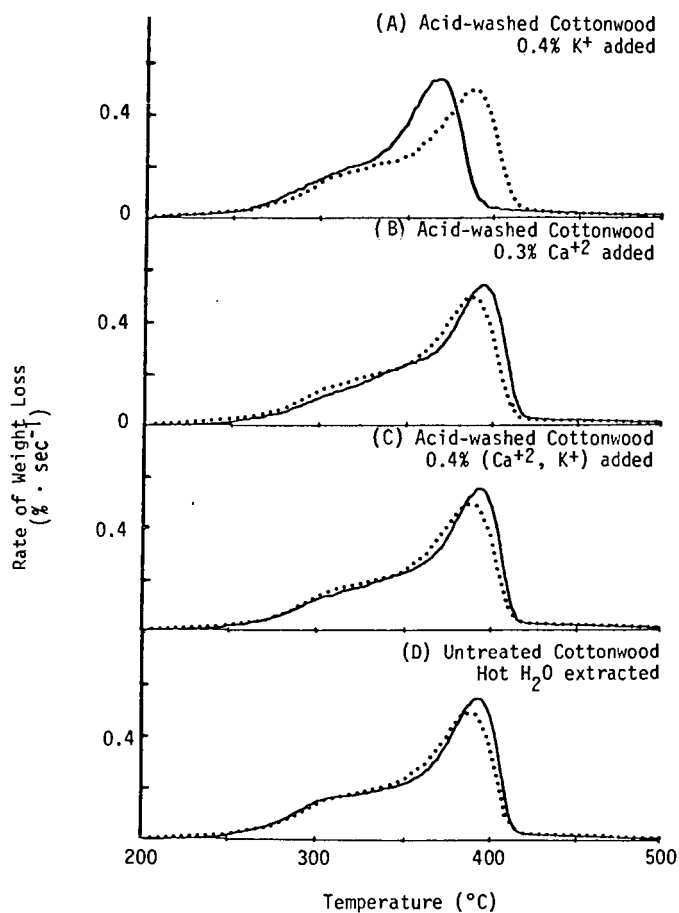
Figure 3. Effects of ion exchange and hot water extraction on the rate of weight loss (DTG) of cottonwood. The DTG of untreated cottonwood is indicated by dotted lines.

Figure 4. Effect of level of addition of calcium (O) and potassium (●) on the char yield from cottonwood.
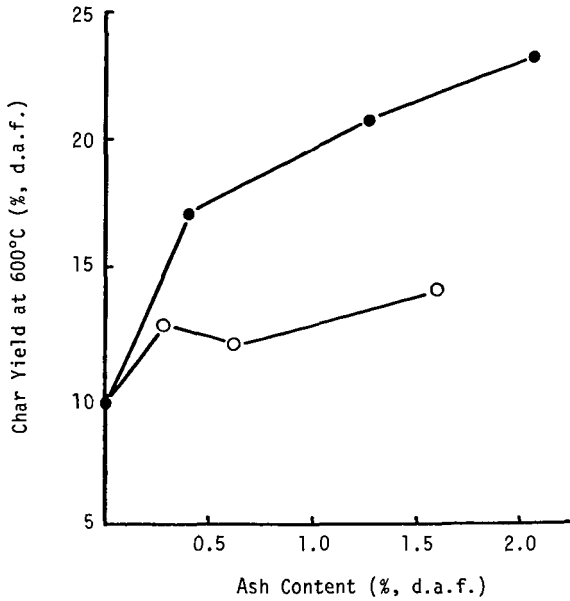
Figure 5. Effect of level of addition of calcium (O) and potassium (●) on the temperature of the maximum rate of weight loss from cottonwood.
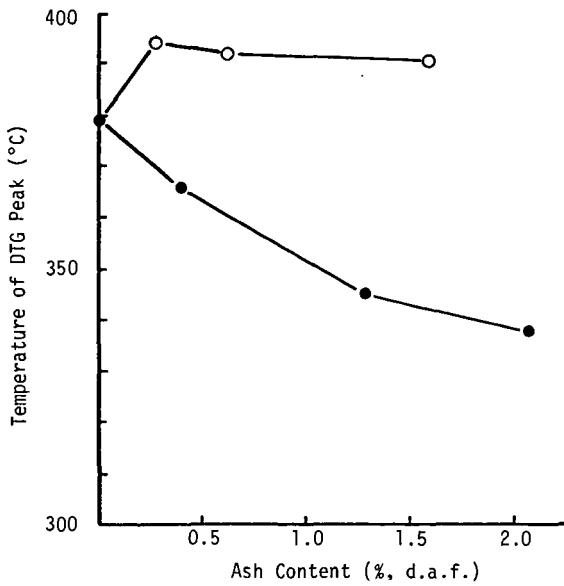
SMALL-ANGLE X-RAY SCATTERING INVESTIGATION OF THE EFFECT OF
HEATING TEMPERATURE ON THE SUBMICROSCOPIC PORE STRUCTURE OF WOOD CHARCOAL*

P. W. Schmidt, M. Kalliat**,

Physics Department
University of Missouri, Columbia, MO 65211

and B. E. Cutter

School of Forestry, Fisheries and Wildlife
University of Missouri, Columbia, MO 65211

INTRODUCTION

One of the important advantages of x-ray techniques in structural studies is that the x-ray data can provide some information about the <u>dimensions</u> of the structure. Small-angle x-ray scattering, which is useful (1,2) for learning about dimensions from about 10 to 2000 Å, is an important method for investigating structures too small to be resolved by optical or scanning electron microscopy.

Small-angle x-ray scattering has been applied (3--8) in several studies of the porosity of charcoal produced by pyrolysis of wood. One of the questions considered in this research was the dependence of the pore dimensions and some other properties, of the pores on the temperature to which the wood was heated during the process of pyrolysis in which the charcoal was produced.

We have already described (6-8) the results of our application of small-angle x-ray scattering in studies of several charcoals prepared by heating to temperatures not exceeding 1000°C. In order to learn about the effects of higher preparation temperatures, we recently examined a series of charcoals from black cherry (<u>Prunus serotina</u> Ehrh.) wood heated to temperatures from 600° to 2000°C. The results are summarized in this report.

In addition to obtaining some information about the pore structure of black cherry charcoal, we have developed a general picture of how the charcoal porosity depends on the temperature to which the wood was heated during pyrolysis. We have found (8) that for wood and for charcoal heated to temperatures not exceeding 350°C, the small-angle x-ray scattering is dominated by the scattering from crystalline cellulose, and little can be learned about the pore structure. At heating temperatures between 350° C and 400°C, this cellulose decomposes, and for charcoals prepared by heating to about 400°C, our scattering data indicate that there are large pores, called (9) macropores, with dimensions of at least a micron, transitional pores, which have dimensions of the order of a few hundrend Å, and a relatively small number of much smaller pores, which, using Dubinin's terminology (9), we will refer to as micropores and which have average dimensions which do not exceed approximately 30 Å. The scattering curves which we have now obtained for charcoals prepared by heating to temperatures above 1000°C show that these higher preparation temperatures have a relatively small effect on the scattering associated with the macropores and transitional pores, but for preparation temperatures above 400°C, the scattering ascribed to the micropores increases rapidly with the preparation temperature. These results have led us to propose that the macropores in charcoals are similar to those in wood and that the main effect which pyrolysis at temperatures above 400°C exerts on the pore structure is to cause the micropores and transtional pores to grow, while leaving the macropores almost unchanged.

**Current Address: Bell Laboratories, 4500 S. Laburnum Ave., Richmond, VA 23231

EXPERIMENTAL TECHNIQUES AND METHODS OF DATA ANALYSIS

The samples were prepared (10) by Paul R. Blankenhorn at the Pennsylvania State University School of Forest Resources by heating black cherry wood to temperatures of 600, 1500, 1750, and 2000°C in a nitrogen atmosphere.

Our scattering data were recorded by the methods discussed in Reference (8), which also reviews the corrections which we applied to the measured scattering curves.

We now will summarize some of the methods and techniques which we employed in the interpretation of our small-angle x-ray scattering data from charcoals. In a typical small-angle scattering study, x-rays from an x-ray tube are formed into a well-defined beam, usually by slits, and strike the sample. A small fraction of these x-rays are re-emitted, without change of wavelength, in directions different from that of the incoming beam. The intensity of these re-emitted x-rays, which are called the scattered rays, and their dependence on the direction in which they are emitted depend on the structure of the sample. In a scattering experiment, the intensity of the x-rays scattered in different directions is recorded, usually with some type of proportional counter. From an analysis of these data, an attempt is made to obtain information about the structure of the sample.

While there is no general prescription for analyzing the scattering pattern from an arbitrary sample, we will review some methods useful for interpretation of scattering measurements from porous materials like charcoals. For a sample which has a structure characterized by a dimension a, most information obtainable from scattering measurements will be found at scattering angles θ in an interval for which

$$0.1 < ha < 10,\qquad\qquad 1)$$

where $h = (4\pi/\lambda) \sin(\theta/2)$; θ is the scattering angle (that is, the angle between the directions of the incident and the scattered beams); and λ is the x-ray wavelength. For angles no greater than about 7 degrees, $\sin\theta/2$ can be approximated by $\theta/2$, and so for small scattering angles, h can be considered proportional to θ. According to Inequality 1), for a structure with dimension a, the scattering is determined by the product ha, so that there is an inverse relationship between the size of the structure and the h values at which the scattered intensity from this structure is appreciable. Since the x-ray wavelengths are normally of the order of 1 or 2 Å, Inequality 1) implies that the x-ray scattering from structures with dimensions between about 20 and 2000 Å will be observed at scattering angles no greater than a few degrees. Small-angle x-ray scattering thus can be used to study these submicroscopic structures.

X-rays are scattered by electrons, and the small-angle scattering will be appreciable when the sample contains regions in which fluctuations or variations in electron density extend over distances of 10 to 2000 Å. At <u>small</u> angles, the scattering process is unable to resolve structures smaller than <u>about</u> 10 Å, and so in the analysis of the scattering data, the atomic-scale structure can be neglected. We therefore found it convenient to consider the charcoal sample to be composed of two phases, with constant but different electron densities. One of the phases is carbonized wood, and the other is air. Because the electron density of air is so small, the scattering from the air in the pores can be neglected, and the pores can be considered to be empty.

When the two phases always are separated by a sharp, discontinuous boundary, and when h is large enough to satisfy the condition $ha_m > 3.5$, where a_m is the <u>minimum</u> characteristic dimension of the structure, the scattered intensity I(h) can be approximated by (11)

$$I(h) = \frac{2\pi\rho^2(S/M)}{h^4}\ \frac{M}{A}\ I_e A,\qquad\qquad 2)$$

where ρ is the difference of the electron densities of the two phases, I_e is the intensity scattered by a single electron; S is the total surface area separating the two phases in the sample; M is the mass of the sample; and A is the cross-sectional area of the sample perpendicular to the incident beam. According to Equation 2), in

the outer part of the small-angle scattering curve (that is, when $ha_m > 3.5$), the scattered intensity is proportional to h^{-4} and thus to the inverse fourth power of the scattering angle. Moreover, when $I(h)$ has this angular dependence, the magnitude of the scattered intensity is proportional to the specific surface S/M, which is the surface area per unit sample mass separating the two phases.

As we explain in Reference (11), the quantities $I_e A$ and M/A can be evaluated from the x-ray data, and so Equation 2) can be employed to calculate the specific surface S/M from the scattering data for samples with submicroscopic porosity.

The specific surface S/M calculated from Equation 2) is often referred to as the "x-ray specific surface", since it is determined from the x-ray scattering data. In this discussion of our studies of charcoal, it is important to remember that the x-ray specific surface includes only the surface of pores large enough to satisfy the condition $ha_m > 3.5$. The x-ray specific surface thus represents only the surface of the macropores and transitional pores and does not include the contribution of the micropores. This result, we believe, is the main reason why specific surfaces measured by adsorption, which often takes account of the surfaces of all three classes of pores, can be much larger than the x-ray specific surfaces.

To analyze the scattering curves which we have obtained from charcoals, we made least-squares fits of a theoretical scattering equation which contained terms representing the contributions to the scattered intensity from all three types of pores. This equation can be expressed

$$I(h) = 2\pi\rho^2 I_e A \frac{M}{A} [\frac{S_1}{h^4} + \frac{S_2}{(c^{-2} + h^2)^2} + \frac{N}{2\pi M} \overline{V^2} F_m(hb)]. \qquad 3)$$

where S_1 and S_2 are the surface areas per unit sample mass associated with the macropores and transitional pores; c is a constant proportional to the average characteristic dimension of the transitional pores; N is the number of micropores in the scattering sample: b is the average dimension of the micropores; V is the volume of a micropores; the bar indicates an average of V^2 over the sample; and $F_m(hb)$ is a function which describes the angular distribution of the scattering from the micropores and which is defined to have the property that $F_m(0) = 1$. The micropores are assumed to scatter independently of each other. The term in Equation 3) proportional to S_2 describes the scattering from the transitional pores and is the expression obtained by Debye, Anderson, and Brumberger (12) for the scattering from a two-phase sample with a random distribution of scatterers. We feel that this expression is a reasonable and convenient way to approximate the scattering from the transitional pores. The macropore scattering is represented in Equation 3) by the term proportional to S_1. The macropores are so large that our scattering data permit only the calculation of the specific surface of these pores and provide no information about their dimensions.

RESULTS AND DISCUSSION

Figure 1 shows the scattering curves which we obtained for southern pine wood heated to 400°C at different rates (8). When the sample temperature was raised at a rate of 50°C per minute, the scattering pattern was quite similar to the curve obtained for wood before heating. For a temperature rise of only 1°C per minute, on the other hand, the inner part of the scattering curve is nearly proportional to the inverse fourth power of h, as would be expected for the scattering from macropores, while in the outer part of the scattering curve, the intensity is nearly constant, as we would predict for micropores. The third curve in Fig. 1 is for a sample with a temperature increase of 10°C per minute and is intermediate beween the other two curves. We have shown (8) that the change from a curve like the curve for a heating rate of 50°C/min to a curve with the form of the curve for 1°C/min is accompanied by the disappearance of the large-angle diffraction peaks from cellulose. We have therefore concluded that the curve for a heating rate of 1°C/min represents the scattering from only the pores in the charcoal.

Figure 2 shows the scattering curves for black cherry samples heated to

156

temperatures of 600, 1500, 1750, and 2000°C. Regardless of the temperature at which the sample was prepared, the inner part of the scattering curve is nearly proportional to h^{-4}. This region of the curve is almost the same for all heating temperatures, but the intensity in the outer part of the curve rises as the heating temperature is increased. This part of the curve contains the information about the micropores.

The curves in Fig. 2 were determined by least-squares fits of Equation (3) to the scattering data for the black cherry charcoals. In the fits of the scattering data recorded for samples produced at 1500°C and above, for $F_m(hb)$ we used the function $P_2(h,1)$ calculated (13) for assemblies of uniform spherical scatterers with different diameters. With this fitting function, we obtained at least an adequate fit. In our analysis of the curve for the sample heated at 600°C we employed an $F_m(hb)$ function of the same form as the function chosen to represent the scattering from the transitional pores. We multiplied the average micropore dimension obtained in this fit by a constant which permitted this b value to be compared with the other average micropore dimensions.

As can be seen from Table 1, which lists some of the quantities obtained from the least-squares fits of Equation (3), when the preparation temperature is raised from 600°C to 2000°C, the constant

$$B = \frac{N}{2\pi M} \, \overline{V^2},$$

which expresses the magnitude of the scattering from the micropores, increases by a factor of almost 50, while the average micropore dimension b is not even doubled. [The rather unusual units $cm^3 \AA^3/gm$ used for B are convenient for some analyses discussed in Reference (8).] If the shape of the micropores is independent of the preparation temperature, the square of the volume of a pore is proportional to b^6, and according to Equation 4), B/b^6 should be proportional to N/M, the number of pores per unit mass. From the values of B and b in Table 1, as the temperature of sample preparation increases from 600°C to 2000°C, B/b^6 varies by about 30% around its average value for the four samples. Within the relatively large uncertainty resulting from the fact that b is raised to the sixth power, B/b^6 thus is independent of the pyrolysis temperature. We therefore can consider that the number of micropores, which according to Equation 4) is proportional to B/b^6, remains very nearly constant, so that higher pyrolysis temperatures lead to charcoals with larger micropores, but the number of micropores does not change appreciably.

In our discussion of data analysis, we have avoided making any precise statements about the meaning of the average pore dimensions, since the definition of these average dimensions depends on the pore shape and on the distribution of pore dimensions. However, Equation 3) contains terms which give the scattering from the the three classes of pores. The models used to obtain the terms for the contributions from the transitional pores and micropores specify what the average pore dimensions represent in these models. In the expression for $F_m(hb)$ which we used to describe the scattering from the micropores for preparation temperatures of 1500°C and above, b is the most probable micropore radius in a system of independently-scattering spheres with different radii. The interpretation of the other average dimensions is discussed in Reference (12).

The quantities S_1, S_2, and B were evaluated by the techniques we employed in our investigation of southern pine charcoal (8). In our calculations, we assumed (8) that the density of the carbon in the charcoals was gm/cm³, while we took the mass absorption coefficient of carbon to be 4.60 cm²/gm.

In Table 1 we show only the total x-ray specific surface $(S_1 + S_2)$, since we found that the region of the scattering curve which was nearly proportional to the inverse fourth power of h was not long enough to permit a good separation of the contributions of the macropores and transitional pores to the total x-ray specific surface. We estimate that the uncertainty in the x-ray specific surfaces in about 25%. Since the x-ray specific surface $S_1 + S_2$ is so nearly the same in all four samples, we suggest that the macropore structure in the charcoal samples is almost the same as in the wood from what the charcoals were prepared.

While the uncertainty in the value of c computed from the least squares fits increases to about ±50% for the sample heated to 2000°C, our fits show a steady

growth in the average dimension c of the transitional pores as the preparation temperature becomes higher.

Unfortunately, we were not able to obtain black cherry samples heated to temperatures between 600°C and 1500°C. Samples prepared in this temperature interval would probably give a more detailed description of the effect of pyrolysis temperature on the number and average dimension of the micropores.

We feel, however, that the scattering curves which we have presented here are sufficient to support our views about the relation between the pore structure and the temperature at which the sample was prepared. From our analysis of the scattering data, we have concluded that when the charcoals are prepared by heating to 400°C, most of the scattering comes from the macropores and transitional pores, with a relatively small contribution from the micropores, the dimensions of which are not large enough to be determined reliably from the scattering data. For pyrolysis at temperatures in the interval from 400°C through 2000°C, the transitional pores and micropores become larger, while the x-ray specific surface and the number of micropores remain nearly the same.

ACKNOWLEDGMENTS

REFERENCES

1. Guinier, A.; Fournet, G.; Walker, C. B.; Yudowitch, K. L.; "Small-Angle Scattering of X-Rays"; Wiley: New York, 1955.
2. Glatter, O., and Kratky, O.; "Small Angle Scattering of X-Rays"; Academic Press: New York, 1982.
3. Jánosi, A.; Stoeckli, H. F. Carbon 1979, 17, 465-469.
4. Hernández, J. G.; Hernández-Calderón, I.; Luengo, C. A.; Tsu, R. Carbon 1982, 20, 201-205.
5. González, J. H.; Torriani, I. L.;, Luengo, C. A. J. Appl. Cryst. 1982, 15, 251-254.
6. Von Bastian, C. R.; Schmidt, P. W.; Szopa, P. S.; McGinnes, E. A., Jr. Wood and Fiber 1972, 4, 185-192.
7. Casteel, J. L.; Pringle, O. A., Jr.; Lin, J. S.;, Schmidt, P. W.; Slocum, D. H.;, McGinnes, E. A., Jr. Wood and Fiber 1978, 10, 6-18.
8. Kalliat, M.; Cutter, B. E.; Kwak, C. Y.; Schmidt, P. W.; McGinnes, E. A., Jr. Wood Science and Technology, in press.
9. Dubinin. M. M.; in "Chemistry and Physics of Carbons"; Walker, P. L., Jr., ed.; Vol II; Dekker: New York, 1954; pp. 51-59.
10. Blankenhorn, P. R.; Barnes, D. P.; Kline, D. E.; Murphey, W. K. Wood Sci. 1978 11, 23-29.
11. Kalliat, M.; Kwak, C. Y.; Schmidt, P. W.; in "New Approaches to Coal Chemistry"; Blaustein, B. D.; Bockrath, B. C.; Friedman, S., eds.; ACS Symposium Series No. 169; Amer. Chem. Soc.: Washington, 1981; pp. 3-22.
12. Debye, P.; Brumberger, H.; Anderson, H. L., Jr. J. Appl. Phys. 1957, 28, 679-683.
13. Schmidt, P. W. Acta Cryst. 1958, 11, 675.

TABLE 1
Quantities Evaluated from the Least-Squares Fits

Pyrolysis Temperature	$S_1 + S_2$ (m^2/gm)	$B(cm^3Å^3/gm)$	$b(Å)$	$c(Å)$
600°C	1.6	2.9	1.3	0.33×10^2
1500	1.7	60	2.0	0.76×10^2
1750	1.9	87	2.1	2.2
2000	1.8	122	2.4	5.3

Figure 2. Scattering curves for black cherry charcoal pyrolized at temperatures of 600 (squares), 1500 (circles), 1750 (triangles) and 2000 (crosses) degrees C. The curves were obtained by least-squares fits of Eq. 3).
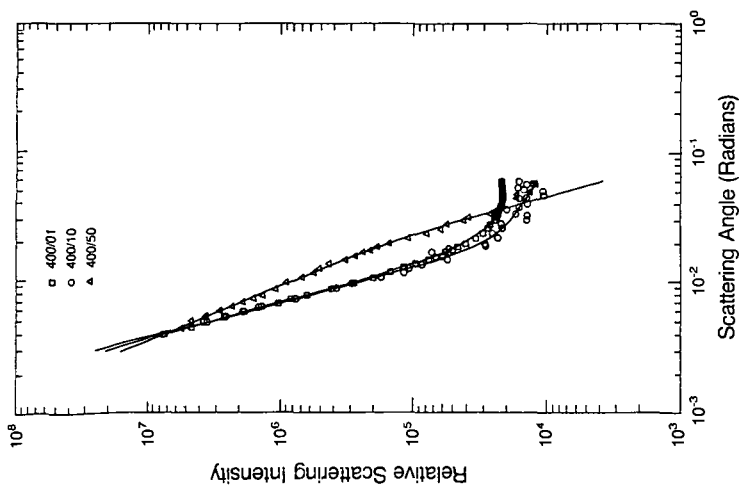

Figure 1. Scattering curve for charcoals produced by increasing the temperature to 400°C at rates of 1 (squares), 10 (circles), and 50 (triangles) degrees C per minute. (Reproduced by permission from Ref. 8.)
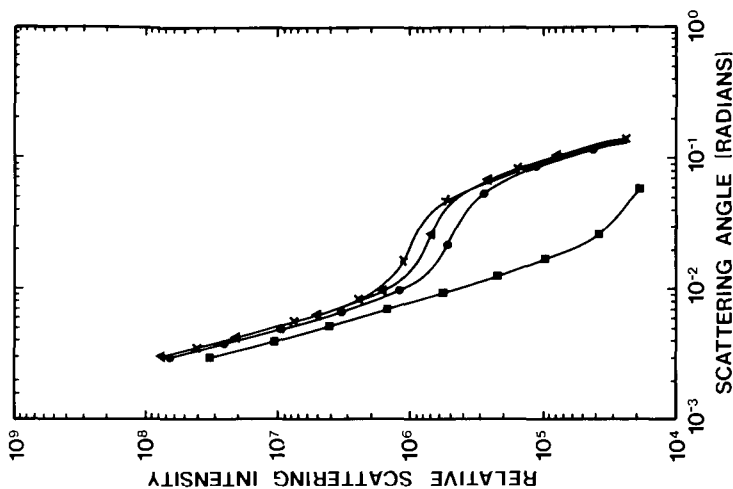
DEFINITION AND DETERMINATION OF THE INTRINSIC RATE
OF CATALYZED BOUDOUARD REACTION

F. Shadman and D.A. Sams

Department of Chemical Engineering, University of Arizona
Tucson, Arizona 85721

During the last decade, increased interest has been focused on the steam gasification of coal using alkali metal catalysis. Various investigators have studied the kinetics of catalytic H_2O/C and CO_2/C gasification reactions and comprehensive reviews are available (1-3).

An important aspect of this gasification process is the variation of the reaction rate during conversion. The primary contributing factors are the change in the reaction area and the change in the amount and distribution of catalyst during gasification. It is important to develop a method and a kinetic model for the characterization of these variations and the determination of the intrinsic rate parameters.

Experimental Method

The char was impregnated with KOH to various concentration levels using an incipient wetting technique. The potassium content of the dried samples was determined by atomic absorption spectroscopy. Char samples were gasified at 800°C, with 15 k Pa CO_2 (balance He) and a total pressure of 100 k Pa. The reactor was operated under differential conditions. The gaseous products were analyzed by on-line GC and IR analyzers. The reaction rate and carbon conversion were calculated from the flow rates and the CO/CO_2 concentrations. The intraphase areas of char samples were measured by a dynamic adsorption/desorption technique using CO_2 as the adsorbing gas with helium as the carrier gas. A schematic diagram of the apparatus is shown in Figure 1.

Results

Surface area measurements have been completed for the char with K/C = 0.0045. The change in the area with conversion is shown in Figure 2. The dependence of carbon conversion on time at various catalyst loadings is shown in Figure 3.

Various definitions for the rate of gasification have been used in the literature. In this study the rates will be defined as:

$$R_m = \frac{-1}{\text{sample mass}} \cdot \frac{d}{dt} \text{ (carbon mass)} \tag{1}$$

The rate of carbon gasification in a char sample is proportional to the total number of surface active sites, ϕ:

$$-\frac{dm_c}{dt} = a \phi \tag{2}$$

During gasification, the rate changes due to various factors including net consumption of sites and catalyst loss. It is assumed that the loss of sites can be represented by an overall first order process:

$$-\frac{d\phi}{dt} = b (\phi - \phi_\infty) \tag{3}$$

where ϕ_∞ is a final limit which depends on the initial properties of the sample.

The initial conditions at t = o are:

$$m_c = m_{co} \qquad\qquad 4)$$

$$\phi = \phi_0 \qquad\qquad 5)$$

After integration and substitutions, the following expressions are obtained for conversion and rate:

$$x = 1 - \frac{m_c}{m_{co}} \qquad\qquad 6)$$

$$x = \frac{R_{mo}}{m_0} \cdot \{ \frac{\phi_\infty}{\phi_0} \, t + \frac{1}{b} \, (1 - \frac{\phi_\infty}{\phi_0})(1 - \exp(-bt)) \} \qquad\qquad 7)$$

$$R_m = - \frac{1}{m} \frac{dm_c}{dt} \qquad\qquad 8)$$

$$R_m = \frac{\dfrac{\phi_\infty}{\phi_0} + (1 - \dfrac{\phi_\infty}{\phi_\infty}) \exp(-bt)}{\dfrac{1}{R_{mo}} - \{ \dfrac{\phi_\infty}{\phi_\infty} \, t + \dfrac{1}{b} \, (1 - \dfrac{\phi_\infty}{\phi_0})(1 - \exp(-bt)) \}} \qquad\qquad 9)$$

At high conversions, Equations 7 and 9 deviate from the data. This is expected because Equation 3 is based on the assumption that the surface is unsaturated with active sites; therefore the number of active sites and not the total reaction area determines the rate. However, as conversion proceeds the surface becomes saturated with active sites. With catalyst, this occurs as K/C increases and surface becomes saturated with catalytic sites. Under the saturation condition, the rate per unit area remains constant but the rate per unit mass, R_m, will be proportional to the reaction area, S_m.

$$R_m = S_m \cdot (\frac{R_m}{S_m})_{x = 0.75} \qquad\qquad 10)$$

The predictions of this kinetic model and the corresponding experimental values of rate are shown on Figure 4.

Conclusions

Impregnation with KOH reduces the surface area of the coal char possibly due to pore plugging. Upon gasification, however, the surface area increases rapidly and goes through a maximum. It is speculated that the increase in area at low conversions is due to catalyst mobility and unplugging of pores.

161

The variation in rate during the catalytic gasification is complex and depends on the initial char properties. In general, the variation is mainly due to the interplay of three factors: the change in area, the change in K/C ratio and the catalyst loss. The catalyst is lost by several mechanisms including deactivation reactions in solid and migration from the char surface. Further study of these complex and important processes is required.

The trend of change in rate with conversion at the onset of gasification depends on the overall rate of loss of active sites. If the loss is fast compared to the main reaction, the gasification rate will decrease with conversion; otherwise it will increase.

As the catalyzed char is gasified, the K/C ratio increases and the surface becomes saturated with catalytic sites. Before surface saturation, the variation in the gasification rate per unit mass is due to the change in K/C ratio and not the change in area. However, after surface saturation, the rate per unit mass is completely determined by the surface

Acknowledgement

References

1. Walker, P.L., Shelef, M. and Anderson, R.A. in 'Chemistry and Physics of Carbon' (Ed. P.L. Walker, Jr), Edward Arnold, London 1968, 4, 287.

2. McKee, D.W. in 'Chemistry and Physics of Carbon' (Ed. P.L. Walker, Jr. and P.A. Thrower), Marcel Dekker, New York, 1981, 16, 1.

3. Wen, W.Y. Catal. Rev.-Sci. Eng. 1980, 22(1),1.
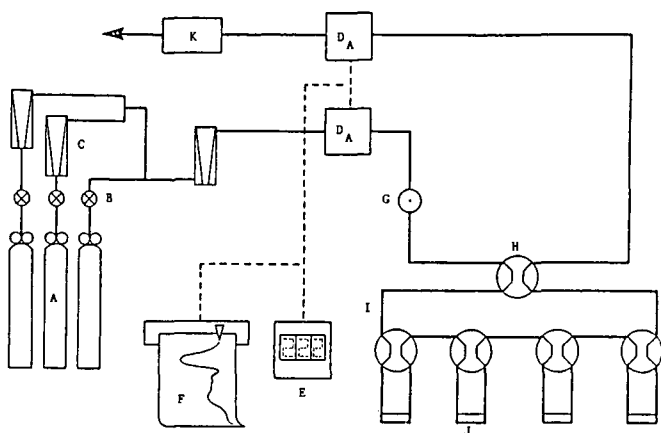
Figure 1. Schematic of the adsorption apparatus.
A) Gas cylinders; B) Toggle valves; C) Rotameters; D) Thermal
conductivity detectors; E) Digital integrator; F) Strip chart
recorder; G) Injection septum; H) Four way valve; I) Multiple
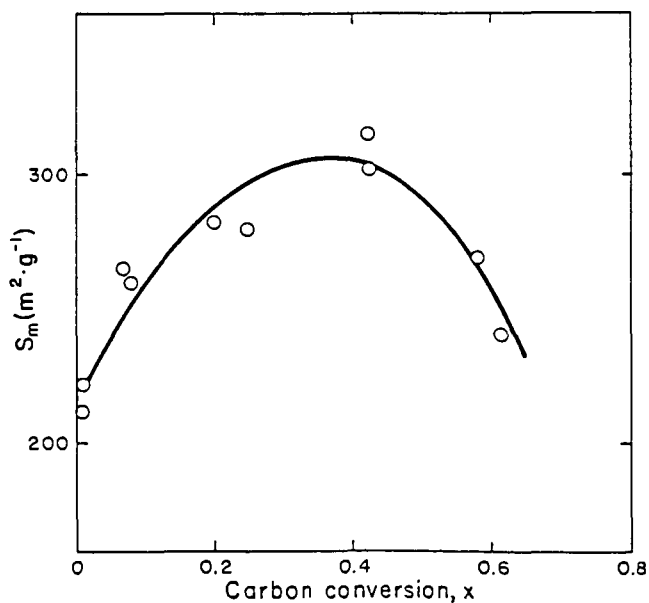sample loop; J) Sample cells; K) Bubble flow meter.

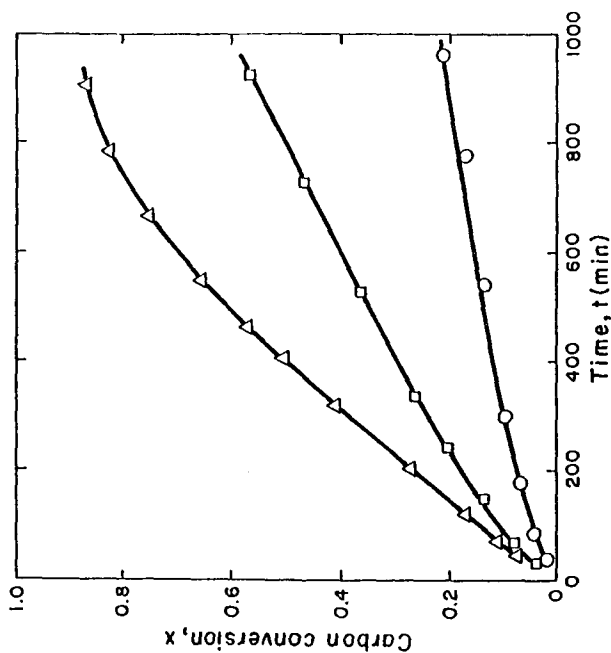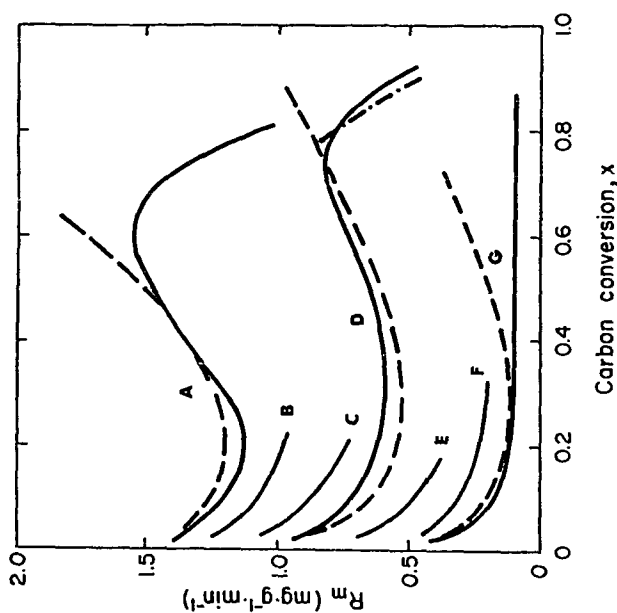Figure 2. Variation of specific surface area during gasification;
K/C = 0.0045.

Figure 4. Variation in rate during gasification, K/C = A, 0.0091; B, 0.0071; C, 0.0060; D, 0.0045; E, 0.0035; F, 0.0025; G, as received. —— data; --- Eqn. 9; —·— Eqn. 10.

Figure 3. Temporal profile of carbon conversion. K/C = △, 0.0091; □, 0.0045; ○, as-received.

164

INFLUENCE OF COKE STRUCTURE ON GASIFICATION KINETICS
AND SELECTIVE GASIFICATION

H. Marsh, C. Calvert and V. Markovic,

Northern Carbon Research Laboratories, School of Chemistry,
University of Newcastle upon Tyne,
Newcastle upon Tyne NE1 7RU, U.K.

1. INTRODUCTION Coals, carbons, cokes and graphites, industrially, are mostly used
in oxidative atmospheres resulting in gasification of the carbonaceous material.
This gasification is often the required process as in steam gasification of coals
and chars and in the electrolytic reduction of bauxite to aluminium where carbon
anodes are consumed. The major part of the world's energy requirements are met by
combustion of coal in electrical power stations. On the other hand, it is undesirable
that metallurgical coke in the blast furnace should undergo gasification to carbon
monoxide whilst in the stack of the blast furnace. The purpose of arc-electrodes in
steel making is to transmit electrical energy to the crucible. Here gasification of
the arc-electrode is detrimental to performance.

     The literature of carbon gasification is dominantly concerned with the kinetics
of gasification reactions using oxygen, steam, nitrous oxide, sulphur dioxide, carbon
dioxide and hydrogen (1-5). An aspect of gasification reactions which has received
much less attention is the role of the structure of the carbon and the influence of
gasification reactions upon the properties of the solid carbon as the reactions
proceed (6-8).   The purpose of this paper is to discuss further the role of carbon
structure during gasification reactions.

1.1. Solid carbons The term 'solid carbon' covers all natural and synthetic
substances consisting mainly of atoms of the element carbon and with the structure
of graphite or at least with two-dimensionally ordered layers of carbon atoms (9).
Solid carbons (referred to as 'carbons') exist as non-graphitic non-graphitizable
forms, as non-graphitic graphitizable forms or as graphitic forms. Non-graphitic
carbons have two-dimensional long range order of carbon atoms in planar hexagonal
networks but without measurable crystallographic order in the third direction. On
heat treatment to above 2500 K the graphitizable carbons adopt a more or less perfect
three-dimensional crystalline order as graphitic carbon, whereas the non-graphitizable
carbons retain only two-dimensional order.

1.2. Formation of solid carbons The non-graphitizable carbons are mostly derived
from parent substances which do not pass through a fluid phase on carbonization.
They are therefore structural pseudomorphs of the parent material, examples being
charcoal from wood, chars from low rank coals and carbonized anthracite. They have
usually surface areas $>>100$ m^2g^{-1}, are microporous and are isotropic in polished
section in plane polarized light optical microscopy. The graphitizable carbons are
mostly derived from parent substances which pass through a fluid phase on carboniza-
tion. Here the resultant solid carbon is formed via an intermediate phase, the
MESOPHASE, of aromatic lamellar nematic liquid crystals (10). The graphitizable
carbons have, usually, surface areas <5 m^2g^{-1}, they contain little or no micro-
porosity and are anisotropic in polished section in plane polarized light optical
microscopy (11). Thus, the term 'solid carbon' is a generic term and contains many
quite diverse materials.

1.3. Anisotropic carbons These materials exhibit a wide range of structure best
characterized by optical microscopy (11). The liquid crystals of the carbonization
process exhibit a size range, observable in optical microscopy, between ~1 μm and
200 μm diameter. The liquid crystals, as carbonization temperatures increase, can
either (a) fuse together without loss of identity or (b) coalesce into each other
with loss of identity to give larger crystals. The structure of the resultant
anisotropic carbon (coke) is a consequence of this fusing or coalescing and is made
up of the 'macrocrystals' from the liquid crystals. The size range of this macro-
crystallinity is described as the optical texture of the carbon and a nomenclature

exists (12) covering from the very fine-grained mosaics (<0.5 μm dia.) to domains (~200 μm dia.). Thus, within anisotropic carbons alone wide variations in structure exist and need to be specified.

1.4. **Influences upon gasification** It has to be emphasized that rarely (if ever) does a solid carbon exist in the pure form, i.e. containing only the element carbon. It is always associated with hydrogen and oxygen, other heteroatoms and mineral impurities. These other elements significantly affect rates of gasification reactions, i.e. CATALYTIC effects exist (3, 4). Gasification reactions of carbon are hetero-geneous processes and a complete specification of the solid carbon of the study is desirable (if not essential). This specification should include (a) for anisotropic carbons, the heat treatment temperature (HTT) and size/shape of optical texture (b) an indication of the impurity content of the carbon, heteroatoms and mineral matter (c) surface area. The surface area of carbons varies from ~2000 m^2g^{-1} to ~0.01 m^2g^{-1} (13, 14). Rates of gasification will accordingly vary considerably, carbon to carbon, simply on the basis of surface availability alone, i.e. total surface area (TSA). However, some twenty years ago, the concept of Active Surface Area (ASA) was introduced and has recently been developed (5). This concept states that surfaces of carbons of equal surface area do not necessarily have the same 'reactivity' under standardized conditions, but can have different surface concentra-tions of active sites. These must be related to structure (i.e. defects and hetero-atom content) within the planar hexagonal network of carbon atoms which make up the structure within carbons.

1.5. **Selective gasification** Solid carbons are essentially non-homogeneous materials (glassy carbons being one of the more homogeneous forms). The non-graphitizing isotropic carbons contain the diverse structures of the parent material and manufactured carbons are mostly composite materials made up of several carbon forms each of which is heterogeneous with a range of size/shape of optical texture. As a consequence of this, during gasification reactions, it is observed that surfaces of carbons exhibit areas of selective preferential gasification, resulting in pitting and fissuring (6, 7). Thus, during gasification, the composition of the carbon material is itself changing. Likewise, physical properties also change such as strength and crack resistance (15). This process of selective gasification can thus influence the 'shift-life' of industrial carbon artifacts, e.g. the aluminium anode and metallurgical coke.

1.6. **The reactivity of carbons** Rate expressions have been developed to describe gasification processes by e.g. steam and carbon dioxide (16). Studies which encompass 'families' of carbons into kinetic data are limited (17) but indicate a spread of reactivities, partly due to lack of ASA data to correct the TSA. The concept that a carbon has a given 'reactivity' which can place it in a given 'pecking-order' could be useful. The limited evidence available suggests that even for a single gasifying gas, e.g. carbon dioxide, 'pecking-orders' depend upon experimental conditions. When several gases are considered the concept of a reactivity pecking-order for all gases is virtually unstudied.

2. **OBJECTIVES** The objectives of this paper are (a) to prepare carbons, with a size range of optical texture, made from pure model organic compounds and Ashland A240 petroleum pitch containing chemical and inert additives; (b) to study the gasification of these carbons by carbon dioxide and relating rates to optical texture and topo-graphical features of pitting etc. using scanning electron microscopy (SEM); (c) to study the relative reactivities of pitch cokes of different optical textures to N_2O, O_2 and CO_2 as well as spontaneous ignition temperatures (SIT) in air; (d) to study the relative efficacies of catalysts in equal concentrations, in carbons of different optical textures from the Ashland A240 pitch.

3. EXPERIMENTAL AND RESULTS
3.1. Use of model compounds (18) Carbons were prepared by carbonization under nitrogen, in tube furnaces to 1273 K (1000°C) at 5 K min^{-1} of acenaphthylene (I), acridine (II), anthrone (III), thianthrone (IV) as well as 9:1 and 1:1 mixtures of acenaphthylene with II to IV and cellulose (V). Optical textures were assessed by optical microscopy (11) and rates of gasification in carbon dioxide were measured gravimetrically using a Stanton Redcroft STA 780 with microbalance facility (DTG)

CO_2 flow rate of 50 $cm^3 min^{-1}$, particle size 250–500 μm, between 1073 and 1273 K. Results are summarized in Table 1.

Table 1.

Carbon	Dominant Size of Optical Texture/μm	Rate at 1240 K/ s^{-1} x 10^{-6}	Activation Energy/ kJ mol^{-1}
I	>60	8	140
II	10–60	20	186
III	<1	28	170
IV	Isotropic	56	180
9:1 (1:II)	>60	19	88
1:1 (1:II)	>60	22	–
9:1 (1:III)	5–30	13	160
1:1 (1:III)	<5–30	185	–
9:1 (1:IV)	5–30	12	–
1:1 (1:IV)	<5–30	17	120
9:1 (1:V)	5–30	23	170
1:1 (1:V)	1.5–5.0	92	200

Rates of gasification are expressed on a $g\ g^{-1} s^{-1}$ (i.e. s^{-1}) basis. Surface areas are not measured. The pure carbon (without heteroatoms) (I) has the lowest reactivity ($8 \times 10^{-6}\ s^{-1}$) and largest optical texture. The three carbons of smallest optical texture from (IV), (1:1 (I:III)) (1:1(I:V)) have the highest reactivity i.e. 56, 185 and $92 \times 10^{-6}\ s^{-1}$ respectively. Certainly, the presence of heteroatoms within the carbon, i.e. nitrogen (II), oxygen (III and V) and sulphur enhance reaction rates, the oxygen being the most effective. As the size of optical texture decreased, the topographical features of gasification changed from fissures to pitting.

3.2. Use of Ashland A240 petroleum pitch (18) Carbons were prepared from Ashland A240 pitch, singly and with additions of cellulose and sulphur, as described above. Reactivities were measured 1073–1273 K and surface areas measured volumetrically at 77 K using krypton as adsorbate. Results are summarized in Table 2.

Table 2.

Carbon	Dominant Size of Optical Texture/μm	Rate at 1240 K/ $s^{-1} x10^{-6}$	Activation Energy/ kJ mol^{-1}	Surface Area/ $m^2 g^{-1}$	Rate at 1240 K $g\ s^{-1} m^{-2} x10^{-6}$
A240	>60	5	205	0.14	37
A240+V 6:4	30–60	15	205	0.52	29
A240+V 1:1	1.5–5.0	19	185	1.21	16
A240+S 9:1	5–10	5	185	0.48	11
A240+S 6:1	Isotropic	8	155	2.04	4

Compared with the data of Table 1, carbons from A240 pitch are less reactive than carbons from acenaphthylene (units of s^{-1}). In these units the addition of oxygen in cellulose (more so) and sulphur (less so) enhances the rates of gasification. But when expressed in units of $g\ s^{-1} m^{-2}$, the rates of gasification decrease with addition of cellulose and sulphur, i.e. the ASA apparently decreases. Activation energies also decrease.

3.3 Addition of TK800 silica to A240 pitch Additions of 'inert' solids, <1 μm diameter, to pitch materials influence the carbonization process by restricting coalescence of mesophase (19, 20). Consequently, the progressive additions of such solids (often referred to as QI material) to a pitch can reduce the size of optical texture of resultant carbon from domains (>60 μm dia) to isotropic (<0.5 μm dia). This 'mechanical' modification to optical texture is distinct from that brought about by 'chemical' additions, as in Tables 1, 2. Experimentally, carbons were prepared from A240 pitch containing known dispersions of TK800 silica (particle dia ~10 nm; surface area ~150 $m^2 g^{-1}$). Rates of gasification and surface areas were measured as described above. Results are summarized in Table 3. Rates are corrected for silica content.

167

Table 3.

Carbon	Dominant Size of Optical Texture/μm	Rate at 1240 K/ s^{-1} $\times 10^{-6}$	Activation Energy/ kJ mol^{-1}	Surface Area/ m^2 g^{-1}	Rate at 1240 K g s^{-1} m^{-2} $\times 10^{-6}$
A240	>60	6	205	0.14	43
+5%	3-20	9	175	0.001	9×10^3
10%	0.5-1.5	26	220	0.09	290
15%	0.5-1.5	83	145	0.22	380
25%	0.5-1.5	130	190	12	11
of TK800					

Additions of 'inert' silica have significant effects on the rates of gasification when expressed in units of g $s^{-1}m^{-2}$, rates varying by three orders of magnitude. The 'inert' material should not be considered as being chemically inert. Its addition to the pitch and its presence in the liquid crystal phase of carbonization must influence the chemistry of conversion of pitch to carbon such that major changes result in the ASA of the carbon, more than observed by chemical additions. In a separate experiment of mechanical mixing of carbon with the TK 800 silica, the latter was not observed to be a catalyst to gasification reactions.

3.4. Relative reactivities of pitch cokes (21) Cokes were prepared from 21 pitch materials and examined by optical microscopy with rates of gasification being measured using oxygen, nitrous oxide and carbon dioxide. Spontaneous ignition temperatures (SIT) (21) were determined in static air. Table 4 lists the pitch cokes in increasing SIT values, i.e. of decreasing reactivity (1 to 21) together with an optical texture index ($\overline{OTI}$) a measure of average size of optical texture (12), QI content of pitch and k_{CO_2} (1240 K) in units of s^{-1}. Table 5 lists the pecking-order of pitch cokes relative to the order established based on SIT. The data within these two Tables suggest broad correlations between SIT and OTI and QI content as well as k_{CO_2} (1240 K). It is seen that the pecking-orders of reactivities in different gases change with the gasifying gas being used. The pecking-order, when using a single gas, i.e. carbon dioxide, depends upon the temperature of measurement of the rate of gasification. There is an identifiable correlation between SIT and k_{O_2} and k_{N_2O}. However, at the higher temperatures needed to determine k_{CO_2} some major displacements of position occur. This suggests that the ASA of carbons could be a function of the gas used as well as being a function of the structure of the carbon. An unknown factor in this particular study is the lack of knowledge of possible catalytic mineral impurities within the pitch coke and derived from the pitch. Catalysis is sensitive to the reacting gas (4) and the temperature of gasification and this factor may account for displacements in the pecking-order.

3.5. Catalyst efficacies in pitch carbon The A240 pitch and pitches No. 16 and 14 were doped with nickel acetylacetonate and sodium chloride according to the ratios in Table 6 and carbonized as described. Reactivities of resultant carbons to carbon dioxide were assessed to give a rate at 1240 K (k_{CO_2}). Relevant details and results are in Table 6. These are preliminary data and suggest that the catalysts may be more effective in carbons of medium sized optical texture, as for pitch carbons (No. 16). Comparison of Table 4 with 6, using k_{CO_2} (1240 K) data, suggest that the carbons of high reactivity, e.g. Nos. 1, 3, 5, 6, 14 may contain catalytically active mineral impurities.

4. CAUSES OF SELECTIVE GASIFICATION Examination of surfaces of carbons, after gasification, by scanning electron microscopy indicates the formation of fissures within carbons of largest size optical texture and of pitting within carbons of smallest size of optical texture. This implies a heterogeneity of structural components within the carbon. In discussing gasification mechanisms the (e.g.) carbon dioxide molecule reacts specifically with only ONE carbon atom in the available surface. The existence of preferential selective gasification to produce (e.g.) pitting implies either that a volume element within the carbon is more 'reactive' than the surrounding carbon, or that the removal of a single carbon atom or even a planar hexagonal network of carbon atoms may induce or create a

<div align="center">Table 4.</div>

<div align="center">Pecking-Order for 21 Pitch-Cokes</div>

Based on SIT values (low to high)	Optical Texture Index	QI Content/ wt. %	k_{CO_2} at 1240 K $s^{-1} \times 10^{-6}$
1	7.3	8.1	68
2	3.2	17.6	36
3	7.6	10.9	42
4	3.6	24.7	25
5	6.4	7.7	67
6	7.2	8.5	49
7	5.7	8.0	14
8	12.8	0.8	33
9	3.6	20.3	31
10	7.4	8.4	29
11	4.7	15.6	19
12	10.2	5.7	26
13	5.2	11.0	21
14	2.9	17.7	42
15	8.7	0.8	27
16	4.6	18.0	11
17	10.8	0.3	35
18	7.0	10.6	14
19	12.8	3.1	11
20	11.4	0.1	10
21	14.0	0.2	7

<div align="center">Table 5.</div>

<div align="center">Pecking-Order for 21 Pitch Cokes</div>
<div align="center">(Most Reactive to Least Reactive)</div>

Based on SIT values (low to high)	Based on k_{O_2}:900 K (high to low)	Based on k_{N_2O}:900 K (high to low)	Based on k_{CO_2} 1173 K (high to low)	1273 K	1423 K
1	3	1	1	14	14
2	1	11	5	1	5
3	2	3	3	5	13
4	6	5	8	3	4
5	7	6	2	10	3
6	10	7	6	9	1
7	11	8	14	20	6
8	8	4	10	6	2
9	5	10	13	4	7
10	4	2	17	13	10
11	12	9	16	8	18
12	13	15	7	17	19
13	9	12	20	2	20
14	14	14	12	12	15
15	16	19	11	15	12
16	18	13	15	18	8
17	15	17	4	11	11
18	19	18	9	7	17
19	17	16	19	19	16
20	20	20	21	16	19
21	21	21	18	21	21
Average displaced position	1.91	1.95	3.82	4.38	4.10

<div align="center">169</div>

Table 6.

Carbon	k_{CO_2} at 1240 K $s^{-1} \times 10^{-6}$	OTI	QI Content/ wt. %
A240	7	14	0
A240 + 0.01 mol Ni	11		
A240 + 0.01 mol Na	39		
A240 + 0.034 mol Na	57		
Pitch No. 16	15	4.6	0.8
+ 0.01 mol Ni	155		
+ 0.01 mol Na	38		
0.034 mol Na	270		
Pitch No. 14	44	2.9	17.7
+ 0.01 mol Ni	120		
+ 0.01 mol Na	100		
0.034 mol Na	140		

more reactive position. The data of Table 3 suggest that carbons of different optical texture can have markedly different reactivities, particularly if optical texture is influenced by the presence of 'inert' (QI) material within the pitch. In carbon composites or even in single carbons, the existence of a range of size of optical texture is common experience. The differences in reactivities between these 'macrocrystals' of optical texture may account for selective gasification processes.

However, the reason why certain 'macrocrystals' are more reactive has to be considered specifically. During gasification, (e.g.) carbon dioxide probably reacts preferentially with carbon atoms at prismatic edge presentations or at defects within the basal planes of the planar networks (22). A study of shape and size of these planar networks (within carbons of several optical textures) by phase contrast high resolution electron microscopy (23) suggests that as the size of optical texture decreases so the size and planarity of the networks of carbon atoms also decreases. This suggests that the ASA of a carbon surface is dependent upon the size and perfection of the networks which make up that plane and that these factors are not independent of optical texture. Variations of 'reactivity' between carbon atoms in different positions within a network have recently been reported (24). However, the presence of catalytic mineral impurities within the carbon can override the above deliberations.

REFERENCES
1. Walker P.L. Jr., Rusinko F. Jr. and Austin L.G., Advances in Catalysis, Vol. 11 (Eds. D.D. Eley, P.W. Selsood and P.B. Weisz) Academic Press, N.Y. :p. 164 (1959).

2. Walker P.L. Jr., Shelef M. and Anderson R.A., Chemistry and Physics of Carbon, Vol. 4 (Ed. P.L. Walker Jr.) Marcel Dekker, N.Y., p. 287 (1966).

3. McKee D.W., Chemistry and Physics of Carbon, Vol. 16 (Eds. P.L. Walker Jr. and P.A. Thrower) Marcel Dekker, N.Y., p. 1 (1981).

4. Walker P.L. Jr., Matsumoto S., Hanzawa T., Muira T. and Ismail I.M.K., Fuel 62 140 (1983).

5. Radovic L.R., Walker P.L. Jr. and Jenkins R.G., Fuel 62 849 (1983).

6. Freeman E.M. and Marsh H., Carbon 8 19 (1970).

7. Adair R.R., Boult E.H. and Marsh H., Fuel 51 57 (1972).

8. Marsh H., Taylor D.A. and Lander J.R., Carbon 19 375 (1981).

9. International Committee for Characterization and Terminology of Carbon, Carbon 20 445 (1982).

10. Marsh H. and Walker P.L. Jr., Chemistry and Physics of Carbon, Vol. 15 (Eds. P.L. Walker Jr. and P.A. Thrower) Marcel Dekker, N.Y. p. 229 (1979).

11. Marsh H. and Smith J., Analytical Methods for Coal and Coal Products, Vol. II (Ed. Clarence Karr Jr.), Academic Press, N.Y. p. 371 (1978).

12. Ōya A., Qian Z. and Marsh H., Fuel 62 274 (1983).

13. Marsh H. and Wynne-Jones W.F.K., Carbon 1 269 (1964).

14. Marsh H., Crawford D., O'Grady T.M. and Wennerberg A., Carbon 20 419 (1982).

15. Ragan S. and Marsh H., Carbon 21 157 (1983).

16. Shaw J.T., Fuel 56 134 (1977).

17. Smith J.W. Fuel 57 409 (1978).

18. Marsh H. and Lander J.R. (Unpublished results).

19. Tillmans H., Peitzka G. and Pauls H., Fuel 57 171 (1978).

20. Stadelhofer J.W., Fuel 59 361 (1980).

21. Calvert C., Marsh H. and Latham C., Ext. Abs. of 16th Biennial Conf. on Carbon, The American Carbon Society, San Diego p. 225 (1983).

22. Thomas J.M., Chemistry and Physics of Carbon, Vol. I (Ed. P.L. Walker Jr.) Marcel Dekker, N.Y. p. 122 (1965).

23. Crawford D. and Marsh H., Carbon '76, Deutsche Keramische Gesellschaft, E.V., Augsburg, p. 231 (1976).

24. Stein S.E., Ext. Abs. of 16th Biennial Conf. on Carbon, The American Carbon Society, San Diego, p. 148 (1983).

CATALYZED CARBON GASIFICATION: THERMAL DESORPTION STUDIES ON CARBON-OXYGEN SURFACE COMPLEXES

Ramkrishna V. Nayak and Robert G. Jenkins

Fuel Science Program
Department of Materials Science and Engineering
The Pennsylvania State University, University Park, PA   16802

INTRODUCTION

The exposure of a clean carbon surface to oxygen results in the formation of stable oxygen complexes (1). A large variety of studies, e.g., chemisorption, desorption, and spectroscopic, have been performed to understand the nature, composition and stability of these complexes (2-12). The programmed temperature desorption techniques have proved to be useful in yielding information on the *total* amount of oxygen present on the carbon surface, the amounts of CO and CO_2 in the desorbed product and the energetics of the complex desorption. Many workers have used temperature programmed desorption techniques to study the carbon-oxygen surface complexes (10-12). However, the majority of the work has been performed on "pure" carbons. Very little work has been conducted previously on the effect of added catalyst(s) on the decomposition of carbon-oxygen surface complexes. In recent studies on a graphatized furnace black, Vulcan 3 (V3G), it has been found that deposition of Pt on the carbon surface leads to significant enhancement of the $C-O_2$ reaction rate (13). To elucidate the cause of this enhanced reactivity it was decided to conduct linear temperature programmed desorption (LTPD) studies of the carbon-oxygen surface complexes formed on the Pt-V3G.

EXPERIMENTAL

i.   Materials - A graphitized furnace black, Vulcan 3, was used in this investigation. The graphitization procedure used is described elsewhere (15). The V3G has a total surface area (BET, N_2, 77 K) of about 60 m^2/g (16). Platinum was deposited on the V3G from a chloroplatinic acid solution. Subsequently, chloroplatinic acid was reduced to Pt by heating the sample to 775 K in flowing H_2 for 15 h. Two samples of V3G with differing amounts of Pt were prepared. The Pt content in the two samples was 0.075% and 1.07% (wt), respectively. These samples are referred as 0.075% Pt-V3G and 1.07% Pt- V3G.

ii. Apparatus - The LTPD studies were conducted in a horizontal mullite tube furnace. Samples (~1-1.2 g) were held in an alumina boat. The furnace temperature was controlled using a Eurotherm analog temperature controller and programmer unit. The sample temperature was measured about 5 mm above the center of the boat using a chromel-alumel thermocouple. Concentrations of CO and CO_2 in the N_2 stream during desorption were measured continuously using nondispersive infrared analyzers (Beckman Model 865). In this system the sensitivity to measure CO and CO_2 in the gas stream was approximately 1 ppm and 0.5 ppm, respectively. Gas flow rates were controlled using fine needle valves and measured using a soap-bubble meter. Oxygen chemisorption was performed using dry grade air. Desorption was performed in flowing ultra high purity nitrogen (99.999%).

iii. Procedure - In the case of 0.075% Pt-V3G and 1.07% Pt-V3G samples, the procedure involved first burning off the sample to 24% weight loss in air at a selected temperature. Subsequently, LTPD was performed. Later a series of oxygen chemisorption-LTPD experiments were carried out on the same sample in-situ. Desorption was always carried out in flowing nitrogen (300 cc/min) at 5 K/min heating rate to the maximum temperature of 1230 K and 3 h soak time. Thus, the sequence for a Pt-V3G sample was (a) initial reaction (B.O.), (b) desorption,

(c) oxygen adsorption, (d) desorption, (e) oxygen adsorption, (f) desorption. In the case of pure V3G, the sample used already had been gasified to 24% burn-off (B.O.) in a separate tube furnace at 723 K in 0.1 MPa of dry air. Therefore, in the case of pure V3G sample the sequence was somewhat different. The gasification reaction temperature selected for the 3 samples (pure V3G, 0.075% Pt-V3G and 1.07% Pt-V3G) were different such that the reaction rate for the three samples would be similar during the gasification. All the three samples were burned-off to the same level of activation (24%). The additional gasification that occurred during adsorption-desorpton cycles was small (~1%) and was neglected.

RESULTS AND DISCUSSION

Data obtained in each run consist of CO and CO_2 desorption rates as a function of temperature/time. Figure 1 and Figure 2 show the desorption profiles of CO and CO_2, respectively, obtained for the 3 samples under the same chemisorption conditions. These figures do not show the desorption rates during the 3 h soak period. The desorption profiles obtained under the different chemisorption conditions were similar in overall nature. The CO desorption rate in all cases did not stop at 1230 K, but upon soaking the sample for 3 h at 1230 K, the desorption rates reduced to a very low level. As can be seen, the CO and CO_2 desorption rate profiles are very different. As examples, CO_2 desorption started at a lower temperature than did the CO desorption; the evolution of CO_2 was complete in a temperature range where the CO desorption rate was reaching a peak; and the CO_2 desorption profiles had more peaks than did the CO profile. In these experiments it was always found that the amount of oxygen complex that desorbed as CO_2 was much less than that desorbed as CO (see Table 1). From the studies performed at different temperatures it was found that as the chemisorption temperature was lowered (713-303 K) then the temperature at which the CO desorption started was also lowered. However, the temperature at which the CO desorption rate was a maximum seemed to be independent of the chemisorption temperature (and, thereby, also was independent of the amount of oxygen on the surface). This suggests that the CO desorption rate is a unimolecular process (17). In all cases, a shoulder in the CO desorption rate appeared at high temperature (1100-1230 K). The presence of a shoulder indicates the presence of more than one kind of sites and/or oxygen complexes desorbing as CO. As was the case for CO desorption, the CO_2 desorption started at lower temperature if the O_2 chemisorption was performed at lower temperature. The temperatures at which peaks in CO_2 evolution rate appeared also seemed to be independent of the chemisorption temperature (and, thus, of the amount of O_2 on the surface). Again, this suggests first order decomposition behavior for CO_2. Presence of Pt appears to have shifted the peak in CO desorption rate to a slightly lower temperature (965 K to 950 K). However, the higher temperature shoulder appears to be little affected by the presence of Pt. It should be noted that desorption of CO_2 appears to be markedly accelerated by Pt. For Pt containing samples the low temperature peak (570 K) was present. However, this peak was absent in the pure V3G desorption profile. Also, proportionately more CO_2 desorbed at lower temperatures in the case of Pt-V3G compared to pure V3G.

The desorption profiles can be integrated to obtain total amount of oxygen desorbed as CO and CO_2 in each case. Table I gives the total amount of oxygen and the amount of oxygen that desorbed as CO and CO_2 from the 3 samples. The amount of oxygen chemisorbed increased with increasing chemisorption temperature. It also increased with increase in Pt content. The amount of O_2 associated with Pt in these cases was very small (~5%) and was neglected.

The amount of oxygen chemisorbed on a carbon sample can be used to determine the active surface area of the carbon as described by Laine et al. (19). In the case of 0.075% Pt-V3G (24% B.O.), the amount of oxygen chemisorbed at 473 K and 0.1 MPa air for 12 h corresponded to about 10% of the total surface area. For 1.07% Pt-V3G (23.5% B.O.) and V3G (24% B.O.) the amount of O_2 chemisorbed at 473 K

173

and 0.1 MPa air corresponded to about 13% and 6.5% of the total surface area, respectively. This significantly higher amount of oxygen adsorbed in the presence of Pt could be due to spillover of O_2 from Pt onto carbon basal planes.

The desorption rate versus temperature data can also be treated mathematically to yield surface complex/site energy distribution as a function of surface coverage (14). Figure 3 and Figure 4 show for CO and CO_2, respectively, the desorption surface site/complex energy (E_d) as a function of surface coverage. For both gases, as the surface was uncovered the activation energy for desorption increased. The variation in E_d for CO desorption (Figure 3) with surface coverage was essentially linear for most of the surface coverage (0.2-0.8) whereas at the beginning and the end of the surface coverage, the variation in E_d was marked. The CO_2 desorption energy varied in a linear fashion for the intermediate surface coverage. But for small surface coverage (<0.2) and large surface coverage (> 0.8), E_d varied rather rapidly. The activation energy for CO_2 desorption varied between 112 KJ/mole to 300 KJ/mole and for CO, the activation energy varied between 200 KJ/mole to 400 KJ/mole. These values agree well with the values listed in the literature (12,14,22).

Figures 3 and 4 also show the variation in E_d for CO and CO_2 as a function of surface oxygen coverage for the 3 different samples, V3G (24% B.O.), 0.075% Pt-V3G (24% B.O.), 1.07% Pt-V3G (23.5% B.O.). Chemisorption on these samples was done under the same conditions of temperature and pressure (473 K, 0.1 MPa air). For the CO desorption energy, the effect of Pt appears to be small. The CO_2 desorption energy as a function of surface coverage shows marked difference as Pt content on V3G increases. The activation energy for the surface complex desorption of CO_2 decreased, at the same surface coverage, with increase in Pt content. In other words, the presence of Pt appears to help in desorption of CO_2 complexes. This agrees with the reactivity measurements performed on these samples using a TGA and a flow reactor with nondispersive infrared detectors (13). In the case of Pt-V3G, CO_2 was found to be the sole gasification product at 723 K (0.1 MPa air). The reactivity of 1.07% Pt-V3G was about 400 times higher compared to that of pure V3G. As Pt content increased the sample reactivity increased. This increase in measured reactivity with Pt content is probably related to the ease of decomposition of oxygen complexes as CO_2 because no CO was detected in the gasification step.

CONCLUSION

The surface of V3G is heterogeneous in nature and several types of surface oxygen species are formed upon its exposure to O_2. With addition of Pt, the amount of O_2 chemisorbed on V3G increases. Under the conditions used in this study, a significant portion of the V3G total surface was covered with oxygen, indicating, probably, spillover of oxygen from Pt onto the carbon surface. The stability of the surface oxygen complexes depends upon the conditions of temperature and pressure under which they are formed. The presence of Pt on the V3G further changes the stability of the surface oxygen complexes. LTPD is a very useful technique to study the stabilites of the surface oxygen species formed on a carbon surface. Using this technique it is found that the presence of Pt affects the stability of both CO and CO_2 forming surface oxygen species. But the effect on the CO_2 forming surface oxygen species is much more than the CO forming surface species. This results in a decrease in activation energy for CO_2 desorption at the same fractional surface coverage from Pt-V3G compared to pure V3G. The reactivity measurements performed on these samples showed that Pt enhances the reactivity of V3G in O_2 by at least 2 orders of magnitude and CO_2 is the sole reaction product upto 775 K.

ACKNOWLEDGEMENT

Table I: Oxygen Chemisorption Conditions and Desorption Product Composition

| Run # | Sample Type | Adsorption Condition | Desorption Products | | Ratio (CO/CO_2) | Total O_2 Desorbed $(\mu mole/g)$ |
			CO $(\mu mole/g)$	CO_2 $(\mu mole/g)$		
1	0.075% Pt-V3G	758 K-0.1 MPa Air-24 h (in-situ B.O. to 24%)	305.0	15.0	20.3	167.5
2	0.075% Pt-V3G (24% B.O.)	473 K-0.1 MPa Air-12 h	154.0	18.5	8.3	95.5
3	0.075% Pt-V3G (24% B.O.)	303 K-0.1 MPa Air-16 h	53.0	7.8	6.8	34.3
4	1.07% Pt-V3G	713 K-0.1 MPa Air-24 h (in-situ B.O. to 23.5%)	388.5	30.1	12.9	224.4
5	1.07% Pt-V3G (23.5% B.O.)	473 K-0.1 MPa Air-12 h	186.5	27.0	6.9	120.2
6	1.07% Pt-V3G (23.5% B.O.)	303 K-0.1 MPa Air-16 h	97.0	15.0	6.5	53.5
7	V3G (24% B.O.)	823 K-0.1 MPa Air-1 h	176.5	6.9	25.6	95.2
8	V3G (24% B.O.)	473 K-0.1 MPa Air-12 h	64.0	8.5	7.6	40.5

175

REFERENCES

1. Donnet, J.B., Carbon, 6, 161 (1968).

2. Hart, P.J., PhD Thesis, The Pennsylvania State University, University Park, PA (1962).

3. Hart, P.J., Vastola, F.J. and Walker, P.L., Jr., Carbon, 5, 363 (1967).

4. Bansal, R.C., Vastola, F.J. and Walker, P.L., Jr., J. Colloid & Interface Sci., 32(2), 187 (1970).

5. Carpenter, D.L. and Sergeant, G.D., Fuel, 45, 311 (1966).

6. Zawadski, J., Carbon, 16, 491 (1978).

7. Mattson, J.S. and Mark, H.B. Jr., J. Colloid & Interface Sci., 31, 171 (1969).

8. Marsh, H., Foord, A.D., Mattson, J.S., Thomas, J.M. and Evan, E.L., J. Colloid & Interface Sci., 49, 368 (1974).

9. Boehm, H.P. and Bewer, G., In 'Fourth Conference on Carbons and Graphite', Society of Chemical Industry, London, p. 344 (1974).

10. Tucker, B.C. and Mulcahy, M.F.R., Trans. Fara. Soc., 65, 274 (1969).

11. Barton, S.S., Harrison, B.H. and Dollimore, J., J. Trans. Fara. Soc., 69, 1039 (1963).

12. Feates, F.S. and Keep, C.W., Trans. Fara. Soc., 66, 31 (1970).

13. Nayak, R.V., Unpublished Results, The Pennsylvania State University, University Park, PA.

14. Tremblay, G., Vastola, F.J. and Walker, P.L., Jr., Carbon, 16, 35 (1978).

15. Ehrburger, P., Mahajan, O.P. and Walker, P.L., Jr., J. Catal., 43, 61 (1976).

16. Taylor, R.L., PhD Thesis, The Pennsylvania State University, University Park, PA, (1983).

17. King, D.A., In 'Chemistry and Physics of Solid Surfaces', Vol. II, Ed. R. Vanselow, C.R.C. Press, Inc., Boca Raton, Florida, 1979.

18. Magne, P. and Duval, X., Carbon, 11, 475 (1973).

19. Laine, N.R., Vastola, F.J. and Walker, P.L., Jr., Proc. of the Fifth Biennial Carbon Conf., Vol II, Pergamon Press, N.Y., 1963, p. 214.

20. Lussow, R.O., Vastola, F.J. and Walker, P.L., Jr., Carbon, 5, 591 (1967).

21. Benson, S., Foundations of Chemical Kinetics, McGraw Hill, N.Y., 1960, pp. 225-266.

22. Dollimore, J., Freedman, C.M. and Harrison, B.H., Proc. Third Conf. on Industrial Carbons and Graphite, Soc. Chemical Industry, London., 1970, p. 250.
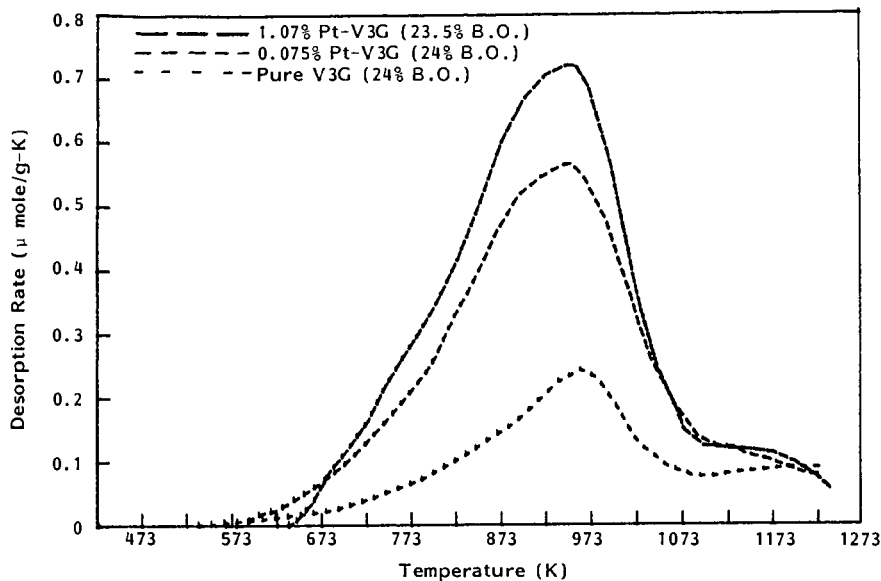
Figure 1: CO Desorption Profiles After 473 K-12 h Chemisorption
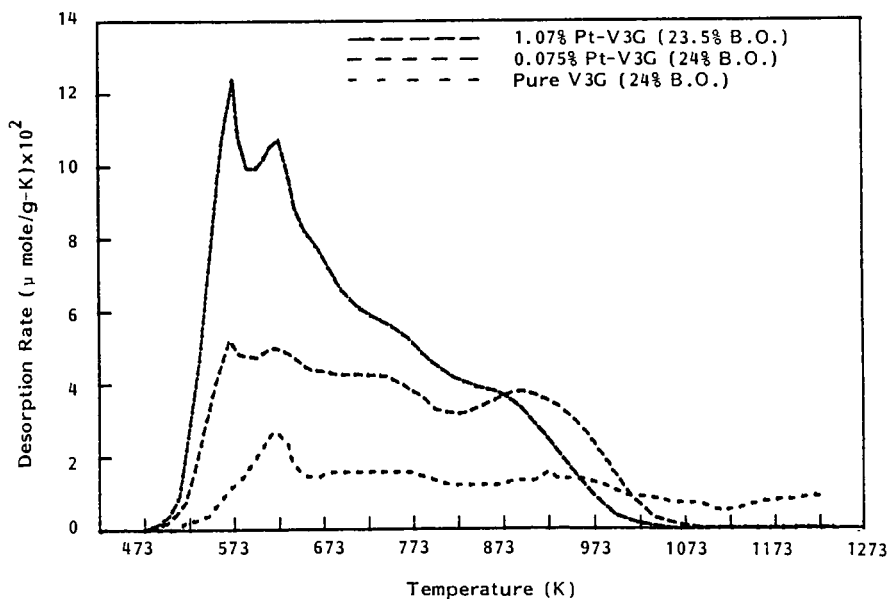
Figure 2: CO_2 Desorption Profiles After 473 K-12 h Chemisorption

177
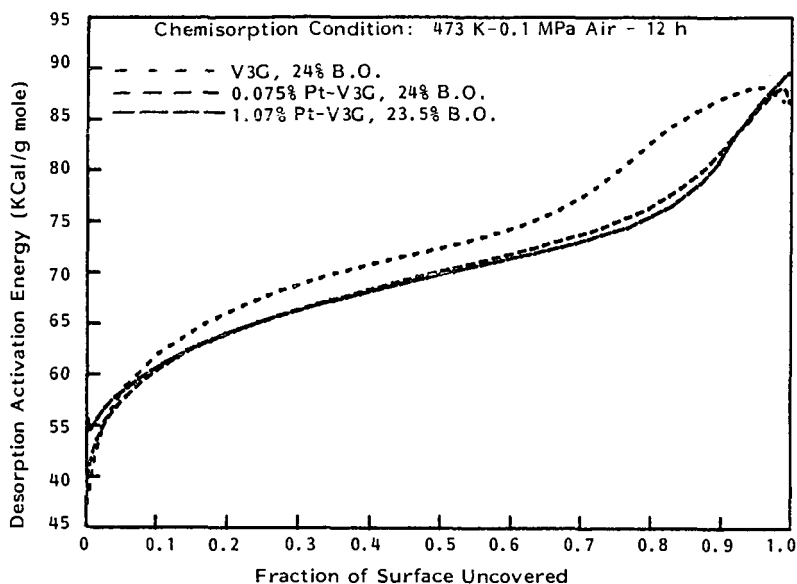
Figure 3: Surface Energy Distribution Profiles Obtained from CO
Desorption Profiles
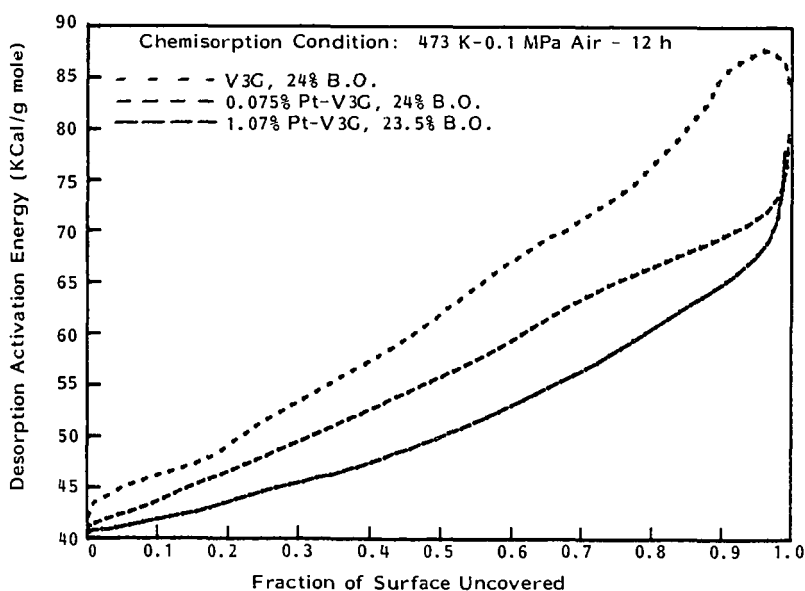
Figure 4: Surface Energy Distribution Profiles Obtained from CO_2
Desorption Profiles

GASIFICATION OF ACTIVE CARBON WITH ALUMINA-SUPPORTED POTASSIUM CARBONATE CATALYST

E.Kikuchi, T.Momoki, M.Hirose, T.Sekiba and Y.Morita

Department of Applied Chemistry, School of Science and Engineering, Waseda University, 3-4-1 Okubo, Shinjuku, Tokyo, 160, Japan.

INTRODUCTION

It was shown in our previous work that carbonaceous residues from petroleum were gasified with extremely high efficiency in the fluidized bed of alumina-supported alkali catalysts.[1] In the present work, we applied the same fluidized bed system to the gasification of solid carbon. Many works have been reported on the catalytic activity of alkali for the gasification of solid carbon such as coal, char and graphite.[2-8] Recent studies have showed that alkali-catalyzed gasification of graphite and char proceeds via oxygen transfer mechanism where the redox of alkali salt is essential.[3,9-11]

In the gasification of petroleum residues, the intermediate was carbon deposited on the catalyst. In the case of solid carbon, however, catalytically active species must travel from catalyst to the surface of solid carbon, and may hopefully return to catalyst after gasification. It is the purpose of the present work to investigate how effectively the alumina-supported potassium carbonate catalyst functions in the gasification of solid carbon.

EXPERIMENTAL

Apparatus and Procedure

Steam gasification of active carbon was carried out in a fluidized-bed and a fixed-bed reactor at 850°C and atmospheric pressure. The fluidized-bed reactor was made of a 40mm diameter and 400mm height stainless steel tube. Steam was supplied in a rate of 4.5 moles/hr at the bottom part of the reactor. Details of the reactor were described in the previous paper.[1] Fixed-bed gasification was studied using five different packing modes of catalyst and carbon, as shown in Fig. 1. Type A and B beds consisted of carbon-catalyst-carbon and catalyst-carbon layers with thin separating layers of alumina, respectively. In Type C bed, a mixture of K_2CO_3 and a small amount of carbon was packed in the upper layer with the major part of carbon in the lower. Type D and E beds contained a carbon-catalyst mixture and carbon impregnated by K_2CO_3, respectively. Each packed-bed contained 4.48×10^{-3} moles K_2CO_3. The feed rate of steam or CO_2 was 0.33 moles/hr.

To investigate the behavior of K_2CO_3 supported on alumina, thermogravimetric analyses were performed by use of Shimadzu thermal analyser DT-30. Measurements were carried out under atmospheric pressure. The sample was heated at a rate of 10°C/min in a stream of H_2, CO or He.

Materials

An active carbon was used in the present work as a feedstock. It was prepared from coconut shell and was supplied by Tsurumi Coal CO. Ltd. The ultimate analysis showed 95% C, 1.7% O, 0.3% H, 0.1% N, 0.1% S and 2.8% ash. An alumina-supported K_2CO_3 catalyst containing 1.28×10^{-3} moles K_2CO_3/g-catalyst, was used in this work. The catalyst was prepared as follows: alumina was impregnated by a solution of K_2CO_3, and dried at 100°C. Alumina was obtained by calcining γ-alumina at 1200°C for 2 hr. The catalyst was dried at 350°C for 2 hr followed by screening and a

portion of the particles in the range of 32-65 mesh were used in the catalytic studies.

RESULTS AND DISCUSSION

Fluidized Bed Gasification

The catalytic activity of K_2CO_3 supported on alumina was compared with that of K_2CO_3 supported on carbon itself. As given in Fig. 2, the variation of gasification rate with reaction time for both cases overlapped in the whole range of carbon conversion. When carbon was completely gasified, another dose of carbon was charged to the residual fluidized bed. In both cases, the carbon was gasified in the same rate with the first run, and it was reproduced on repeated several doses of additional carbon charge. These results seem to show that catalytically active species rapidly transfer from catalyst to the surface of carbon and return to alumina surface after gasification. As the reaction temperature (850°C) was far below the melting point of K_2CO_3 (891°C), decomposition or reduction of K_2CO_3 should be involved in the transfer of the active species. The gasification rate was found to be a function of the amount of carbon in the fluidized bed, being independent of the catalyst amount in the range tested (bulk K/C $\geq$ 0.015). Thus, the amount of active species required is not very large.

Thermogravimetric (TG) Study

Reactions of K_2CO_3 on alumina in a stream of reducing or inert gas were investigated, the results being shown in Fig. 3. In flowing He or CO, K_2CO_3 decomposed above 650°C to CO_2 and K_2O which was retained by alumina. In a stream of H_2, the weight reduction exceeded that of decarboxylation, showing a further reduction of K_2O to K. Carbon physically mixed with the catalyst was also found to reduce K_2CO_3 to potassium metal in flowing He.

Packed-bed Gasification

TG experiments showed that K_2CO_3 in the catalyst was reduced by flowing H_2 but not by CO. To examine the effect of catalyst reduction on gasification, C-H_2O and C-CO_2 reactions were performed using packed-beds of Type A and Type B. The results are shown in Fig. 4. For C-H_2O reaction, the carbon/catalyst/carbon triple-layer bed (Type A) was gasified with a greater rate than the catalyst/carbon double-layer bed (Type B). The rate of C-CO_2 reaction was not influenced by the mode of bed-packing. It is thus deduced that non-catalytic C-H_2O reaction in the upper layer of Type A bed to yield H_2 is effective to form K in the middle layer and to make the gasification in the lower layer catalytic.

Further evidence for the transport of K vapor was obtained by the run using a Type C packed-bed where K_2CO_3 was mixed with a small amount of carbon in the upper layer. The solid contact reduction of K_2CO_3 by carbon was very rapid and K was mounted on carbon in the lower layer in a stream of nitrogen. As shown in Fig. 5, transfered K gave a rate of gasification greater than non-catalytic one. As gasification proceeded and K/C ratio increased to some extent, the rate of gasification decreased with decreasing amount of carbon. When the catalyst instead of K_2CO_3 was packed with carbon in the upper layer, no appreciable enhancement of gasification rate was observed probably due to the adhesion of K on alumina which did not enable the distant transport of K in gas phase.

Figure 6 shows the rate of gasification in a uniform mixture of carbon and catalyst, compared with that of carbon impregnated by K_2CO_3. With increasing amount of carbon in the bed and decreasing K/C ratio, the rate of gasification increased and saturated at a bulk K/C ratio around 0.03-0.05. Reduction of K_2CO_3

180

and transfer of K would create active centers on carbon surface. The rate of gasi-fication should be proportional to the number of active centers. At K/C ratios above saturation, the number of active centers seemed to be determined by the amount of carbon, and the gasification rates in both cases coincided. At K/C ratios below saturation, however, K_2CO_3 on alumina seems to create larger numbers of active centers than K_2CO_3 on carbon.

Overall Kinetics

Recent studies of Mims et al.[5,6] have indicated that the rate of K_2CO_3-catalyzed gasification of amorphous carbon is proportional to the $(H_2O)/(H_2)$ ratio, in agreement with their gasification mechanism. The results obtained in the present work were also found to obey the following rate expression meaning product inhibition:

$$rate = k \cdot Cx \cdot (H_2O/H_2) \qquad 1)$$

where Cx meant the number of active centers. Figures 7 and 8 show $rate \cdot (H_2/H_2O)$ vs the amount of total carbon (Ct) for packed-bed and fluidized-bed experiments, respectively. Here, (H_2/H_2O) was obtained by averaging ratios at reactor-inlet and outlet. Assuming that $Ct=Cx$ in the region of large K/C ratio, the rate co-efficients for packed-bed and fluidized-bed gasification were determined to be 0.54 and 0.48 (hr^{-1}), respectively. Roughly coincident rate coefficients seem to mean a common gasification mechanism operating in the packed-bed and fluidized-bed gasi-fication.

REFERENCES

1. E.Kikuchi, H.Adachi, T.Momoki, M.Hirose and Y.Morita, Fuel 62,226 (1983)

2. N.Kayembe and A.H.Pulsifer, Fuel 55, 211 (1976)

3. M.J.Veraa and T.Bell, Fuel 57, 194 (1978)

4. C.A.Mims and J.K.Pabst, Prepr. Pap. Am. Chem. Soc. Div. Fuel Chem. 25, 258 (1980)

5. C.A.Mims and J.K.Pabst, Prepr. Pap. Am. Chem. Soc. Div. Fuel Chem. 25, 263 (1980)

6. C.A.Mims and J.K.Pabst, Fuel 62, 176 (1983)

7. D.W.McKee, C.L.Spiro, P.G.Kosky and E.J.Lamby, Prepr. Pap. Am. Chem. Soc. Div. Fuel Chem. 27, 74 (1982)

8. M.V.S.Sekhar and M.Tarnan, Fuel Processing Technology 6, 61 (1982)

9. D.W.McKee and D.Chatterji, Carbon 16, 53 (1978)

10. D.W.McKee, A.I.P. Conf. Proc. 70, 236 (1981)

11. D.W.McKee, Fuel 62, 170 (1983)
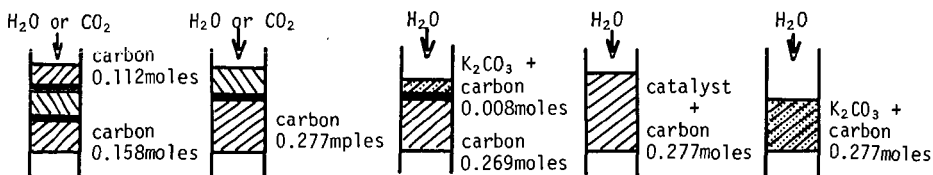
Figure 1. Packed bed reactors of different types A-E. The amount of catalyst in packed beds A, B and D were 3.5g which contained 4.48×10^{-3} moles K_2CO_3. The same amount of K_2CO_3 were packed in beds C and E. ■, Al_2O_3 isolater; ▨, carbon; ▨, catalyst; ▨, K_2CO_3.
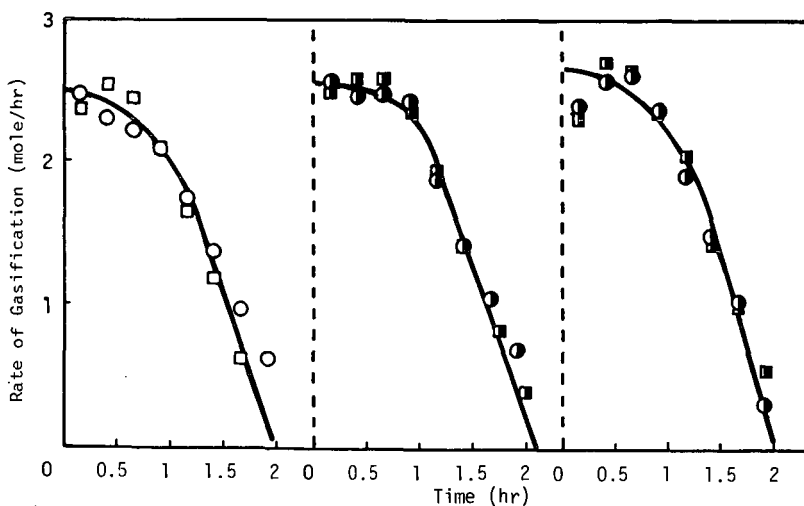
Figure 2. Rate of fluidized-bed gasification in Runs; A (○) with K_2CO_3 (0.123moles) on alumina (83g) + carbon (3.96moles) followed by Run B (●) with freshly charged carbon (3.96moles) after a complete consumption of carbon in the preceding run; and C (□) with K_2CO_3 on carbon (3.96moles) + alumina (83g) followed by D (■) as Run B after Run A.
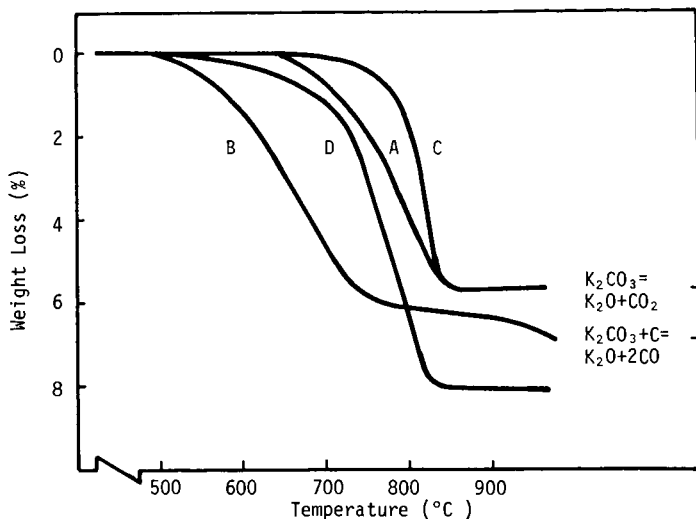
Figure 3. Thermogravimetric analyses on decomposition and reduction of K_2CO_3 supported on alumina: A, in He; B, in H_2; C, in CO; D, mixed with active carbon (K/C=0.17) in He.
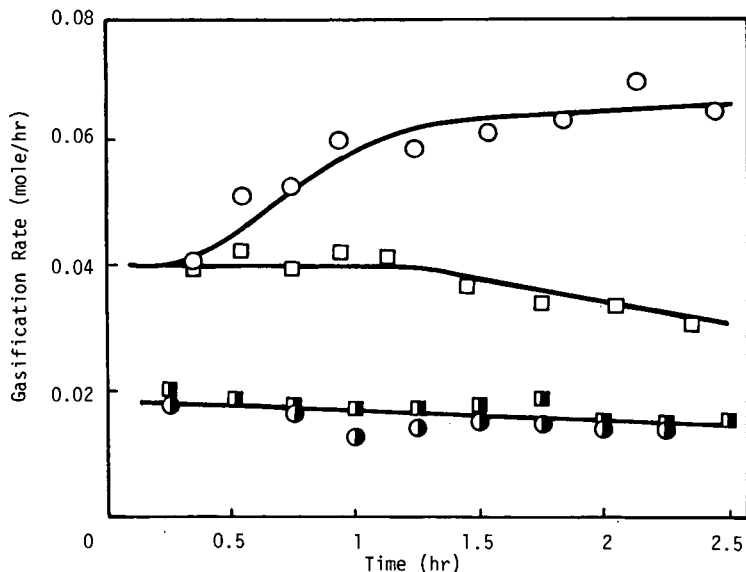
Figure 4. Variation in rates of $C-H_2O$ and $C-CO_2$ reactions in packed-beds Type A (catalyst-carbon-catalyst) and Type B (catalyst-carbon) with reaction time: ○ and ◐ , $C-H_2O$ and $C-CO_2$ reactions in Type A, respectively; □ and ◧ , those in Type B. Initial amounts of carbon and catalyst were 0.277 moles and 3.5g, respectively.
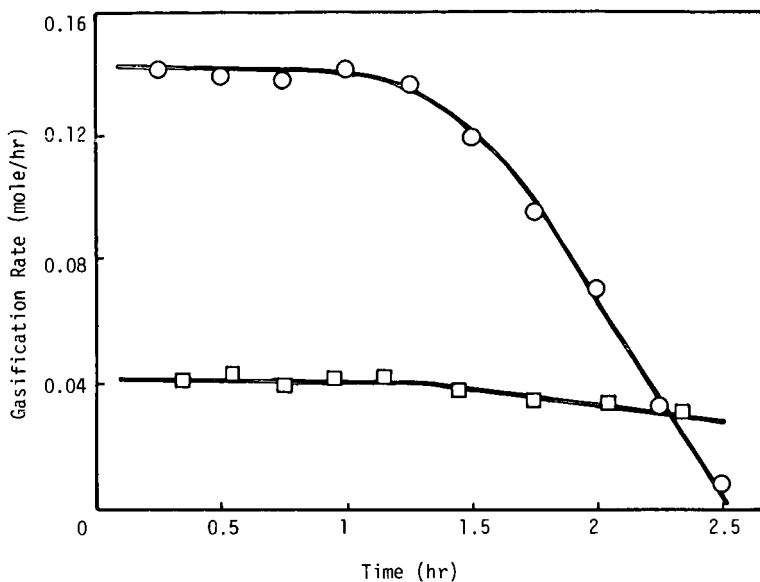
Figure 5. Enhancement of gasification rate in packed-bed Type C
($\bigcirc$) where K_2CO_3 was reduced by a small amount of carbon in the
upper layer, in comparison with Type B ($\square$).
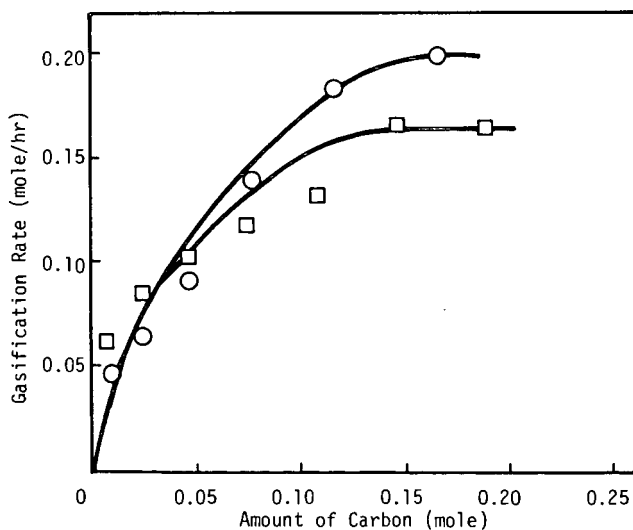
Figure 6. Rates of packed-bed gasification of carbon mixed
with catalyst (Type D, $\bigcirc$) and K_2CO_3 (Type E, $\square$) as a
function of the amount of carbon in the beds.
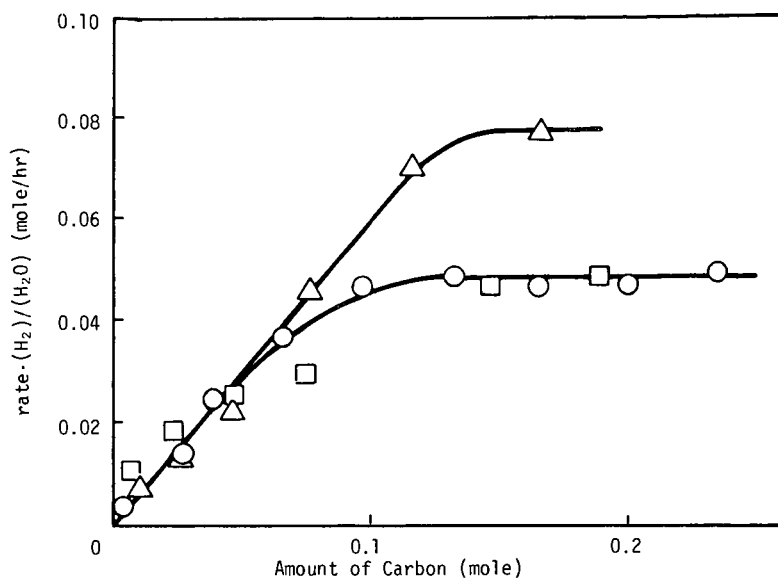
Figure 7. Plots between rate·(H_2)/(H_2O) and Ct for data from packed-bed experiments: ◯, Type C; △, Type D; ▢, Type E.
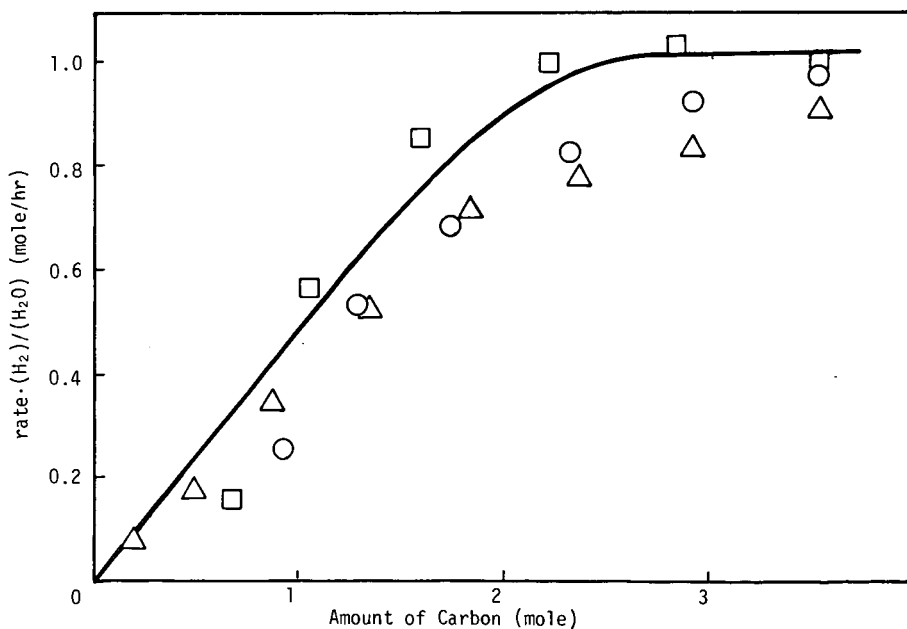
Figure 8. Plots between rate·(H_2)/(H_2O) and Ct for data on fluidized-bed gasification: catalyst weight ◯, 150g; △, 100g; ▢, 25g.

Gasification of Carbon Using Calcium Oxide

H-C. zur Loye, R. Kershaw, K. Dwight, and A. Wold
J.K. Pabst[+] and R.J. Lang[+]

Department of Chemistry, Brown University
Providence, Rhode Island 02912
[+]Exxon Research & Engineering
Post Office Box 4255, Baytown, Texas 77520

Introduction

Extensive investigations of the catalytic action of potassium under the conditions of steam and hydrogen gasification have been reported (1-4). Calcium oxide, as a catalyst, has also been studied under various conditions of temperature and pressure (5,6); however, the nature of the calcium oxide catalysts as a function of time during gasification has not been investigated in detail. It was shown by Lang and Neavel (6) that calcium, in contrast to potassium, was not very active as a gasifying catalyst unless it was very well dispersed by chemical reaction with the organic matter.

Gasification of carbon depends upon the experimental conditions of preparation of the catalyst, as well as on the percent loading, temperature, and time of the gasification reaction. The temperature for maximum gasification rate varies, however, with the type of carbon as well as the catalyst present and its degree of dispersion. The crystallinity and structure of the carbon and the extent of crystallinity of the catalyst also are major factors that influence the rate of the gasification reaction. Because Spherocarb is an extremely pure, high-surface form of amorphous carbon, it has been chosen in this study as the support for the dispersed calcium oxide particles.

In order to understand the carbon-calcium oxide system in more detail, a study was undertaken to prepare dispersed calcium oxide on Spherocarb supports and to measure the change in crystallinity of the catalyst as well as the amount of carbon gasified at 760°C as functions of time. Hence, any changes in catalytic activity of calcium oxide might be correlated with the observed changes in its crystallinity.

Experimental

The Spherocarb particles supplied by Analab (GC012) were of high purity and possessed large surface areas. Impregnation of these particles was accomplished with an aqueous solution of calcium nitrate ($Ca(NO_3)_2 \cdot 4H_2O$ Reagent Grade, MCB) to give a final calcium oxide loading of 5% by weight. The concentration of the aqueous solution of calcium nitrate was such that the desired degree of loading could be achieved by the addition of 1 ml solution to the Spherocarb. The loaded sample was dried under an infrared lamp for 2.5 hours and then transferred to a small silica tube which was stoppered at the narrow end with silica wool (Fig. 1). The sample was purged for one hour with dry nitrogen at a flow rate of 100 cm^3/min and then the temperature was raised from room temperature to 540°C. The decomposition of calcium nitrate tetrahydrate was allowed to proceed for 4 hours. The temperature was then raised to the gasification temperature of 760°C. Once this temperature was reached, the gas flow was switched to a hydrogen/water mixture. The flow rate of the hydrogen was 100 cm^3/min and the rate of water injection was 4.82 cm^3/hr. This combination gave a mole ratio of hydrogen to water of 1:1. The water vapor was introduced by injection of distilled water from a syringe pump (Sage Instrument Model 355). The complete reactor as well as the point of injection, which was kept at or above 200°C, is shown in Fig. 1. After the desired time under gasification conditions, the gas flow was switched back to nitrogen and the sample temperature was maintained at 760°C for an additional 30 minutes to

ensure complete dryness. The reaction tube was removed from the furnace and allowed to cool under flowing nitrogen. The sample was weighed immediately after cooling in order to minimize uptake of water. It was stored under vacuum over P_2O_5 until x-ray diffraction patterns could be taken with a Philips Norelco diffractometer using copper radiation ($\lambda CuK\alpha_1 = 1.5405 \text{Å}$); data were obtained with a graphite monochrometer at a scan rate of $1°2\theta/\text{min}$.

Results and Discussion

It was found that calcium oxide was the species present after gasification of the Spherocarb, was converted to calcium carbonate. This was verified by x-ray diffraction analysis of the products. Conversion of the carbonate to the oxide took place upon heating of the sample to 760°C. X-ray analysis showed that after only 15 minutes of gasification, only calcium oxide is present in the sample. There is no x-ray evidence for the presence of $CaCO_3$. The sole presence of calcium oxide in the product after gasification indicated that this was the only well-crystallized compound of calcium formed during the gasification process.

A number of gasification experiments were performed on Spherocarb samples containing 5 weight % calcium oxide. The percent of carbon gasified as a function of time is plotted in Fig. 2. There is an increase in the weight loss with time as gasification proceeds, but this loss persists for only one hour after which no additional weight loss is observed. At the end of 60 minutes, approximately 60% of the carbon is gasified and the calcium oxide appears to become deactivated.

There appears to be a correlation between the degree of gasification of Spherocarb, as indicated by weight loss, and the degree of crystallinity of the calcium oxide. Whereas the crystallite sizes were not determined quantitatively, it can be seen from Fig. 3 that as gasification proceeds there is a marked increase in the crystallinity of the catalyst. After only 15 minutes of gasification, the CaO peaks are broad and their sharpness continues to increase until at the end of 60 minutes x-ray diffraction patterns indicate the formation of a well-crystallized product. As loss of carbon takes place during the gasification process, segregation and crystal growth of the catalyst occur. It is apparent that the calcium oxide prefers to segregate rather than redisperse to occupy new active sites.

Potassium nitrate was also dispersed on Spherocarb and decomposed; gasification was allowed to proceed under identical conditions used for the calcium oxide experiments. It was observed that after two hours, a 5% loading of potassium oxide gasified 85% of the Spherocarb compared to 60% for calcium oxide. Hence, it appears that potassium is a more efficient catalyst at this level of loading. No distinct potassium species could be identified by x-ray analysis of the gasified products; this would seem to indicate that the potassium oxide remains poorly crystallized during the entire gasification process.
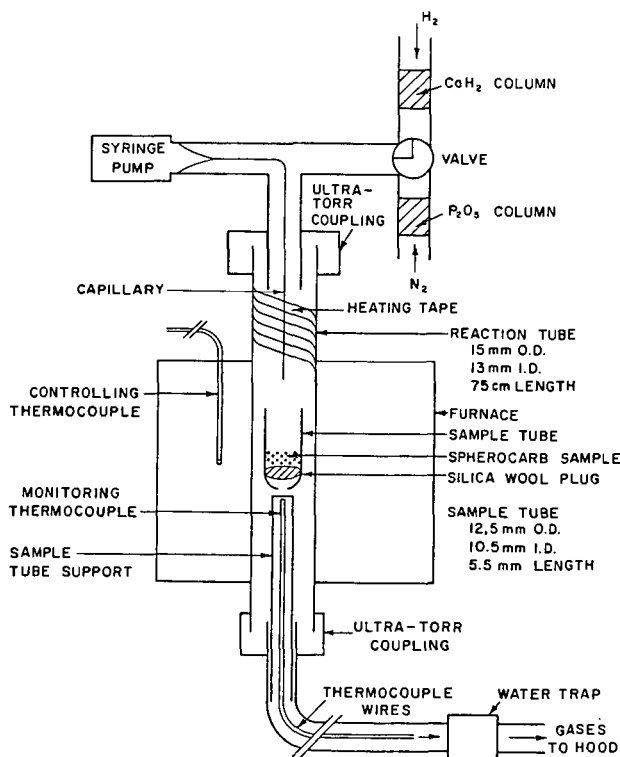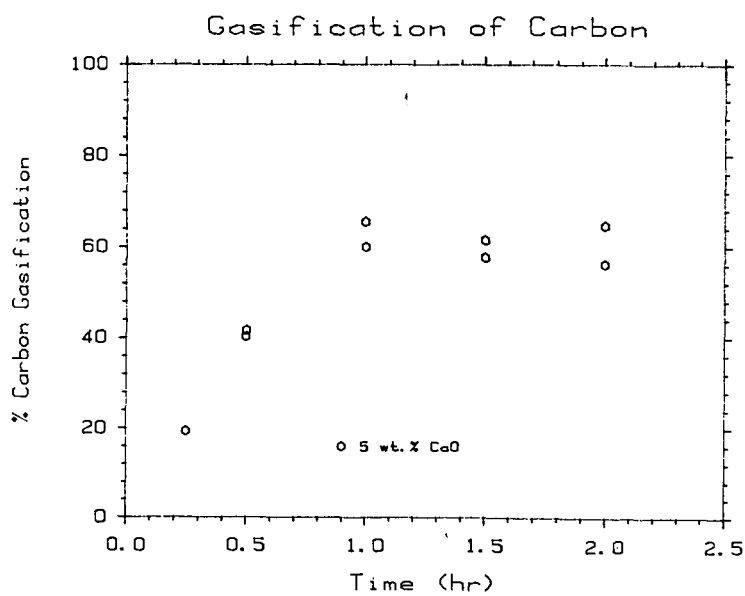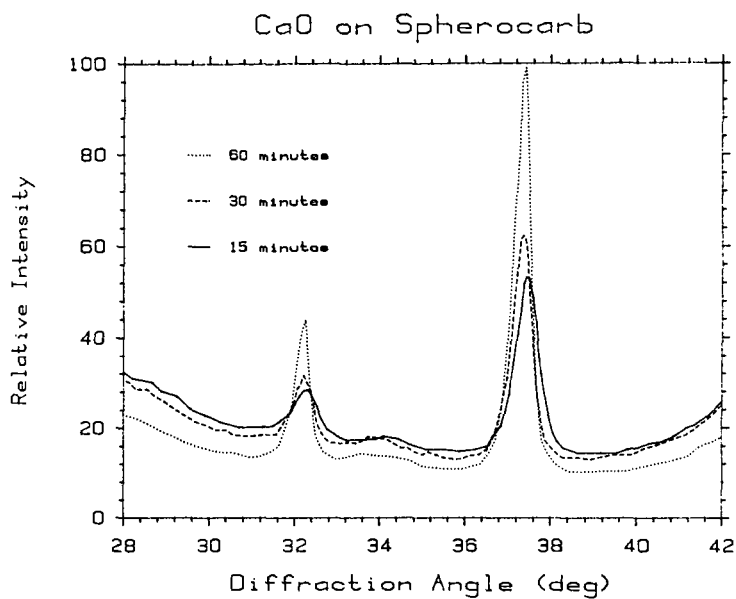
Acknowledgments

References

1. C.A. Mims and J.K. Pabst, Am. Chem. Soc., Div. Fuel Chem., Prepr. 25 (3), 258, 263 (1980).
2. C.A. Mims and J.K. Pabst, Fuel 62, 176 (1983).

3. S. Yokoyama, M. Koshiro, J. Kenichi, J. Tashiro, and I. Takakuwa, Nippon Kagaku Kaishi 6, 974 (1980).
4. I.L.C. Freriks, H.M.H. van Wechem. J.C.M. Stuiver, and R. Bouwman, Fuel 60, 463 (1981).
5. L.R. Radovic, P.L. Walker, Jr., and R.C. Jenkins, Proceedings of the International Symposium on the Fundamentals of Catalytic Coal and Carbon Gasification, Amsterdam, Sept. 27-29, 1982.
6. R.J. Lang and R.C. Neavel, Fuel 61, 620 (1982).

CaO on Spherocarb

Relative Intensity vs Diffraction Angle (deg)

· · · · · · 60 minutes
- - - - 30 minutes
——— 15 minutes

Gasification of Carbon

% Carbon Gasification vs Time (hr)

o 5 wt.% CaO

THE ADSORPTION AND CATALYZED REACTIONS OF CO AND CO_2 ON GRAPHITE SURFACES

By W. T. Tysoe, J. Carrazza and G. A. Somorjai

Materials and Molecular Research Division
Lawrence Berkeley Laboratory
and
Department of Chemistry
University of California
Berkeley, California 94720

1. Introduction

The use of ultra-high vacuum (10^{-10} – 10^{-11} torr) in conjunction with various electron spectroscopies has, over the past twenty years, provided considerable insight into adsorption on well-characterized transition metal surfaces. The incorporation of a high-pressure cell into the vacuum chamber has allowed surface species to be related to the mechanism of catalytic reactions (1).

A similar approach is adopted in this work in the study of catalytic reactions of graphite with CO and CO_2. Prior to studying catalytic reactions, results are presented in this paper on the interaction of these molecules with a clean graphite surface.

The experimental probes that are brought to bear on this problem are Auger electron spectroscopy (AES) for elemental analysis of the surface, temperature programmed desorption (TPD) to examine thermal decomposition of adsorbate species and, finally, x-ray photoelectron spectroscopy (XPS) in order to identify surface entities.

2. Experimental

The experimental apparatus is shown in Figure 1, and has been described in detail elsewhere (2). Briefly, it consists of a UHV chamber which contains a high-pressure cell, a double-pass cylindrical mirror analyzer with co-axial electron gun for Auger spectroscopy, and an X-ray source with a magnesium anode for XPS. The chamber is also equipped with a quadrupole mass spectrometer for residual gas analysis and TPD experiments. Two types of carbon were used in these experiments: a polycrystalline carbon for high pressure reactions and TPD, and a piece of oriented graphite from the Carbon Products Division of Union Carbide for XPS.

3. Results

Oxygen was the major contaminant of both graphite samples as revealed by AES. This could be effectively removed by extensive outgassing at 1500K in UHV. Hydrogen, another possible contaminant is not detectable by AES, but since C–O bond strengths are likely to be greater than for C–H, thermal removal of oxygen implies that all hydrogen has also been removed.

3.1 CO and CO_2 Adsorption and Reaction

Shown in Figure 2 are 28 amu (CO) and 44 amu (CO_2) desorption spectra after high exposures ($>10^8$L) of CO and CO_2 onto clean polycrystalline graphite at room temperature. No other desorption species were detected. The large exposures required to saturate the surface imply very low sticking probabilities.

Surprisingly, both CO and CO_2 give rise to identical 28 and 44amu spectra above 600K, exhibiting a CO_2 peak at 740K and a CO peak at 1230K. Features below 600K may originate from "physisorbed" molecules (3) or from desorption from supports. (Platinum, the support material, has a CO desorption peak at $\sim$500K).

The number of adsorption sites on the polycrystalline sample may be estimated at $\sim$5 x 10^{14} cm^{-2} from a comparison of these data with a desorption spectrum from a CO saturated Pt foil. The reaction between CO or CO_2 and polycrystalline graphite was investigated as a function of sample temperature in the high pressure reactor. The results for the reaction $CO_2 + C \rightarrow 2CO$, using a gas pressure of 230 torr, are shown in Figure 3a. These results were obtained by measuring the gas production rate, and the turnover frequencies calculated assuming the active site concentration obtained from TPD experiments ($\sim$5 x 10^{14} cm^{-2}). Measurement of the slope of this curve yields an activation energy for CO production of 67 $\pm$ 3 kcal/mole. This is in good agreement with values of 59 kcal/mole obtained in a flow reaction (4).

Figure 3b shows a similar plot for the reverse reaction ($2CO \rightarrow CO_2 + C$). An activation energy may be extracted from the linear region and yields a value of 24 $\pm$ 2 kcal/mole. The difference between these activation energies, i.e. the enthalpy for reaction is -43 ± 5 kcal/mole, which is in good agreement with the literature value of -41.2 kcal/mole (5).

Oriented graphite was used for X-ray photoelectron experiments since polycrystalline samples exhibited a broad feature on the high binding energy side of the Cls peak due to excitation of a plasmon (6). This peak is sufficiently intense to effectively obscure any adsorbate induced features. However, the plasmon satellite is strongly attenuated with the X-ray beam impinges at grazing incidence onto an edge plane which allows chemically shifted species to be observed. This sample orientation is also likely to lead to increase in number of adsorbate sites.

Figure 4a shows a MgKα Cls x-ray photoelectron spectrum from the edge plane of an oriented graphite sample after exposure to $\sim$ 10^8L CO_2 and flashing to 450K to remove "physisorbed" species. The solid line depicts the spectrum of clean graphite taken under identical conditions. The graphite Cls peak has a binding energy of 285.0 eV, and the adsorbate induced peaks occur at 281.7 eV and 280.6 eV constituting chemical shifts of 3.3 $\pm$ 0.2 and 4.4 $\pm$ 0.1 eV) remains. This peak may be removed by heating to $\sim$1400K corresponding to the desorption of CO.

191

4. Discussion

The use of single crystal graphite aligned so that the x-ray source
impinges onto the edge plane atoms allows adsorbate induced Cls features
to be observed. It is well established (7) that these shifts may be due
to carbon species that can be categorized as follows: ether and hydroxyl
groups $\sim$1.6 eV, carbonyl groups $\sim$3 eV and carboxyl groups, $\sim$4.2 eV. The
trend in Ols binding energies is less clear cut. On this basis, the peaks
that arise after CO_2 exposure may be identified as being due to carboxyl
(280.6 eV) and carbonyl (281.7 eV) species. The XPS data indicates that
the carboxyl species disappears on heating to above 850K. CO_2 is
desorbed at this temperature in TPD so that carboxyl species thermally
decomposes to yield CO_2. The $\pi \rightarrow \pi^*$ shake-up satellite also disappears.
Such behavior has been observed by Schlogel after similar treatments of
graphite samples (6). Further heating to 1400K evolves CO in TPD and the
remaining adsorbate induced peak due to a carbonyl species disappears.
High pressure reactions on a polycrystalline graphite sample result in the
formation of CO_2 from CO in the temperature range 800-900K and CO from
CO_2 in the range 1000-1100K. These temperatures correspond to those at
which CO_2(740K) and CO(1230K) are evolved, so that the rate limiting
step for CO_2 formation may be the decomposition of carboxyl species.
Similarly, the reaction to form CO may take place via carbonyl
decomposition.

Further work is required to identify the exact nature of the surface
carbonyl and carboxyl species so that their interconversion mechanism may
be elucidated in greater detail.

5. Conclusion

The interaction of clean graphite surfaces with CO and CO_2 is amenable
to investigation using conventional surface science techniques such as
AES, TPD and XPS. Preliminary studies indicate that carboxyl and carbonyl
species may be identified and appear to arise from exposure to either CO
or CO_2. CO_2 production at similar temperatures in both high pressure
reactions and in TPD suggests that carboxyl decomposition may be the rate
limiting step to CO_2 formation. Analogously, carbonyl decomposition
appears to be rate limiting for the formation of CO.

6. Acknowledgements

7. References

1. G. A. Somorjai and S. M. Davis, Platinum Metals Review, 27, 54(1983).

2. A. L. Cabrera, Heinz Heinemann and G. A. Somorjai, J. Catalysis, 75, 7(1982).

3. T. Wigmans, J. van Doorn, and J. A. Moulyn, Fuel, 62, 190(1983).

4. S. Ergun, J. Phys. Chem., 60, 480(1956).

5. Handbook of Chemistry and Physics, 61st ed., R. C. Weast, ed., CRC Press, 1980-81.

6. Schlogel and H. P. Boehm, Carbon, 12, 345(1983).

7. D. T. Clark and H. R. Thomas, J. Polymer Science (Polymer Chem Ed.), 16, 791(1978).
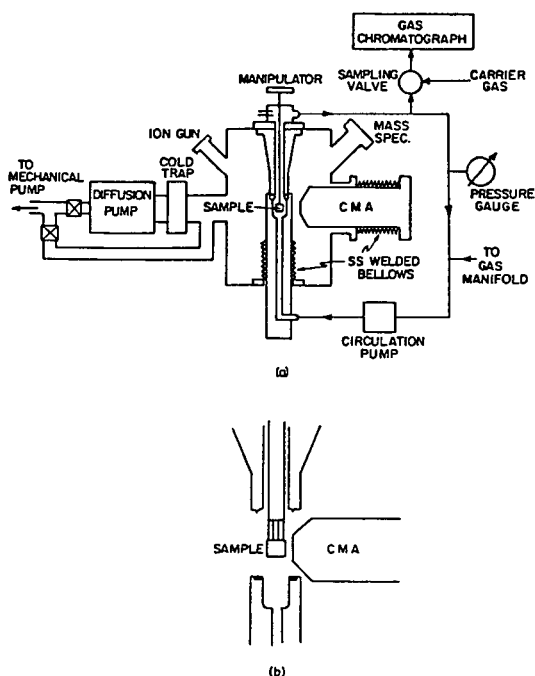
Fig. 1   (a)   Schematic diagram of apparatus with high pressure cell closed;
         (b)   detail with high pressure cell open.
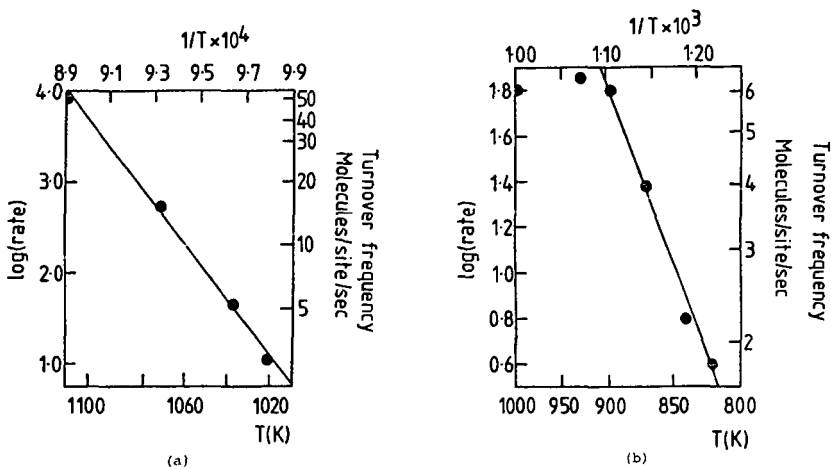
Fig. 3 (a) Arrhenius plot for the reaction, $CO_2 + C \rightarrow 2CO$; (b) Arrhenius plot for the reaction $2CO \rightarrow CO_2 + C$.
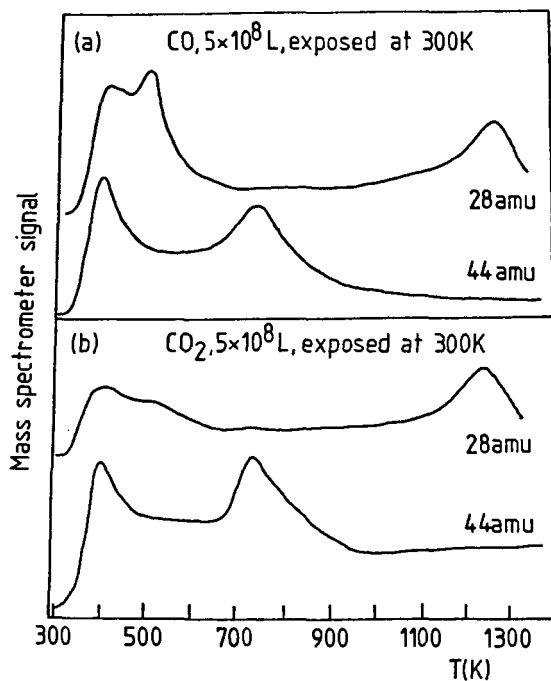
Fig. 2 28 and 44 amu desorption spectra obtained after (a) 5×10^8 L exposure of CO and (b) 5×10^8 L exposure of CO_2 onto poly-crystalline.

194

KINETICS AND MECHANISM OF CATALYTIC GASIFICATION OF COAL

H. Jüntgen and K.H. van Heek

Bergbau-Forschung, 4300 Essen 13, West Germany

1. Introduction

In the recent years experiments for the gasification of German hard coal have been carried out using several alkaline compounds, especially K_2CO_3, as catalysts. The work has been performed within the framework of the project "Prototype Plant Nuclear Process Heat" aiming at the use of heat from high temperature nuclear reactors (HTR) for the performance of the gasification. In this case the use of catalysts has special interest as the outlet temperature of the HTR is limited to about 950° /1,2/. Therefore, gasification temperature should be as low as possible (e.g. 750°C) to keep the temperature difference between the heat exchanger flown through by hot helium from the HTR and the reacting coal as high as possible. Special interest has been directed to kinetics and mechanism in order to get a basis for modelling of gasification reactors. In the following firstly experiments will be described which have been performed in laboratory scale. Then the effects of the catalysts in a big fluidized bed will be shown.

2. Order of Reaction with Respect to C and Related Reaction Models

Carbon conversion during gasification of coal is particularly dependent on the C-concentration in the solid, on temperature, on total pressure and on the partial pressures of the gasifying agent and the products. Thus, it is generally described by complex equations for the reaction rates assuming a Langmuir-Hinshelwood mechanism. For steam gasification at low partial pressures of the products H_2 and CO and at constant partial pressure of the steam reaction rates r can be described much more simple as it is only a function of the C-concentration of the solid and the temperature as follows:

$$r = k_o \exp(-E/RT)\ c^n \qquad 1)$$

with n: order of the reaction with respect to C
    k_o: frequency factor
    E: activation energy
    c: C-concentration.

For the uncatalyzed reaction values of n have been found between 2/3 and 1. Then r can be expressed as

$$r_s = \frac{dX}{dt} \; \frac{1}{(1 - X)^{2/3}} \qquad \text{for } n = 2/3 \text{ or} \qquad 2)$$

$$r'' = \frac{dX}{dt} \; \frac{1}{1 - X} \qquad \text{for } n = 1 \qquad 3)$$

with X = carbon conversion.

For coal gasification catalyzed with alkaline compounds Mims and Pabst /3/ have reported that n can be 0 at low degree of carbon conversion and will change to n = 1 and beyond at higher degrees of conversion corresponding to

$$r' = \frac{dX}{dt} \qquad \text{for } n = 0. \qquad 4)$$

The existence of different values for n can be explained as follows: If all C-atoms are equally accessible and active during the course of the gasification reactions between C and H_2O then the assumption of n = 1 makes sense. However, in a more detailed consideration it has to be taken into account that the different C-atoms may show different activities to gasification and that the reaction will occur at the internal surface of the porous solid. Both effects are complex and not predictable by a simple theory. The reaction order of n = 2/3 can be deduced on the basis of a geometric pore model if the effects of crystalline structure of the C-matrix are neglected. For catalyzed gasification it can be assumed that the C-atoms in the neighborhood of catalytically active particles show a much higher reaction activity. Consequently, they are preferably consumed. The reaction order will then be a function of the accessibility of these "catalyzed C-atoms" during the course of conversion. Provided that the catalyst atoms are mobile, the concentration of the C-atoms has no influence, and the reaction order will be 0.

3. Experimental Results Concerning the Reaction Order and the Influence of the Catalyst Concentration

First of all the reaction order for the uncatalyzed gasification of a char shall be discussed. Fig. 1 shows as an example the measured reaction rates r_s and r'' plotted against the degree of gasification assuming a reaction order of 2/3 or 1, respectively /4/. The reaction rate r_s remains constant for a degree of conversion ranging between 20 and 70 % and decreases rapidly beyond 70 %. That means that the assumption of n = 2/3 gives the best fit for the experimental values for this char. In other experiments, however, reaction orders closer to 1 than 2/3 have been determined.

A reaction order of 2/3 has been found for the catalytic gasification, too, adding 0.56 to 5.1 % K to a low ash char made from the coal Westerholt, as can be seen by fig. 2 /5/. The mode of char preparation is also given in /5/. It can be stated that r_s remains constant in a wider range of C-conversion (burn-off) as compared with the uncatalyzed case (fig. 1). It follows that the K-atoms are excellently distributed in the char and that the C-atoms in the neighborhood of the catalysts are equally well accessible by the steam during the course of burn-off.

As these experiments are carried out at 700°C a free mobility
of the catalyst cannot be expected as will be shown later on.
A detailed analysis of the results leads to the following equation
for the description of the rate of the catalyzed reaction r_s
dependent on X and the K-concentration c_K:

$$r_s = \frac{dX}{dt} \cdot \frac{1}{(1 - X)^{2/3}} = (k_1 + k_2\, c_K) \qquad 5)$$

$$k_1 = 0{,}00276\ \frac{1}{\min}$$

$$k_2 = 0{,}00953\ \frac{1}{\min \cdot wt\%K}$$

As it is shown in fig. 3 the rate r_s increases linear with the
K-concentration c_K in the sample.

Different results have been found at gasification temperatures
of 880°C and a pressure of 1 bar with coal "Lohberg" (35.7 % v.m.
m.a.f., 5.3 % ash m.f.) /6,7/ using different alcaline compounds.
In fig. 4 reaction rates r' are plotted depending on the degree
of conversion assuming a reaction order n = 0. This assumption
is confirmed by the horizontal slope of the curve for carbon
conversions up to 90 %. This deviation from the findings given
in fig. 2 may be explained by the assumption that the catalyst
is free mobile at this higher temperature as will be discussed
later.

Fig. 5 demonstrates the different effects of equal alkali con-
centrations (in mole/g coal) for the different alkali group
elements. For each alkali metal there is a concentration range
in which the zero-order reaction rate r' increases nearly propor-
tionally to the catalyst concentration. The slope of this straight
line is increasing with increasing atomic number of the alcaline
metals. It is remarkable that the boiling point of the metals
decreases in the same order (table 1). As will be discussed
later, our experiments have shown that the alcaline carbonates
are reduced to the metals by the carbon while heated up to reac-
tion temperature. The metals are bound to the C-atoms by a mech-
anism which is not yet clear. Obviously, the effectiveness of
these metals is strongly related to their mobility on the surface
and the latter surely depends on the boiling point relative
to the reaction temperature. As shown in table 1 the boiling

Table 1: Boiling Point of Alkaline Metals

Metal	Atomic Number	Boiling Point °C
Cs	55	690
K	19	760
Na	11	892
Li	3	1330

temperatures of Cs and K are lower than the reaction tempera-
ture of 880°C (fig. 5). In this case a high mobility of both
metals results in a high catalytic effectiveness. The boiling
temperature of Na is beyond, that of Li is far beyond 880°C
with the effect that the catalytic activity is decreasing in
this order. Furthermore, our experiments have shown that Li
probably is present as oxide instead of metal.

4. Desactivation of the Alkali by Mineral Matter

It can already be seen from fig. 5 that low concentrations of
catalyst lead to no increase of the reaction rate. As has been
confirmed by detailed studies this observation can be explained
by reactions of alkali with clay minerals in the coal which
lower the catalytic activity. Relevant results are shown in
fig. 6 whereby different concentrations of K_2CO_3 have been added
to chars of ash content between 6 and 30 %.

For the 6.6 % ash char the catalytic effects are observed after
3 % K_2CO_3 have been added. The rates then increase proportional
to the concentration. For the 18.8 % ash char catalytic gasifi-
cation starts distinctly with a minimum of 7.5 % K_2CO_3 addition
and in the case of the 13 % ash char approximately 12.5 % K_2CO_3
seem to be necessary. From the shape of the curve depending
on burn-off it can be derived that n = 2/3 is valid to some
extent for the char with a relatively low ash content. For the
chars containing a higher amount of mineral matter the reaction
rates decrease systematically with burn-off whereby different
slopes have been measured in the different ranges of burn-off.
It can be concluded that rapid and slow reactions of desactivation
take place, as the alkali reacts with different components of
the mineral matter. Active in consuming alkali have been proven
to be the clay minerals kaolinite and illite and kaliophilite
is found as a product of the reaction of both clay minerals
with potassium carbonate /8/.

5. Activation Energy and Frequency Factor

Investigating the kinetics of catalytic gasification, special
attention has to be paid to the temperature region in which
chemical reaction is rate determining. In this region catalysts
are expected to have maximum effect. However, in consequence
of the reaction rate increase the transition temperature between
the chemical viz. diffusion controlled regions should change
to lower values. This effect has been verified experimentally.
In the Arrhenius-type diagram (fig. 7) the transition temperature
can be located at 700°C, whereas for the uncatalyzed gasifi-
cation no transition is to be observed up to 850°C.

The investigations described below are therefore restricted
to the domain of chemical reaction controlled gasification rate.
As shown in fig. 8 increasing amounts of potassium shift the
lines in the Arrhenius diagram without changing the slope /6,7/,
i.e. the activation energy is nearly unaffected by the cata-
lyst while the frequency factor increases proportional to the
amount of potassium added. In the case of Na-catalyzed gasific-
ation, results were similar besides the fact that the uncatalyzed
reaction exhibits an activation energy slightly different from
those found in the experiments with distinct Na-concentrations.

6. Chemical State of the Alkali Catalysts and Mechanism

Thermogravimetric analyses were performed to examine the de-
composition reaction of K_2CO_3 on the surface of char and the
evaporation of elemental potassium from a char-potassium-mix-
ture /6,7/. It can be concluded that the first reaction step
is the reduction to elemental potassium by the carbon:

$$K_2CO_3 + C \longrightarrow 2K + CO + CO_2 \qquad\qquad 6)$$
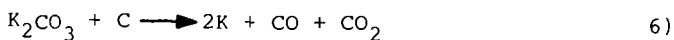
The potassium has been found to undergo a relatively strong bonding to the carbon. This is indicated by an extremely small evaporation rate of potassium metal in the presence of carbon. Thus the conclusion seems to be justified that the second step consists in the formation of a potassium-carbon-complex KC_n:

$$K + nC \longrightarrow (KC_n) \qquad\qquad 7)$$

The value of n is approximately 5.5 which results from our evaporation experiments. The exact status of the bonding between alkaline metal and the carbon is not yet understood, however, we assume that there is a bonding by an electron transfer from the K-metal to the C-atom. Other authors stress the possibility of a bonding between carbon-oxygen complexes and the K-metal /9/.

The next reaction steps are speculative. The assumption seems reasonable that in a third step K-C-complexes are converted to surface oxides and hydrogen by the steam:

$$(KC_n) + H_2O \longrightarrow (KC_n)O + H_2 \qquad\qquad 8)$$
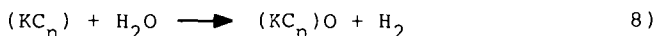
The fourth step should be the desorption of the surface oxide as CO thereby restoring the metallic state of the potassium:

$$(KC_n) \longrightarrow K + (n-1)\ C + CO \qquad\qquad 9)$$
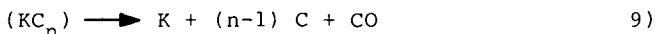
Migration of potassium may form a K-C-complex again because potassium is mobile - at least at temperatures of 800 to 880°C thus repeating step 2 (equation 7) and completing the reaction cycle. In parallel to the gasification the desactivating reactions with coal minerals mentioned above occur. In addition potassium may be desactivated by re-establishing the potassium oxide or carbonate by reactions with steam or product gases. At high degrees of C-conversion the oxides or salts may form larger crystallites because of the high K-concentrations. Potassium then looses contact to the carbon atoms and reduction into the metal is no longer possible. This results in a severe desactivation. As to be seen in fig. 2, 4, and 6 such a desactivation occurs at C-conversions beyond 80 or 90 %.

7. Experiments on Larger Scale

On the basis of results of exploratory research in the laboratory a number of runs have been performed in a semi-technical plant with a fluidized bed of about 4 m^3 volume heated by an immersed helium-flow heat exchanger /10/. K_2CO_3 and other active substances have been fed along with the coal in a dry mixture into the gasifier. Fig. 9 summarizes the reaction rates for an anthracite, a high volatile bituminous coal without catalyst and doped with different amounts of K_2CO_3. For high volatile bituminous coal an increase of the reaction rate compared to anthracite by a factor of 2.5 can be stated. A doping with 2 or 3 % K_2CO_3 to the latter has a relatively modest effect. This can be explained by side reactions of K_2CO_3 with mineral compounds in the coal ash with the consequence of loss of catalytic activity. However, if 4 % K_2CO_3 are added a steep increase

of reaction rate by a factor of about 20 can be achieved. As has been predicted theoretically, the mean fluidized bed temperature decreases to 740°C. A steam decomposition of 30 % at a coal feed rate of 400 kg/h and an average carbon conversion of 37 % (in the fully back-mixed system) have been measured.

7. Discussion

Steam gasification catalyzed by potassium has been found to follow a varying reaction order with respect to carbon depending on the kind of char, ash content, and temperature. For the gasification of low-ash char, deviations of zero-order is ascribed to a restricted mobility of the catalyst, as it is found to occur especially at low temperatures, whereas mineral matter change the amount of active catalyst during gasification and thus produces apparent reaction orders that can even exceed n = 1. Chemical state of the catalyst on char under inert conditions has been found to be rather metallic than oxidic, but a bonding to carbon has been proven. Concerning reaction mechanism, the principle of catalytic action seems to be not a reaction path with a lower activation energy than for uncatalyzed reaction but an increase in the number of active sites. In this aspect, the mechanism of alkali catalysis is like that of earth alkali catalysis for which Otto et al /11/ reported a constant activation energy and an increased frequency factor.

Literature

/1/ Jüntgen, H., FUEL 1982, Vol. 62, Feb., p. 234

/2/ Kubiak, H., Schröter, H.-J., Sulimma, A., and van Heek, K.H., FUEL 1982, Vol. 62, Feb., p. 242

/3/ Mims, C.A., Pabst, J.K., private communication

/4/ Mühlen, H.J., Thesis, University of Essen (FR of Germany)

/5/ Leonhardt, P., Sulimma, A., van Heek, K.H., and Jüntgen, H., FUEL 1982, Vol. 62, Feb., p. 200

/6/ Huhn, F., Klein J., and Jüntgen, H., FUEL 1982, Vol. 62, Feb., p. 196

/7/ Huhn, F., Thesis, University of Essen 1983 (FR of Germany)

/8/ Kühn, L., Plogmann, H., FUEL 1982, Vol. 62, Feb. p. 205

/9/ Mims, C.A., Pabst, J.K., FUEL 1980, Vol. 62, Feb., p. 176

/10/ Kirchhoff, R., van Heek, K.H., Jüntgen, H., and Peters, W., "Nuclear Engineering and Design" (in press)

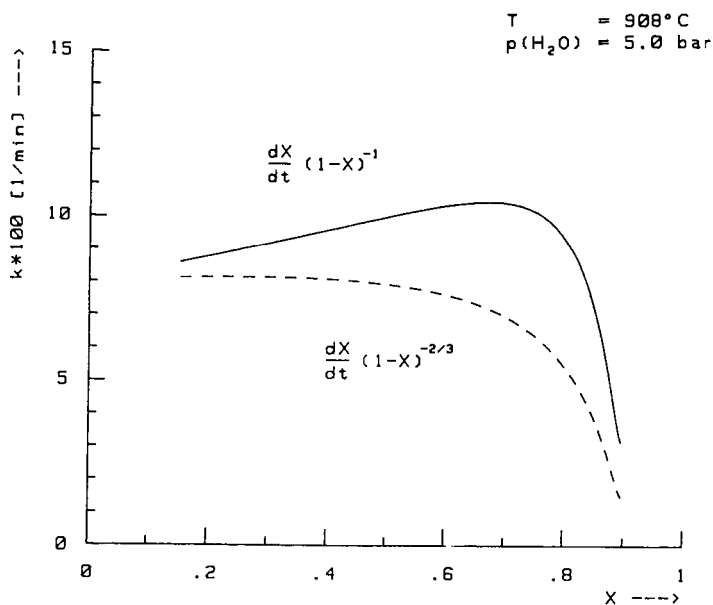/11/ Otto, K., Bartosiewicz, L., and Shelef, M., Carbon 1979, Vol. 17, p. 351

Fig. 1: Comparison of 1st-order and 2/3rd-order-reaction
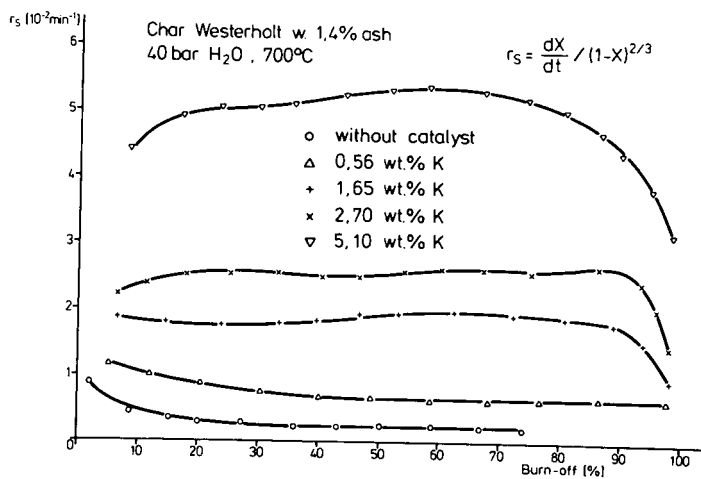rate of a steam gasification run

Fig. 2: Reaction rate based on order 2/3 for catalytic
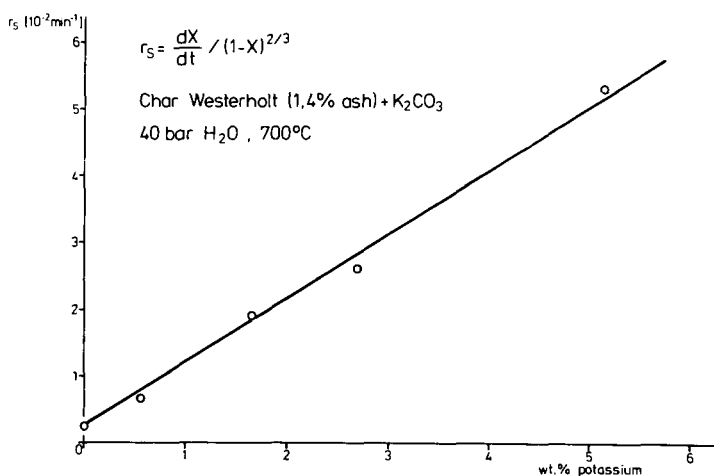gasification of a low-ash char

Fig. 3: Correlation of reaction rate r_s with potassium concentration for steam gasification of a low-ash char
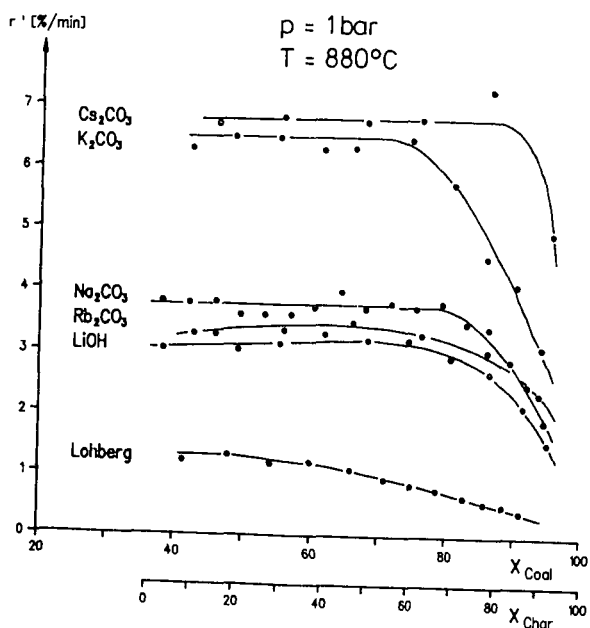

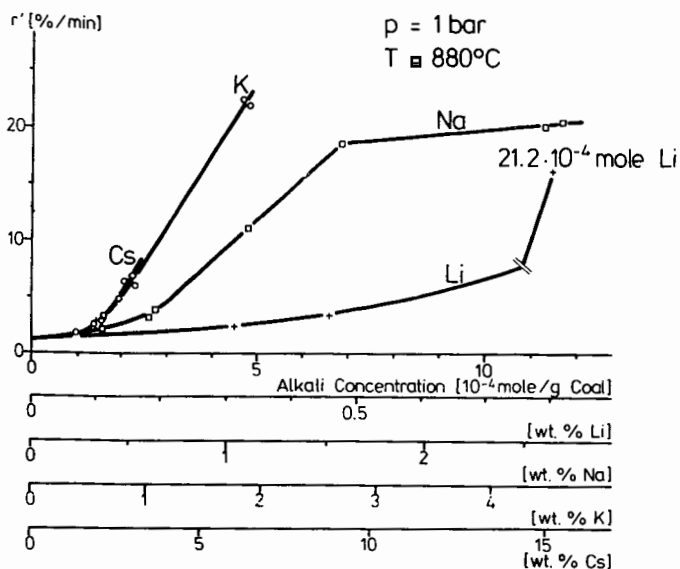Fig. 4: Steam gasification of "Lohberg" coal with alkali catalysts as a function of C-conversion

Fig. 5: Concentration dependance of steam gasification
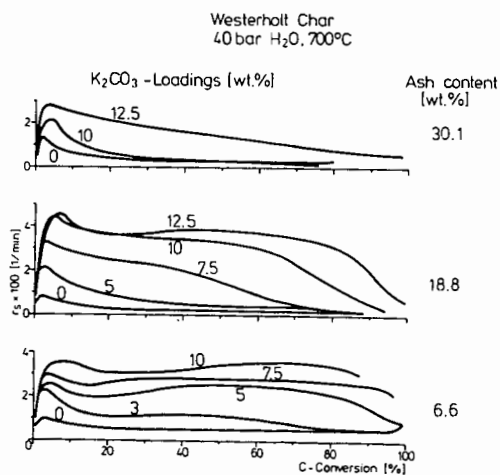of coal "Lohberg" with different group elements

Fig. 6: Catalytic steam gasification of Westerholt char
with different potassium and ash contents - eva-
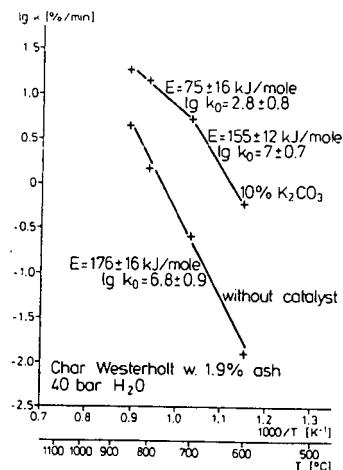luated assuming reaction order n = 2/3 -

203

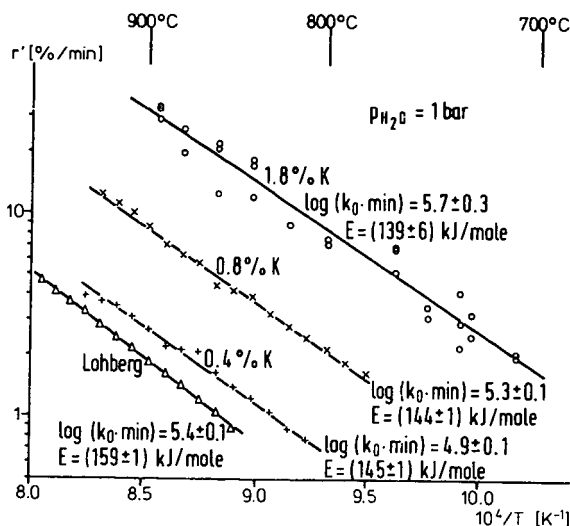Fig. 7: Activation energy for non-catalytic and potassium-
catalyzed steam gasification

Fig. 8: Activation energy and frequency factor as function
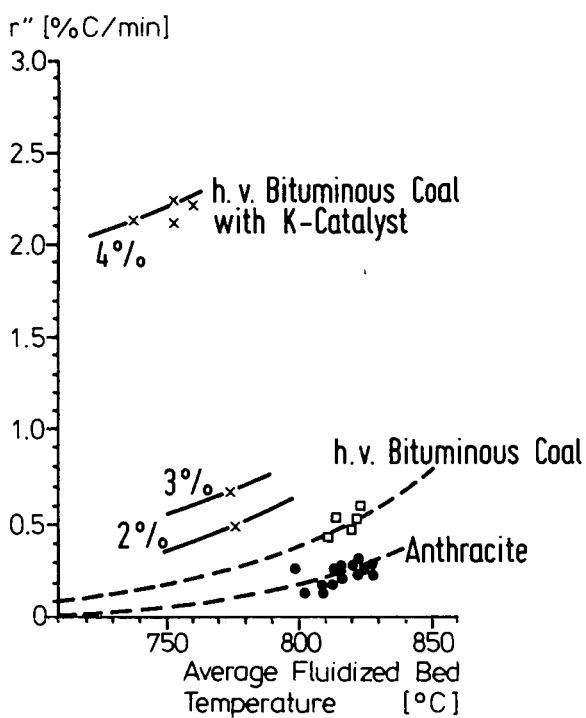of potassium catalyst for the gasification of
"Lohberg" coal

204

Fig. 9: Rates of catalyzed and uncatalyzed gasification
in a fluidized bed reactor (height 4 m, pressure
40 bar) – The weight percent of K_2CO_3 added is
noted at the curves

FTIR STUDIES OF THE EFFECT OF ALKALI METAL SALTS AND THE USE OF ALKALI METAL CHLORIDES IN THE CATALYTIC GASIFICATION OF COAL CHARS

Shang Jung Yuh and Eduardo E. Wolf[*]

Department of Chemical Engineering
University of Notre Dame
Notre Dame, Indiana 46556

INTRODUCTION

Catalytic gasification of coal provides a direct route for producing synthetic natural gas (SNG). It has long been known that certain alkali metal salts can catalyze the steam gasification of carbonaceous materials[1-2]. As a result, lower gasification temperatures can be employed creating a thermodynamically favorable condition for methane production. Several interpretations have been proposed to explain the catalytic mechanism of coal gasification by alkali metal salts. Various redox cycles involving alkali metal[3-5], alkali oxide[6-8], and alkali metal-carbon intercalates[9-10] as the reaction intermediates, have been suggested. Alternatively, Mims and Pabst have proposed that surface complexes such as -C-O-K, -C-K are possible sites of catalytic activity during coal gasification[11-13]. Our previous infrared studies of partially gasified coals originally treated with alkali salts showed the presence of a common infrared spectrum for all salts except for the inactive chlorides[14-15]. In the Exxon catalytic coal gasification (CCG) process, only about two-third of the original K_2CO_3(or KOH) catalyst can be recovered by water leaching from the ashes due to the formation of insoluble aluminosilicates[11]. Procedures to activate the less expensive alkali salts have been investigated. Wood et al.[16] reported that at modest temperatures, a steam pretreatment of KCl-impregnated carbon may activate this otherwise inactive but inexpensive salt. Lang and Pabst[17] showed that high gasification rates can be attained by employing mixtures of strong acid salts of potassium and, any weak acid salts or certain strong acid salts of sodium as the catalyst. Chauhan et al.[18] found that coal treated with CaO using NaOH at an elevated temperature is much more reactive than that impregnated with aqueous CaO slurry. Lang and Neavel[19] also concluded that calcium must be atomically dispersed throughout the coal to obtain good activity.

This paper describes kinetic and infrared studies of the steam gasification of coal catalyzed by alkali metal salts. These studies have subsequently led us to the formulation of a procedure by which alkali metal chlorides are used as the source of alkali metals for catalytic coal gasification.

---

* To whom correspondence should be addressed.

EXPERIMENTAL

Kinetic experiments were performed in a quartz flow reactor equipped with a Cahn RG 2000 electrobalance which can continuously monitor the weight loss of the sample as it reacts with flowing steam. During the course of the gasification, effluent gas was periodically analyzed by a gas chromatograph. The infrared spectra were recorded on a Digilab FTS-15C fourier transform infrared spectrometer (FTIR) using coal samples pressed with KBr at a ratio of 1:400. A spectrum was obtained by co-adding fifty scans at a resolution of 4 cm^{-1} wavenumber using a pure KBr disc as the reference. In all experiments, reagent grade chemicals and high purity gases were used as received. Further details about the experimental apparatus, operating procedures, and sample preparation have been described elsewhere[14].

RESULTS AND DISCUSSION

Figure 1 summarizes the gasification rates at 20% conversion and 750°C versus metal/carbon ratio. The data were obtained using an Illinois #6 coal treated with various sodium salts and different catalyst loadings. All sodium salts studied, except NaCl, exhibit good catalytic activity for steam gasification of coal. The gasification rate follows a linear relation with sodium/carbon ratio until a saturation point at about Na/C=0.12 is reached. This trend is similar to the observation reported by Mims and Pabst[11] for K_2CO_3 with various carbon substrates. The dependence of the gasification rate on the catalyst contacting method, namely incipient wetness, aqueous impregnation, and mechanical mixing is not significant. Figure 1 shows that the gasification rate varies at most 10% among three contacting methods. Furthermore, based on the same metal/carbon ratio potassium salts are more effective than sodium salts. However, untreated NaCl and KCl are inactive as catalysts for steam gasification of coal.

The infrared spectrum of Na_2CO_3-impregnated coal is shown in Figure 2A. The absorption band at 1610 cm^{-1} has been assigned to the chelated conjugated carbonyl structure and carboxylates contained in coal[20] whereas the 1450 and 880 cm^{-1} bands are due to sodium carbonate[21]. Upon devolatilization, the 1610 cm^{-1} band disappeared while the carbonate bands were still present but less intense as shown in Figure 2B. Since about 44% of the Na initially loaded was lost after devolatilization along with 34% release of volatile matter, the Na/C ratio of the devolatilized sample should have remained the same as that of the impregnated sample. Thus, the decrease in infrared absorbance of the carbonate bands in the devolatlized sample indicates that the missing fraction had reacted with the carbon substrate. Moreover, upon partial gasification to 25% conversion, the intensity of the carbonate bands decreased even further as shown in Figure 2C, even though the Na/C ratio increased due to the carbon consumption. Furthermore, the infrared spectrum of an almost completely gasified sample(94% conversion, Figure 2D) shows an increase of intensity of the carbonate bands as well as the appearance of additional
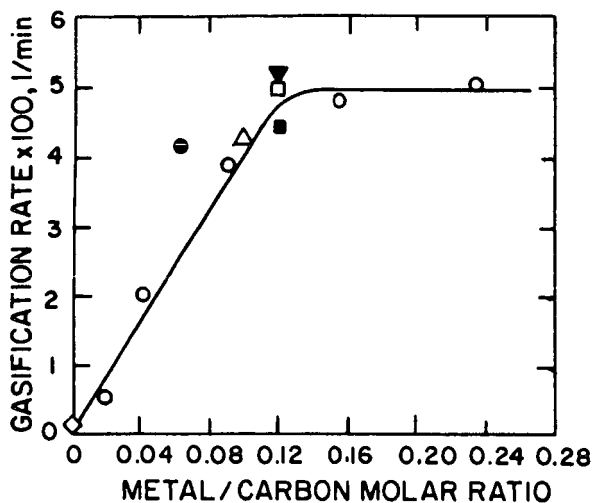
Figure 1 Effects of loading, anion, and contacting method of catalyst on the gasification rate. O, NaOH; Δ, Na_2CO_3; ▼, $NaNO_3$; □, $NaHCO_3$ (incipient wetness); +, $NaHCO_3$ (aqueous impregnation); ■, $NaHCO_3$ (mechanical mixing); ●, K_2CO_3; ◇, without catalyst.
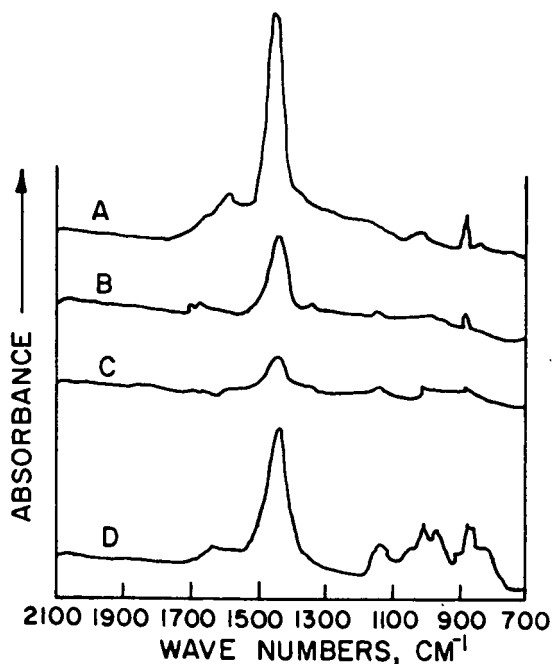

Figure 2 FTIR spectra of Na_2CO_3 coal samples. A, impregnated; B, devolatilized; C, partially gasified (25% conversion); D, gasified (94% conversion).

bands in the 1200-800 cm^{-1} region which corresponds to mineral matters. Atomic absorption measurements of the sodium contained in this sample gave a similar percentage of Na losses(43%) as in the devolatilized sample demonstrating that the interaction of sodium with the carbon substrate occurs at the initial stages of gasification but it disappears at the end with the release of sodium due to the depletion of carbon. It is also interesting to note that all devolatilized and partially gasified samples treated with catalytically active sodium salts exhibit a common infrared spectrum regardless of the anion of the parent salt(15).

In addition, the interaction of sodium and carbon substrate has also been documented by our and other's thermogravimetric results(4,11,15). We found that the weight loss of Na$_2$CO$_3$-char in helium starts at temperature much lower than the melting point of Na$_2$CO$_3$(851°C), with CO and CO$_2$ being the gas products. In the case of char impregnated with NaCl, the temperature at which the weight loss begins is similar to that of NaCl, without any detectable gas product. The infrared and thermogravimetric results clearly demonstrate the importance of the direct interaction of coal with the alkali metal in catalytic activity. Thus, the lack of catalytic activity of alkali metal chlorides results from the high stability of the alkali metal-chlorine bond which prevents the interaction of the carbon substrate with the alkali metal. Further proof of this point is illustrated in Figure 3 in which HCl was added to three Na$_2$CO$_3$-treated chars. It can be seen that as the amount of chlorine increases, the catalytic activity decreases accordingly. Moreover, infrared spectra of the HCl-treated samples show a corresponding decrease in the intensity of the carbonate absorbance indicating that the reaction of sodium to form chloride which is infrared inactive, was favored over the interaction of sodium with the carbon substrate.

A corollary of the above results is that Na has to be freed from the chlorine ion in order to use NaCl as the source of Na to catalyze coal gasification. On this basis, we have developed a process which ultilizes alkali chlorides as the source of alkali metals for catalytic coal gasification. The process consists of slurrying the coal with an aqueous solution of the chlorides and a suitable solvent, and subsequent saturation with CO$_2$. The solid is separated, washed, and dried and is then ready for gasification. All operations except drying are carried out at room temperature. The chlorine ions could be removed in the form of CaCl$_2$ and the solvent can be regenerated and reused. The advantage of this procedure is that the consumption of CO$_2$ required can be supplied by the gasification itself and alkali chlorides are less expensive than other alkali salts.

Figure 4 shows the gasification rates (at 20% conversion and 750 ^{o}C) of coals treated with different amounts of NaCl and KCl according to the above mentioned procedure, versus metal/carbon ratio. The sodium and potassium loadings were determined by an atomic absorption spectrophotometer(Perkin-Elmer, Model 305). As expected the KCl-treated coals show higher activity than NaCl-treated coals. Also included in Figure 4 are points obtained with Na$_2$CO$_3$-impregnated and K$_2$CO$_3$-impregnated coals showing that the activities of these samples are equivalent to those obtained with chloride-treated samples.
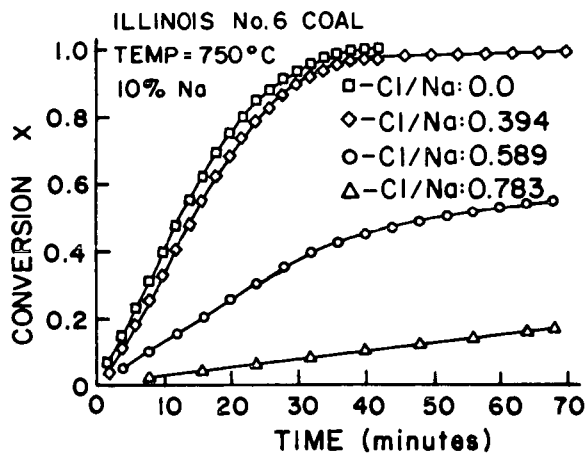
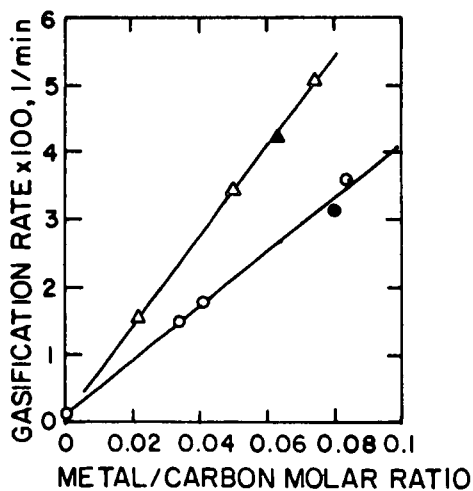Figure 3 Effect of chlorine addition to Na_2CO_3 coal samples.

Figure 4 Gasification rates of KCl treated coals ($\triangle$), NaCl treated coals (O), K_2CO_3 impregnated coal ($\blacktriangle$), Na_2CO_3 impregnated coal ($\bullet$).

CONCLUSION

　　Laboratory results demonstrate that alkali metal chlorides can provide the source of alkali metals required for catalytic steam gasification of coals via a process involving contact of coal with an aqueous solution of alkali chloride, a suitable as well as regenerable solvent, and CO_2. The catalytic activities of the samples prepared by this procedure are equivalent to those impregnated with other alkali salts.

REFERENCES

1. Walker, P. L., Jr., Shelef, M., and Anderson, R. A., "Chemistry and Physics of Carbon", Vol. 4(Ed. Walker, P. L., Jr.), Edward Arnold, Landon, 287, 1968.
2. McKee, D. W., "Chemistry and Physics of Carbon", Vol. 17(Eds. Walker, P. L., Jr. and Thrower, R. A.), Marcel Dekker, New York, 1, 1980.
3. Fox, D. A. and White, P. H., Ind. Eng. Chem., 23,259, 1931.
4. McKee, D. W. and Chatterji, D., Carbon, 16(1), 53, 1978.
5. Veraa, M. J. and Bell, A. T., Fuel, 57(4), 194,1978.
6. McKee, D. W. and Yates, J. T., J. Catal., 21(2),308, 1981.
7. Yates, J. T. and McKee, D. W., J. Chem. Phys., 75(6), 2711, 1981.
8. Wigmans, T. et al., Carbon, 21(1), 1, 1983.
9. Wen, W.-Y., Catal. Rev. Sci. Eng., 22(1), 1, 1980.
10. Kapteijn, F., Jurriaans, J., and Moulijn, J. A., Fuel, 62(2), 249, 1983.
11. Mims, C. A. and Pabst, J. K., Preprints Am. Chem. Soc. Div. Fuel Chem., 25(3), 258, 1980.
12. Mims, C. A. and Pabst, J. K., "Proc. Inter. Conf. Coal Sci.", 730, 1981.
13. Mims, C. A. and Pabst, J. K., Fuel, 62(2), 176, 1983.
14. Yuh, S. J. and Wolf, E. E., Fuel, 62(2), 252, 1983.
15. Yuh, S. J. and Wolf, E. E., Submitted for publication in Fuel.
16. Wood, B. J. et al., SRI International, Quarterly Technical Progress Report No. 6, DOE Contract No. AC21-80MC14593, June 18, 1982.
17. Lang, R. J. and Pabst, J. K., U. S. Patent 4318712, 1982.
18. Chauhan, S. P. et al., Preprints Am. Chem. Soc. Div. Fuel Chem., 22(1), 38, 1977.
19. Lang, R. J. and Neavel, R. C., Fuel, 61(7), 620, 1982.
20. Friedel, F. A., Retcofsky, H. L., and Queiser, J. A., U. S. Bu. Min. Bul., 640, 1, 1967.
21. Miller, F. A. and Wilkins, C. H., Anal. Chem., 24(8), 1253, 1952.